

# **Grinding Wheel Surface Texture Characterization Using Scale Sensitive Fractal Analysis.**

By: David Greaves  
John Niewola  
Garrett Vandette

A Major Qualifying Project

Submitted to the Faculty of

WORCESTER POLYTECHNIC INSTITUTE

In Partial Fulfillment of the Requirements for the

Degree of Bachelors of Science

In

Mechanical Engineering

April 2007

APPROVED:

Prof. Christopher A. Brown, Project Advisor

# Table of Contents

<b>1. Introduction</b> .....	<b>4</b>
1.1 Objectives .....	4
1.2 Rationale .....	4
1.3 State of the Art .....	6
1.4 Approach.....	7
<b>2. Methods</b> .....	<b>8</b>
2.1 Grinding .....	8
2.2 Replication .....	10
2.3 Measurement.....	12
2.5 Characterization .....	16
2.5 Differentiation.....	19
<b>3. Results</b> .....	<b>21</b>
3.1 Grinding .....	21
3.2 Replication .....	23
3.3 Measurement.....	24
3.4 Characterization .....	27
3.5 Differentiation.....	30
<b>4. Conclusions</b> .....	<b>38</b>
<b>5. Discussion</b> .....	<b>39</b>
<b>6. References</b> .....	<b>41</b>
<b>7. Appendices</b> .....	<b>41</b>

## List of Figures

Figure 1: Outline of State of the Art references.....	6
Figure 2: Flow chart of sequence of events .....	8
Figure 3: Table of grinding wheels examined .....	9
Figure 4: Replica material left on grinding surface .....	10
Figure 5: Measurement principal of a confocal point sensor.....	13
Figure 6: Table of Measurement Parameters .....	14
Figure 7: Table of Conventional Parameters .....	16
Figure 8: Length-Scale Illustration .....	17
Figure 9: Area-Scale Illustration.....	18
Figure 10: Differentiation Matrix .....	20
Figure 11: Regions of the grinding surface.....	21
Figure 12: Performance graphs.....	22
Figure 13: Replica quality inspection .....	23
Figure 14: Noise Comparison .....	24
Figure 15: Three-dimensional representations of noise test results.....	25
Figure 16: Height-Height plot of repeatability tests .....	26
Figure 17: Table of conventional parameter results .....	27
Figure 18: Comparison of area-scale curves.....	28
Figure 19: Comparison of filling-scale curves.....	29
Figure 20: Sa differentiation matrix.....	30
Figure 21: Sq differentiation matrix .....	30
Figure 22: Sp differentiation matrix .....	31
Figure 23: Sv differentiation matrix .....	31
Figure 24: St differentiation matrix .....	31
Figure 25: Ssk differentiation matrix.....	32
Figure 26: Sku differentiation matrix .....	32
Figure 27: Sz differentiation matrix.....	32
Figure 28: Pa differentiation matrix.....	33
Figure 29: Pq differentiation matrix .....	33
Figure 30: Combined conventional parameter differentiation matrix .....	34
Figure 31: F-test results of area-scale comparisons.....	34
Figure 32: Relative area differentiation matrix.....	35
Figure 33: F-test results of a filling-scale comparison.....	36
Figure 34: Average texture depth differentiation matrix .....	36
Figure 35: Combined relative-area and average texture depth differentiation matrix.....	37

## **Abstract**

The objective of this project is to characterize grinding wheel surface texture using conventional parameters and scale sensitive fractal analysis, for the purpose of differentiation. Combining this knowledge with grinding performance data will allow wheels to be designed and/or dressed to custom specifications. Replicas were made of grinding wheel surfaces and measured. Conventional and fractal parameters were calculated using software, and F-tests were performed to differentiate surface texture based on these parameters. The fractal method was found to differentiate surface textures better.

## **1. Introduction**

### ***1.1 Objectives***

The aim of this research is to measure the surface texture of grinding wheels for the purpose of differentiating between wheel composition (abrasive, bond) and degree of wear (dressed, ground).

### ***1.2 Rationale***

A grinding wheel's surface texture has a strong influence upon its grinding performance. This is clearly evidenced by the increase in grinding forces, power consumption, and cutting zone temperatures as a wheel wears [Butler and Blunt, 2002]. If the surface texture of a grinding wheel could be measured and quantified, then it could be

compared to known grinding performance data for similar texture. Grinding wheels could also be designed and/or dressed to take advantage of better textures leading to wheels that stay sharper longer.

Sharper wheels generally have high material removal rates and low grinding forces and power consumption. High material removal rates shorten cycle times, which allow more parts to be made in less time. Low grinding forces and power consumption reduces wear on grinding machinery and improves the surface finish of the work piece. Due to these properties it stands to reason that producing grinding wheels that remain sharp longer will save consumers time and money.

Understanding the connection between surface textures and grinding performance also benefits quality control. Currently wheels are tested by performing a grinding operation and examining the performance data, which generally consists of material removal rate, grinding force, power consumption, specific energy, and grinding ratio. This process is time consuming, destroys the product, and is an indirect method of characterizing the wheel.

Measuring the surface texture, however, would be faster and automatable, be completely non-contact, and give a direct characterization of the wheel. The wheel surface could easily be compared to an industry standard and assigned a value of how well it fits the standard, similar to the ratings of electrical resistors. This would all work together to reduce the time and money spent testing wheels, reduce the time to market, and allow for a guarantee of wheel performance.

### 1.3 State of the Art

Figure 1 shows a table outlining the sources described below, and the methods used in their research.

<b>Names:</b>	<b>Measurement Technique:</b>	<b>Parameter Examined:</b>
Zhou and Xi (2002)	Contact Stylus	Active cutting edges vs. Grinding power
Blunt and Ebdon	Contact Stylus	Static Cutting Points
Butler, Blunt, See, Webster, and Stout	Contact Stylus	Summit density and curvature

**Figure 1: Outline of State of the Art references**

Zhou and Xi (2002) developed a new analytical method for predicting the surface roughness of a grinded work piece for a variety of different grinding conditions. This was accomplished by applying the stochastic distribution model of grain protrusion heights to kinematic analyses. The surface texture of the grinding wheel was measured using a contact stylus, and the coinciding points on the trajectories of multiple grains were sorted consecutively from highest to lowest. This model of the grinding wheel surface texture was regressed with grinding performance data and the number of active cutting edges to predict the surface roughness of a work piece after grinding. They found that this model of the surface texture more accurately predicted the surface roughness of a work piece than previous models. This is important to our research because it is an attempt to relate the surface texture of a grinding wheel to aspects of grinding performance.

Blunt and Ebdon (1995) characterized the surface topography of grinding wheels in terms of static cutting points and static cutting grains using three-dimensional contact profilometry techniques. The advantage of having a three-dimensional plot over a two-dimensional profile is discussed. Static cutting points and static cutting grains were quantified by producing highly magnified stereographic images of the grinding surface to

produce contour maps and cutting edges and grains were counted by hand. Blunt and Ebdon also discuss sampling strategies for the characterization of grinding wheel topographies and outline optimum sampling spacing criteria.

Butler, Blunt, See, Webster, and Stout (2002) examined the topographical change occurring on a conventional aluminum oxide wheel as it machined steel work pieces. The same three-dimensional contact profilometry techniques suggested by Blunt and Ebdon (1995) were employed. The team investigated how the grinding force, summit density, and summit curvature changed as a function of stock removal. They found that the grinding force had a brief first phase where the force steeply climbs to a maximum level, and then a prolonged phase where the force tapers off from the maximum value. The change between these two phases was found to occur when the force reached a point that deflects the machine to the point where the measured depth of cut is equal to the true depth of cut.

## ***1.4 Approach***

In this work six different aluminum carbide inside diameter grinding wheels were examined after dressing and after grinding. The surface texture of the grinding wheels was characterized by making replicas of the grinding surface and measuring them using a non-contact optical profilometry technique. The conventional surface texture parameters, a complete list of which can be found in figure 7, are calculated using Mountains software. The fractal properties of relative area and average texture depth of the surface textures are calculated using the surface metrology and fractal analysis software package

SFRAX. Scale based F-tests are performed to find the scales, if any, at which fractal properties become differentiable.

## 2. Methods

The methods used to obtain and analyze the data necessary to meet the objectives of this work are outline in the following sections. The results of the analyses are explained in full detail in the results section of this report. The subsequent flow chart shows the sequence of necessary steps to achieve the objectives, and is followed by a series of sections with a detailed description of each step.

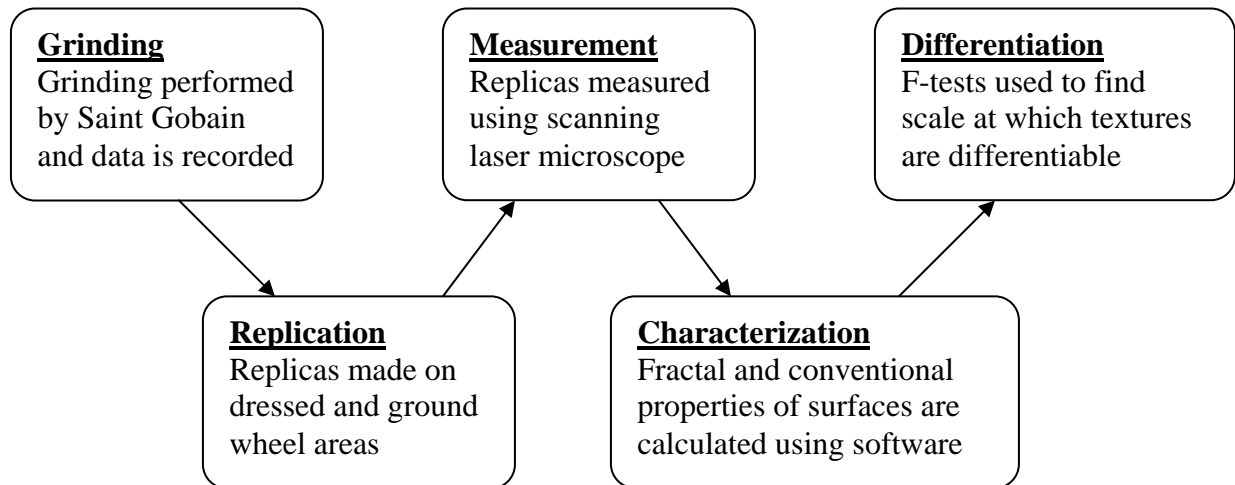


Figure 2: Flow chart of sequence of events

### 2.1 Grinding

Saint Gobain Abrasives performed dressing and grinding on a Bryant OD/ID grinder. A sample of 6 inside diameter grinding wheels was tested. The wheels had

dimensions 1.15”x 0.39” x 1.0” and a grit number of 100, and were composed of an assortment of aluminum oxide abrasives and vitrified bond types shown in the following table:

<b>Name</b>	<b>Wheel Code</b>	<b>Grade</b>	<b>Structure</b>	<b>Bond No</b>	<b>Grain No</b>
Blue 1	428.1.3	L	10	Bond2	Grain6
Blue 2	927-4	L	10	Bond2	Grain2
Blue 3	927-5	L	7	Bond3	Grain3
White 1	428.3.3	L	10	Bond2	Grain5
White 2	927-2	L	10	Bond1	Grain1
White 3	928-4.1	L	10	Bond2	Grain4

**Figure 3: Table of grinding wheels examined**

The wheels were 14 mm wide and had an initial diameter of approximately 30 mm. The wheels were brought up to 32,000 rpm, and cooled using Trim e-210 coolant diluted with 5% distilled water. The wheels were dressed using a CDP diamond roll dresser with a speed of 5,200 rpm and a dress lead of 32 mm. The wheels were used to grind a work piece 6.35 mm wide, an initial diameter of 33 mm, and a Rockwell C hardness of 61 Rc at an infeed rate of 0.06477 mm/s. Plunge grinding was conducted in climb mode and each wheel completed twenty 1.6 second runs for a cumulative grinding time of 32 seconds. Grinding power, as well as normal and tangential force, was measured using a Norton Field Instrumentation System (FIS), and recorded to an Excel spreadsheet. The change in work piece diameter was measured periodically using a bore gauge, and was used in conjunction with grinding power as well as normal and tangential force to calculate grinding performance parameters, specifically: material removal rate, specific energy, and grinding ratio. Surface roughness and waviness of the work piece were also measured periodically to further characterize grinding performance.

## 2.2 Replication

Measurements of the surface textures were made from replicas of the grinding wheels surfaces. Replication is the process of producing a mirror image of a surface by applying an impressionable material to a surface, allowing it to set and then separating it from the surface. The downside of using replicas is that they are not a direct measurement of the grind wheel surface, which means that surface texture information is either not captured by the replica material or information is sheared from the replica material when removed from the surface. The latter of which is illustrated in the following image:

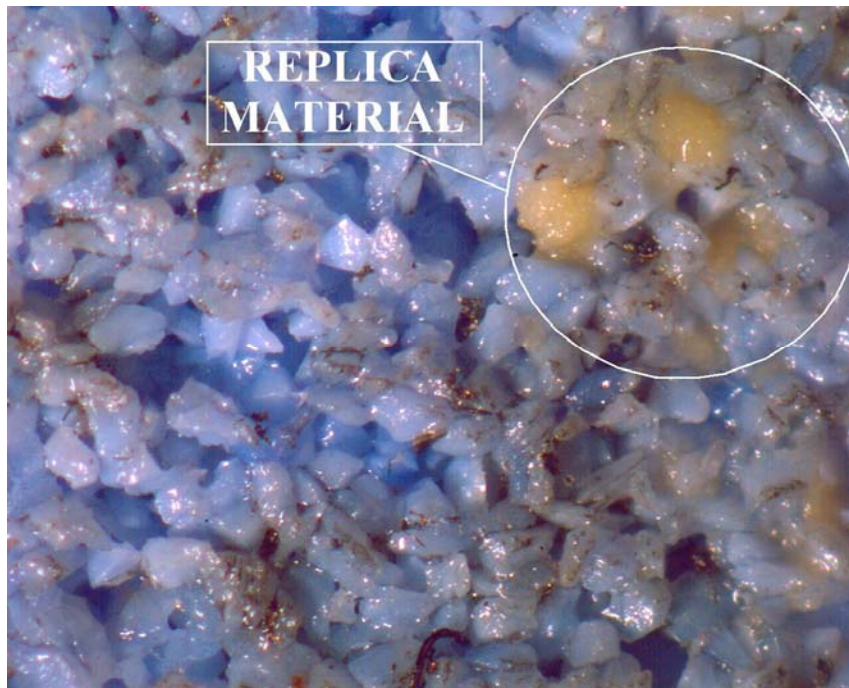


**Figure 4: Replica material left on grinding surface**

Attempts to measure the grinding surface of grinding wheels directly using optical techniques proved unsuccessful due to inherent properties of bonded abrasives. The fact that some grains are more transparent than others makes it difficult for the light source to

find the top of the grain. High reflectivity of the grain also poses a problem by saturating the measurement equipment with light. Also, measurement equipment cannot easily transition from focusing on bond to focusing on grain. Using replicas removes all of these problems by providing an opaque, non-reflective image of the grinding surface that is made out of consistent material.

Replicas were prepared using Coltène President, a polyvinylsiloxane base and catalyst system generally used to make dental molds, which is commercially available from Coltène-Whaledent. The area on the wheel for replication was prepared by holding the wheel steady in a custom made fixture and applying a size 10 washer to the top of the wheel using scotch tape. A small amount of base material and catalyst, less than a gram of each, were mixed together at a one to one ratio. The replica material was then placed in the center of the washer and held under a 200g weight for a total time of 10 minutes.

In order to determine the quality of the replicas taken a number of tests were performed. The first test was performed as the replica was removed from the wheel. The ease with which the replica was removed from the grinding surface, the amount of material left behind on the grinding surface, and the apparent texture transferred to the replica material were noted. If any of these seemed to be irregular that replica was discarded and another was taken.

The second test was performed after all replicas had been made. Each wheel was placed under a high-resolution camera and highly magnified. The wheels were then visually inspected for replica material left behind on the grinding surface. If this amount was small then it was an indication that the texture transferred to the replica material was not greatly altered when the replica was removed. High-resolution images were also

taken of the replicas, and were visually compared to the images taken of the grinding wheel surface. If the two images resembled each other it was an indication that the replica closely approximated the grinding surface.

### **2.3 Measurement**

Initially a Micromasure made by Microphotonics, located at Saint Gobain Abrasives in Worcester MA, was used in an attempt to measure the surface texture of the grinding wheels directly. This method was abandoned for two reasons. The primary reason was that after completing a test to measure the noise recorded by the system it was deemed too high to obtain an accurate measurement at the desired scale of 10 microns. The results of this noise test are discussed in detail in the results section. The second reason was that the intensity of the light generated by the xenon bulb in the equipment was too great to measure the reflective grinding surface. For these reasons the measurements were made using replicas, and measured using the UBM scanning laser microscope located at Worcester Polytechnic Institute in Worcester MA.

Replicas were measured using a UBM scanning laser microscope, located in the surface metrology lab at Worcester Polytechnic Institute. The UBM uses a Keyence LC-2210 confocal point sensor, which reflects a laser light source off of a surface and through a detector pinhole to determine height information. The laser beam is shown through an objective lens that rapidly oscillates on a vertical axis. When the surface being measured crosses the focus of the lens the light intensity reaches its maximum value. Conversely, when the distance between the surface and the lens is greater than or less than the radius of curvature of the lens the reflected light reaching the pinhole is faint

and is not detected. Therefore a height measurement is only recorded when the maximum intensity of light goes through the pinhole. This process is illustrated in the following picture:

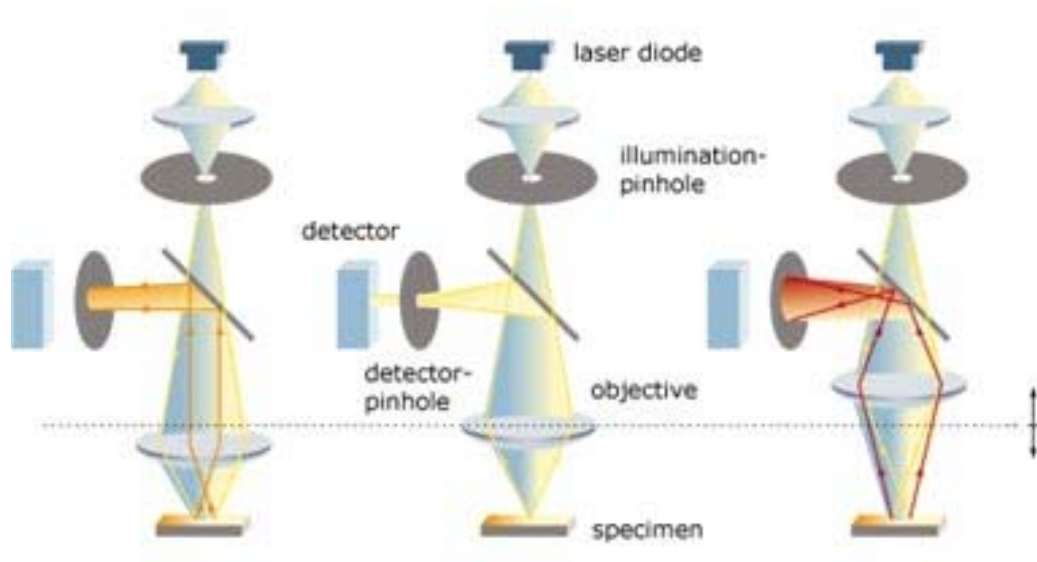


Image from <http://www.solarius-inc.com/html/confocal.html>

**Figure 5: Measurement principal of a confocal point sensor**

A test was performed on the UBM equipment to measure the internal and external noise experienced by the system while a measurement is being made. Because the measurements being made are on the order of microns, very small ambient vibrations and vibrations from the equipments motors could skew the final outcome of the measurements. Noise testing was performed by attached a 90 degree bracket to the height sensor in a manner that would allow a stationary point on the bracket to be measured. Arbitrary parameters were entered in the UBM software, and the equipment was left to run for several minutes. Therefore, any height data recorded by the UBM during this procedure was purely from noise affecting the system. This data was then

analyzed and the amount of noise was found to be negligible. The results of the noise test are discussed in further detail in the results section.

Measurement of the replicas was performed in batches. Each batch was first arranged in a systematic pattern that would easily allow files to be associated with their correct surface texture afterwards. Once on the table of the replicas were held in place using magnets. Then a check was made to confirm that the replica was situated near the center of the range of the height sensor by moving the height sensor and noting its uppermost and lowermost limits. Once the replicas were in the range of the sensor, the table was moved to align the upper left hand corner of each measurement area with the laser and the UBM software recorded the positions. The UBM was then able to begin measuring the replicas. The following table shows the parameters used for measurement:

	<b>Parameter</b>	<b>Value</b>
<b>Area</b>	Length Ground/Dressed	2.54 mm/2.0 mm
	Width Ground/Dressed	2.54 mm/2.0 mm
	Vertical Range	30 mm
	Step Size	10 $\mu$ m
<b>Light Source</b>	Wavelength	780 nm
	Spot Diameter min/max	70-90 $\mu$ m
	Pulse Width	12.5 $\mu$ m
	Power	3 mW
<b>Data Acquisition</b>	Sampling Rate	40 KHz
	Response Frequency	16 KHz
	Response Time	100 $\mu$ s
	Averaging	128 pts
	Measurement Rate	100 pixel/s
	Table Speed	1 mm/s

**Figure 6: Table of Measurement Parameters**

When the UBM finished measuring, the data files were renamed to correspond with their respective replica and saved in a .UB3 file format. The data was then manipulated by leveling it using the UBM software. This was done by performing a linear regression to remove any inherent slope or form from the measurement.

The data was then transferred into MountainsMap software to calculate the conventional parameters, which will be discussed in detail later in the methods. After the conventional parameters were calculated the format of the files was changed to .SUR to be compatible with the software used to calculate the fractal properties of the surface, which will be discussed later in the methods. The values obtained for the conventional parameters are discussed in detail in the results section.

To ensure that the UBM was in fact generating a clear portrayal of the textures captured by the replicas a test was performed to judge the equipments ability to reproduce a result. This was done simply by measuring a batch of replicas using the method previously outlined and then, without moving or reorienting any of the replicas, remeasuring the batch under the same conditions. Each surface was then compared to its counterpart from the other trial by using a height-height diagram. A height-height diagram works by plotting the height of every x-y position of one surface versus another surface. The closer the surfaces are the being the same the closer the points on the plot should align along the line  $y = x$ . The results of this test are discussed in detail in the results section.

## 2.5 Characterization

The surface files were characterized using two different methods. The following displays the list of conventional surface parameters that were calculated for every surface file using MountainsMap software:

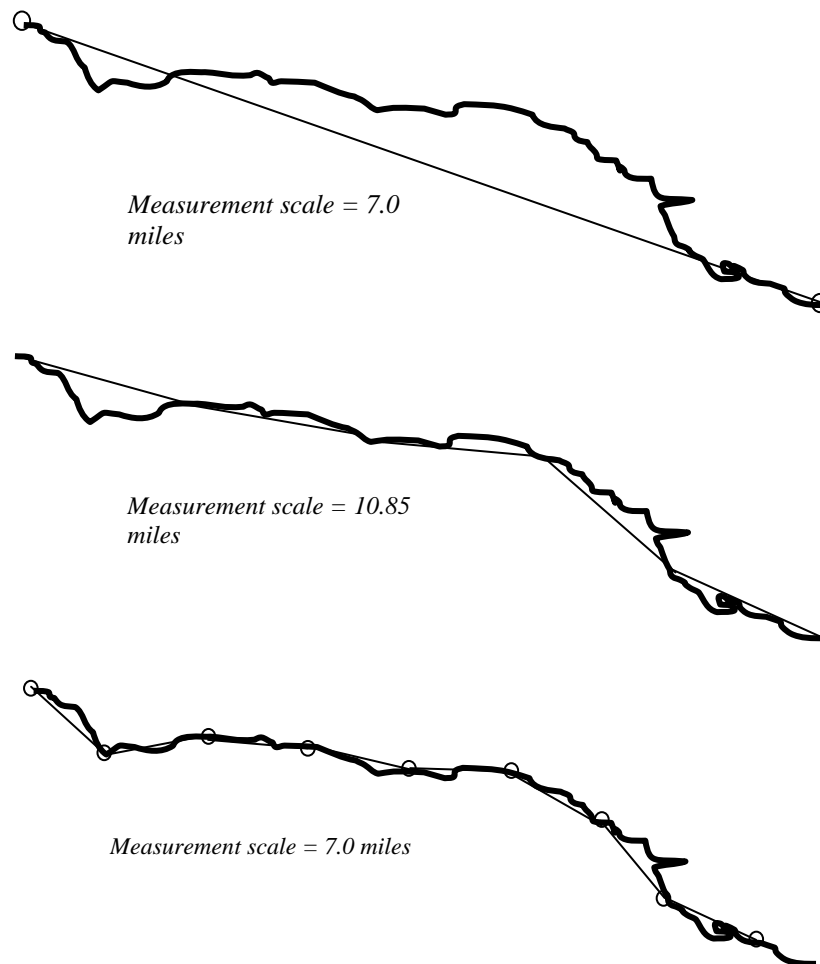
Symbol	Description	Definition (ASME B46)
<b>Sa</b>	<b>Average Roughness</b>	$S_a = \frac{1}{MN} \sum_{k=0}^{M-1} \sum_{l=0}^{N-1}  z(x_k, y_l) - \mu ^\dagger$
<b>Sq</b>	<b>Root Mean Squared (RMS) Roughness</b>	$S_q = \sqrt{\frac{1}{MN} \sum_{k=0}^{M-1} \sum_{l=0}^{N-1} [z(x_k, y_l) - \mu]^2}^\dagger$
<b>Sp</b>	<b>Maximum Peak Height</b>	$S_p = Z_{max}^\dagger$
<b>Sv</b>	<b>Maximum Valley Depth</b>	$S_p = Z_{min}^\dagger$
<b>St</b>	<b>Maximum Peak to Valley Distance</b>	$S_t = Z_{max} - Z_{min}^\dagger$
<b>Ssk</b>	<b>Surface Skewness</b>	$S_{sk} = \frac{1}{MNS_q^3} \sum_{k=0}^{M-1} \sum_{l=0}^{N-1} [(z(x_k, y_l) - \mu)]^{3\dagger}$
<b>Sku</b>	<b>Surface Kurtosis</b>	$S_{ku} = \frac{1}{MNS_q^4} \sum_{k=0}^{M-1} \sum_{l=0}^{N-1} [z(x_k, y_l) - \mu]^4^\dagger$
<b>Sz</b>	<b>Ten Point Height</b>	$S_z = \frac{\sum_{i=1}^5 (z_{pi} - \mu) + \sum_{i=1}^5 (z_{vi} - \mu)}{5}^\dagger$
<b>Pa</b>	<b>Unfiltered Average Roughness</b>	$Pa = \frac{1}{lb} \int_{lb} z(x) dx^*$
<b>Pq</b>	<b>Unfiltered RMS Roughness</b>	$Pq = \sqrt{\frac{1}{lb} \int_{lb} z^2(x) dx}^*$

† - Equation from [http://www.imagemet.com/WebHelp/spip.htm#roughness\\_parameters.htm](http://www.imagemet.com/WebHelp/spip.htm#roughness_parameters.htm)

\* - Equation from <http://www.digitalsurf.fr/en/guideparam2D.htm>

**Figure 7: Table of Conventional Parameters**

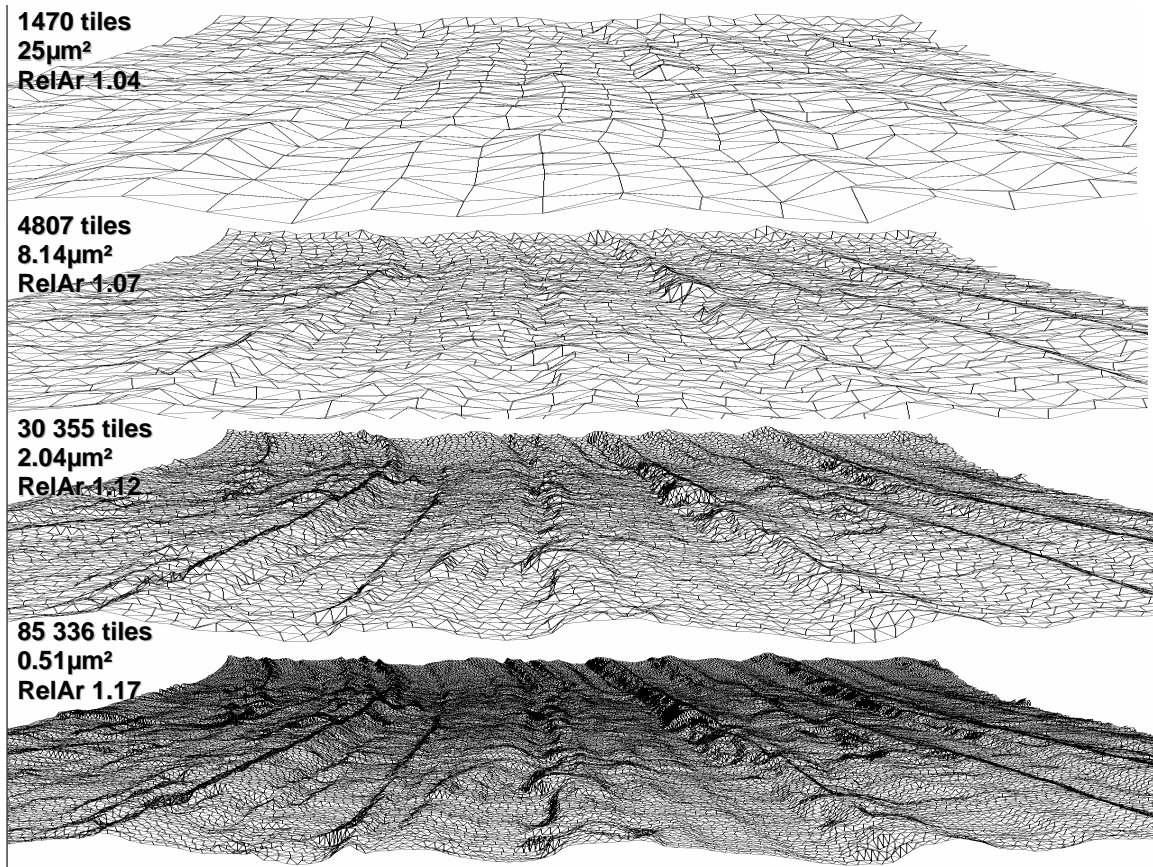
The second method used to characterize the surface textures was scale sensitive fractal analysis. This method can be used to analyze linear profiles, surface area, and surface depth and volume, denoted length-scale, area-scale, and filling scale respectively. Length-scale can be described by asking the question, how long is the coast of California? One might first draw a line from the northern most point to the southern most point tip of the coastline, but this only accounts for one scale of observation. By breaking that line into progressively smaller segments of equal length more and more detail of the bays and coves come into view. As illustrated in the following figure:



From [Recent Developments in Surface Metrology Using Fractal Analysis](#) by Christopher A. Brown, Slide 17.

**Figure 8: Length-Scale Illustration**

Similarly, area-scale analysis is used to find the area of surface at progressively smaller scales. The apparent area is calculated by covering the surface with a patchwork of triangular tiles with progressively smaller areas, which is illustrated in the following figure:



From Recent Developments in Surface Metrology Using Fractal Analysis by Christopher A. Brown, Slide 94.

**Figure 9: Area-Scale Illustration**

The relative area at a particular scale is then calculated as the measured area (area of a single tile multiplied by the total number of tiles) divided by the nominal area (area of the x-y plane). Filling-scale analysis is performed in a similar fashion by replacing the triangular patches with rectangular prisms and adding their volumes together.

Fractal analysis of the surface textures was performed using SFRAX software. Once a surface file was loaded into the software alterations were performed on the data. First the data had to be inverted to account for the negative image of the grinding wheel surface produced by replication. Second the data was distorted by a factor of 9.95 to correct a calibration error inherent to the UBM measurement equipment.

Area-Scale analysis was performed to calculate the relative area of the surface texture of each replica measurement across a range of scales, using the four corners full overlap method. The area-scale curves produced were then grouped together by the wheel used to produce the replicas. As was stated previously 6 wheels of distinct bond-grain composition were measured 12 times each, 6 on the ground region and 6 on the dressed region, producing 72 unique area-scale curves.

Filling-Scale analysis was performed to calculate to average texture depth of the surface texture of each replica measurement across a range of scales, using the Volume Absolute analysis method. The filling-scale curves produced were then grouped together by the wheel used to produce the replicas. As was stated previously 6 wheels of distinct bond-grain composition were measured 12 times each, 6 on the ground region and 6 on the dressed region, producing 72 unique filling-scale curves.

## ***2.5 Differentiation***

Differentiation of the surface textures was done by performing F-tests. An F-test is a statistical method for comparing the difference in the standard deviation of 2 sets of data. Differentiation was performed for every conventional parameter listed in section 2.5, as well as for relative area and average texture depth.



### 3. Results

#### 3.1 Grinding

After grinding was performed on each of these wheels there were clear differences on the surface of the wheel. The width of the work piece was smaller than the width of the grinding wheel, so the dressed section was able to be visually distinguished from the ground section. The following picture shows the differences between the ground and dressed regions of the wheel.

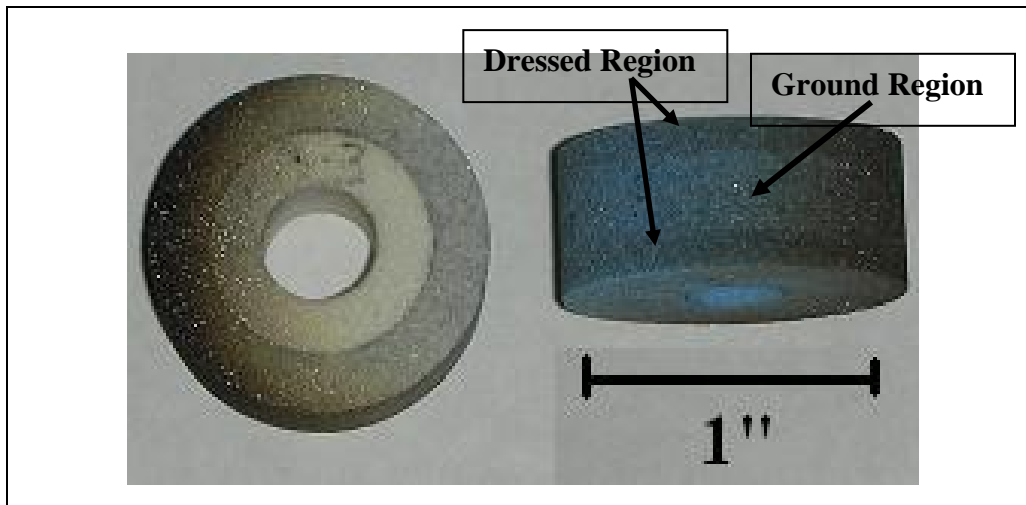


**Figure 11: Regions of the grinding surface**

The grinding performance of the wheel is generally gauged by plotting the cumulative material removed as a function of the power consumed by the grinder. The greater the slope of the resulting line the more material it can remove while consuming less power. Below are the performance graphs for each of the wheels examined.

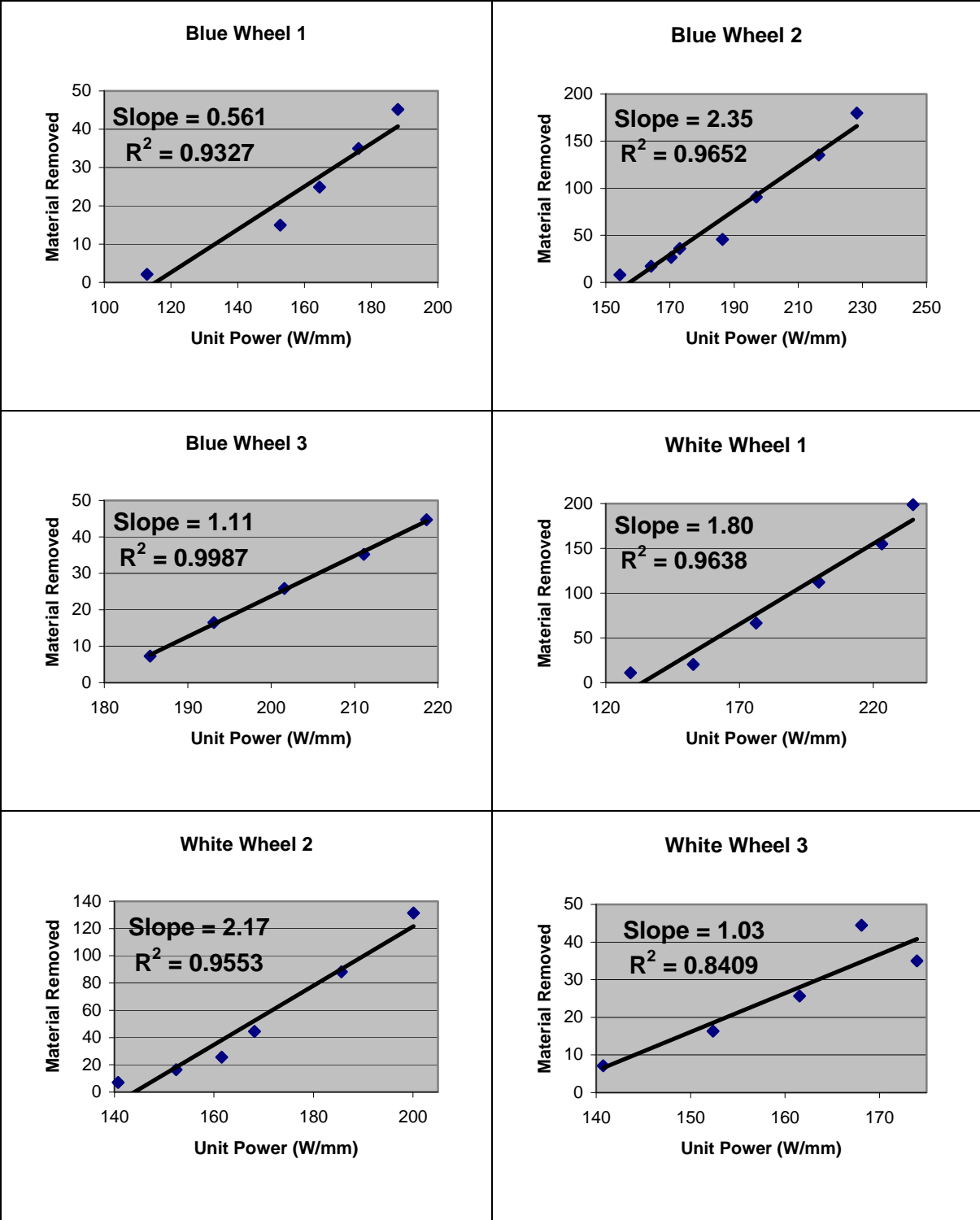


Figure 12: Performance graphs

These graphs clearly indicate that there is a large amount of variance in the performance of these wheels, which means there should be noticeable differences in each of the wheels surface textures.

The performance graphs were all measured in metric units. The Power was measured in W/mm and Cumulative Material Removed measured in  $\text{mm}^3/\text{mm}$ . Some points were interpreted as outliers if their deviation from the average was more than twice the standard deviation and were removed from the graphs. These points are most likely measurement artifacts as the result of equipment error. These points generally occurred at the very beginning or very end of the tests. The data used to create these plots along with other performance data generated from the tests can be found in the appendix.

### **3.2 Replication**

Below are highly magnified images of a grinding wheel surface and its corresponding replica surface.

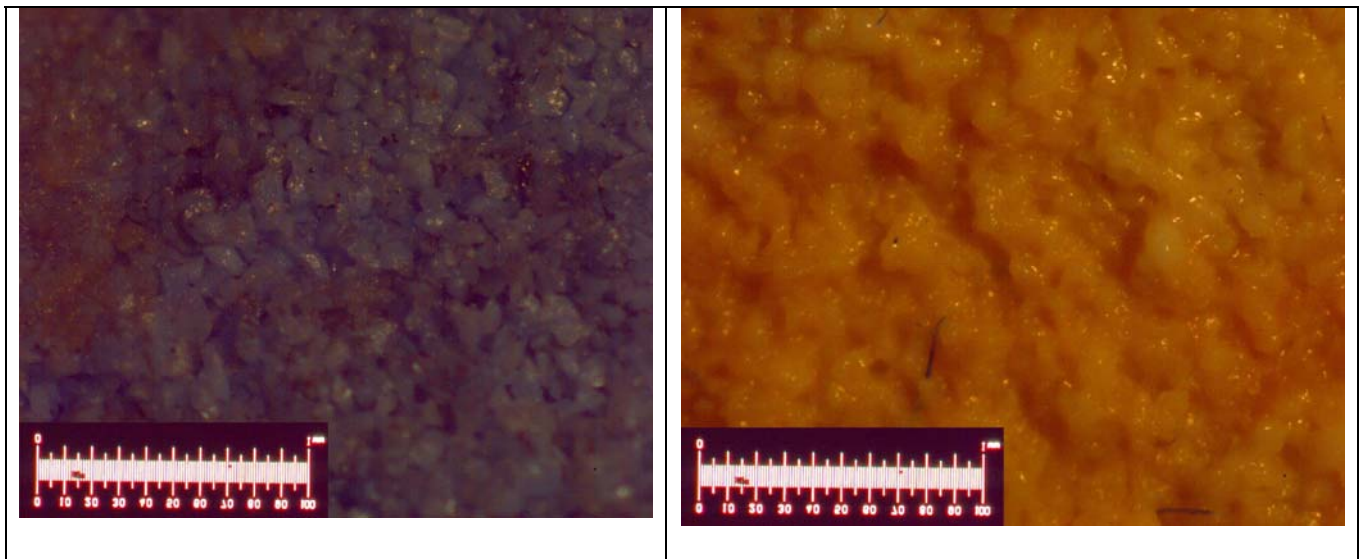


**Figure 13: Replica quality inspection**

The wheels were then visually inspected for replica material left behind on the grinding surface. As can be seen in Figure 13 the amount of replica material left on the grinding surface is minimal, which is a good indication that the texture transferred to the grinding surface is minimal, which is a good indication that the texture transferred to the replica material was not greatly altered when the replica was removed.

A visual inspection of the similarity in surface texture was also performed. It can be seen in Figure 13 that the texture transferred to the replica material closely approximates the texture of the grinding surface. Since the two images resemble each other it is a good indication that the replica is an accurate approximation the grinding surface.

### 3.3 Measurement

Figure 14 shows a comparison of the noise inherent to the Micromasure located at Saint Gobain Abrasives and the UBM located at Worcester Polytechnic Institute.

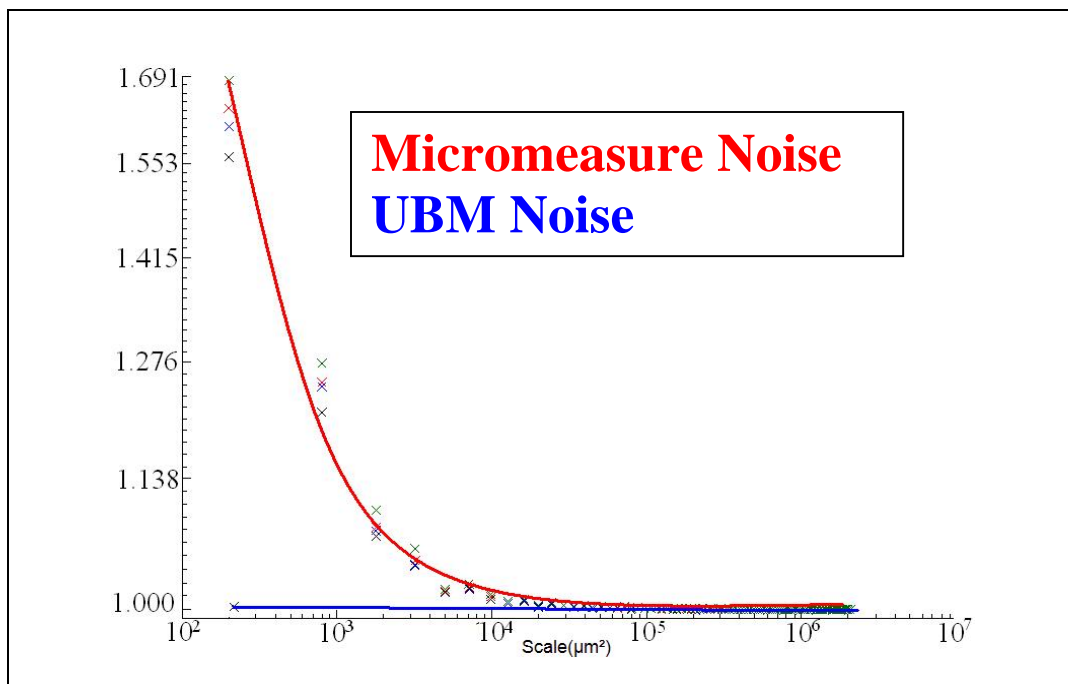
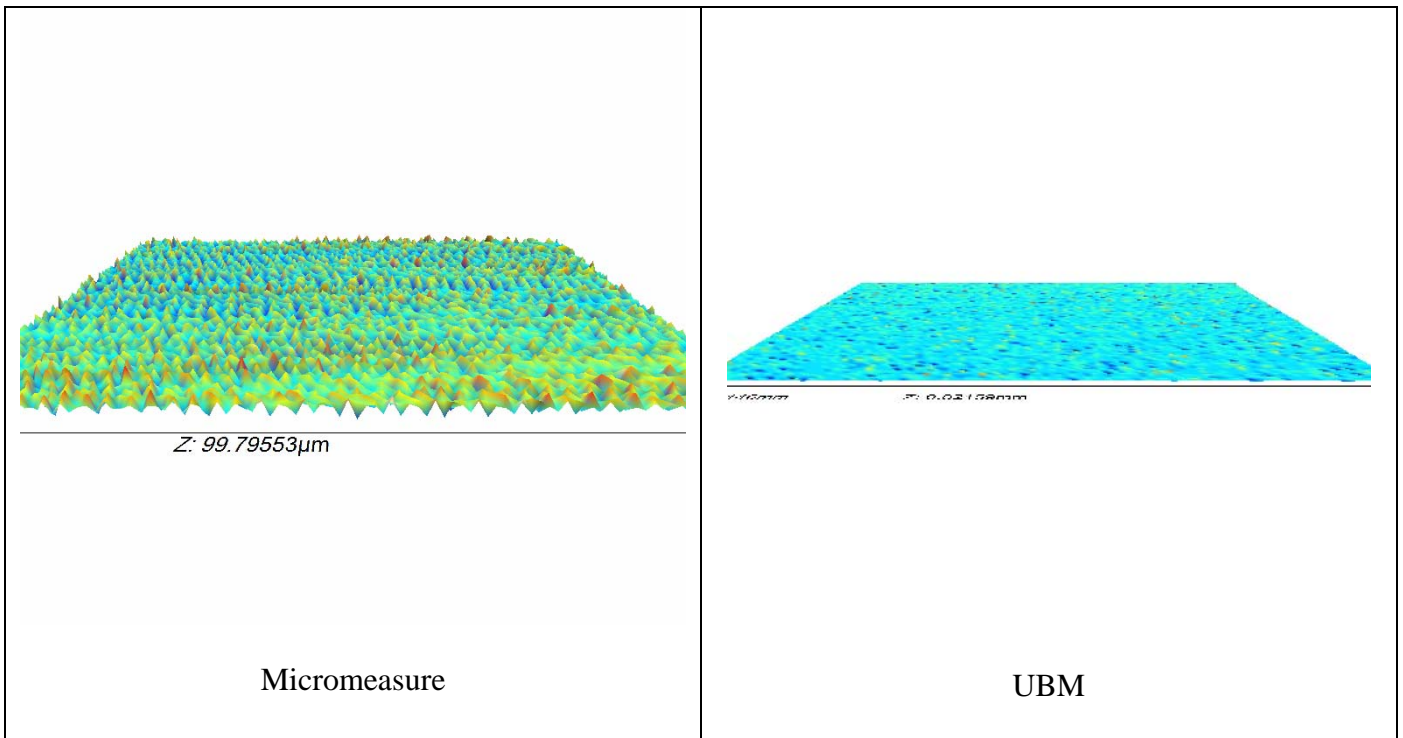


Figure 14: Noise Comparison

The noise tests run on the Micromesure and UBM scanning laser microscope were analyzed in SFRAX. Figure 14 is the result of area-scale analysis that was run on the surface files created by the noise tests, and shows the relative area as a function of scale. Ideally these plots should show a horizontal line at a relative area of 1.00 at all scales, which would be a perfectly flat surface. From these plots it is clearly shown that at the scale of  $200\mu\text{m}^2$  the Micromesure is measuring a high level of noise whereas the UBM is not. The Micromesure measures a high level of noise because it set directly on a table with no means of damping ambient vibrations. The following pictures show three-dimensional representations to further characterize the noise collected during the noise tests.



**Figure 15: Three-dimensional representations of noise test results**

Figure 16 shows the height-height plot used to determine the repeatability of the measurements using the UBM scanning laser microscope.

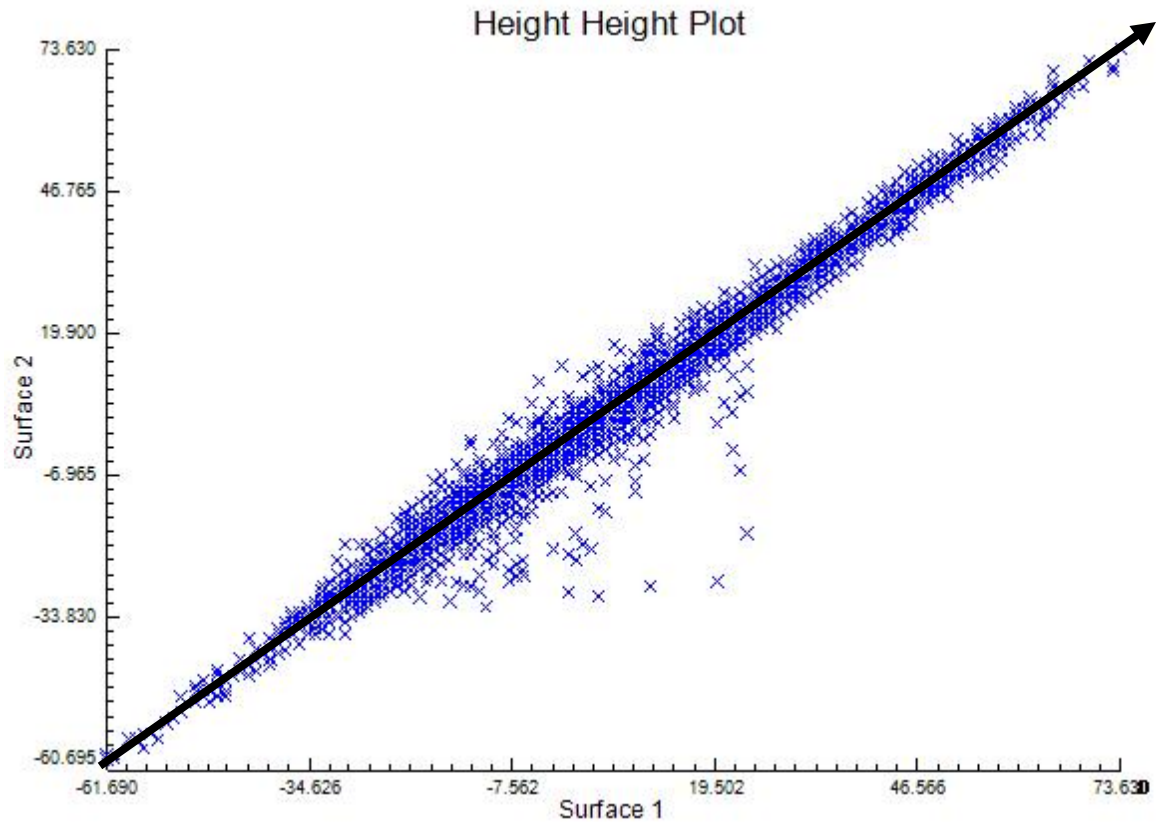


**Figure 16: Height-Height plot of repeatability tests**

While measuring the replicas, it was important to know that the results could be repeated, which was accomplished by measuring the same surface twice and creating a height-height diagram. A height-height diagram works by plotting the height of every x-y position of one surface versus another surface. The closer the surfaces are to being the same the closer the points on the plot should align along the line  $y = x$ . Since the data in Figure 16 follows the form of the equation  $y = x$  it shows that the UBM is accurately measuring the surface of the replicas. Because the points on this graph are not random, this test also shows a low level of noise in the UBM equipment.

### 3.4 Characterization

Figure 17 displays the calculated average and standard deviation of every conventional parameter listed in Figure 7 broken down by wheel and region.

	B1D		B2D		B3D		B1U		B2U		B3U	
Symbol	Avg	S. D.										
<b>Sa</b>	2.22	0.18	1.60	0.12	1.19	0.18	2.48	0.39	2.05	0.18	1.94	0.27
<b>Sq</b>	2.81	0.22	2.01	0.14	1.52	0.22	3.16	0.56	2.63	0.21	2.41	0.33
<b>Sp</b>	7.25	1.00	5.77	0.62	4.38	0.38	8.40	1.13	6.95	0.93	6.38	0.49
<b>Sv</b>	12.13	1.32	7.75	1.05	6.48	1.42	13.87	2.95	12.25	2.26	9.82	2.52
<b>St</b>	19.38	1.83	13.52	1.38	10.87	1.71	22.27	3.29	19.20	2.18	16.20	2.91
<b>Ssk</b>	-0.58	0.21	-0.41	0.16	-0.48	0.27	-0.57	0.37	-0.68	0.34	-0.45	0.23
<b>Sku</b>	3.49	0.20	3.12	0.33	3.51	0.68	3.68	0.86	3.84	0.90	3.11	0.45
<b>Sz</b>	14.73	1.16	10.44	1.64	8.36	0.86	15.43	2.00	13.35	2.07	11.38	2.12
<b>Pa</b>	1.98	0.09	1.45	0.10	1.06	0.15	2.01	0.46	1.70	0.26	1.49	0.14
<b>Pq</b>	2.45	0.11	1.80	0.12	1.33	0.17	2.48	0.58	2.13	0.32	1.86	0.18

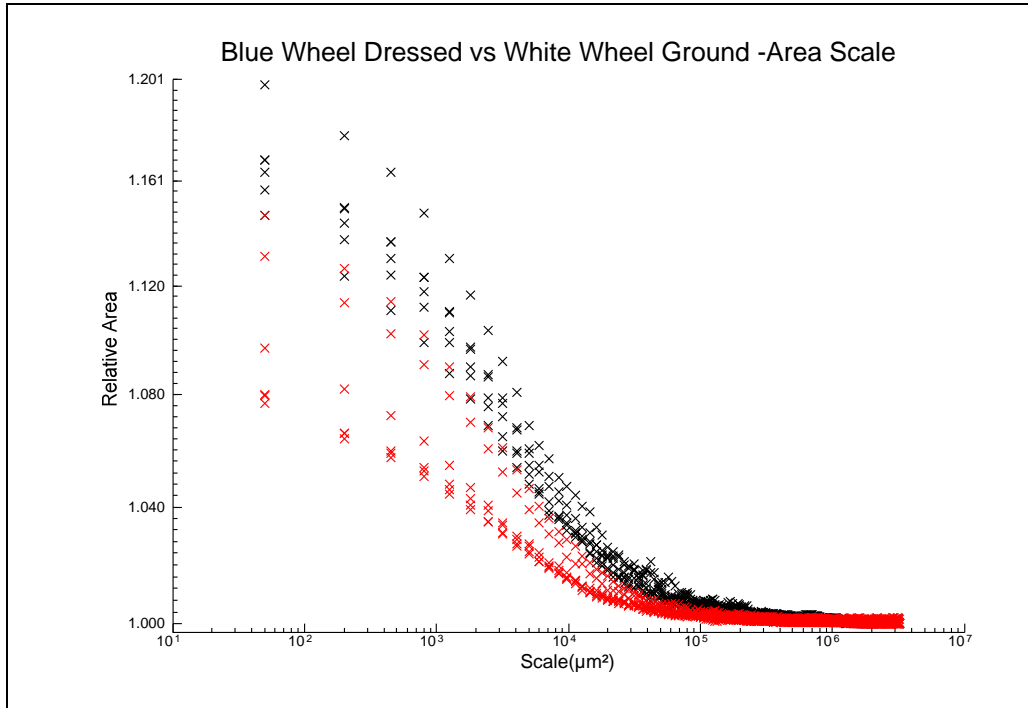
  

	W1D		W2D		W3D		W1U		W2U		W3U	
Symbol	Avg	S. D.										
<b>Sa</b>	2.17	0.25	1.36	0.25	1.49	0.14	2.58	0.15	1.82	0.37	1.97	0.17
<b>Sq</b>	2.74	0.32	1.72	0.31	1.88	0.15	3.24	0.20	2.28	0.46	2.44	0.22
<b>Sp</b>	7.48	0.84	5.32	0.66	6.28	1.11	8.55	0.55	6.27	0.71	6.60	0.88
<b>Sv</b>	12.62	3.53	6.90	1.49	7.43	1.16	15.00	3.52	9.03	2.43	9.80	1.60
<b>St</b>	20.10	4.08	12.22	1.63	13.62	1.47	23.55	3.85	15.30	2.80	16.40	2.06
<b>Ssk</b>	-0.57	0.14	-0.42	0.19	-0.32	0.24	-0.59	0.24	-0.39	0.34	-0.45	0.21
<b>Sku</b>	3.55	0.46	3.23	0.24	3.31	0.53	3.59	0.79	3.11	0.15	2.96	0.33
<b>Sz</b>	13.69	2.56	9.31	1.00	9.55	1.00	17.48	1.88	10.58	1.88	11.17	0.58
<b>Pa</b>	1.93	0.22	1.24	0.24	1.34	0.09	2.08	0.11	1.36	0.13	1.47	0.15
<b>Pq</b>	2.41	0.28	1.54	0.28	1.68	0.10	2.60	0.17	1.69	0.15	1.82	0.18

Figure 17: Table of conventional parameter results

These results are used for the purpose of differentiating surface textures, the result of which will be discussed later in the differentiation section of the results.

Figure 18 is an example of the area-scale curves of two distinct regions plotted on the same graph. Each region is designated by a different color red or black.



**Figure 18: Comparison of area-scale curves**

This graph shows that there is a clear difference in the relative area of the two regions. This implies that the regions will be differentiable. The complete set of area-scale comparisons can be found in the appendix.

Along with area-scale analysis, filling scale analysis was also run on the measurements. Figure 19 shows a graph comparing the filling-scale curves of two distinct regions.

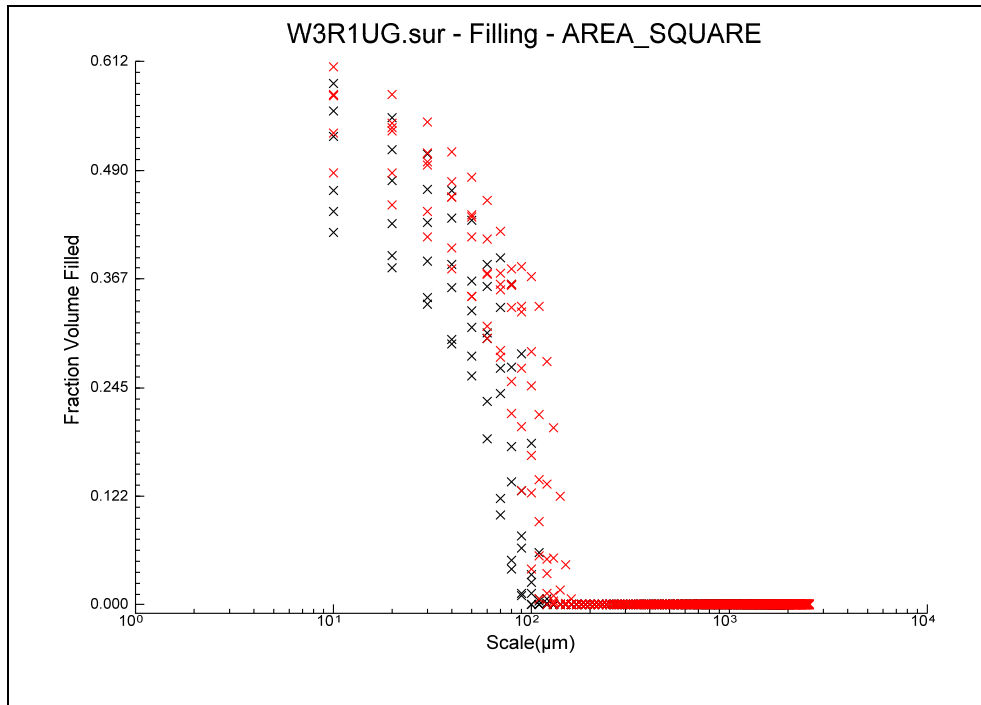


**Figure 19: Comparison of filling-scale curves**

This plot shows less distinction between the two data sets, which indicates that the regions will be harder to differentiate based on filling-scale analysis. The complete set of filling-scale comparisons can be found in the appendix.

### 3.5 Differentiation

The following figures (20-29) show the results of differentiation by conventional parameters.

<b>Sa</b>		<b>5% Differentiability</b>											
B1D	B1D												
B2D	0.339	B2D											
B3D	0.919	0.391	B3D										
B1U	0.132	0.020	0.111	B1U									
B2U	0.947	0.372	0.973	0.117	B2U								
B3U	0.406	0.085	0.353	0.473	0.370	B3U							
W1D	0.525	0.122	0.463	0.361	0.484	0.840	W1D						
W2D	0.514	0.118	0.452	0.370	0.473	0.854	0.986	W2D					
W3D	0.554	0.708	0.623	0.044	0.599	0.165	0.228	0.222	W3D				
W1U	0.620	0.637	0.692	0.053	0.667	0.193	0.266	0.258	0.922	W1U			
W2U	0.151	0.024	0.127	0.938	0.135	0.521	0.402	0.412	0.051	0.061	W2U		
W3U	0.859	0.432	0.939	0.096	0.912	0.317	0.419	0.409	0.677	0.749	0.111	W3U	

Figure 20: Sa differentiation matrix

<b>Sq</b>		<b>9% Differentiability</b>											
B1D	B1D												
B2D	0.340	B2D											
B3D	0.992	0.335	B3D										
B1U	0.067	0.009	0.069	B1U									
B2U	0.862	0.431	0.854	0.048	B2U								
B3U	0.410	0.086	0.416	0.280	0.322	B3U							
W1D	0.433	0.093	0.439	0.263	0.342	0.967	W1D						
W2D	0.498	0.113	0.504	0.222	0.397	0.881	0.913	W2D					
W3D	0.371	0.950	0.366	0.011	0.467	0.097	0.104	0.127	W3D				
W1U	0.851	0.440	0.843	0.047	0.988	0.315	0.335	0.389	0.476	W1U			
W2U	0.143	0.023	0.146	0.677	0.106	0.497	0.472	0.409	0.026	0.103	W2U		
W3U	0.996	0.343	0.987	0.067	0.867	0.407	0.430	0.494	0.374	0.855	0.142	W3U	

Figure 21: Sq differentiation matrix

<b>Sp</b>		<b>3% Differentiability</b>											
B1D	B1D												
B2D	0.315	B2D											
B3D	0.055	0.318	B3D										
B1U	0.781	0.205	0.032	B1U									
B2U	0.879	0.390	0.074	0.668	B2U								
B3U	0.148	0.634	0.592	0.090	0.190	B3U							
W1D	0.723	0.507	0.107	0.529	0.839	0.262	W1D						
W2D	0.380	0.893	0.260	0.253	0.465	0.543	0.595	W2D					
W3D	0.821	0.223	0.036	0.958	0.706	0.099	0.563	0.275	W3D				
W1U	0.224	0.824	0.433	0.142	0.283	0.799	0.379	0.721	0.155	W1U			
W2U	0.484	0.751	0.195	0.333	0.582	0.431	0.727	0.854	0.359	0.590	W2U		
W3U	0.791	0.453	0.091	0.588	0.910	0.228	0.929	0.536	0.624	0.334	0.661	W3U	

Figure 22: Sp differentiation matrix

<b>Sv</b>		<b>9% Differentiability</b>											
B1D	B1D												
B2D	0.626	B2D											
B3D	0.876	0.522	B3D										
B1U	0.102	0.040	0.134	B1U									
B2U	0.263	0.118	0.331	0.572	B2U								
B3U	0.183	0.077	0.235	0.736	0.818	B3U							
W1D	0.050	0.019	0.068	0.707	0.352	0.479	W1D						
W2D	0.797	0.460	0.919	0.160	0.382	0.274	0.082	W2D					
W3D	0.787	0.827	0.671	0.062	0.171	0.115	0.030	0.600	W3D				
W1U	0.051	0.019	0.068	0.709	0.353	0.480	0.998	0.083	0.030	W1U			
W2U	0.208	0.090	0.265	0.678	0.880	0.938	0.433	0.308	0.132	0.434	W2U		
W3U	0.684	0.376	0.801	0.205	0.467	0.342	0.108	0.880	0.501	0.109	0.382	W3U	

Figure 23: Sv differentiation matrix

<b>St</b>		<b>5% Differentiability</b>											
B1D	B1D												
B2D	0.551	B2D											
B3D	0.884	0.651	B3D										
B1U	0.223	0.079	0.176	B1U									
B2U	0.705	0.335	0.602	0.390	B2U								
B3U	0.331	0.127	0.267	0.794	0.545	B3U							
W1D	0.102	0.032	0.078	0.647	0.196	0.474	W1D						
W2D	0.806	0.724	0.921	0.149	0.535	0.229	0.065	W2D					
W3D	0.643	0.893	0.749	0.101	0.404	0.160	0.042	0.826	W3D				
W1U	0.128	0.042	0.099	0.739	0.239	0.554	0.899	0.082	0.054	W1U			
W2U	0.371	0.146	0.301	0.732	0.599	0.935	0.427	0.260	0.183	0.502	W2U		
W3U	0.799	0.398	0.689	0.328	0.902	0.467	0.160	0.618	0.475	0.197	0.518	W3U	

Figure 24: St differentiation matrix

<b>Ssk</b>		<b>0% Differentiability</b>											
B1D	B1D												
B2D	0.570	B2D											
B3D	0.593	0.278	B3D										
B1U	0.258	0.099	0.539	B1U									
B2U	0.335	0.135	0.658	0.861	B2U								
B3U	0.836	0.441	0.743	0.351	0.444	B3U							
W1D	0.393	0.770	0.175	0.057	0.080	0.293	W1D						
W2D	0.832	0.720	0.458	0.184	0.244	0.675	0.517	W2D					
W3D	0.798	0.413	0.779	0.375	0.473	0.961	0.272	0.641	W3D				
W1U	0.785	0.404	0.792	0.384	0.483	0.948	0.265	0.629	0.986	W1U			
W2U	0.334	0.135	0.657	0.863	0.998	0.443	0.080	0.243	0.471	0.482	W2U		
W3U	0.942	0.620	0.545	0.231	0.301	0.779	0.433	0.889	0.743	0.730	0.300	W3U	

Figure 25: Ssk differentiation matrix

<b>Sku</b>		<b>26% Differentiability</b>											
B1D	B1D												
B2D	0.311	B2D											
B3D	0.019	0.135	B3D										
B1U	0.006	0.053	0.612	B1U									
B2U	0.005	0.045	0.552	0.929	B2U								
B3U	0.104	0.507	0.382	0.177	0.152	B3U							
W1D	0.097	0.484	0.403	0.188	0.162	0.970	W1D						
W2D	0.716	0.508	0.039	0.014	0.011	0.195	0.183	W2D					
W3D	0.052	0.306	0.610	0.316	0.277	0.710	0.738	0.103	W3D				
W1U	0.009	0.074	0.739	0.861	0.792	0.234	0.249	0.020	0.403	W1U			
W2U	0.528	0.111	0.005	0.002	0.001	0.031	0.029	0.325	0.014	0.002	W2U		
W3U	0.291	0.964	0.146	0.058	0.049	0.536	0.511	0.480	0.327	0.080	0.102	W3U	

Figure 26: Sku differentiation matrix

<b>Sz</b>		<b>12% Differentiability</b>											
B1D	B1D												
B2D	0.462	B2D											
B3D	0.534	0.184	B3D										
B1U	0.255	0.674	0.088	B1U									
B2U	0.229	0.625	0.078	0.946	B2U								
B3U	0.210	0.586	0.070	0.901	0.955	B3U							
W1D	0.106	0.351	0.032	0.602	0.649	0.690	W1D						
W2D	0.749	0.297	0.761	0.151	0.135	0.122	0.059	W2D					
W3D	0.753	0.299	0.756	0.153	0.136	0.123	0.059	0.995	W3D				
W1U	0.309	0.770	0.112	0.896	0.843	0.799	0.516	0.188	0.190	W1U			
W2U	0.310	0.771	0.112	0.895	0.842	0.798	0.515	0.189	0.190	0.999	W2U		
W3U	0.151	0.038	0.395	0.016	0.014	0.012	0.005	0.254	0.252	0.021	0.021	W3U	

Figure 27: Sz differentiation matrix

<b>Pa (AVG)</b>	<b>15% Differentiability</b>												
B1D	B1D												
B2D	0.853	B2D											
B3D	0.317	0.411	B3D										
B1U	0.003	0.004	0.025	B1U									
B2U	0.037	0.053	0.231	0.239	B2U								
B3U	0.368	0.471	0.917	0.020	0.196	B3U							
W1D	0.072	0.101	0.382	0.137	0.734	0.330	W1D						
W2D	0.055	0.078	0.313	0.174	0.843	0.267	0.887	W2D					
W3D	0.974	0.827	0.302	0.003	0.035	0.352	0.067	0.051	W3D				
W1U	0.647	0.784	0.579	0.008	0.089	0.652	0.163	0.128	0.624	W1U			
W2U	0.441	0.556	0.811	0.015	0.157	0.893	0.270	0.217	0.423	0.751	W2U		
W3U	0.281	0.368	0.935	0.030	0.263	0.852	0.426	0.351	0.268	0.525	0.748	W3U	

Figure 28: Pa differentiation matrix

<b>Pq (AVG)</b>	<b>18% Differentiability</b>												
B1D	B1D												
B2D	0.883	B2D											
B3D	0.388	0.472	B3D										
B1U	0.003	0.004	0.018	B1U									
B2U	0.039	0.052	0.193	0.218	B2U								
B3U	0.328	0.403	0.904	0.023	0.234	B3U							
W1D	0.069	0.090	0.301	0.135	0.774	0.358	W1D						
W2D	0.066	0.087	0.293	0.140	0.788	0.349	0.985	W2D					
W3D	0.788	0.678	0.263	0.001	0.023	0.218	0.041	0.039	W3D				
W1U	0.398	0.482	0.986	0.017	0.187	0.890	0.294	0.285	0.270	W1U			
W2U	0.554	0.655	0.781	0.010	0.120	0.691	0.196	0.190	0.393	0.795	W2U		
W3U	0.355	0.434	0.948	0.020	0.214	0.955	0.331	0.322	0.238	0.935	0.732	W3U	

Figure 29: Pq differentiation matrix

The differentiation was performed using the FTEST function in Microsoft Excel. The function returned a value from 1 to 0, which can be seen in each cell of the matrices. A cell containing a number less than or equal to 0.05 was interpreted to be differentiable and is highlighted in green. The percent of surface textures that were differentiable is also shown in the upper right-hand corner of each figure. From these matrices it can be determined that kurtosis is the best conventional parameter to use for differentiation while skewedness is the worst.



Any point of the graph that lies above the horizontal bar is differentiable with 95% confidence. A differentiation matrix was filled out that shows the result of each F-test comparing all regions of all wheels, and can be seen in Figure 32.

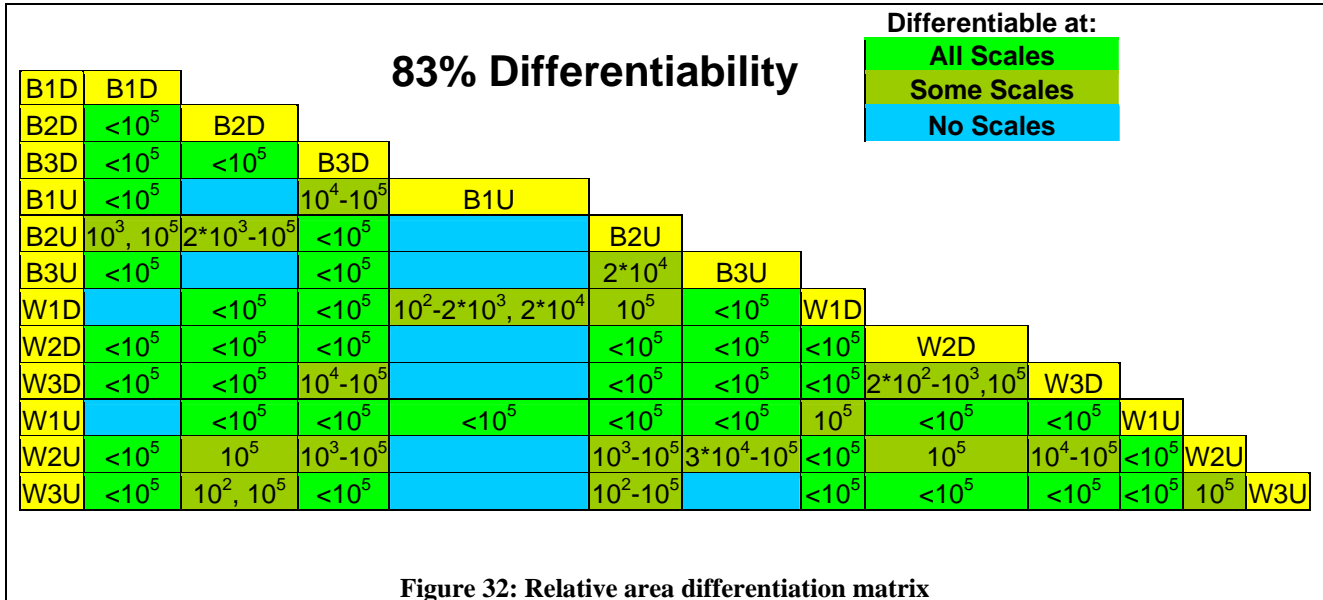


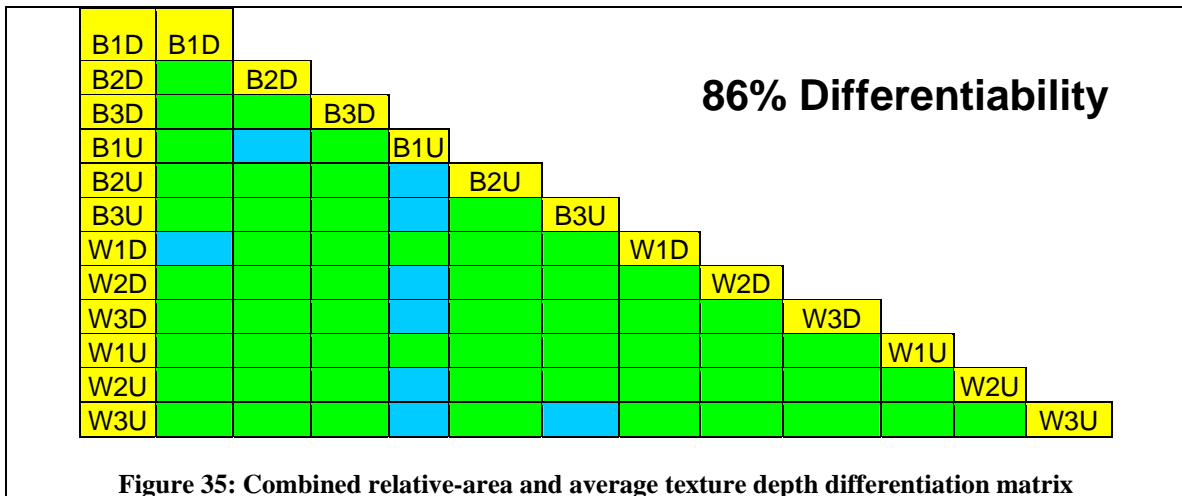
Figure 32 clearly shows that relative area is a much better way to differentiate surface textures than the best conventional parameter. Green cells represent comparisons in which the F-test produced results that were differentiable at all scales below the smooth rough crossover at 10<sup>5</sup> μm<sup>2</sup>, while dark green cells represent comparisons where the F-test produced results that were differentiable only at a particular scale or range of scales that is contained within the cell.

Figure 33 shows examples of F-tests performed on two sets of filling-scale curves showing the mean square ratio of both as a function of scale.



This matrix shows that average texture depth does not do as good a job as relative area at differentiating the surface textures. One advantage that it does have is that textures are either differentiable or they are not. The results do not change with scale like they do with the relative area F-tests. This can be advantageous in the sense that the wheels do not have to be measured at a specific scale to be differentiated using this method.

Figure 35 shows the combined differentiability of relative area and average texture depth.



This figure shows that there is some improvement in the success rate of differentiation using fractal techniques. However, many of the surface textures differentiable by average texture depth are already differentiable by relative area. Only 2 surface comparisons were added by superimposing the two matrices.

## 4. Conclusions

1. Because the performance of the grinding wheels decay in a linear fashion, sharpness of the surface texture must decay in a similar fashion.
2. The type of inside diameter grinding wheel used in this research cannot be measured directly using a chromatic white light profilometer or scanning laser microscope.
3. The replica material can be used to replicate surfaces at a scale of 10 microns, and can successfully capture features of the surface texture at this scale.
4. Fractal techniques, especially relative-area, can be used to differentiate surfaces with a much higher success rate than conventional parameters.
5. The difference in differentiability by relative area/average texture depth at different scales could be due to features on the surface that are prominent at those scales and account for the difference in grinding performance.

## 5. Discussion

Measuring a grinding wheels performance by plotting the cumulative material removed as a function of power shows a high linear correlation. This implies that the surface texture of a grinding wheel must also wear in a linear fashion, and some link must exist between the starting texture and ending texture of the wheel. In order to find this link relative area and average texture depth must be correlated with the grinding performance at differentiable scales.

Originally the approach to measuring the surface textures of the grinding wheels was to use a chromatic white light profilometer. Aside from technical difficulties and scheduling conflicts with the equipment, this equipment could not be used due to problems encountered in measuring grinding surfaces directly, which are attributed to inherent properties of bonded abrasives. One of these properties is the reflective nature of the grains, which would reflect enough light back into the equipment to saturate the reading even at the lowest intensity levels. Also, the transparency of some grains makes it difficult for the light source to find the actual surface. The grinding surfaces could not be measured directly on the UBM scanning laser microscope either due to its inability to adjust to the changes in focus caused by the light moving between bond and grain.

When it was realized that the grinding wheel surfaces were not able to be measured directly using a chromatic white light profilometer or scanning laser microscope, it was decided that replication of the surface textures of the grinding wheels was the next best option, but it was uncertain whether or not the material used to make replicas was going to be able to capture enough detail of the surface at very small scales.

It was determined retrospectively that the replicas were providing information at a scale of 10 microns by examining the relative area plots. If there were a decrease in the amount of new area covered by triangular patches as the tiling routine moved to a sequentially smaller scale, then there would be a noticeable decrease in the slope of relative-area curve at the scale this would begin to occur. Because the slopes of the relative area curves all remain increasing to the finest measurable scale it can be inferred that detail of the surface textures at these scales was captured by the replica material.

The best differentiation using conventional parameters was found using kurtosis, which produced a 26% success rate. This is in stark contrast to average texture depth, which had a 47% success rate, and relative area, which produced an 83% success rate. Even superimposing every conventional parameter matrix still only produced a 59% success rate. This can be attributed to the fact that each conventional parameter only examines one specific detail of a surface. This is like trying to differentiate waves by looking at their amplitude. Although many waves can have similar peak heights their wavelengths could vary by miles, yet by only examining the amplitude would be considered non-differentiable. Fractal techniques, however, examine all aspects of the surface texture at the same time, and consequently do not produce such high levels of erroneous results.

Another added benefit to using fractal analysis to differentiate surface texture is that the differentiation is broken down by scale. In the case of conventional parameter differentiation, surface textures are either differentiable or they are not. This is not the case with fractal parameters. Some surfaces are only differentiable at a certain scale or a range of scales. This shows that there is a specific feature or group of features at those

scales that is very different between the two surface textures. Surface features that exist at these highly differentiable scales are most likely responsible for differences in grinding performance.

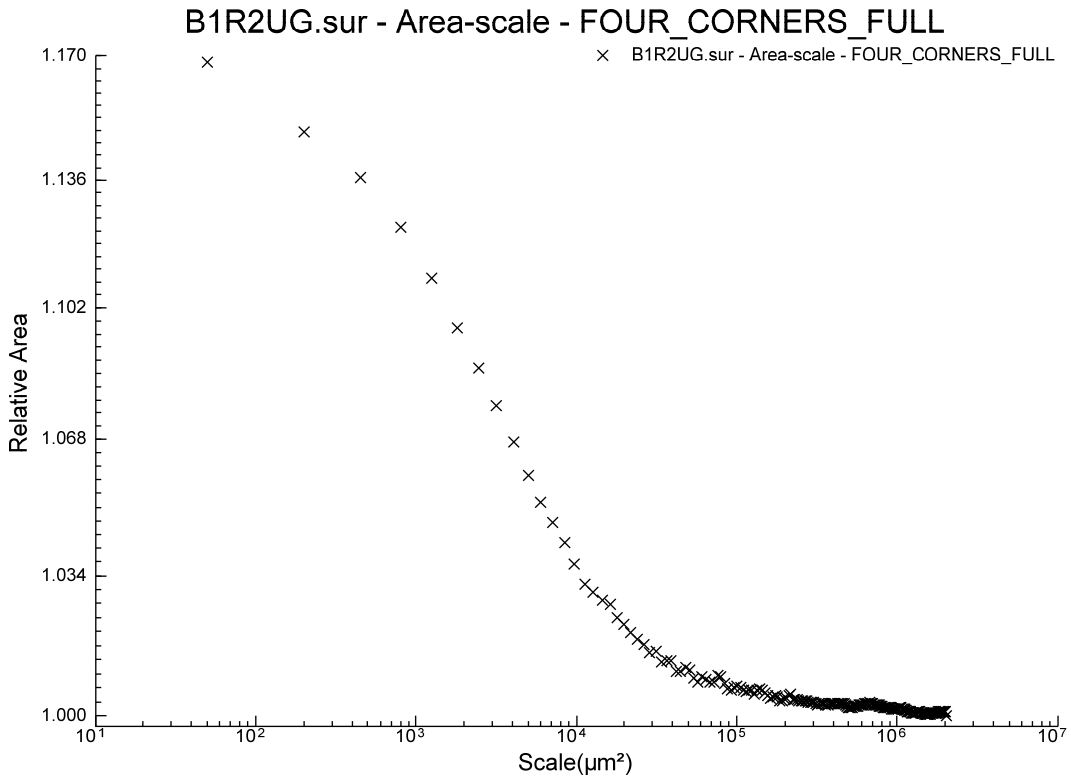
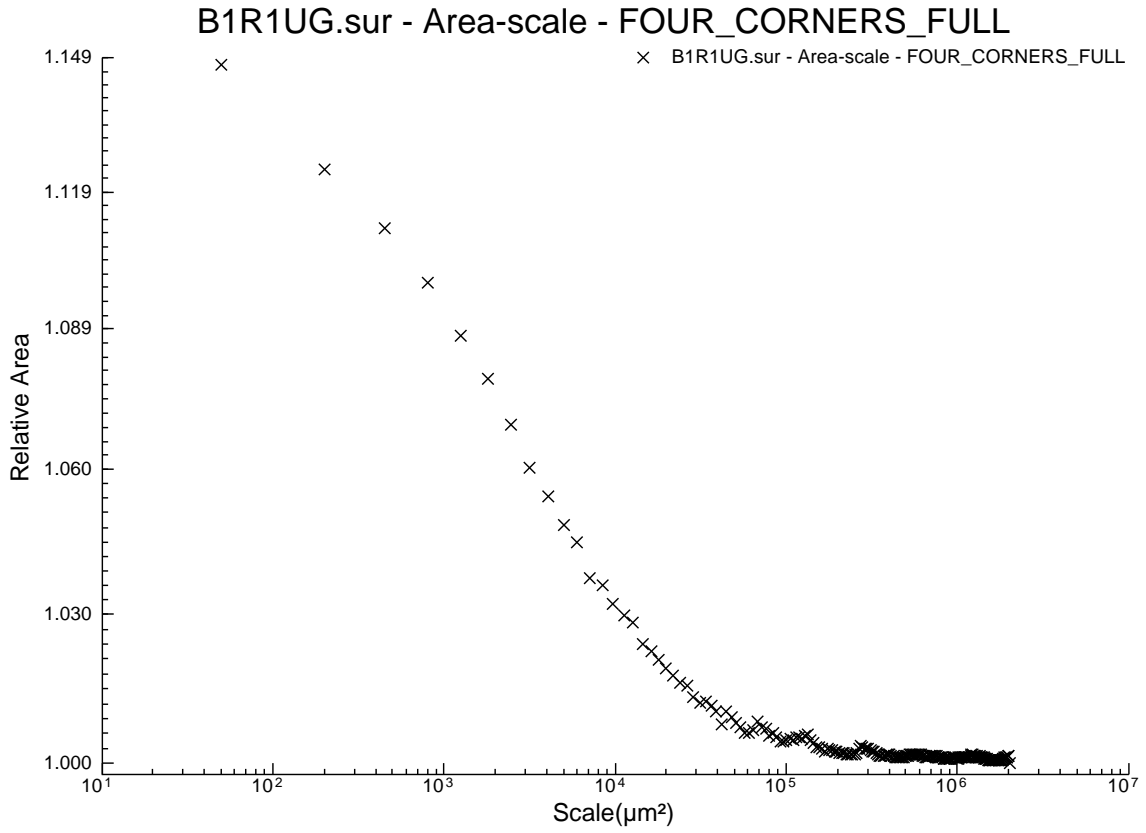
## 6. References

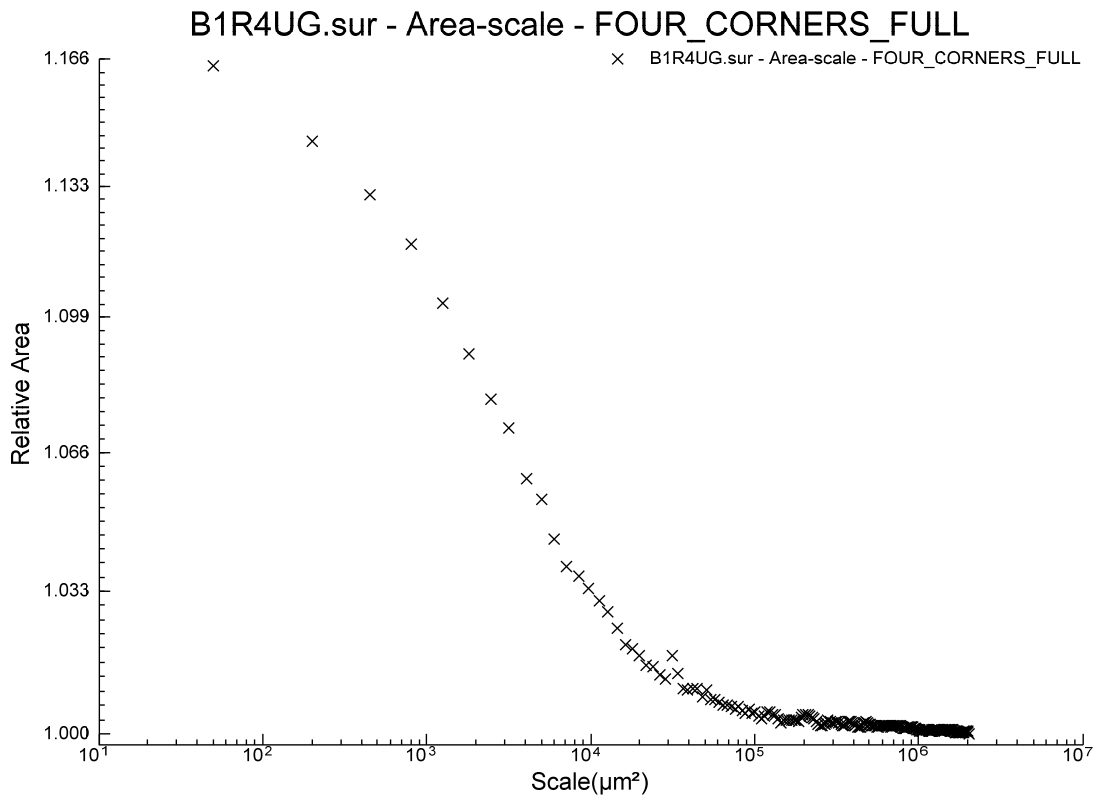
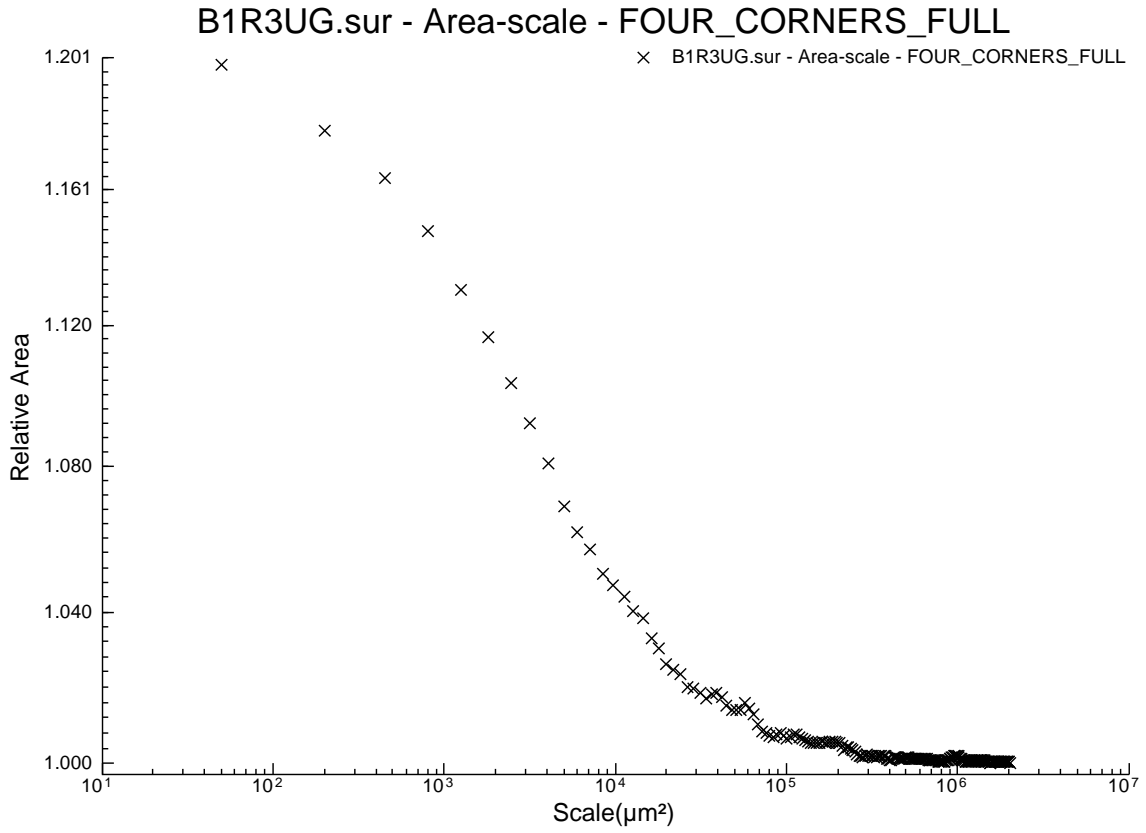
- [1] Blunt, L. and Ebdon, S. The Application of Three-Dimensional Surface Measurement Techniques to Characterize Grinding Wheel Topography. *Int. J. Mach. Tools Manufact.* Vol. 36, No. 11, pp. 1207-1226, 1996.
- [2] Brown, C. A. Recent Developments in Surface Metrology Using Fractal Analysis. *Presented at Saint Gobain Abrasives in Worcester MA*, November 29, 2006
- [3] Butler, Blunt, See, Webster, and Stout The characterization of grinding wheel surfaces using 3D surface techniques. *Journal of Materials Processing Technology* 127. pp. 234-237, 2002.
- [4] Malkin, Stephen. Grinding Technology: Theory and applications of machining with abrasives. Dearborn, MI: Society of Manufacturing Engineers, 1989.
- [5] Multiple Authors ASME B46: Surface Texture, Surface Roughness, Waviness, and Lay. *American Society of Mechanical Engineers.* 2002.
- [6] Zhou, X. and Xi, F. Modeling and Predicting Surface Roughness of the Grinding Process. *Int. J. Mach. Tools Manufact.* Vol. 42, No. 8, pp. 969-977, 2002.

## 7. Appendices

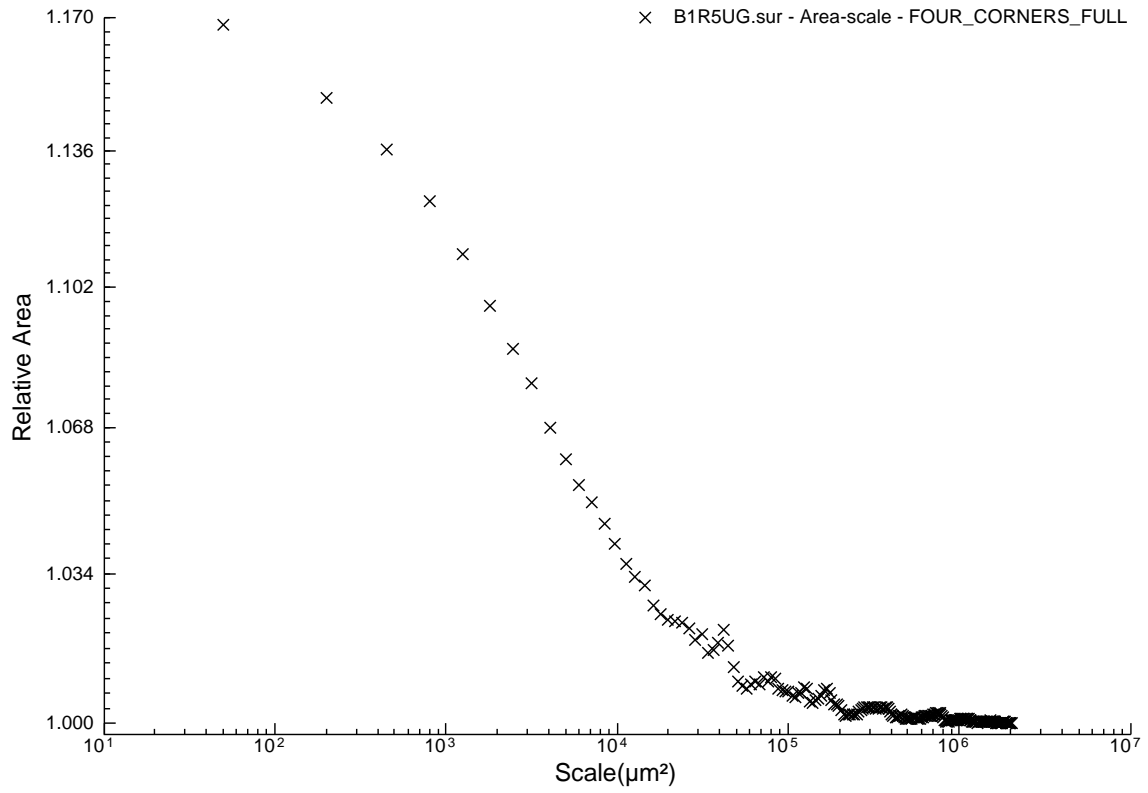
# Appendix A

## Relative-area plots

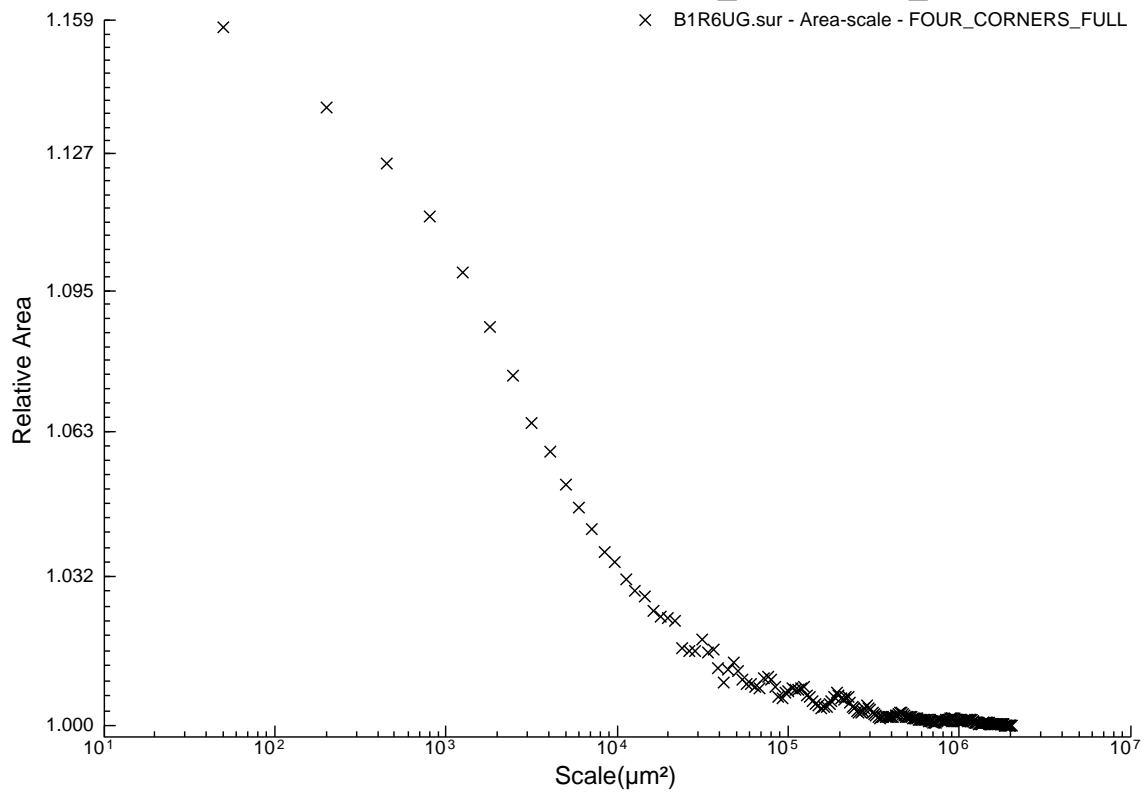




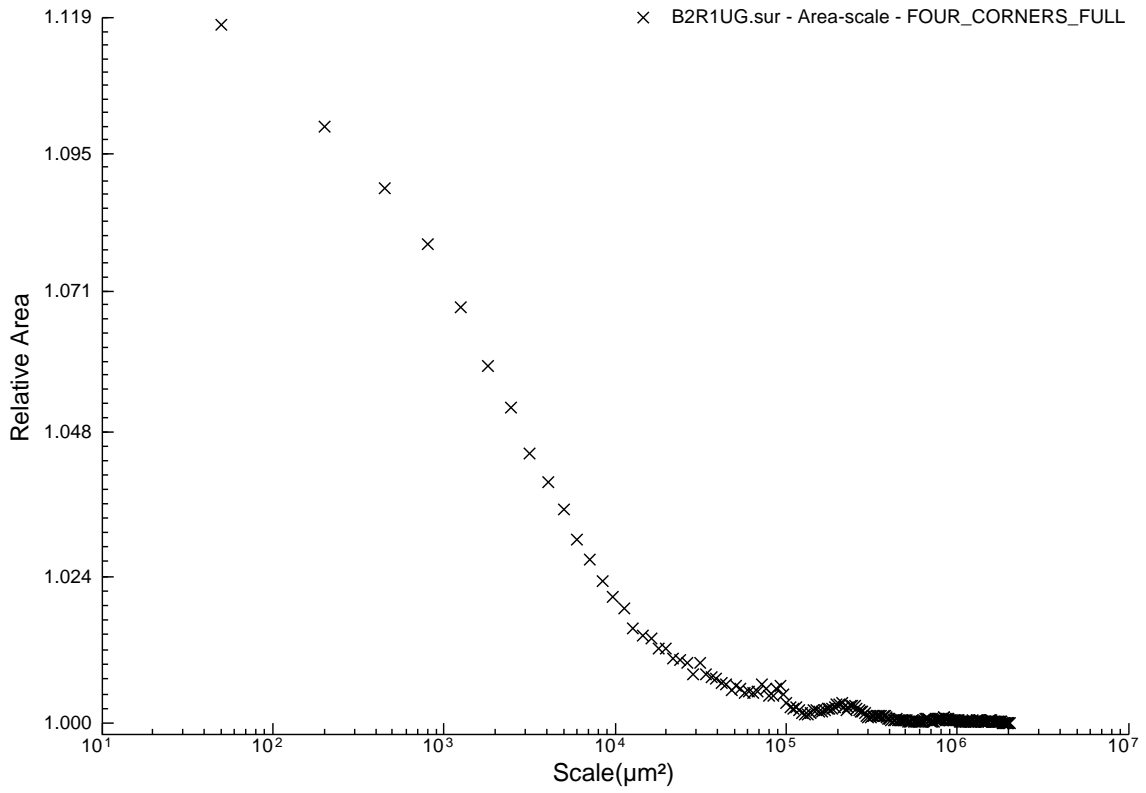
B1R5UG.sur - Area-scale - FOUR\_CORNERS\_FULL



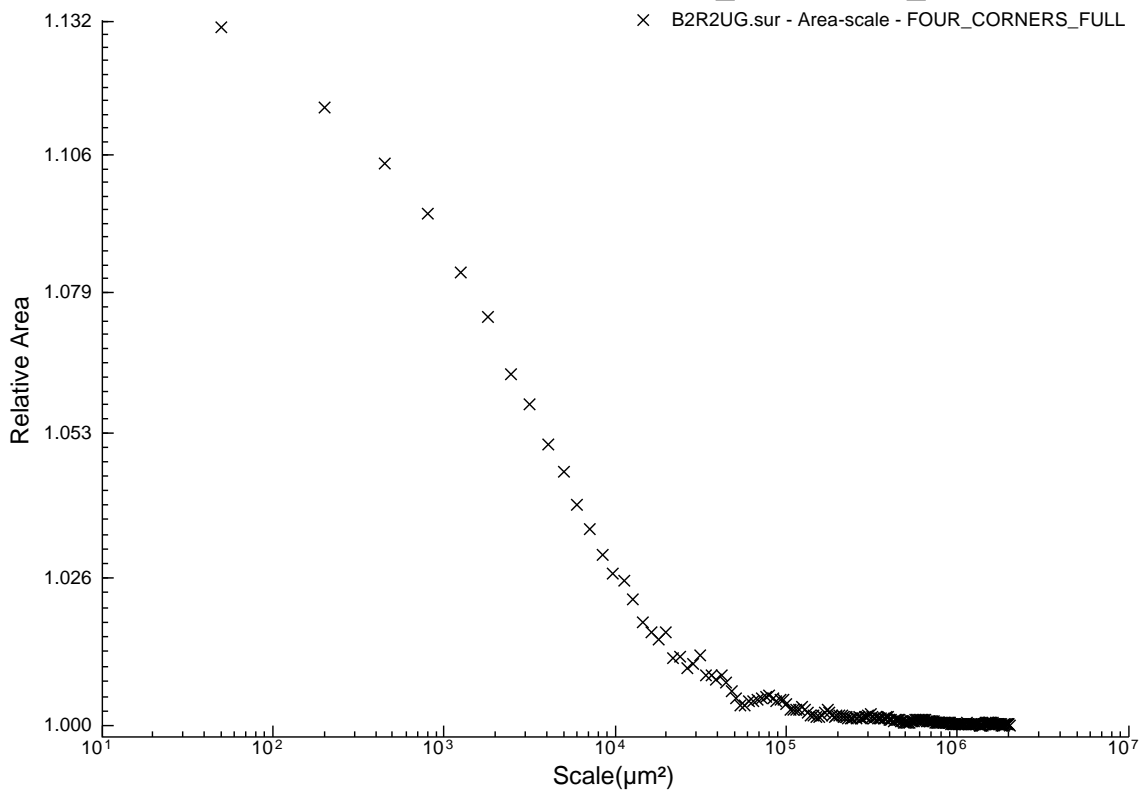
B1R6UG.sur - Area-scale - FOUR\_CORNERS\_FULL

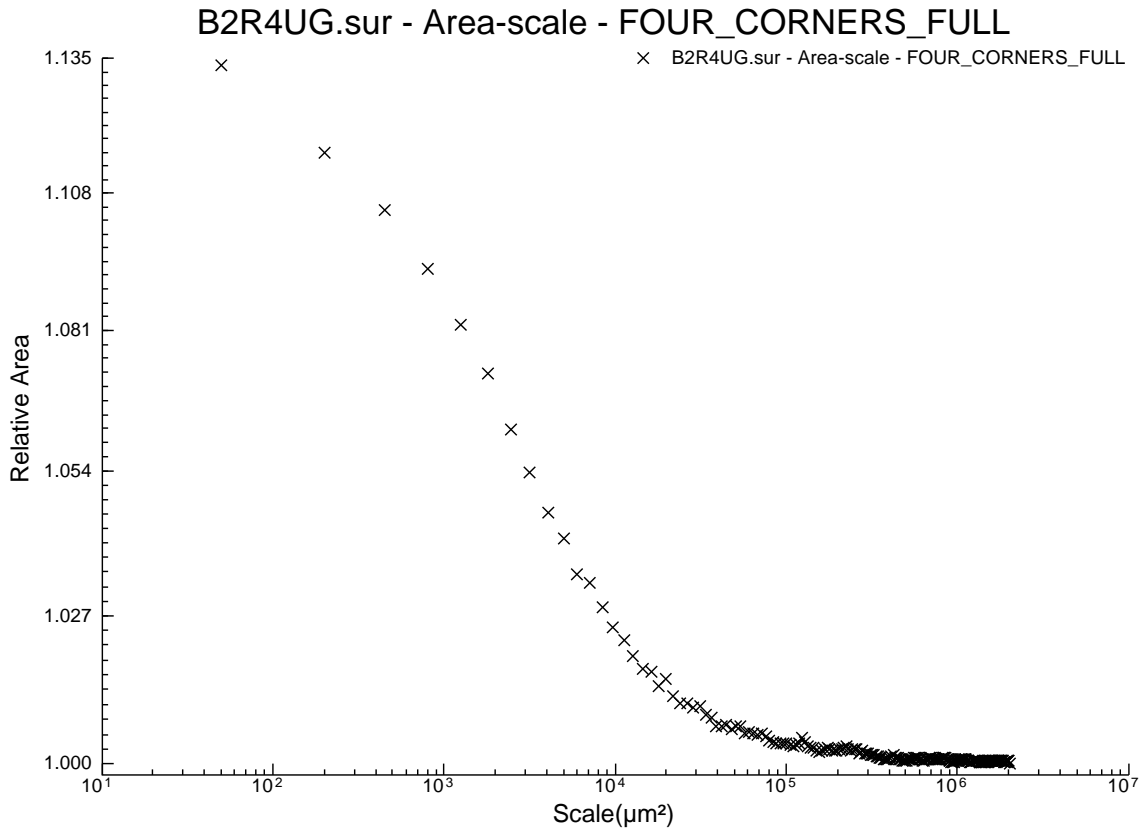
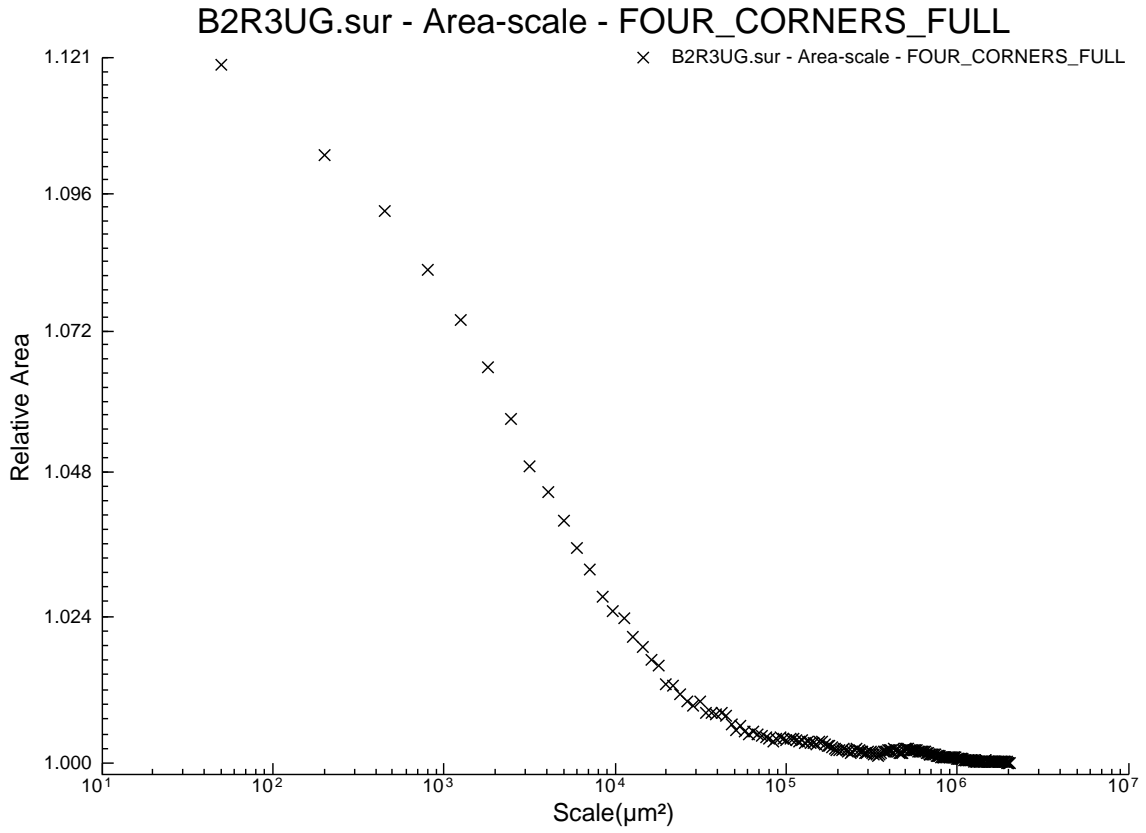


B2R1UG.sur - Area-scale - FOUR\_CORNERS\_FULL

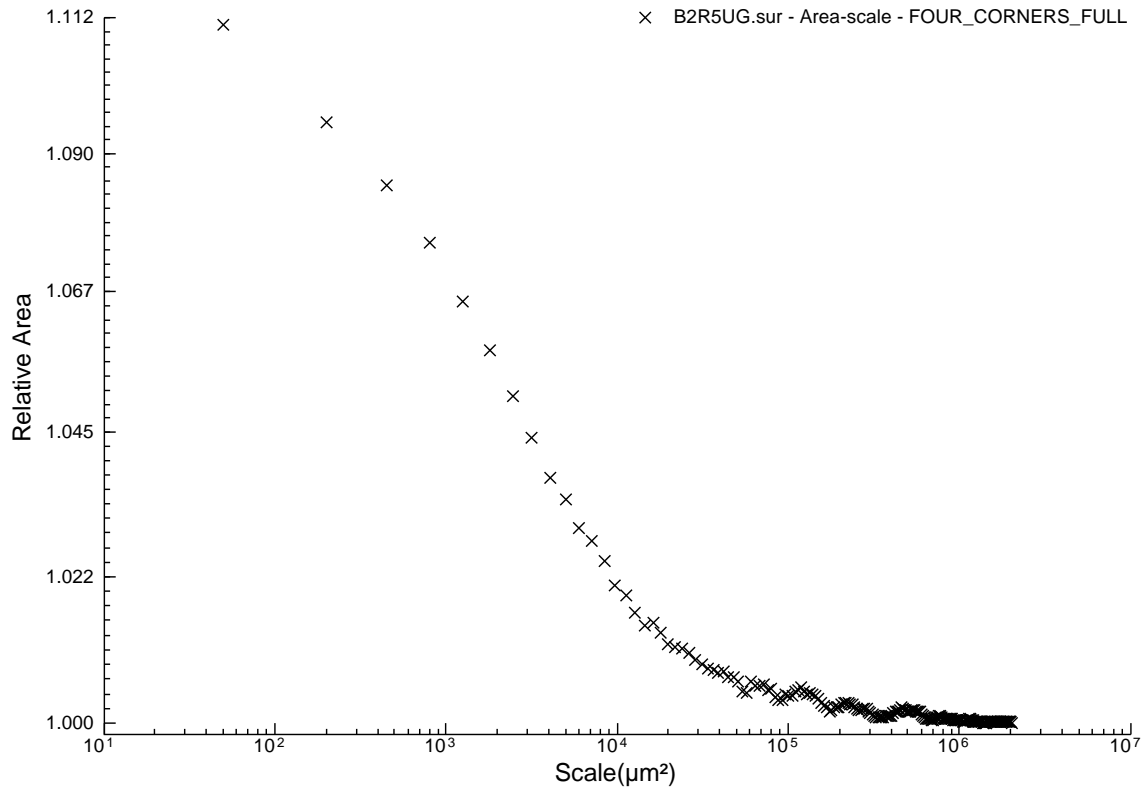


B2R2UG.sur - Area-scale - FOUR\_CORNERS\_FULL

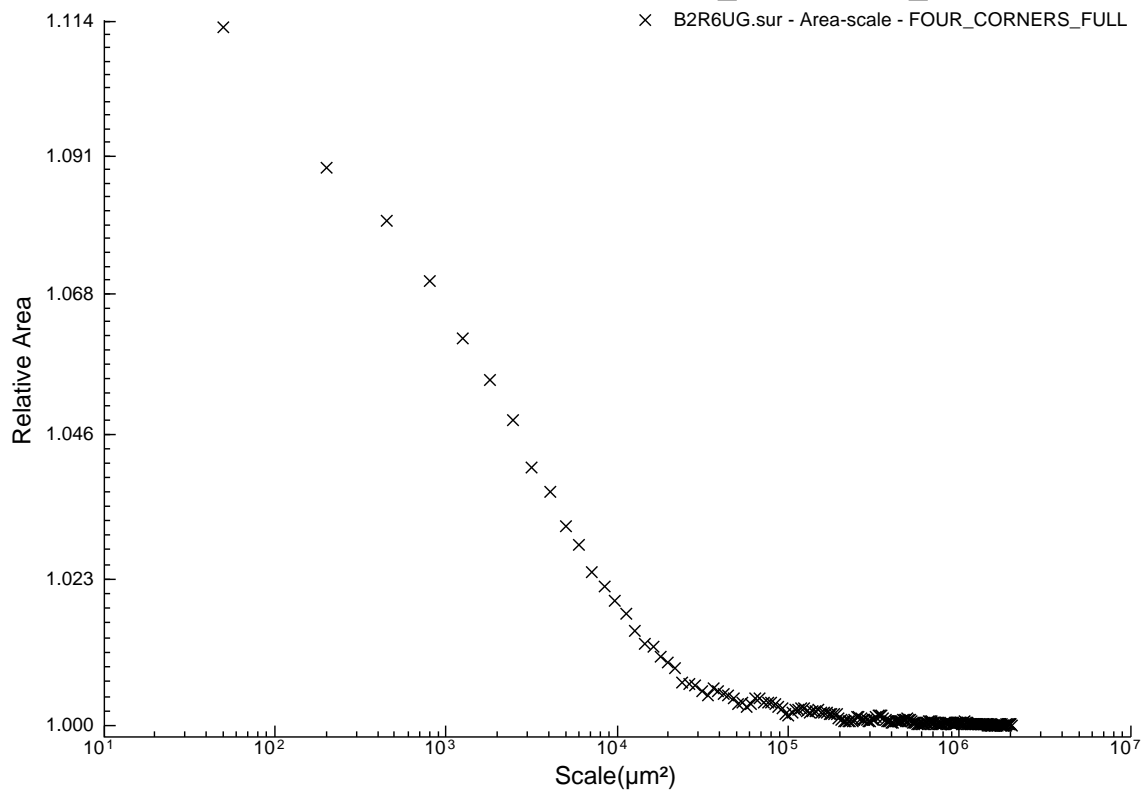




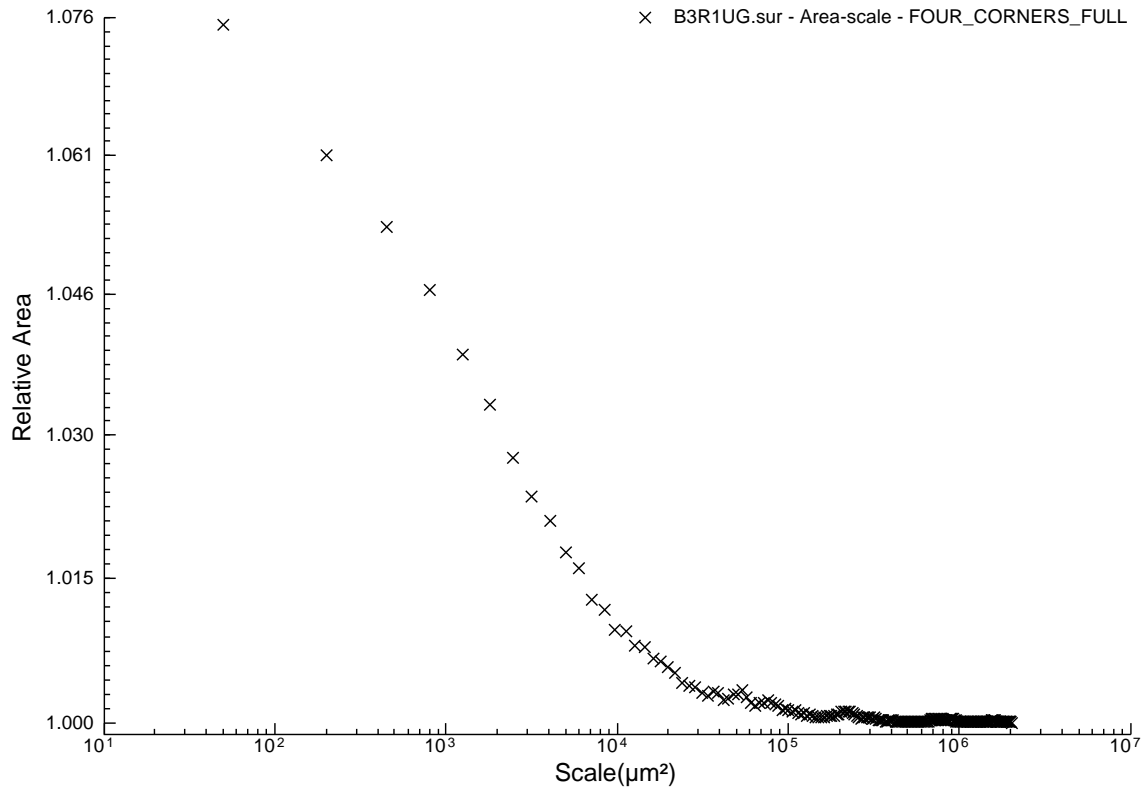
B2R5UG.sur - Area-scale - FOUR\_CORNERS\_FULL



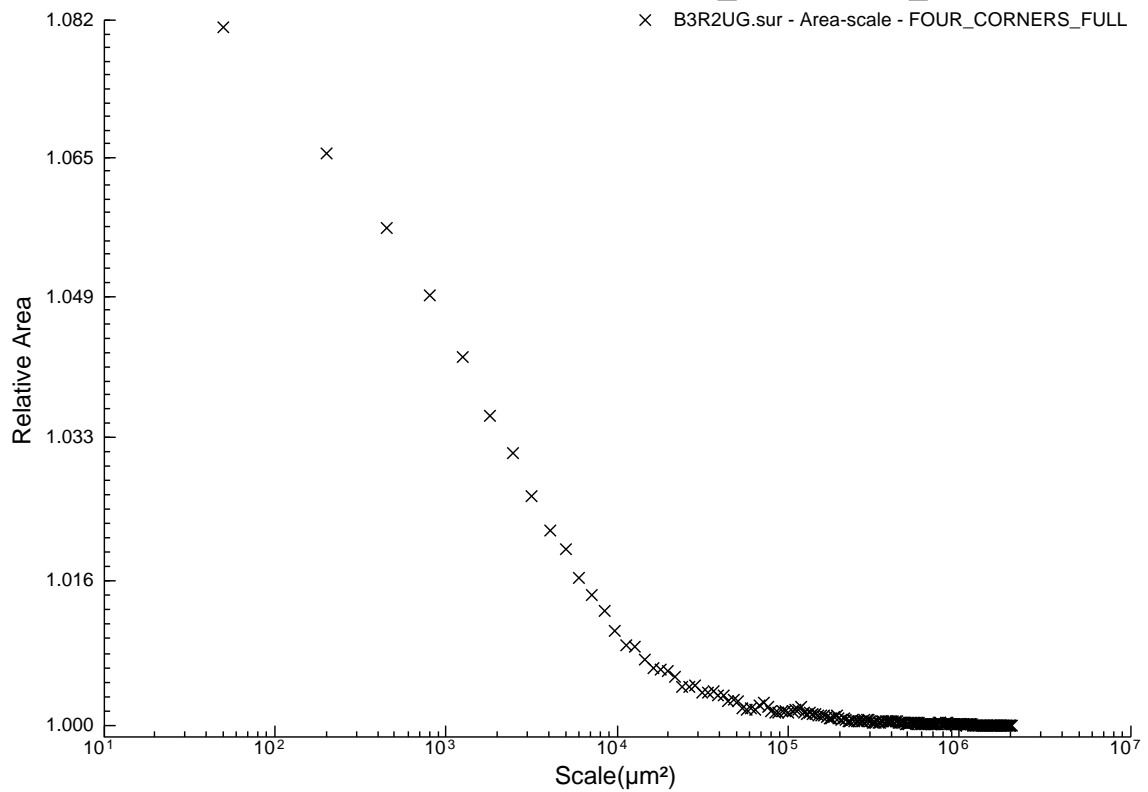
B2R6UG.sur - Area-scale - FOUR\_CORNERS\_FULL



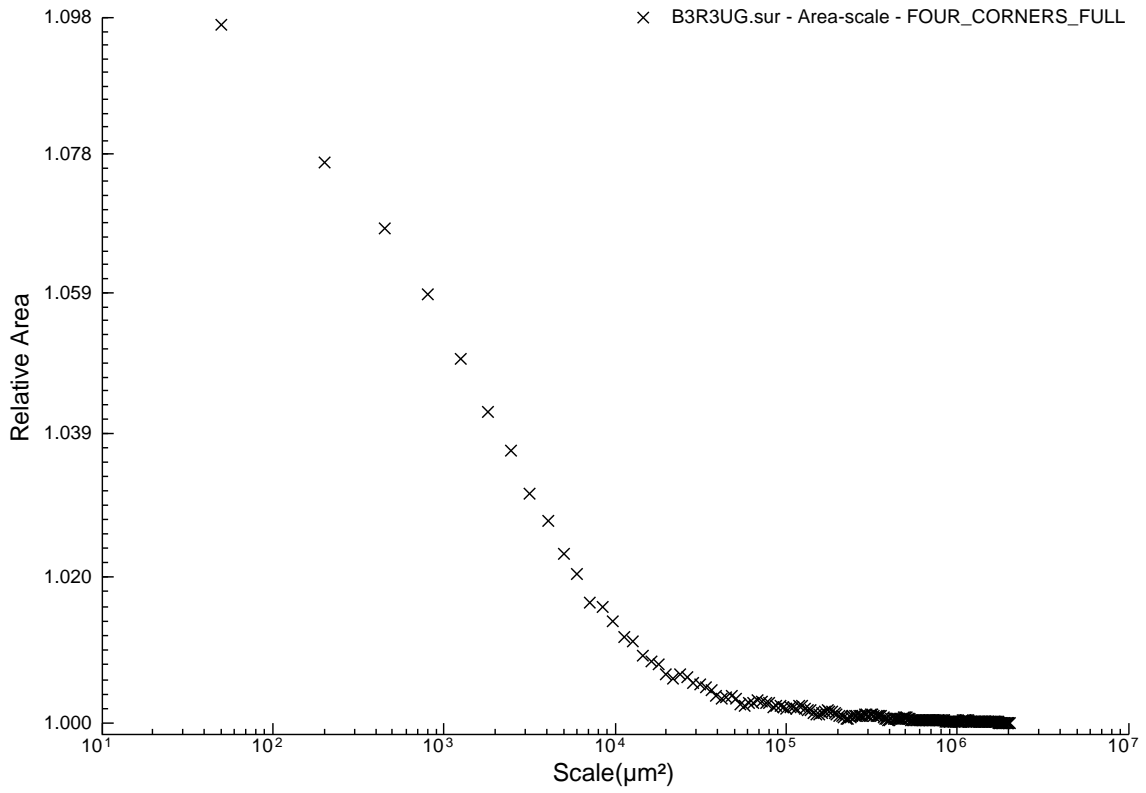
B3R1UG.sur - Area-scale - FOUR\_CORNERS\_FULL



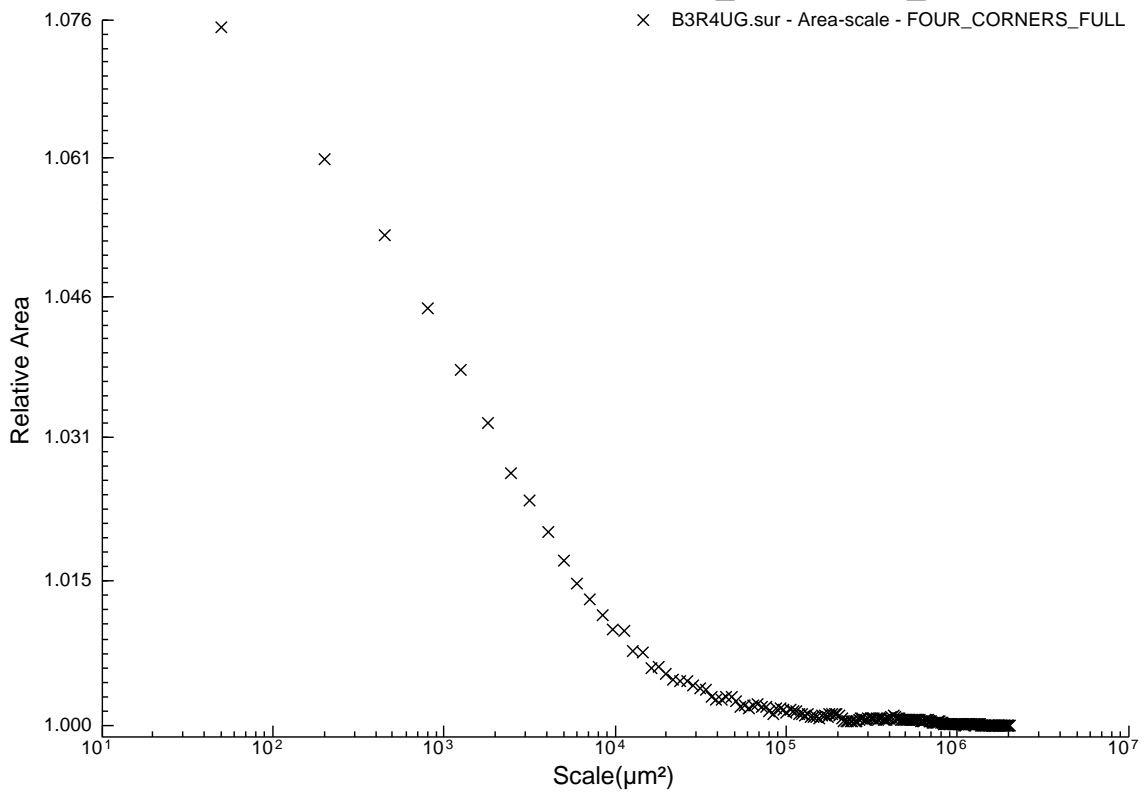
B3R2UG.sur - Area-scale - FOUR\_CORNERS\_FULL

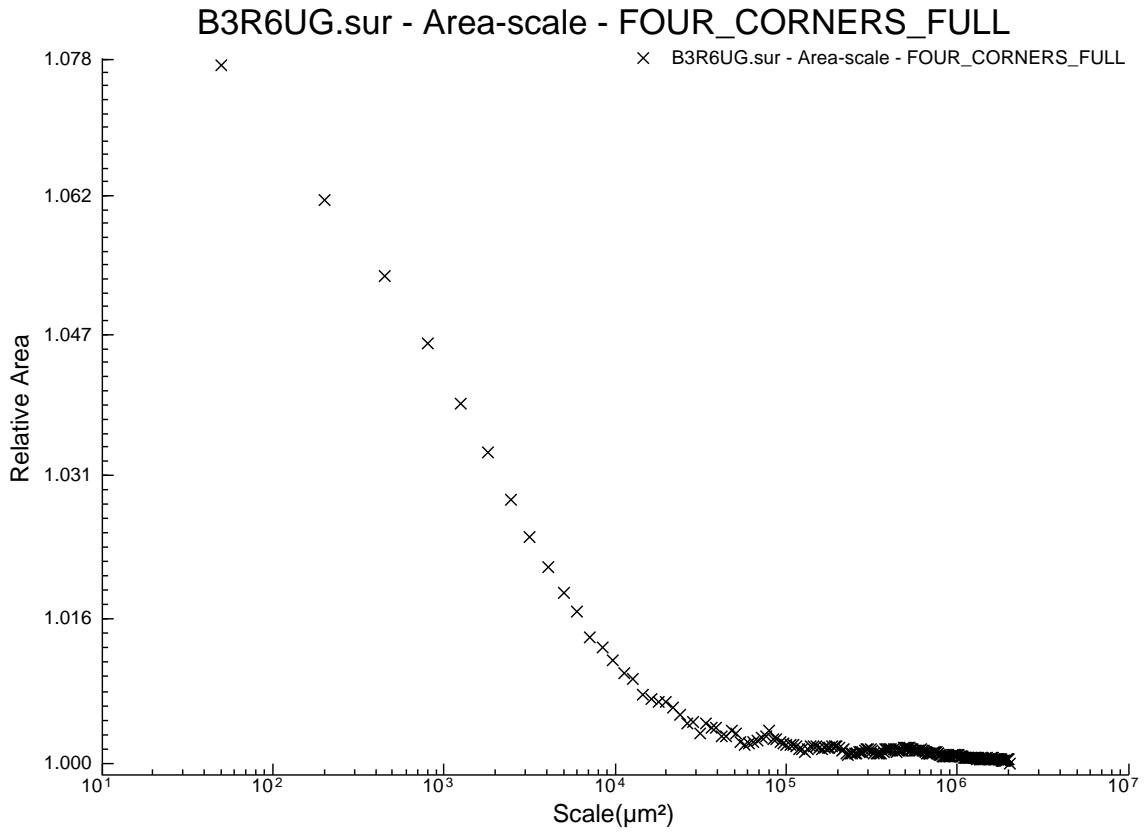
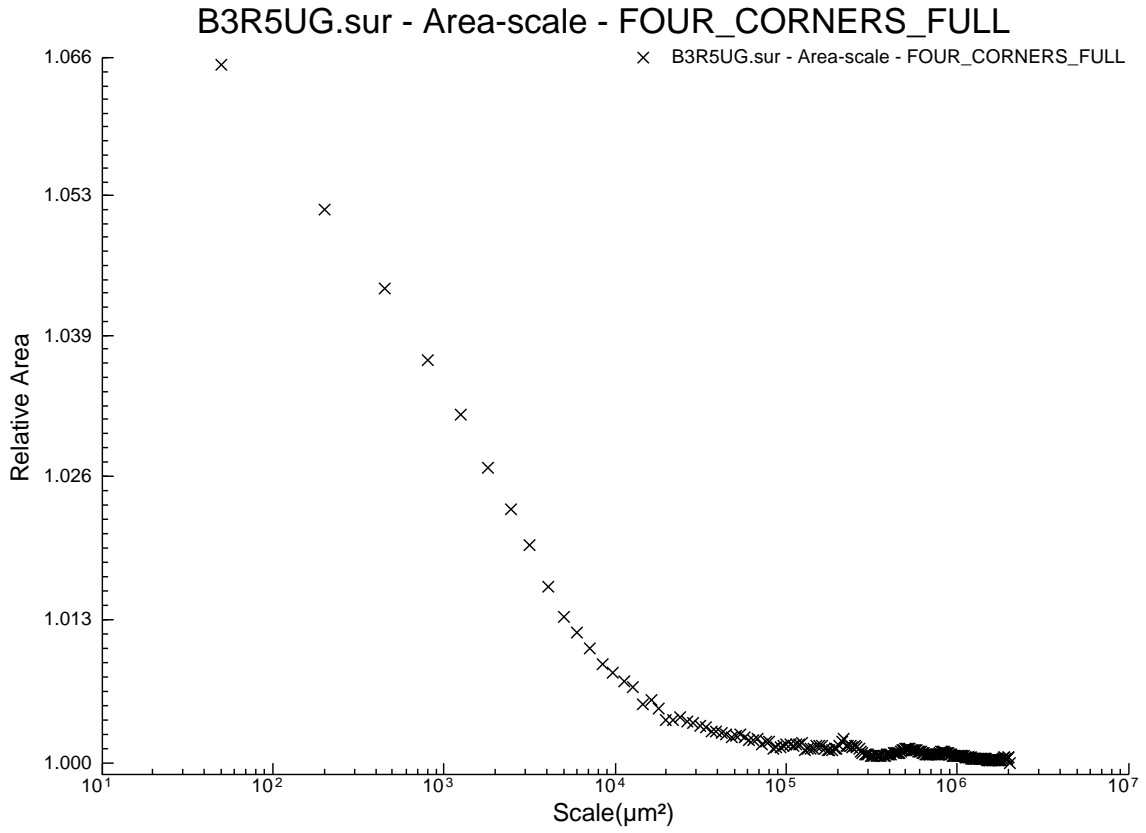


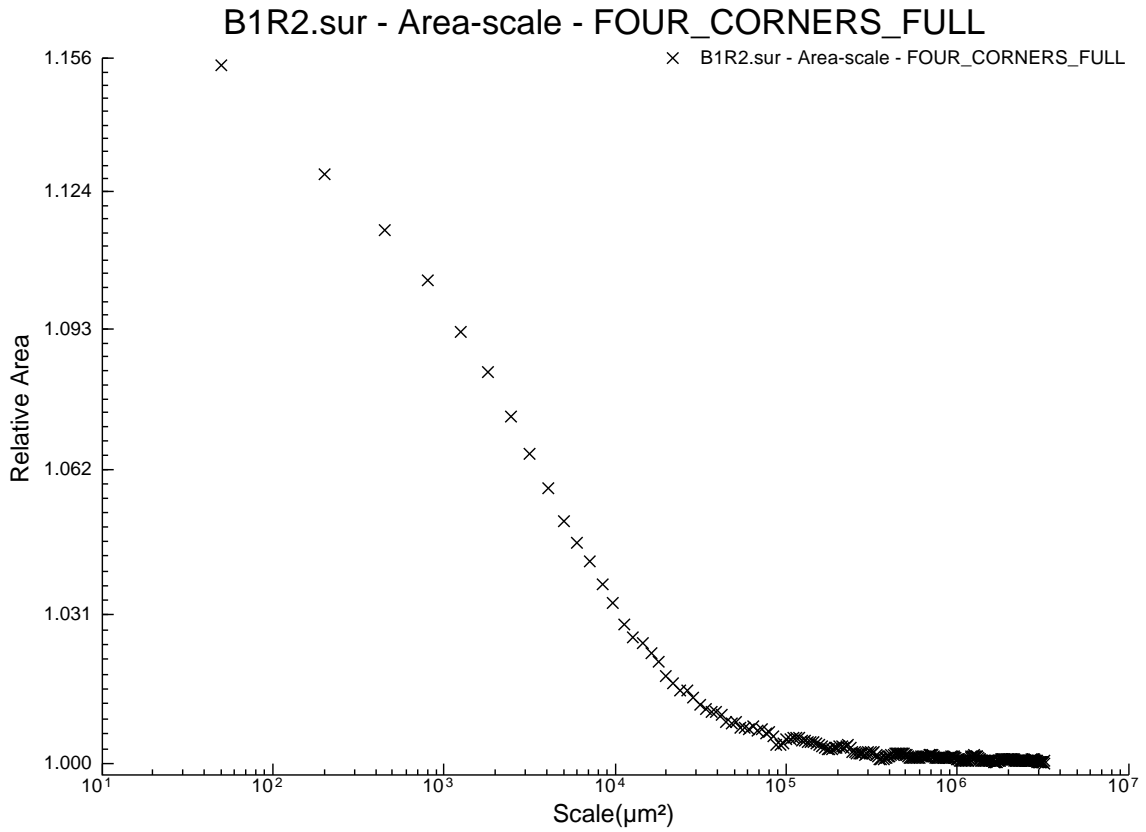
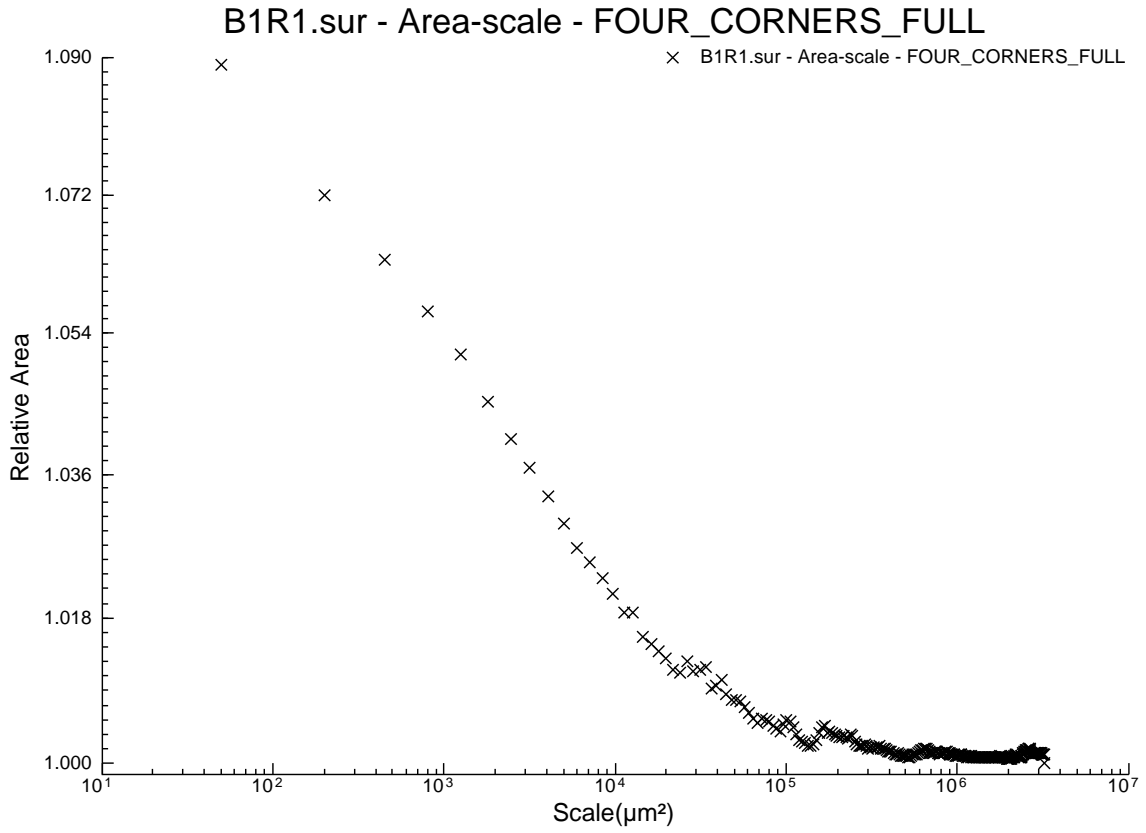
B3R3UG.sur - Area-scale - FOUR\_CORNERS\_FULL

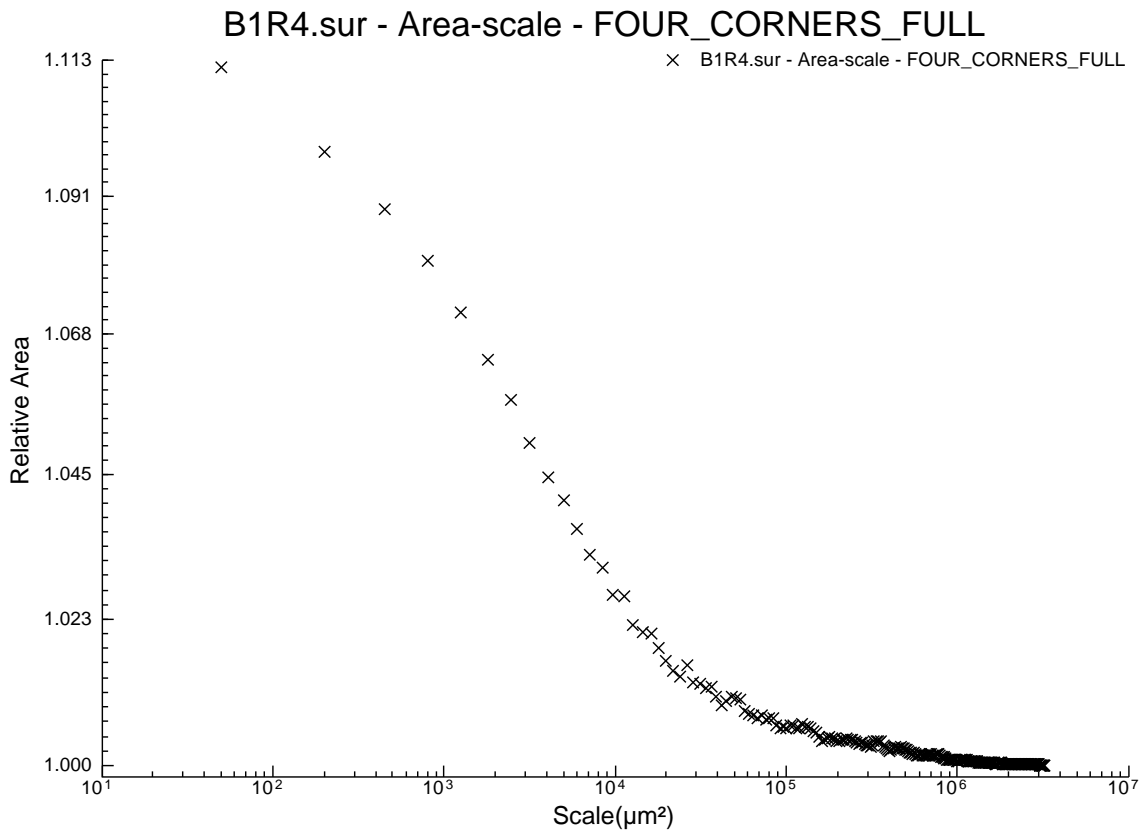
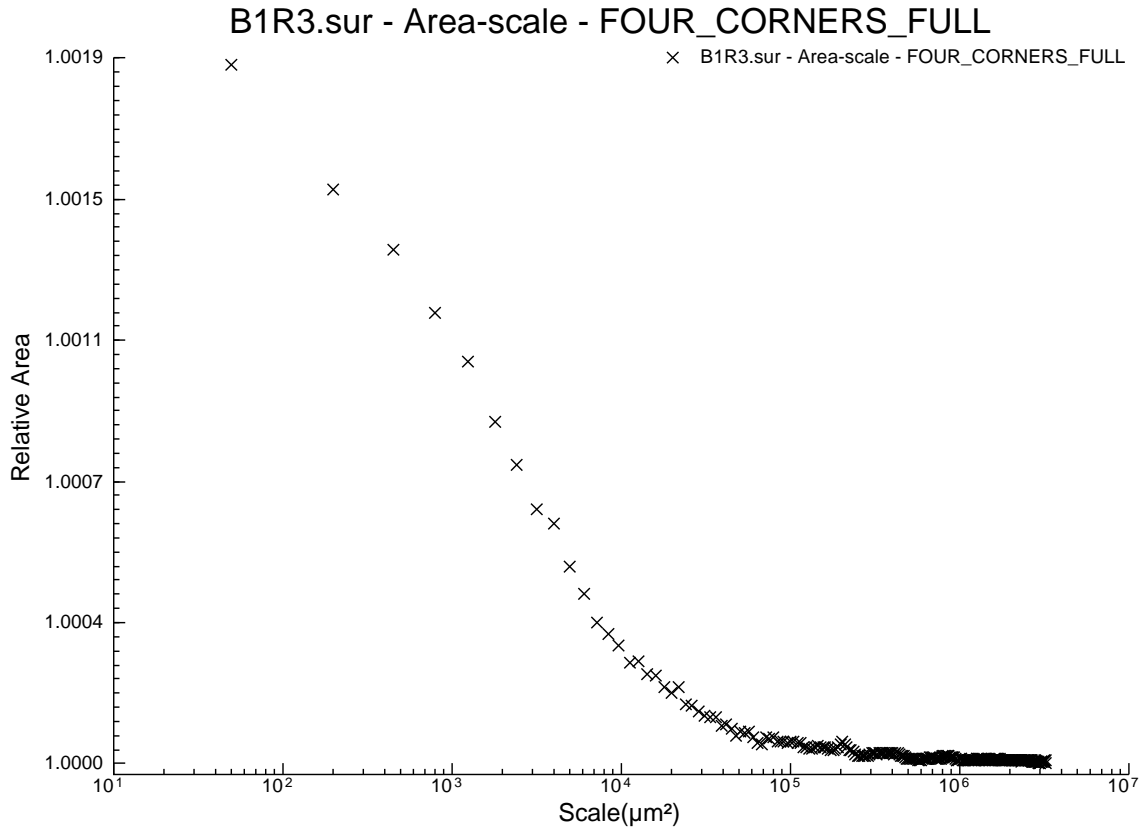


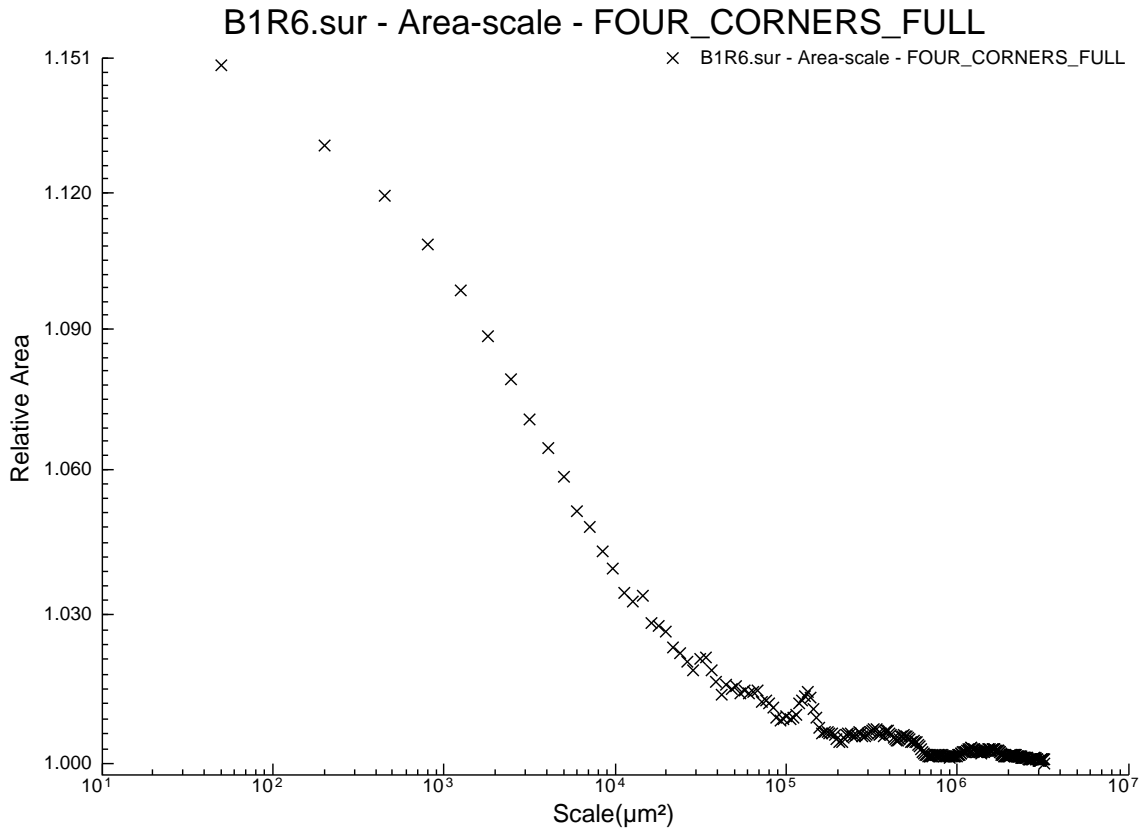
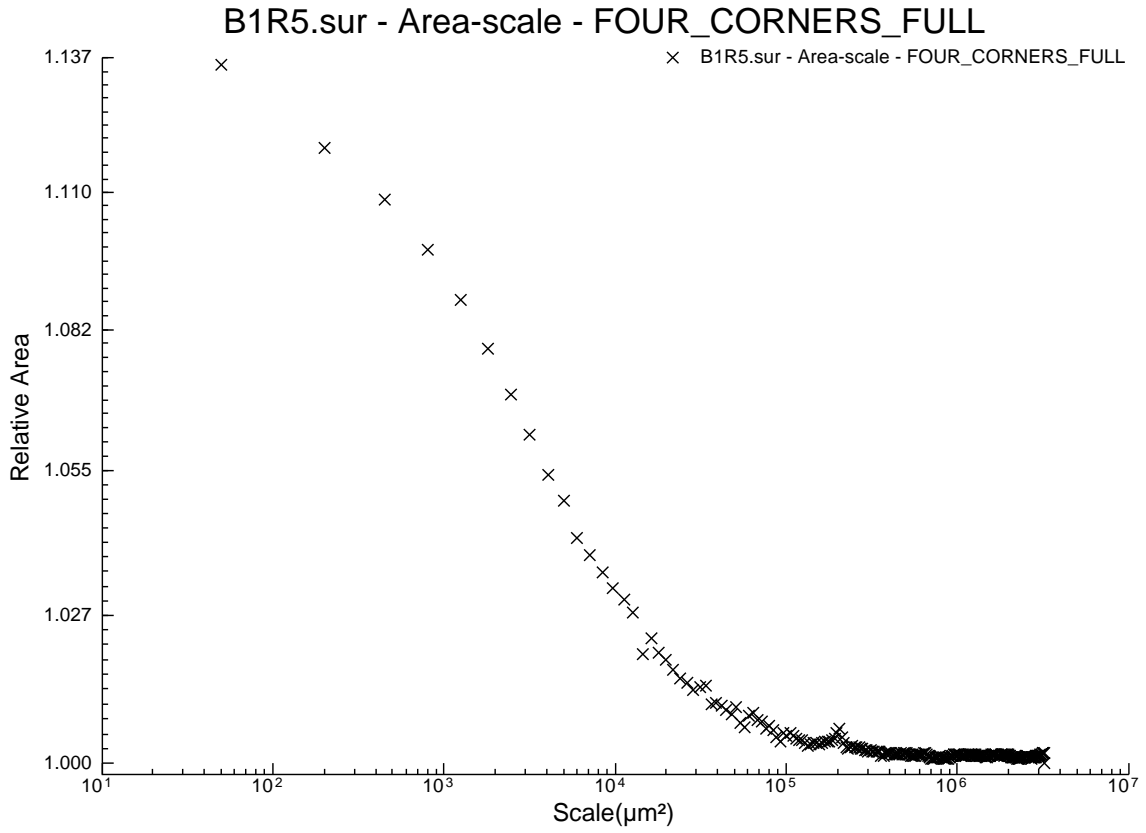
B3R4UG.sur - Area-scale - FOUR\_CORNERS\_FULL

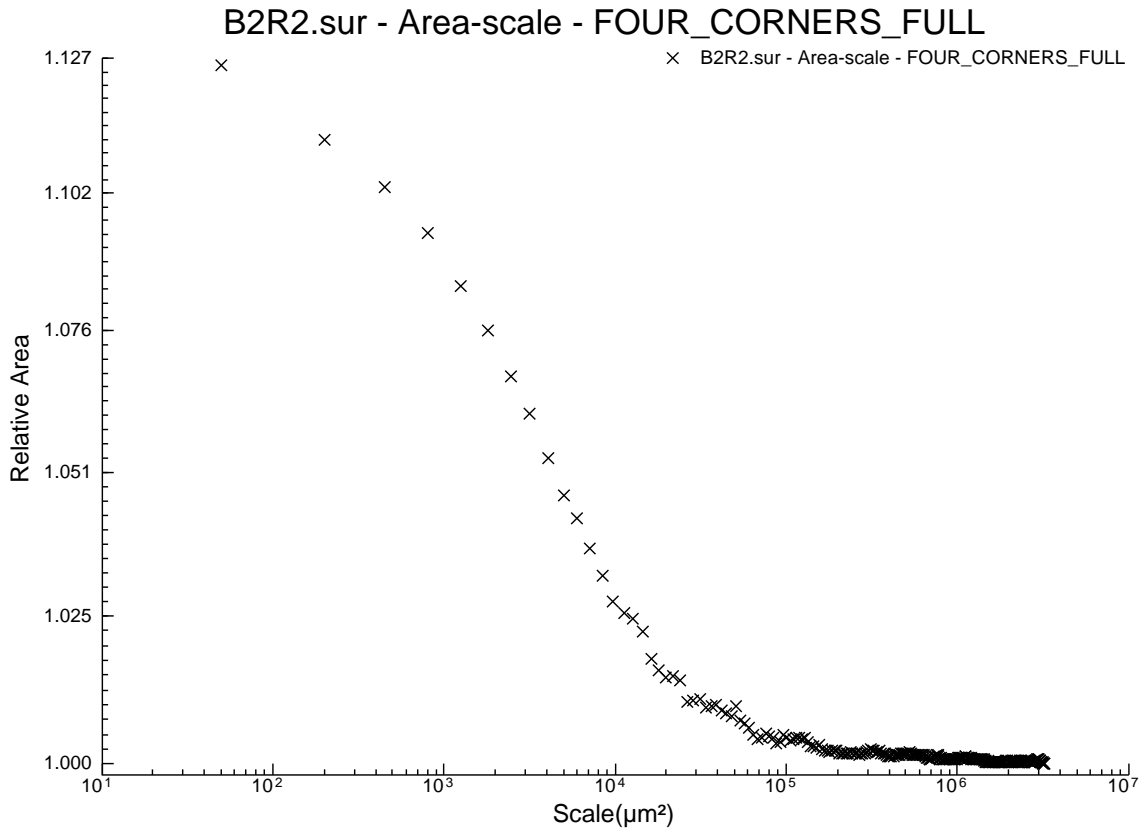
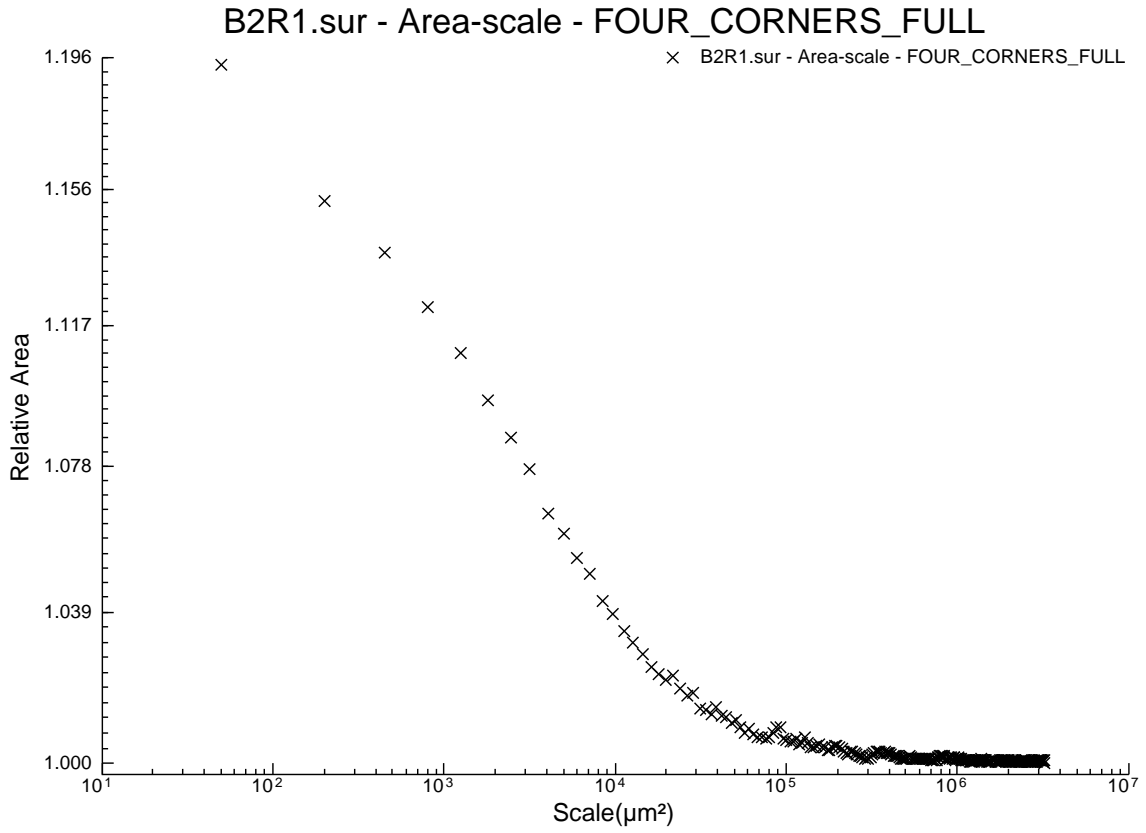


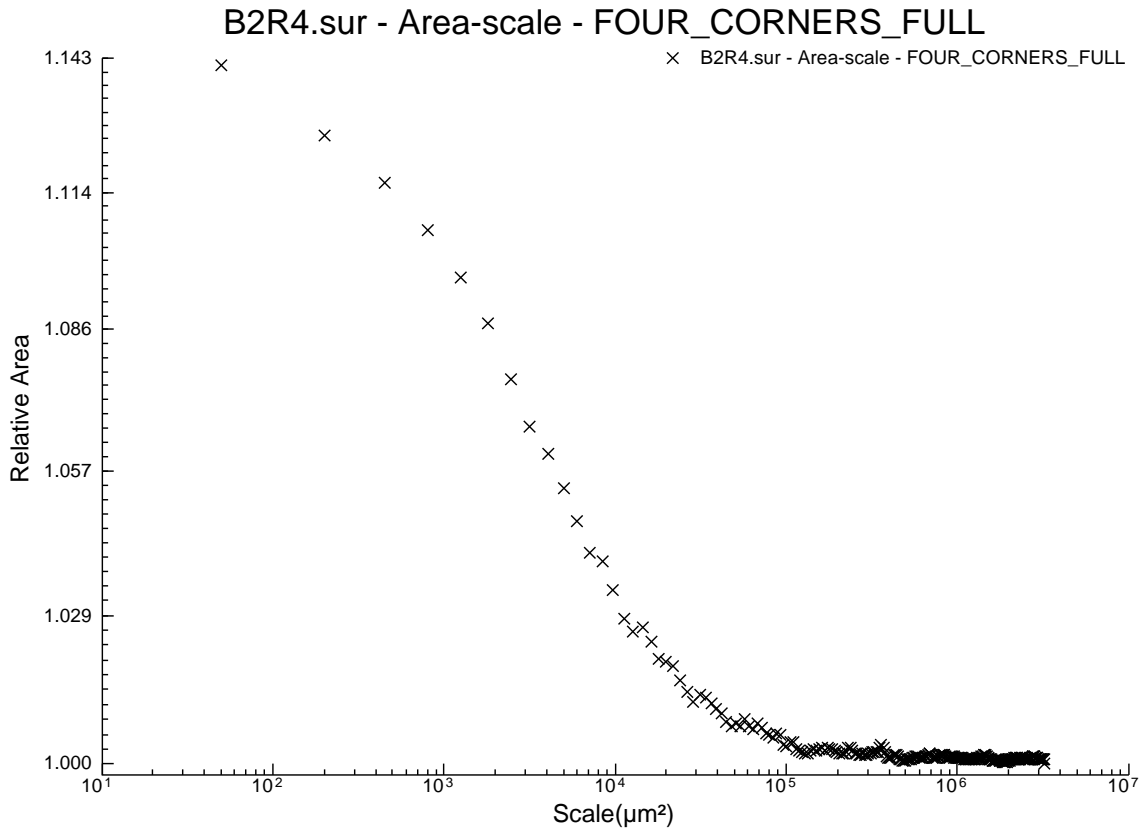
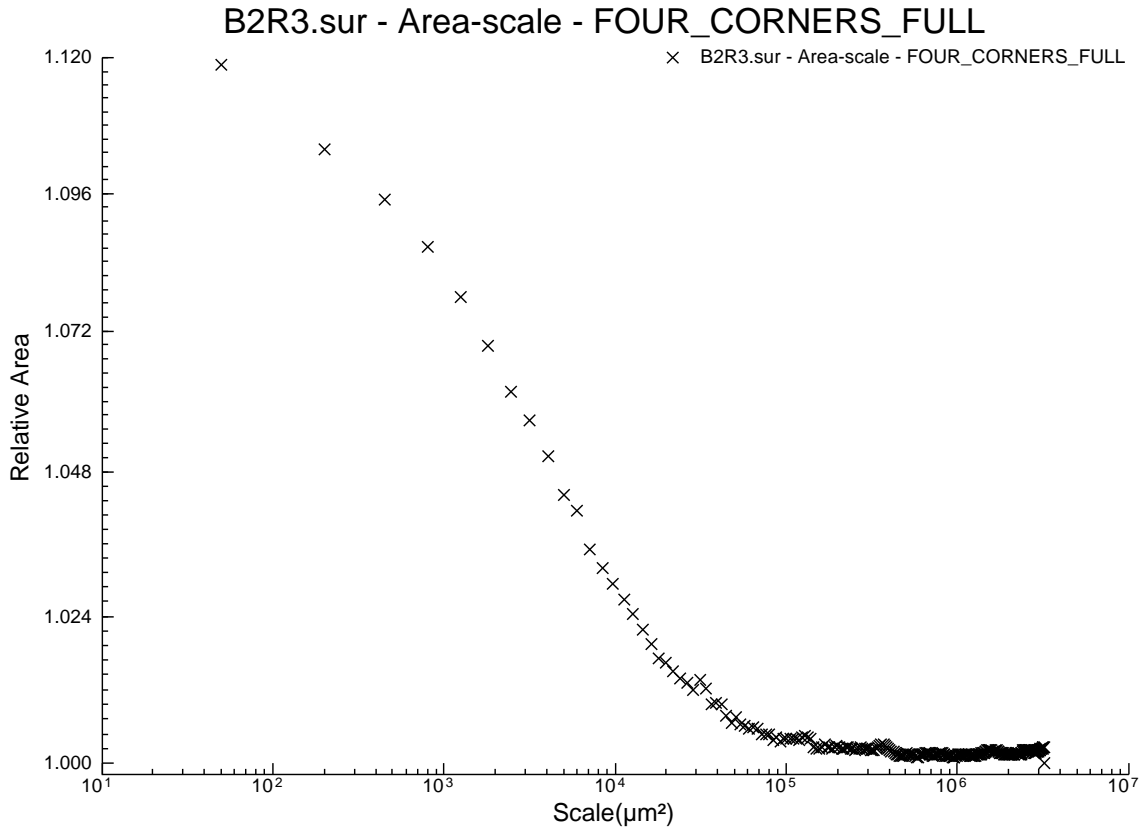


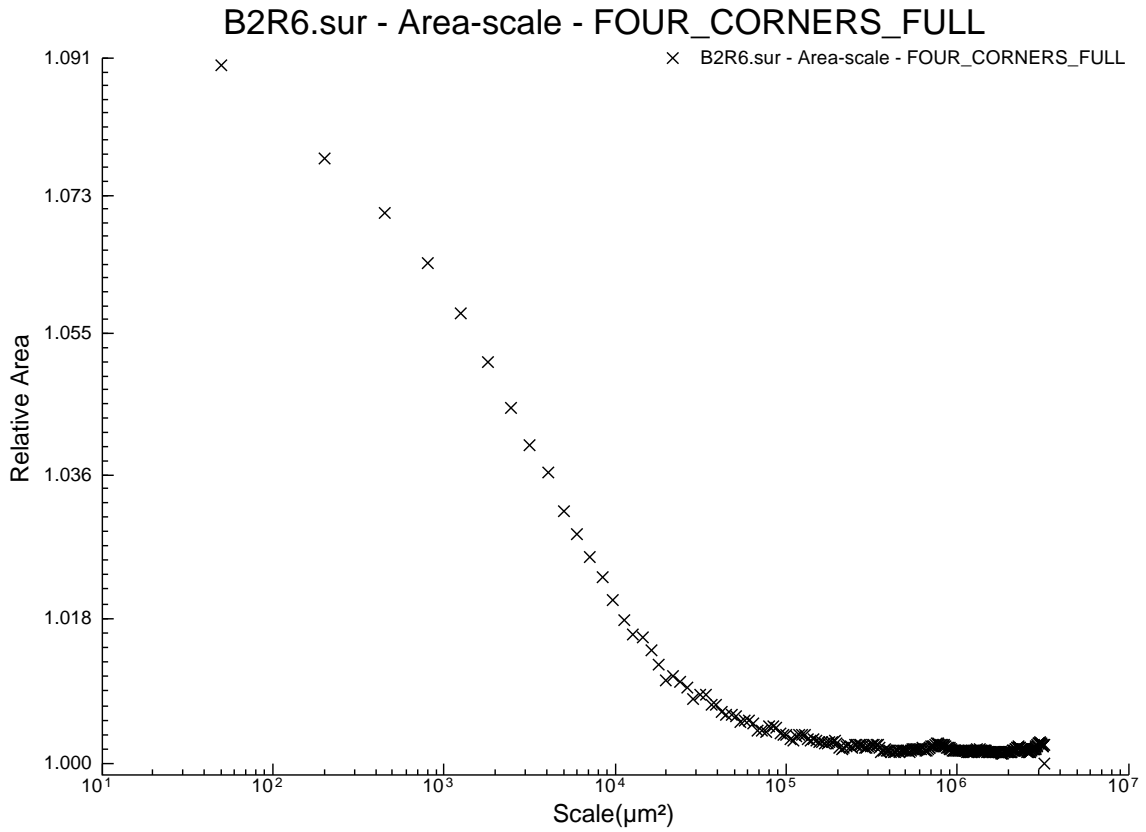
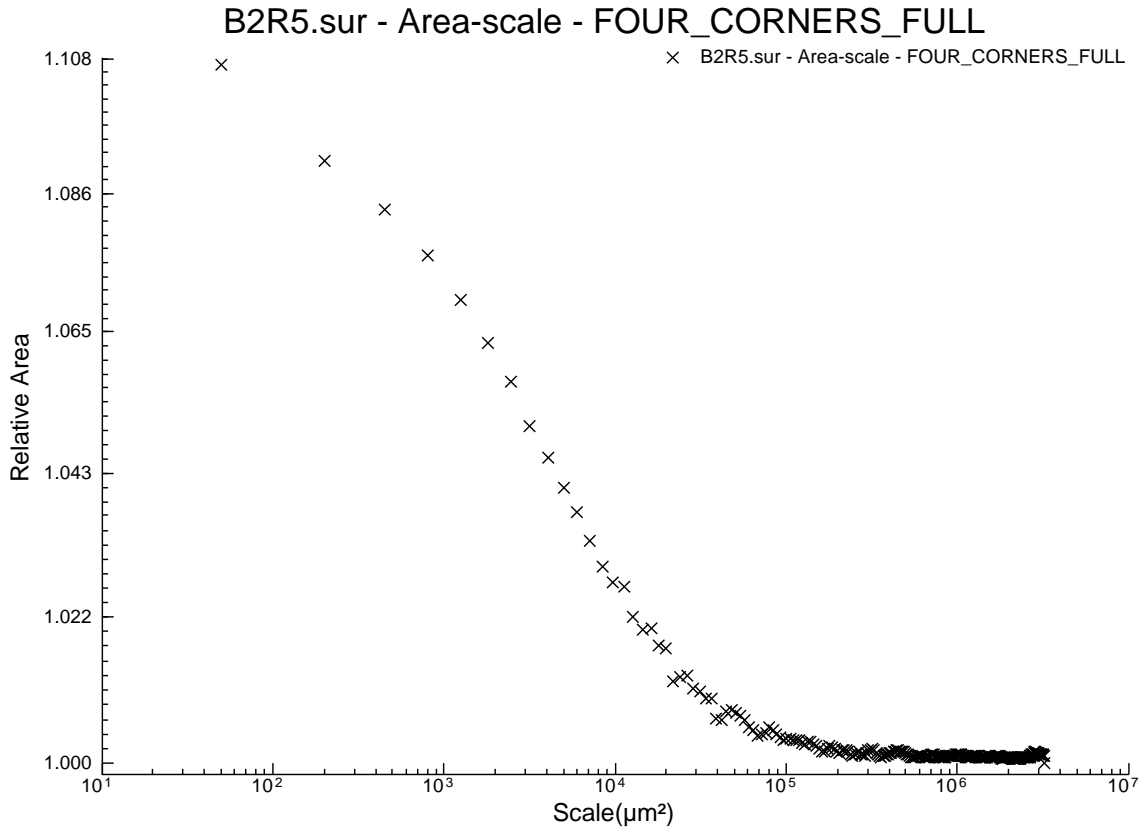


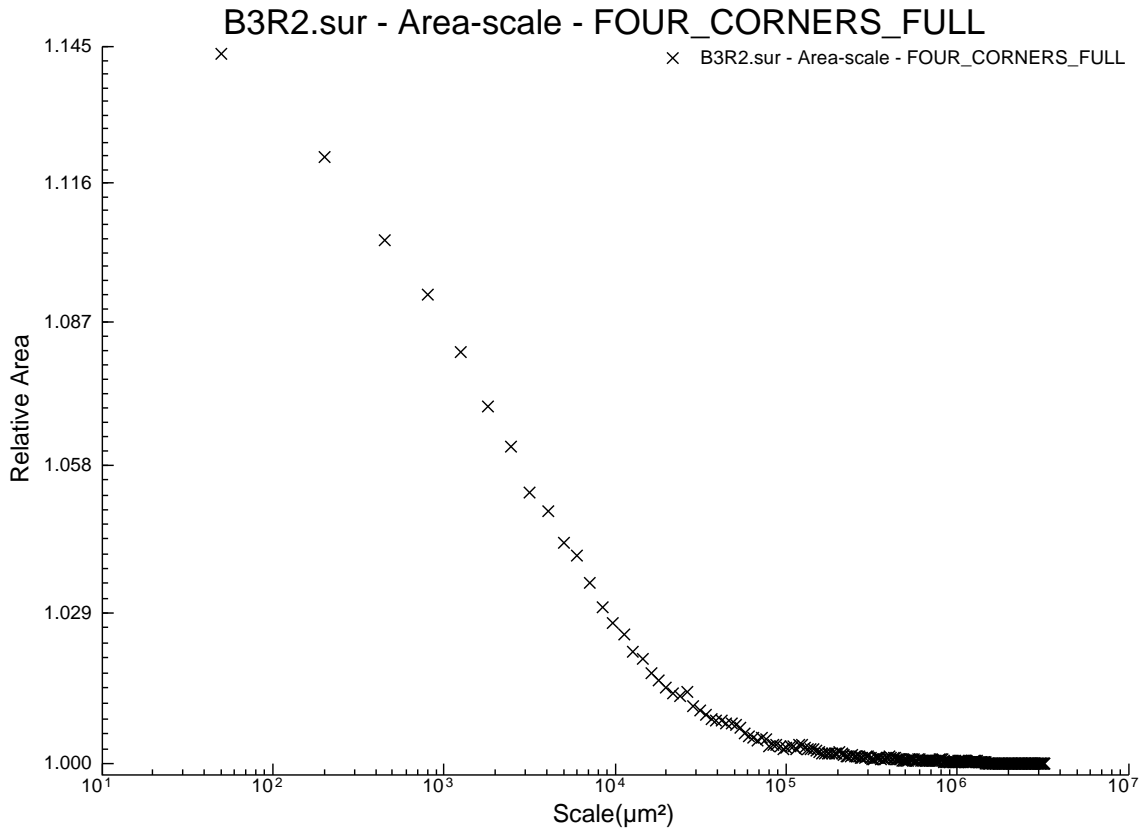
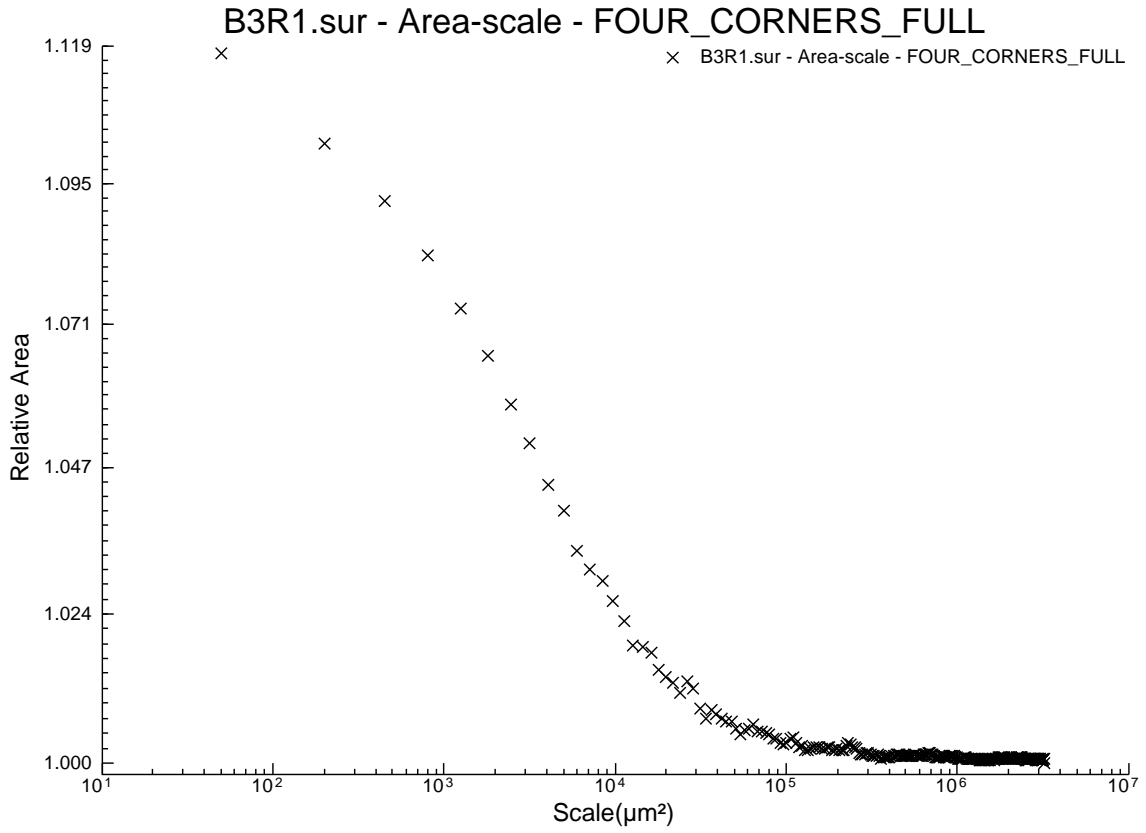


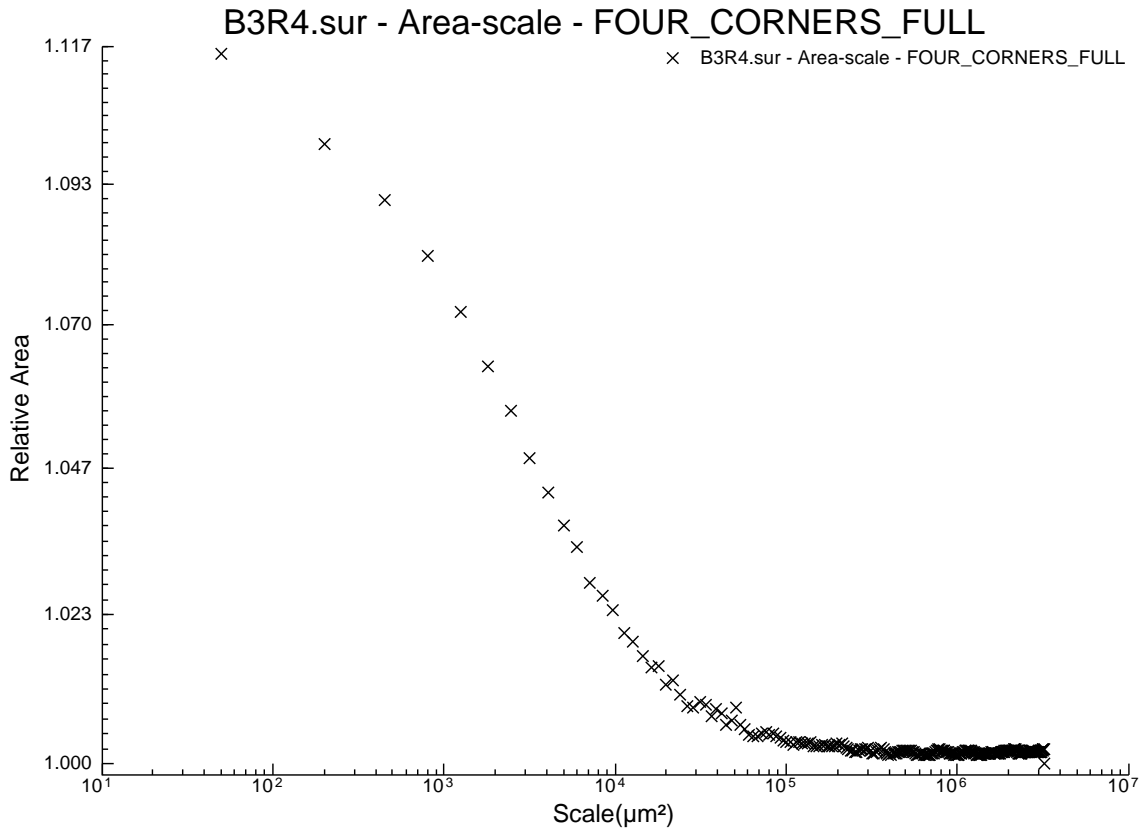
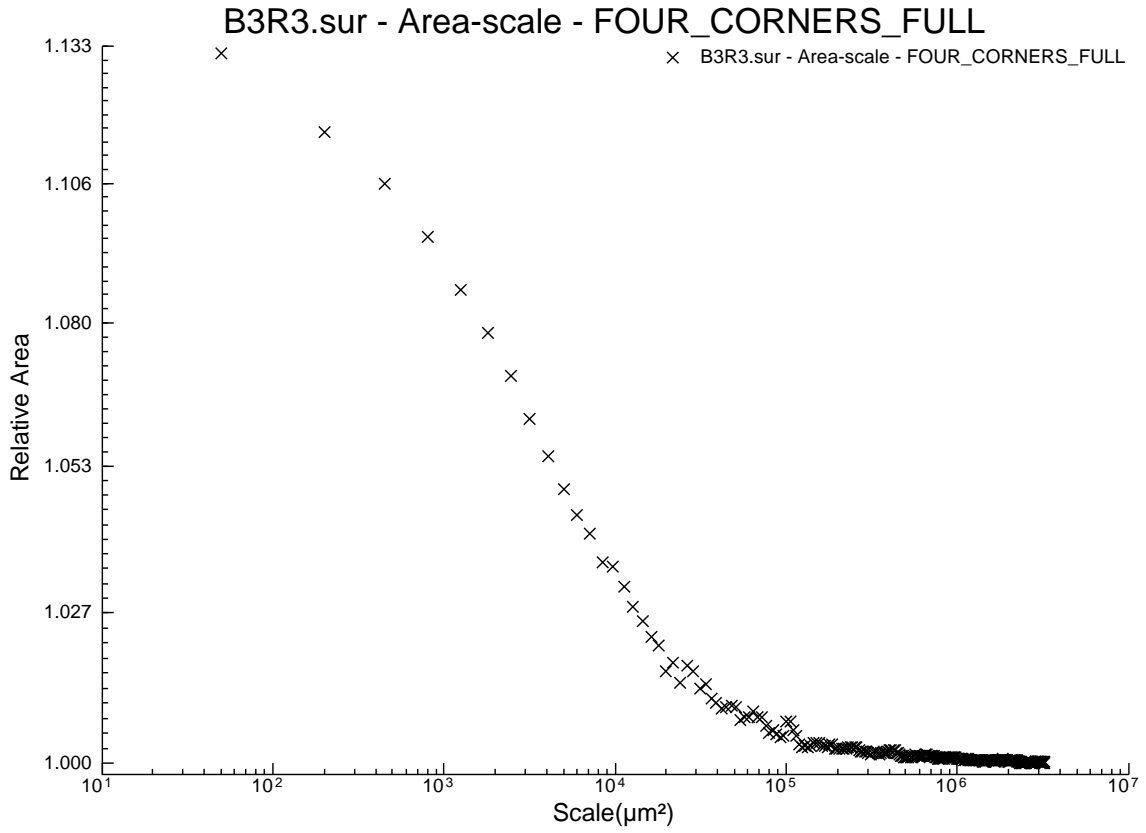


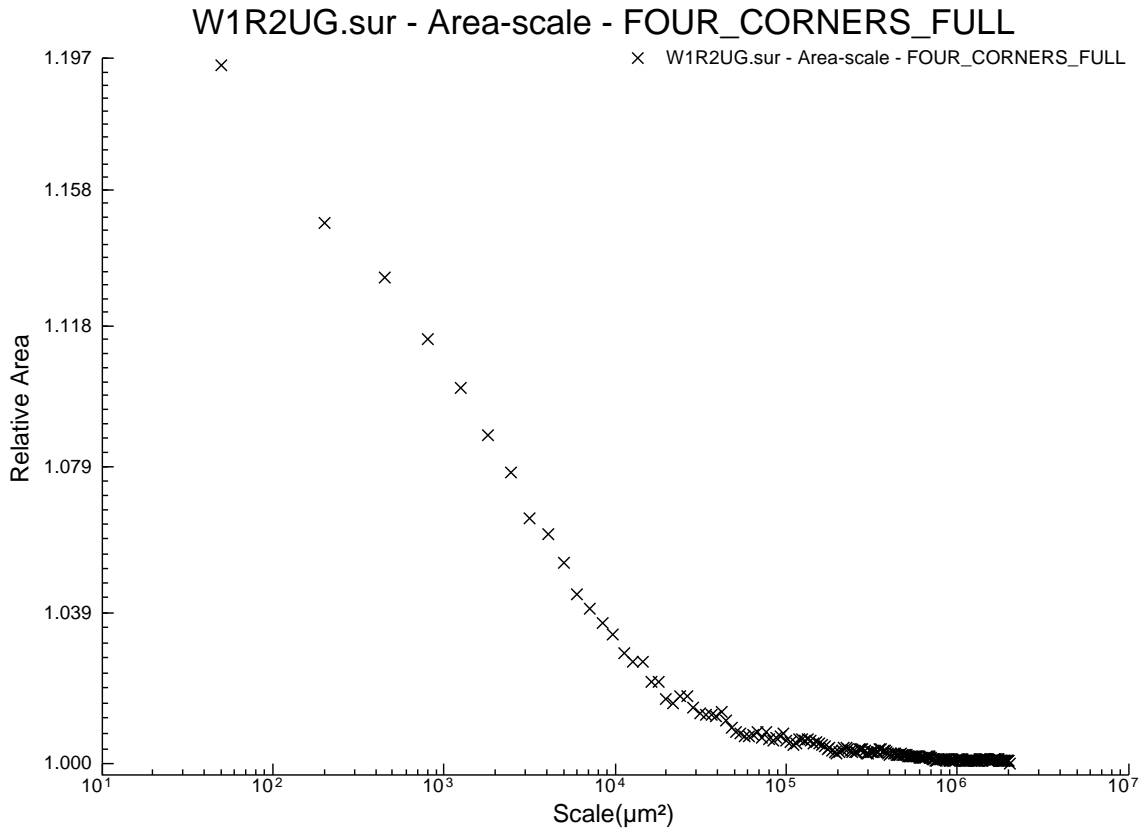
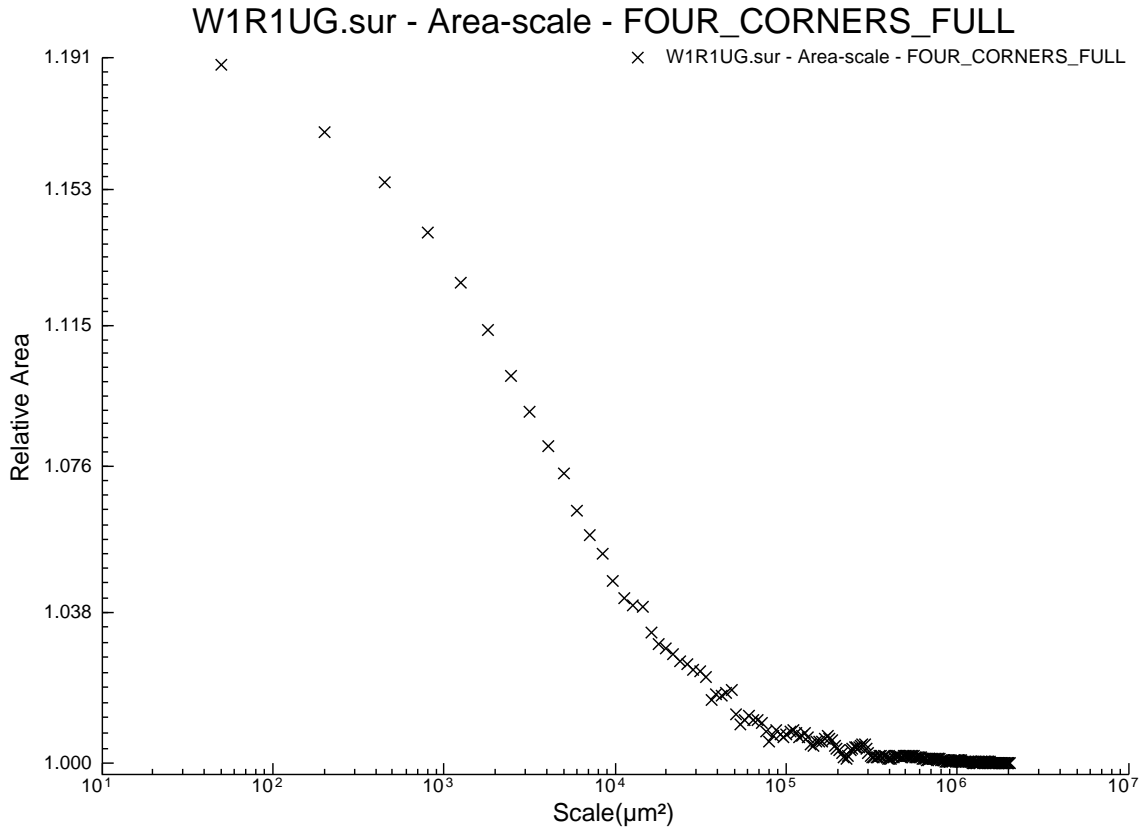


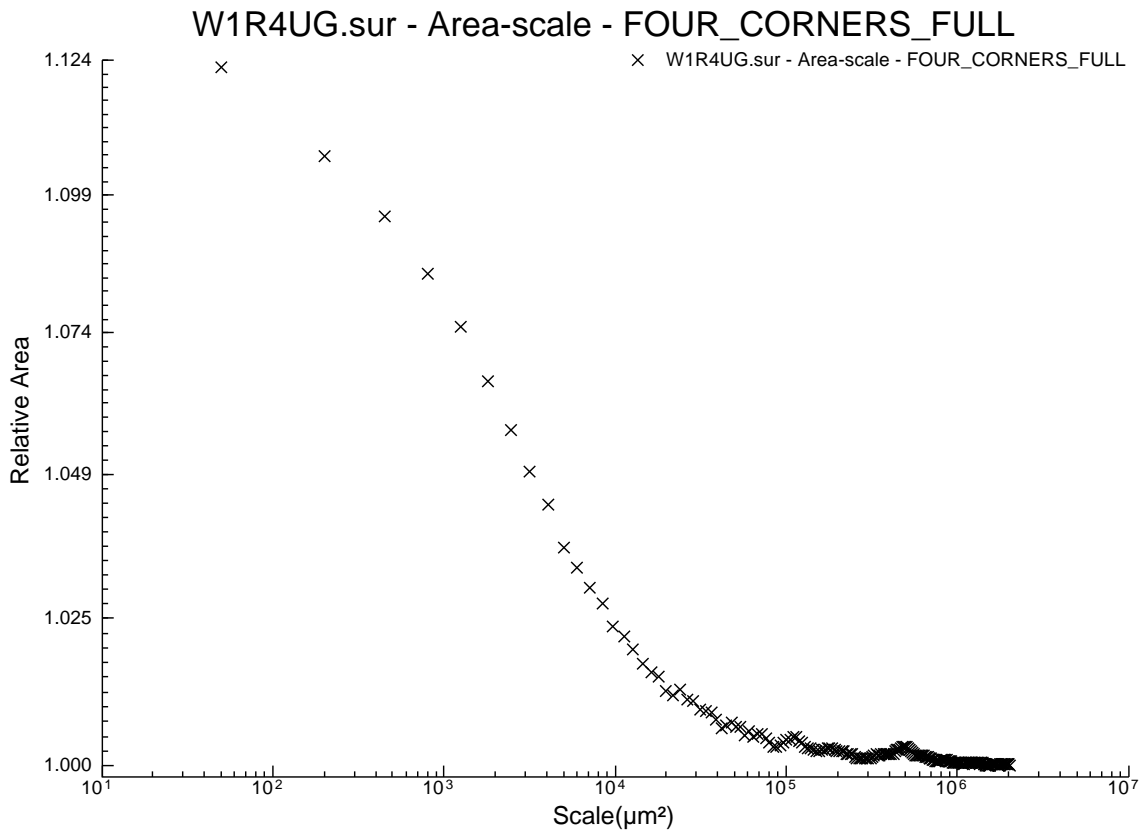
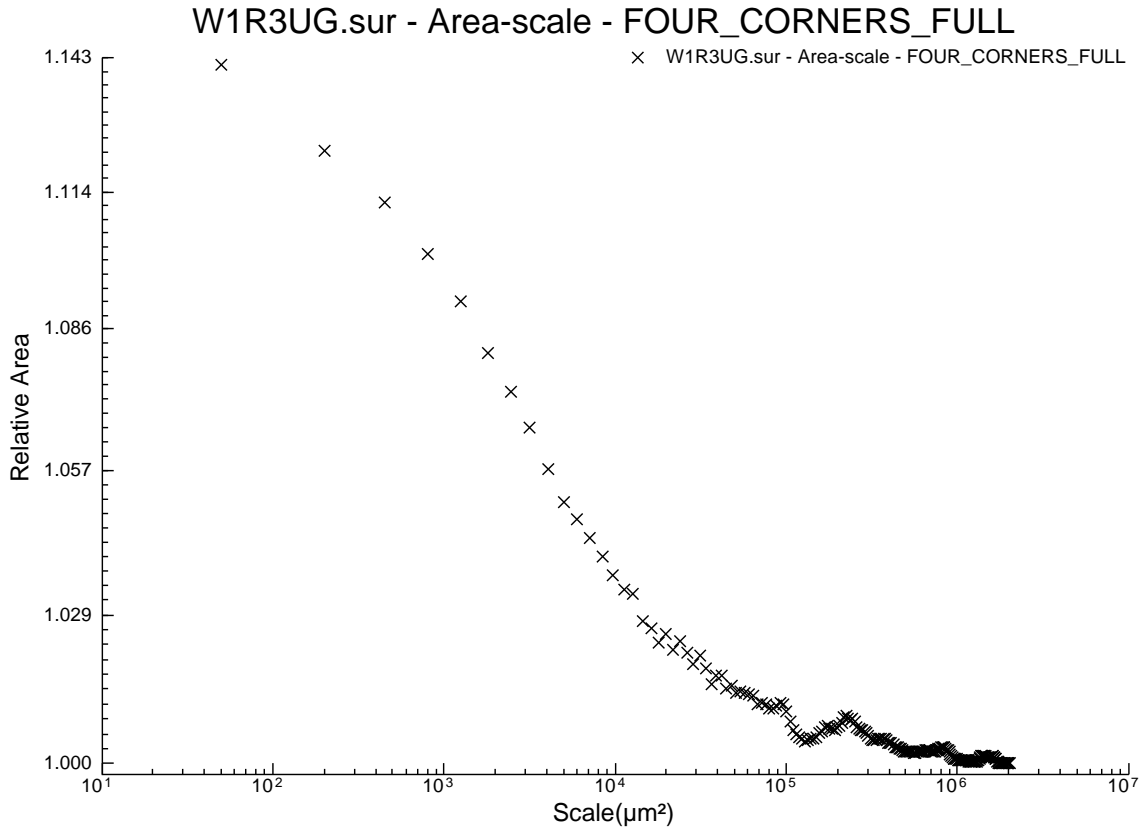


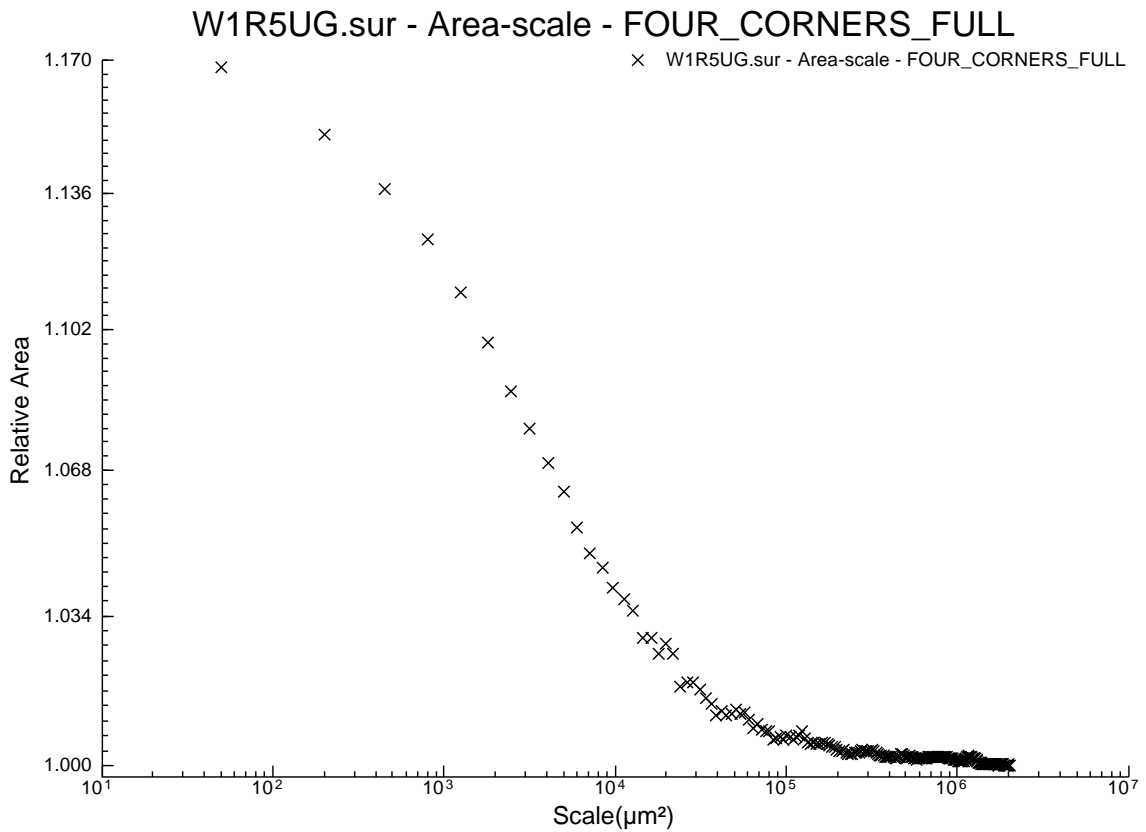
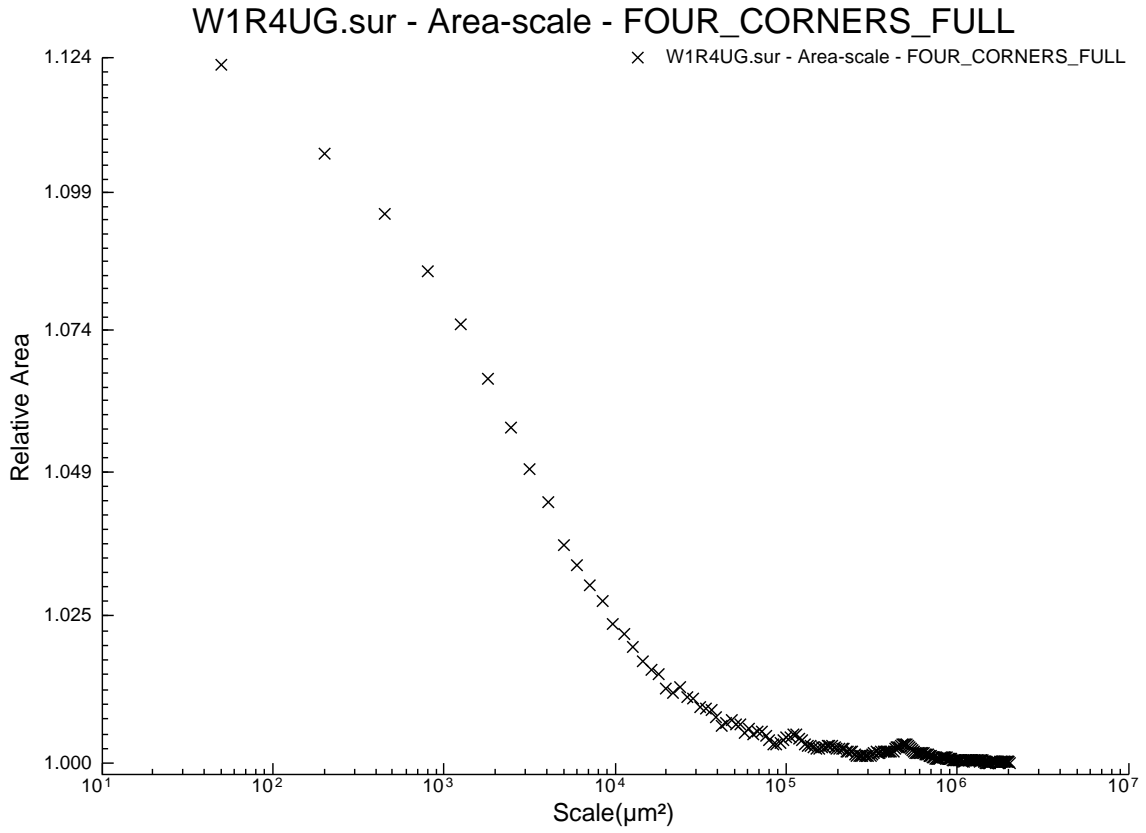




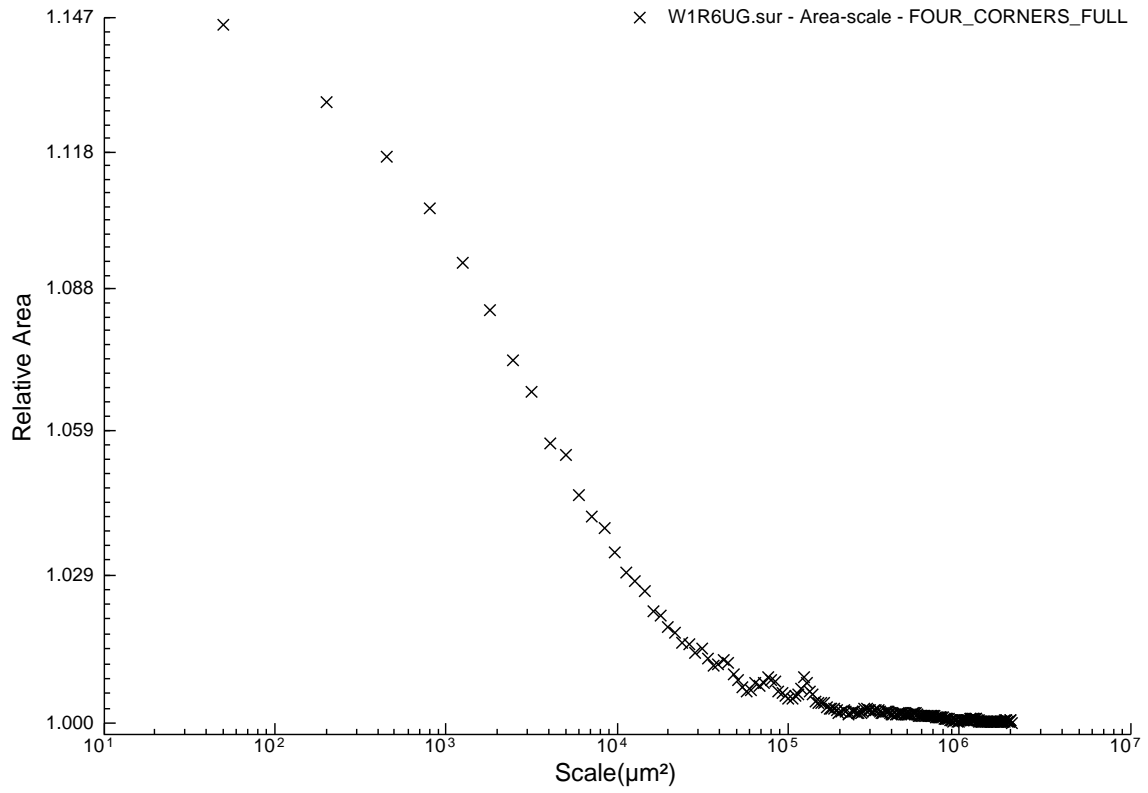




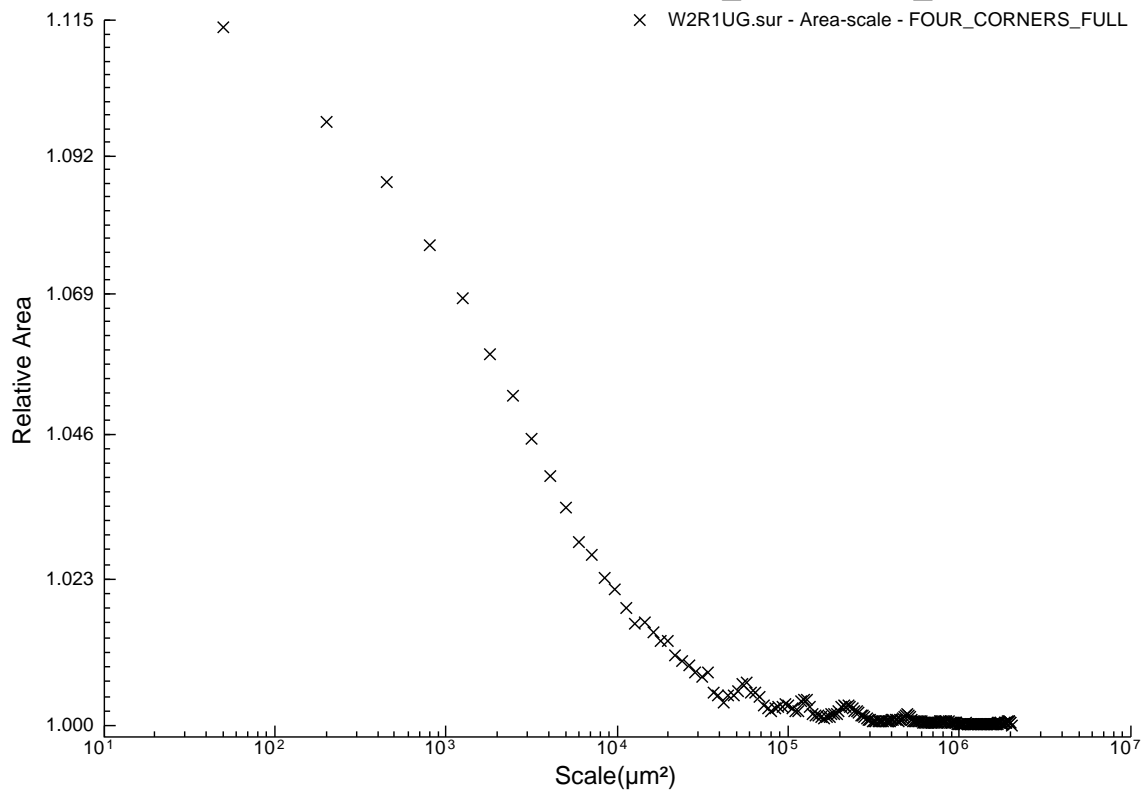


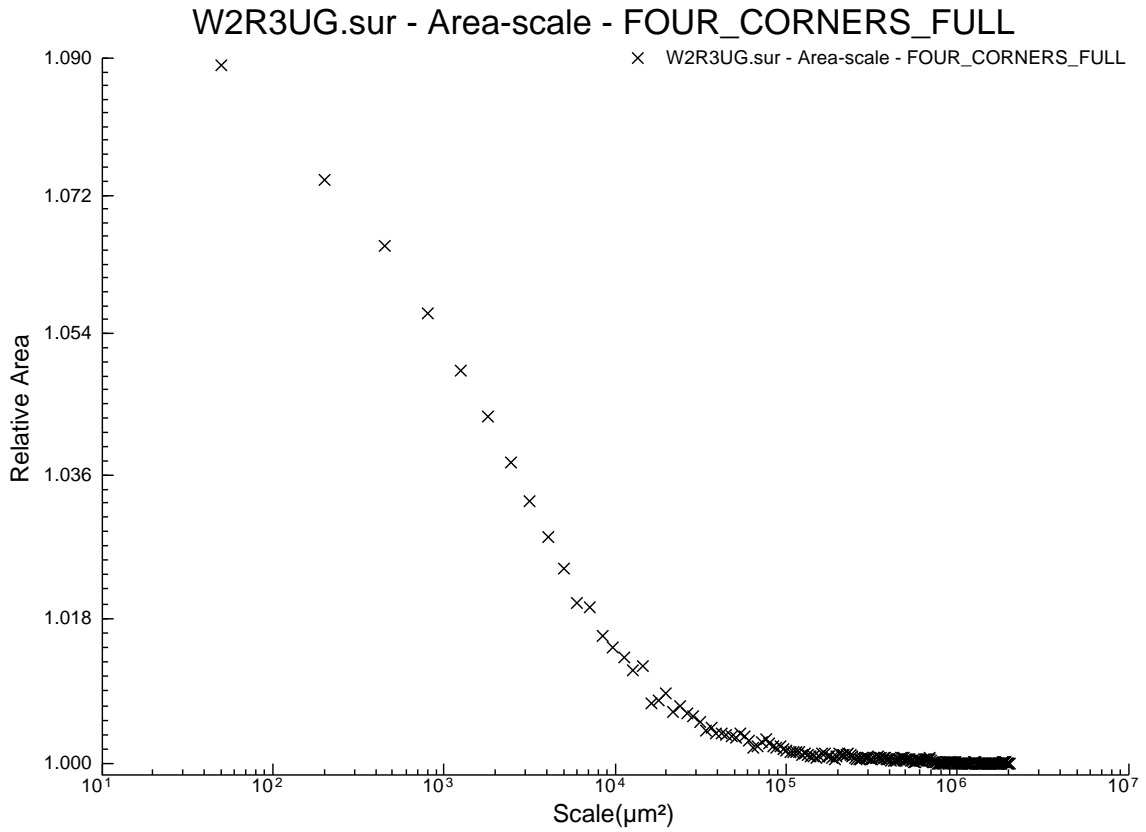
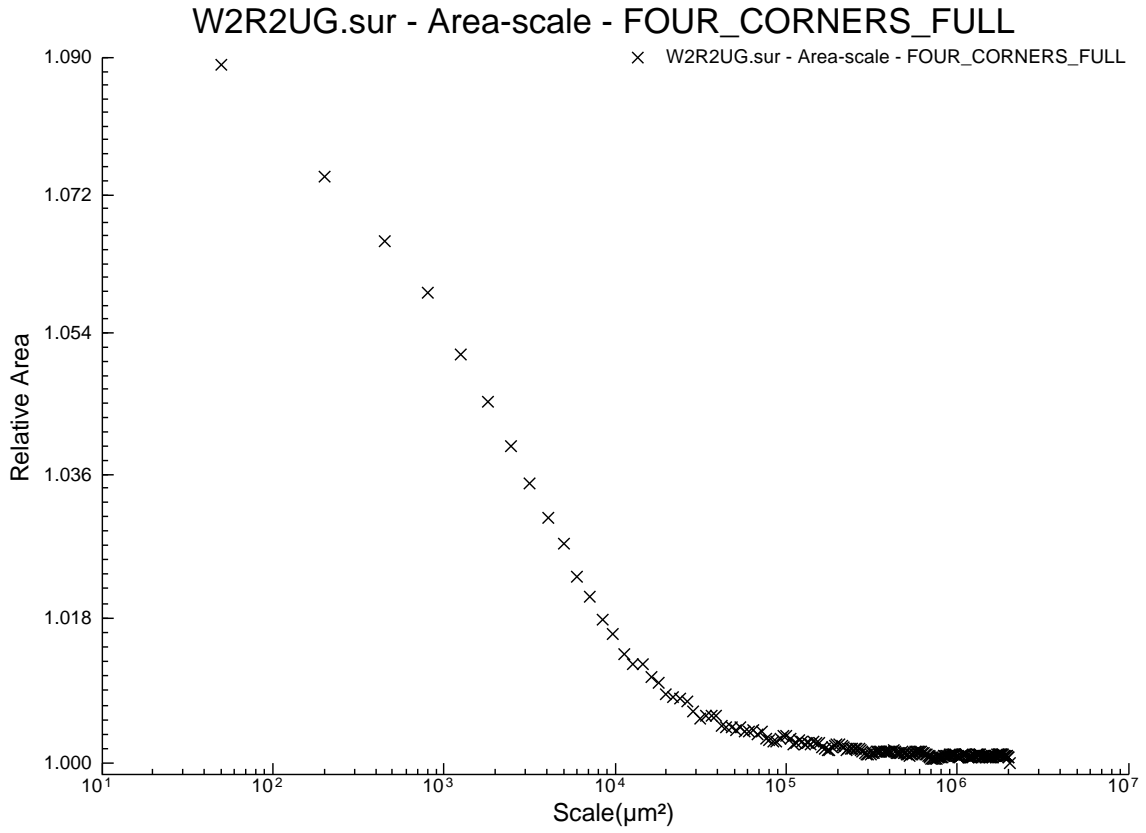


W1R6UG.sur - Area-scale - FOUR\_CORNERS\_FULL

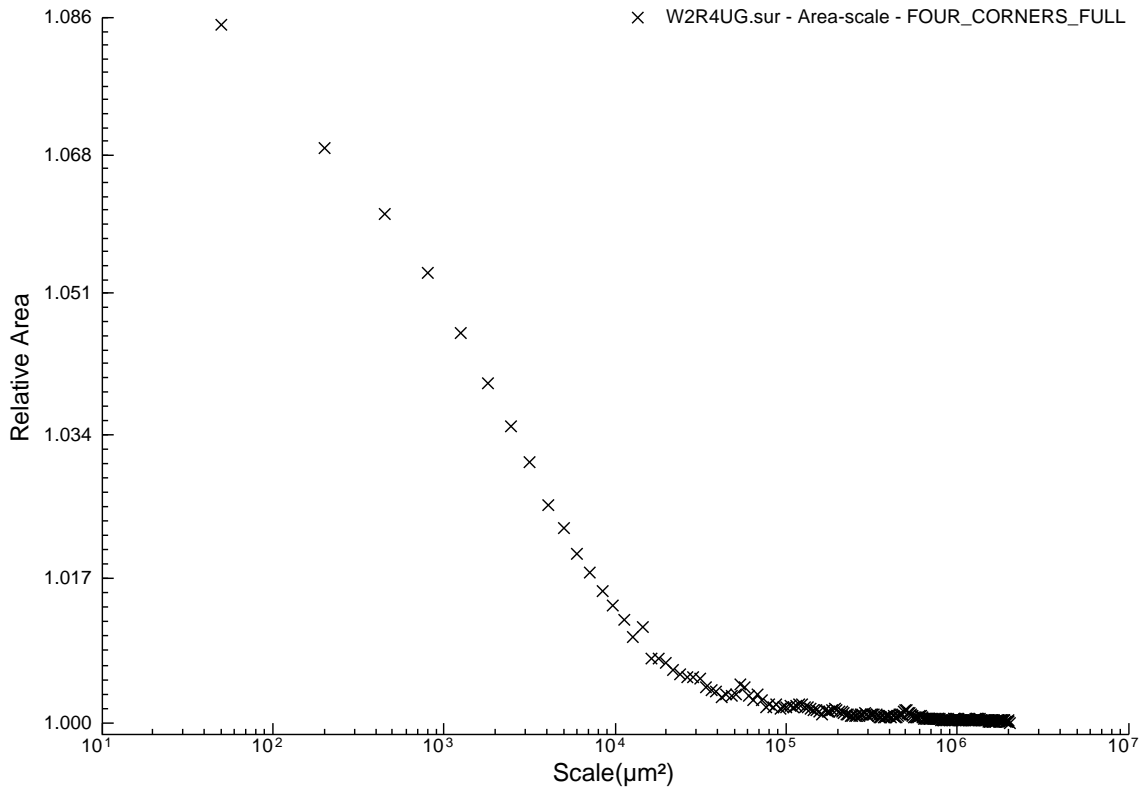


W2R1UG.sur - Area-scale - FOUR\_CORNERS\_FULL

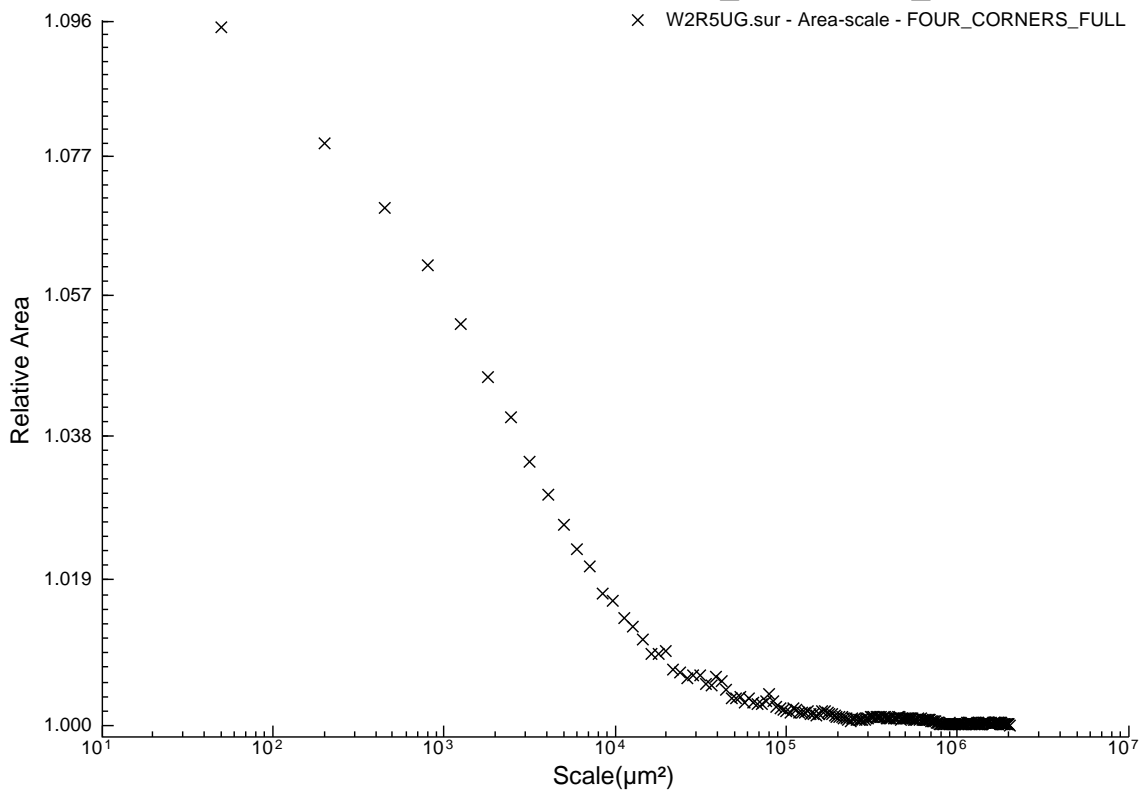


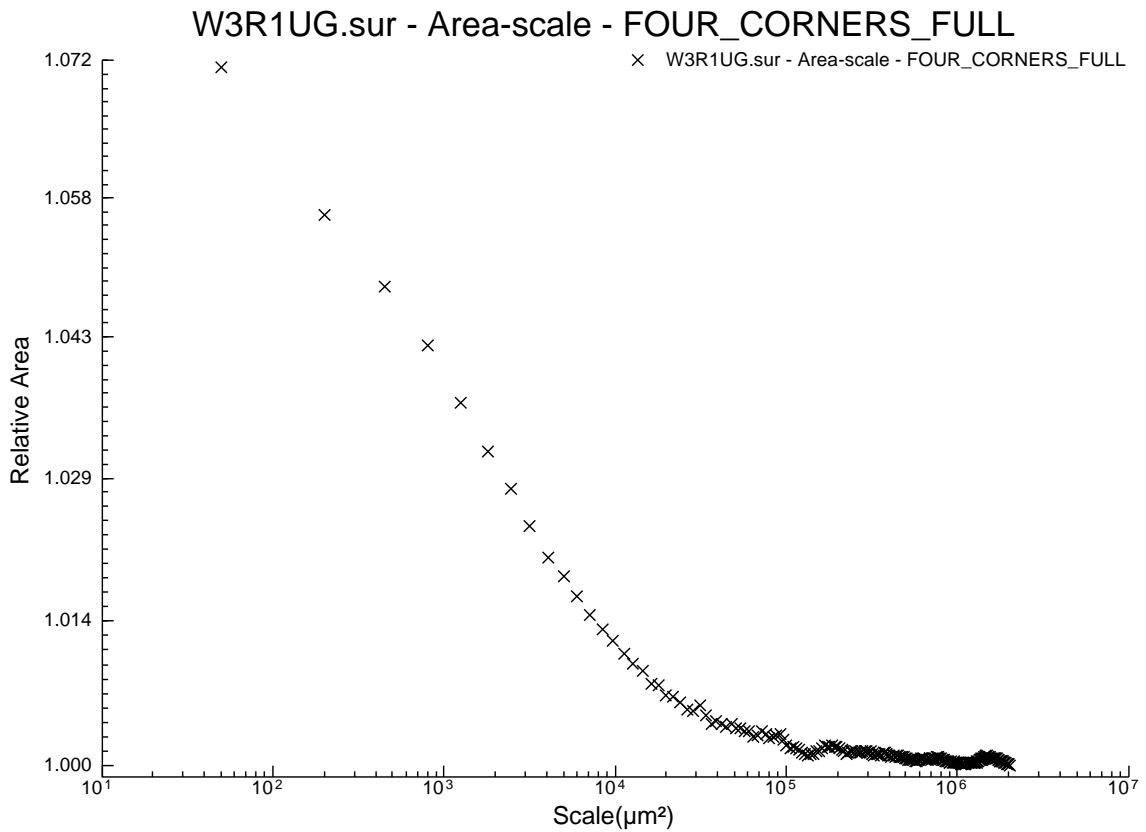
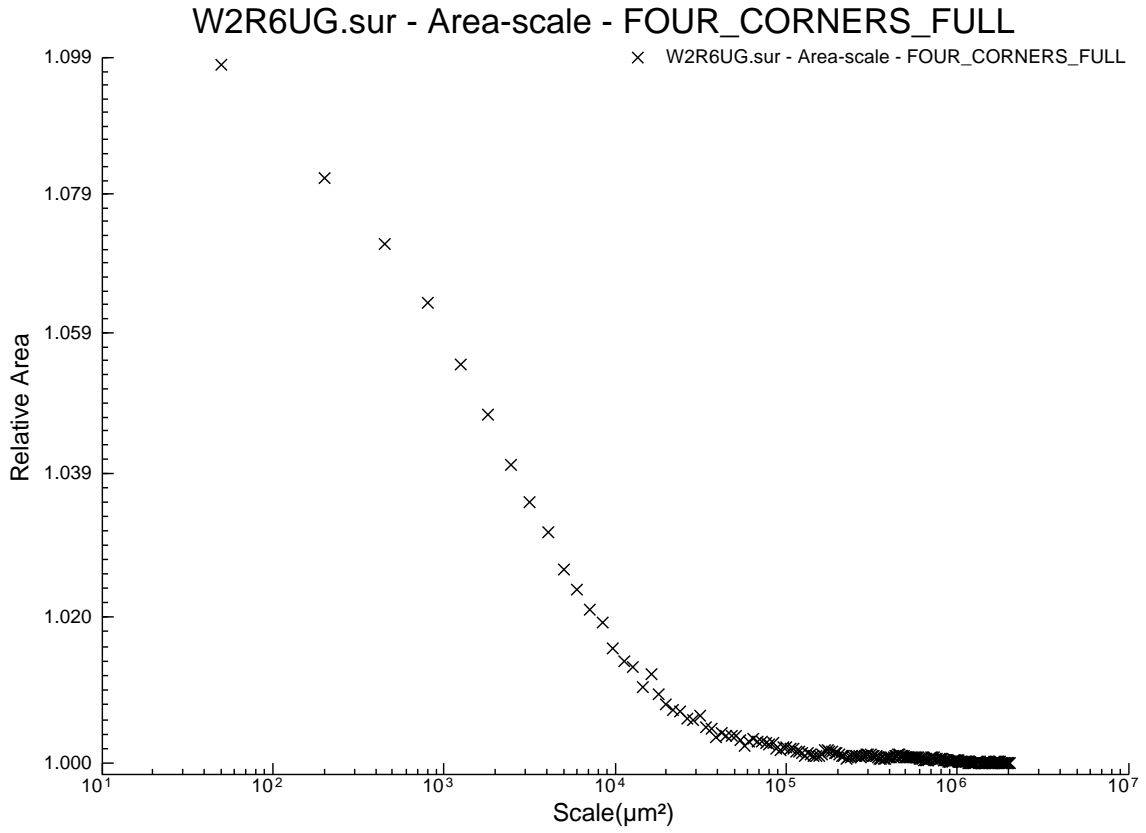


W2R4UG.sur - Area-scale - FOUR\_CORNERS\_FULL

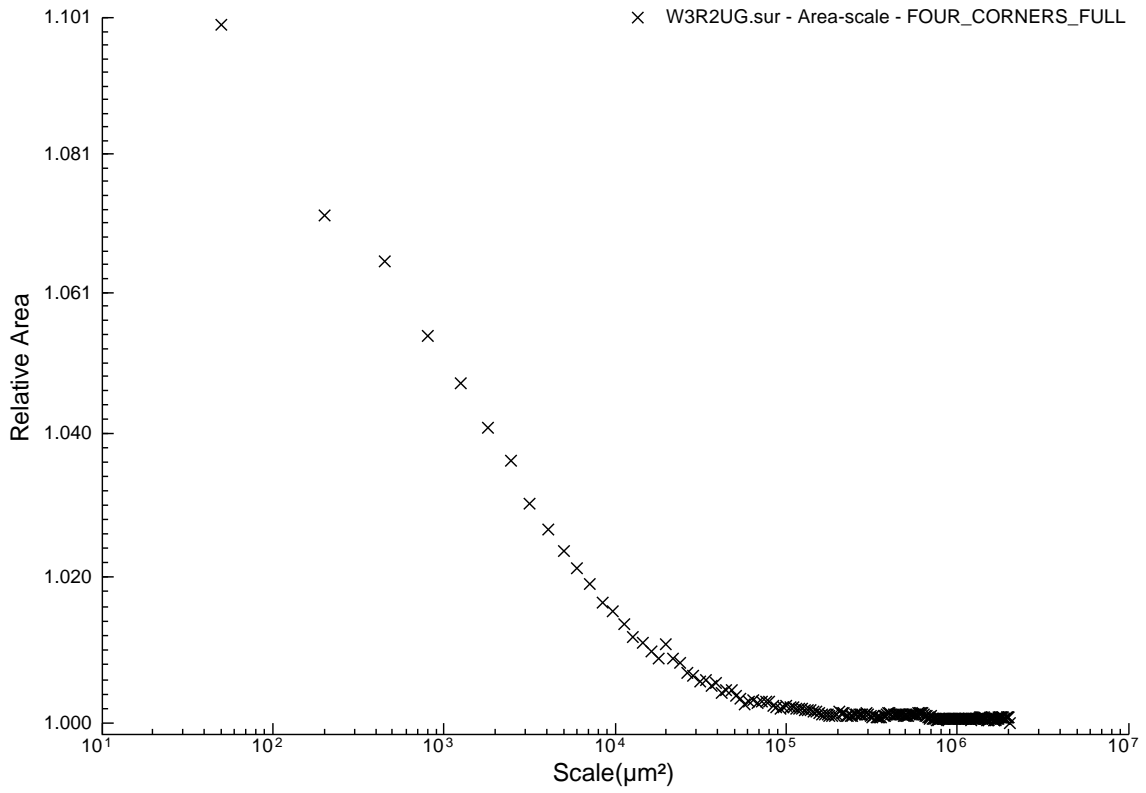


W2R5UG.sur - Area-scale - FOUR\_CORNERS\_FULL

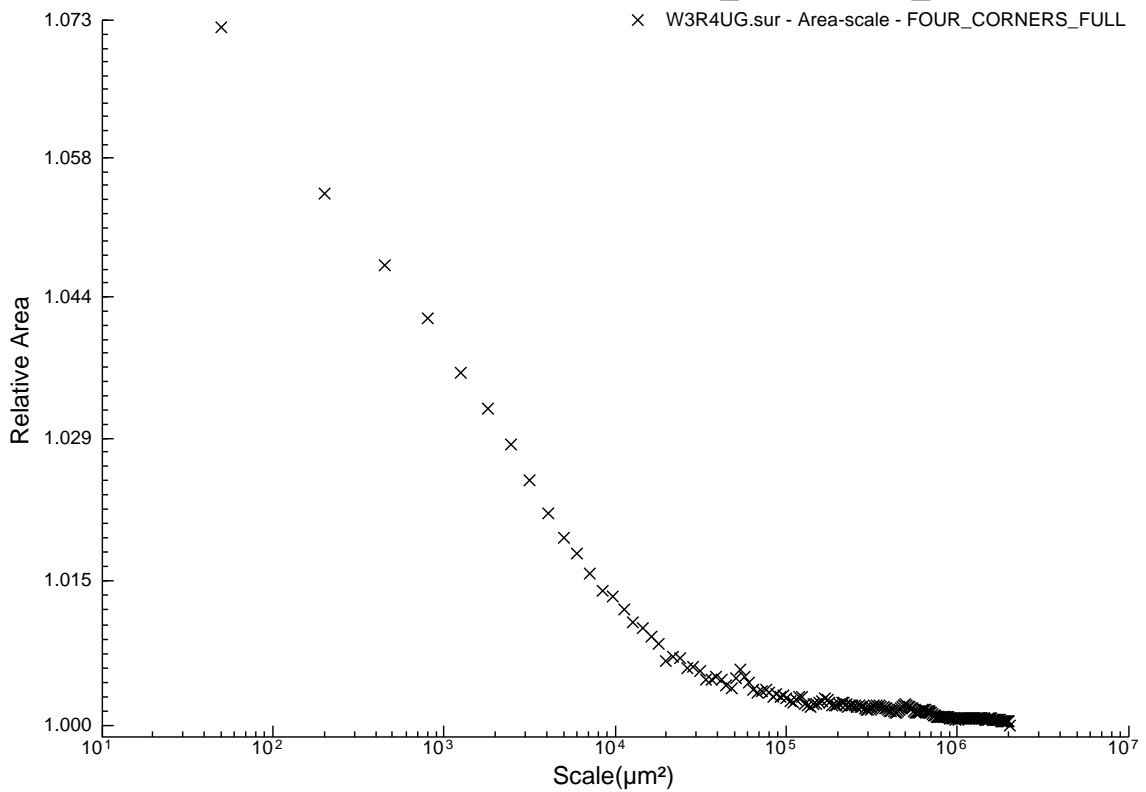




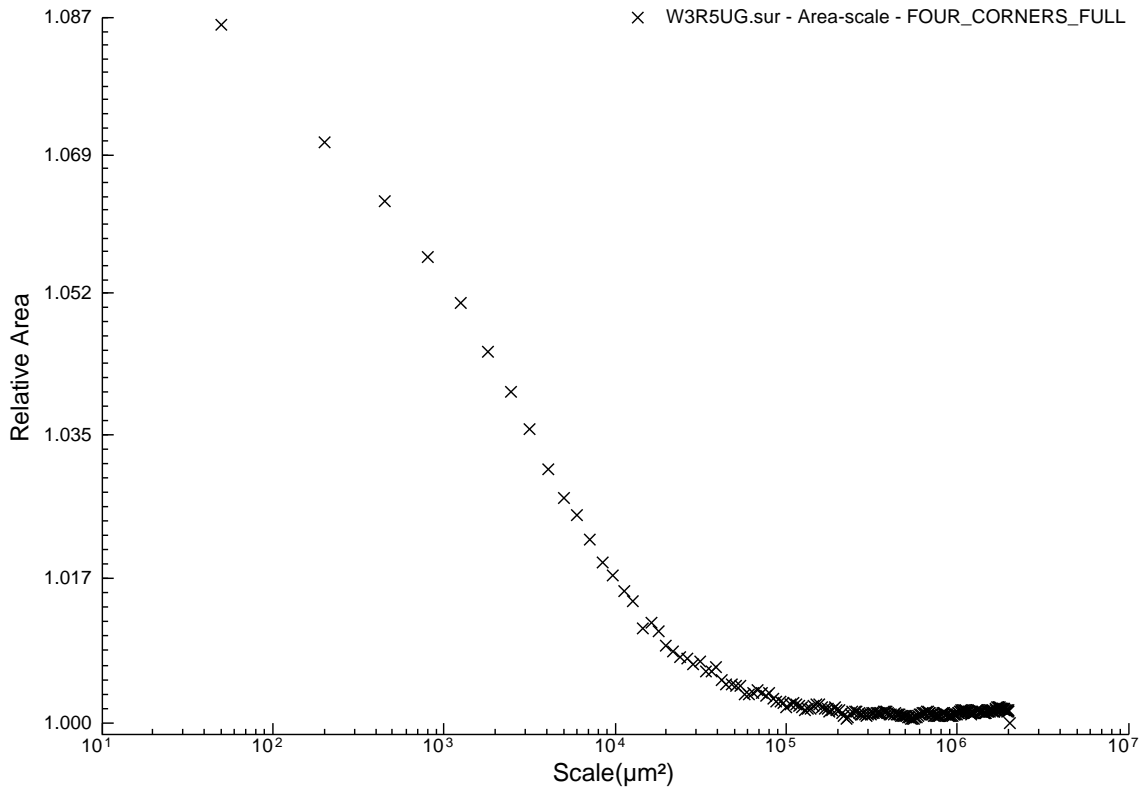
W3R2UG.sur - Area-scale - FOUR\_CORNERS\_FULL



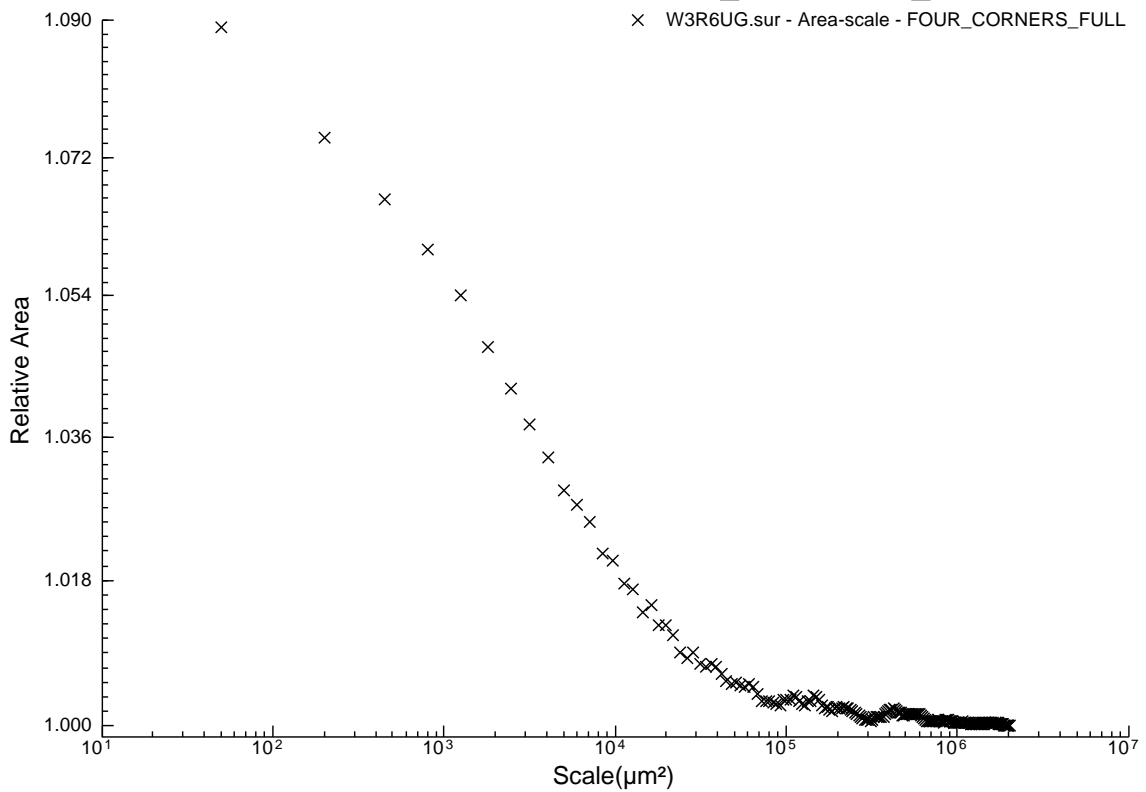
W3R4UG.sur - Area-scale - FOUR\_CORNERS\_FULL

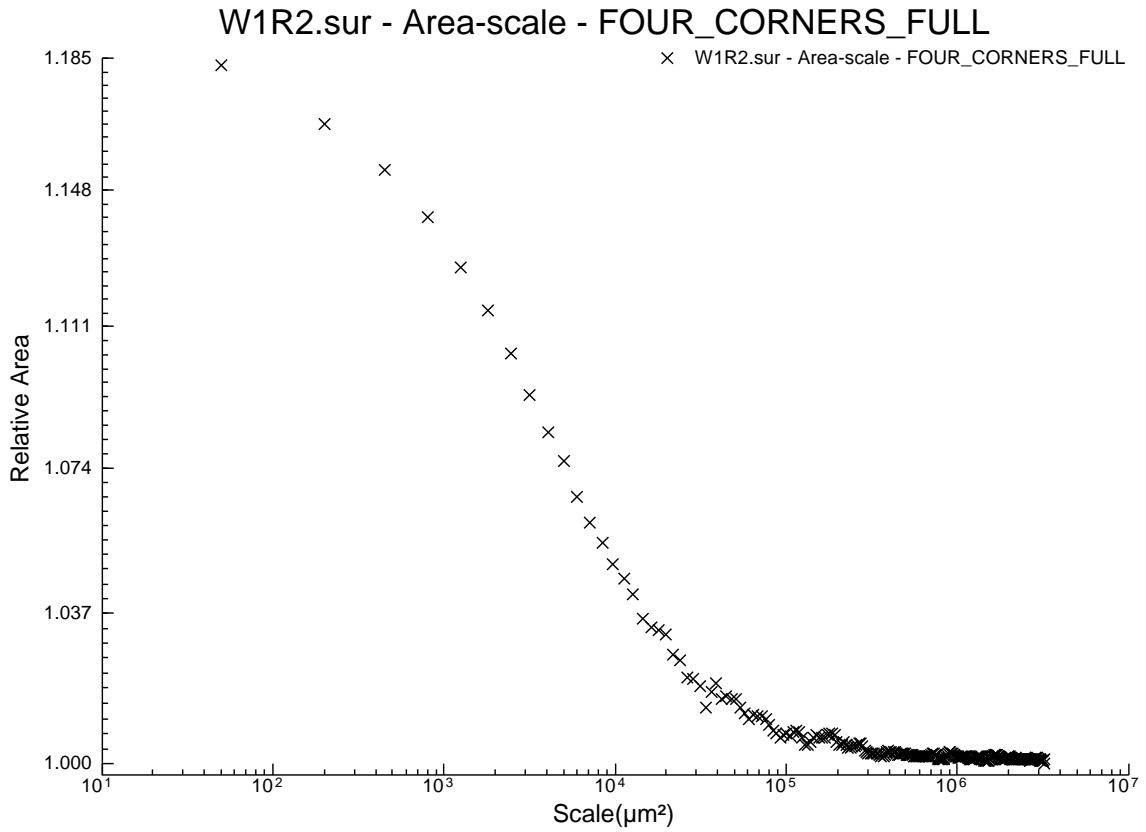
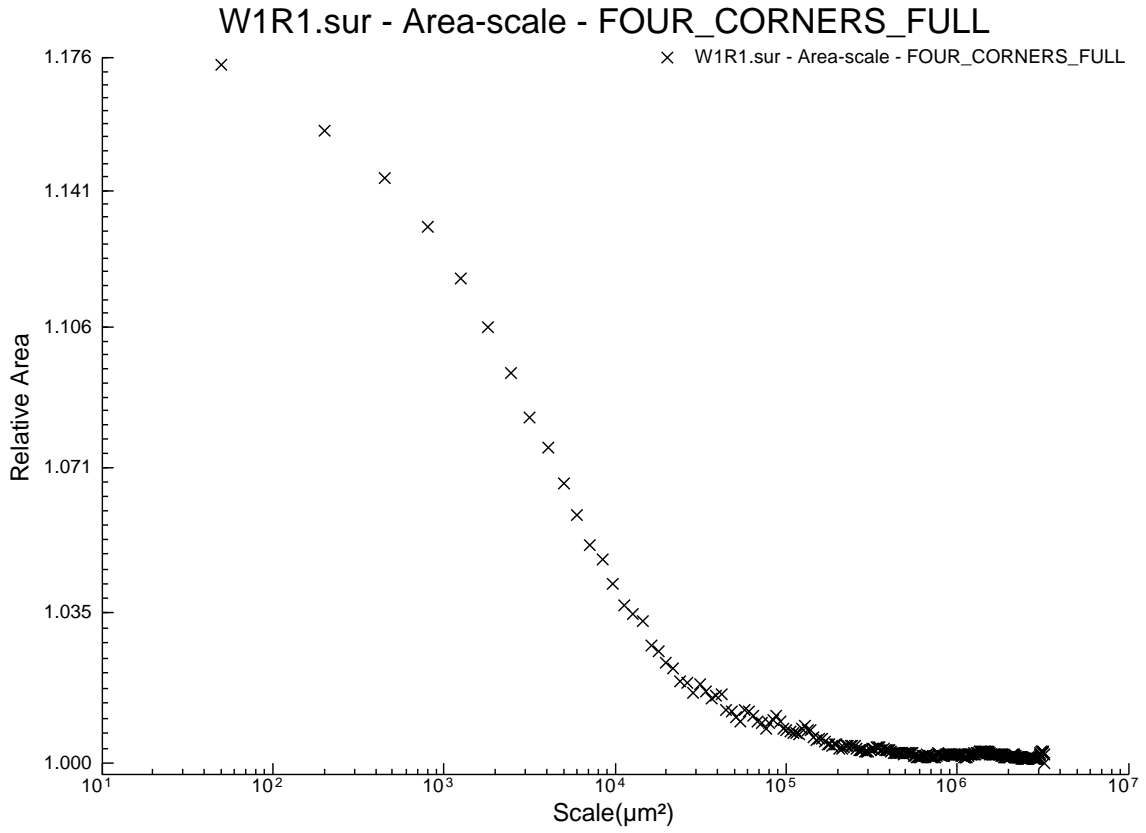


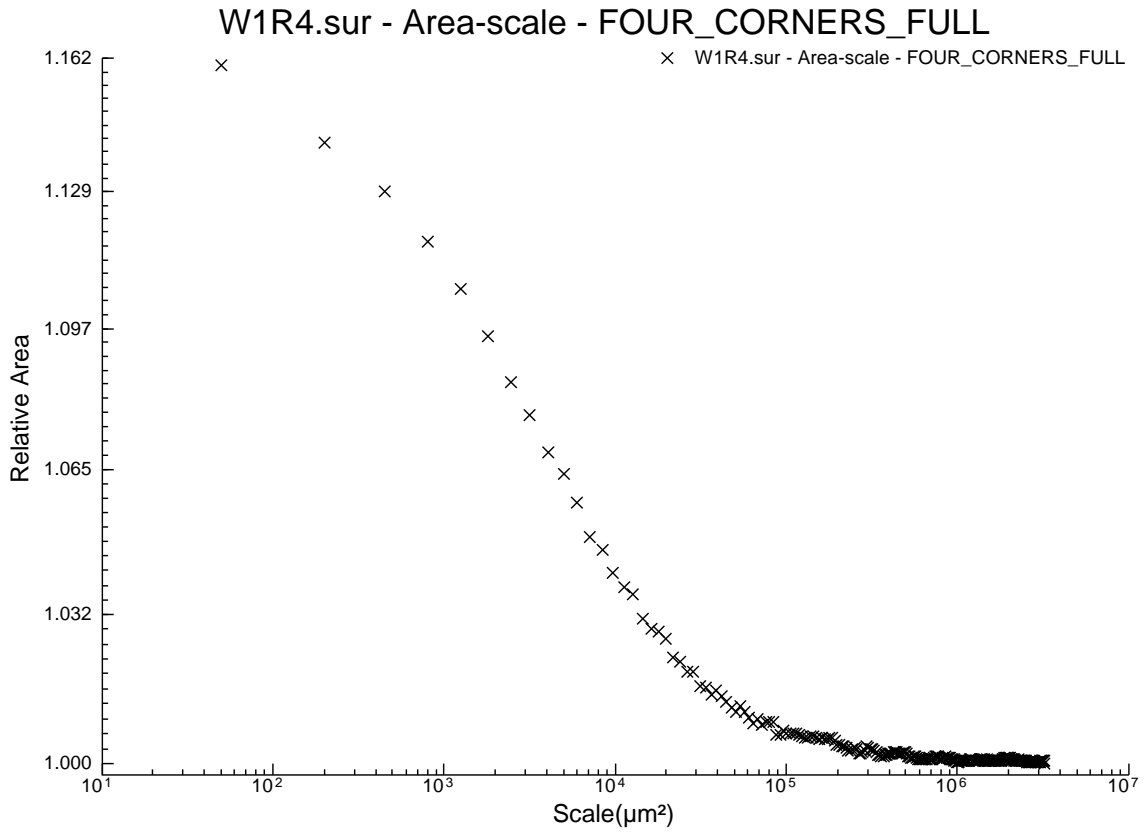
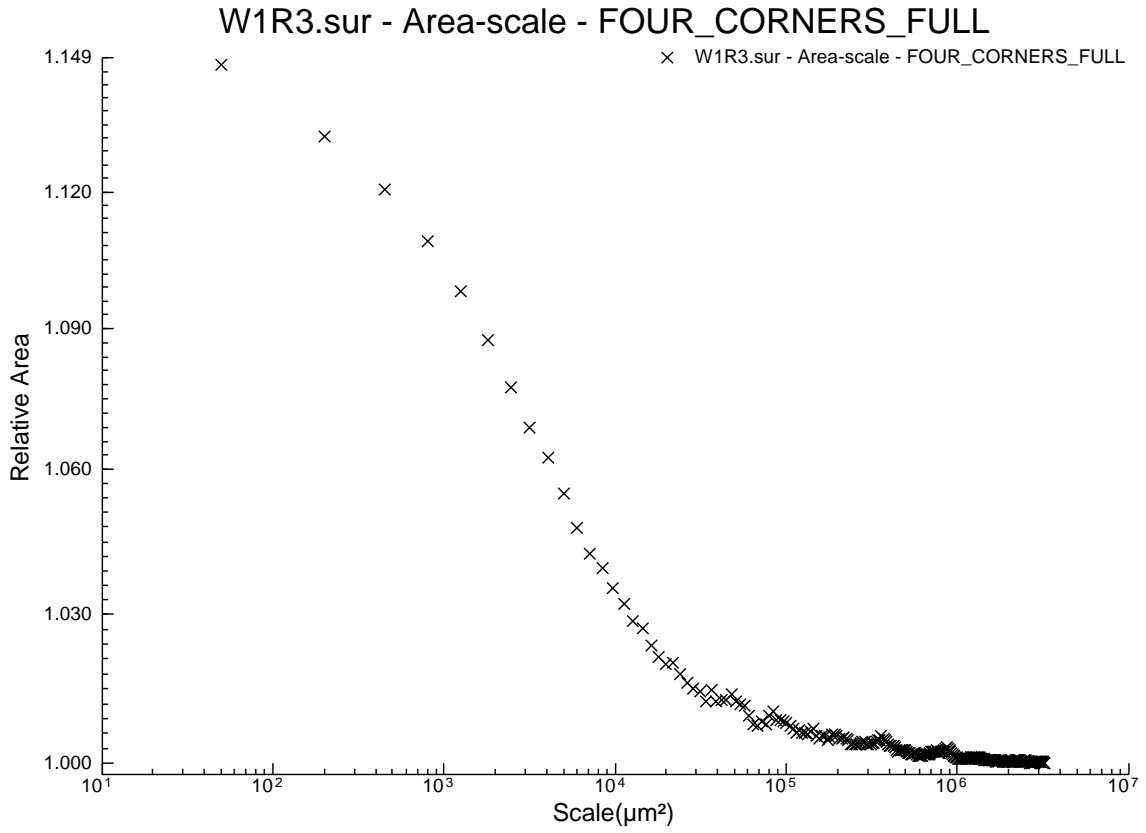
W3R5UG.sur - Area-scale - FOUR\_CORNERS\_FULL

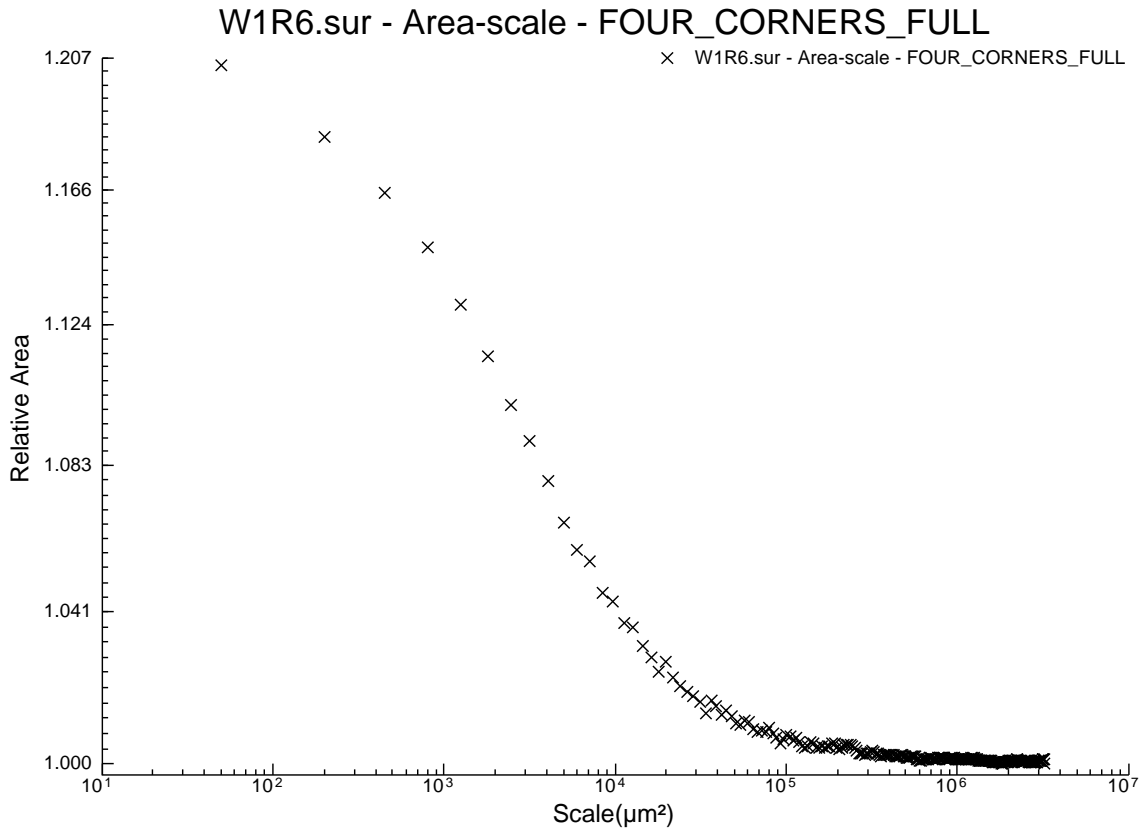
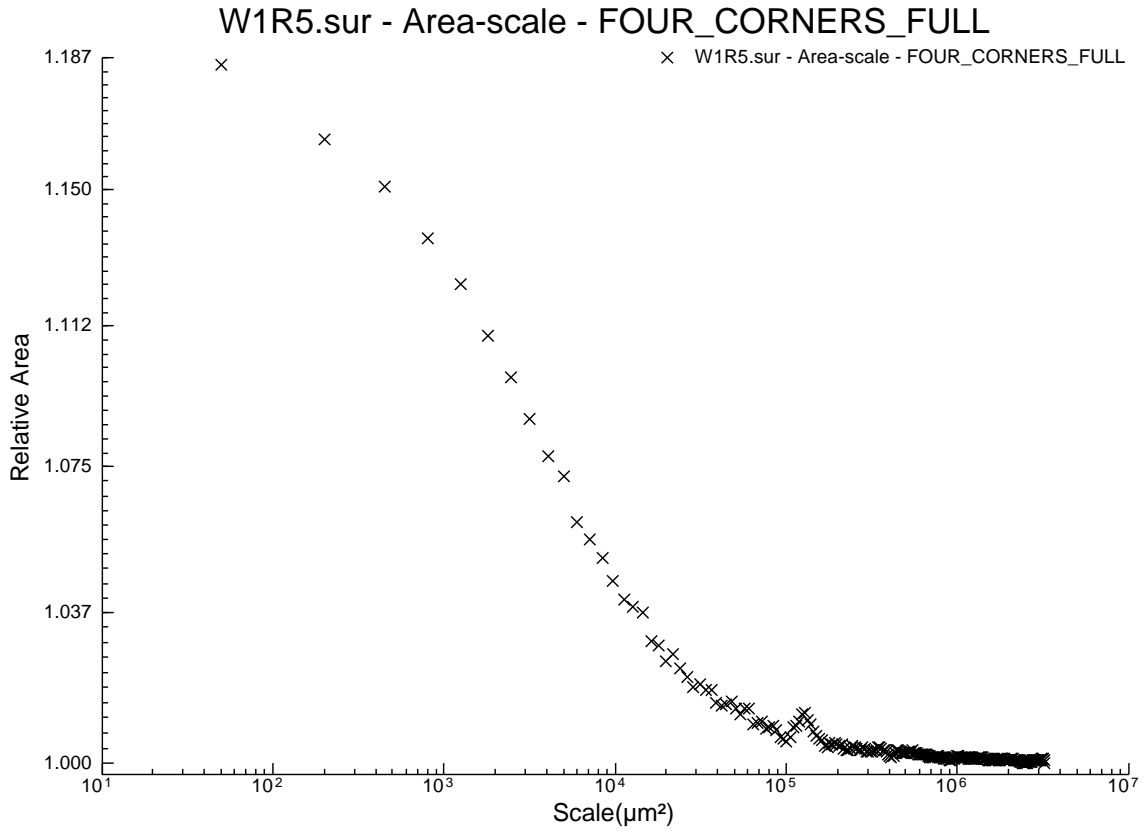


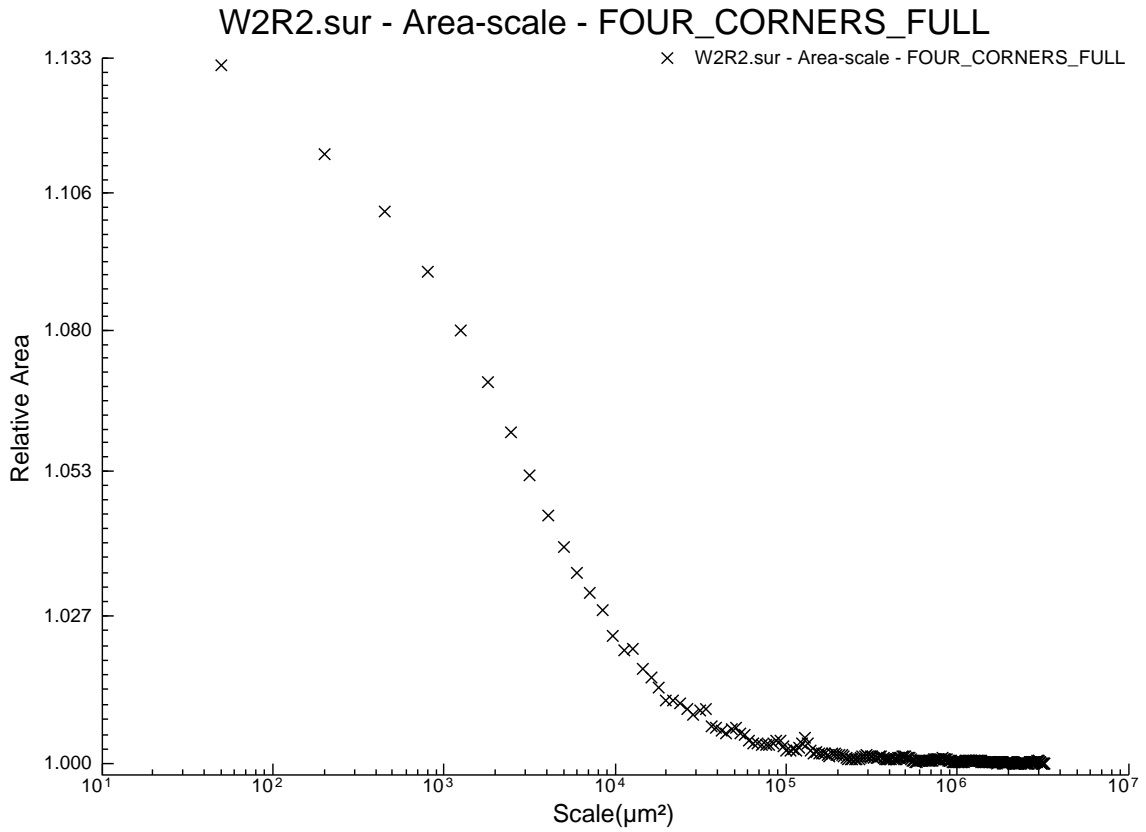
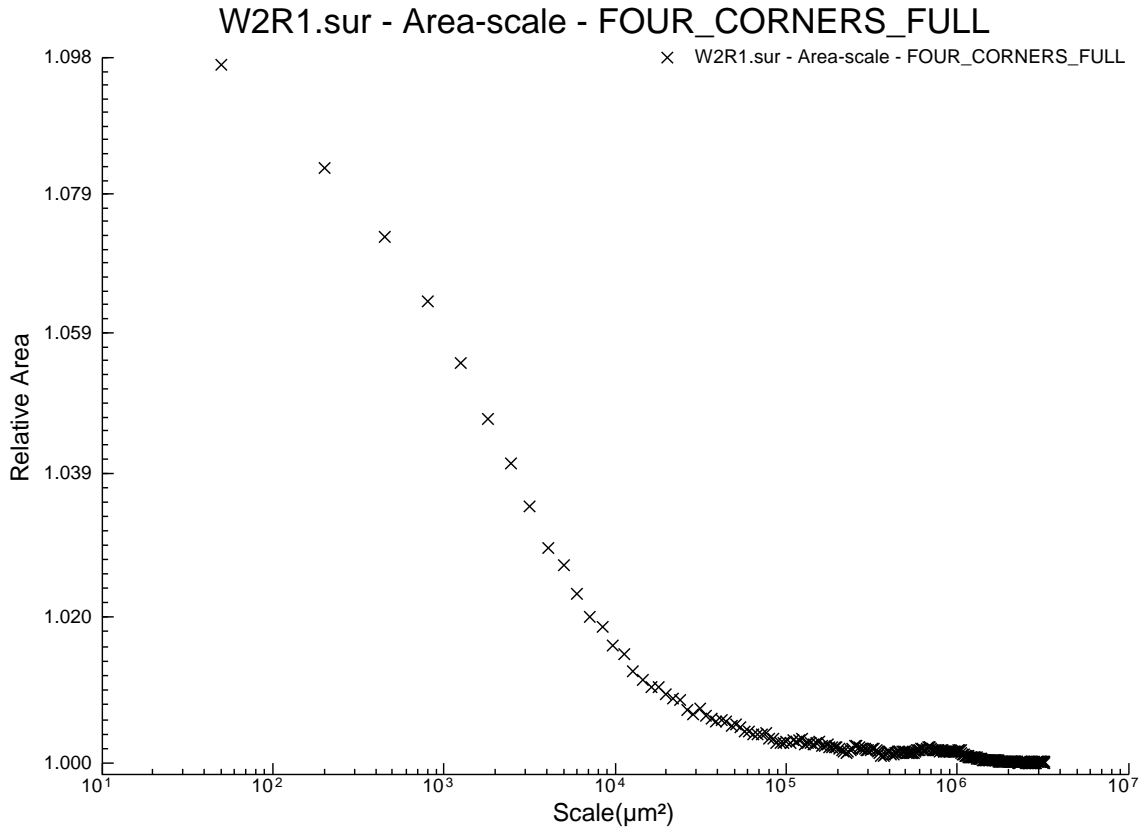
W3R6UG.sur - Area-scale - FOUR\_CORNERS\_FULL

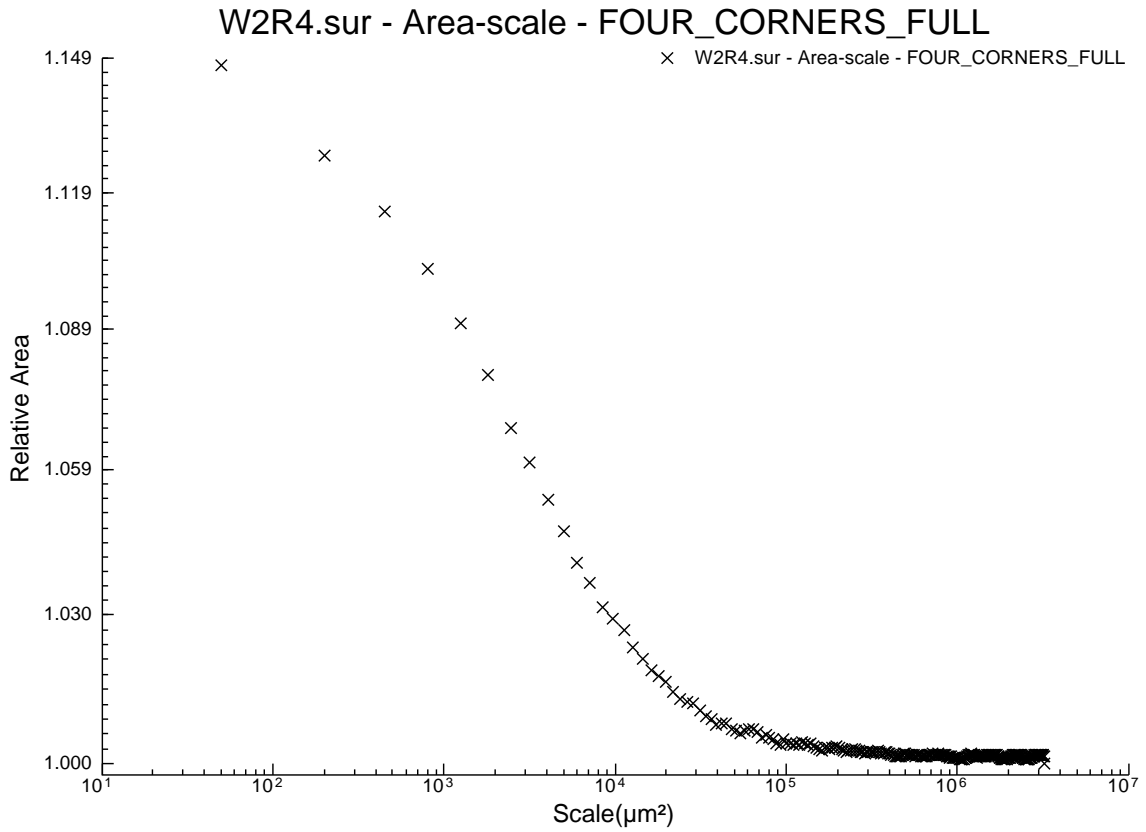
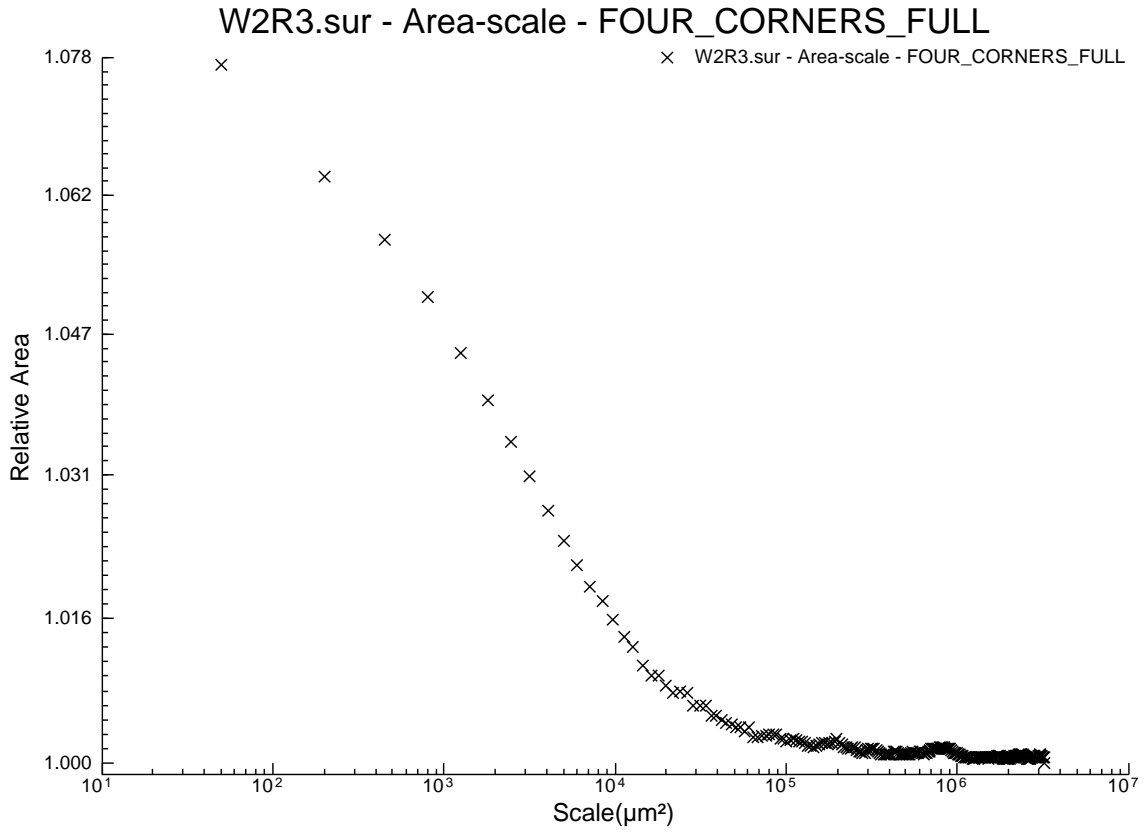


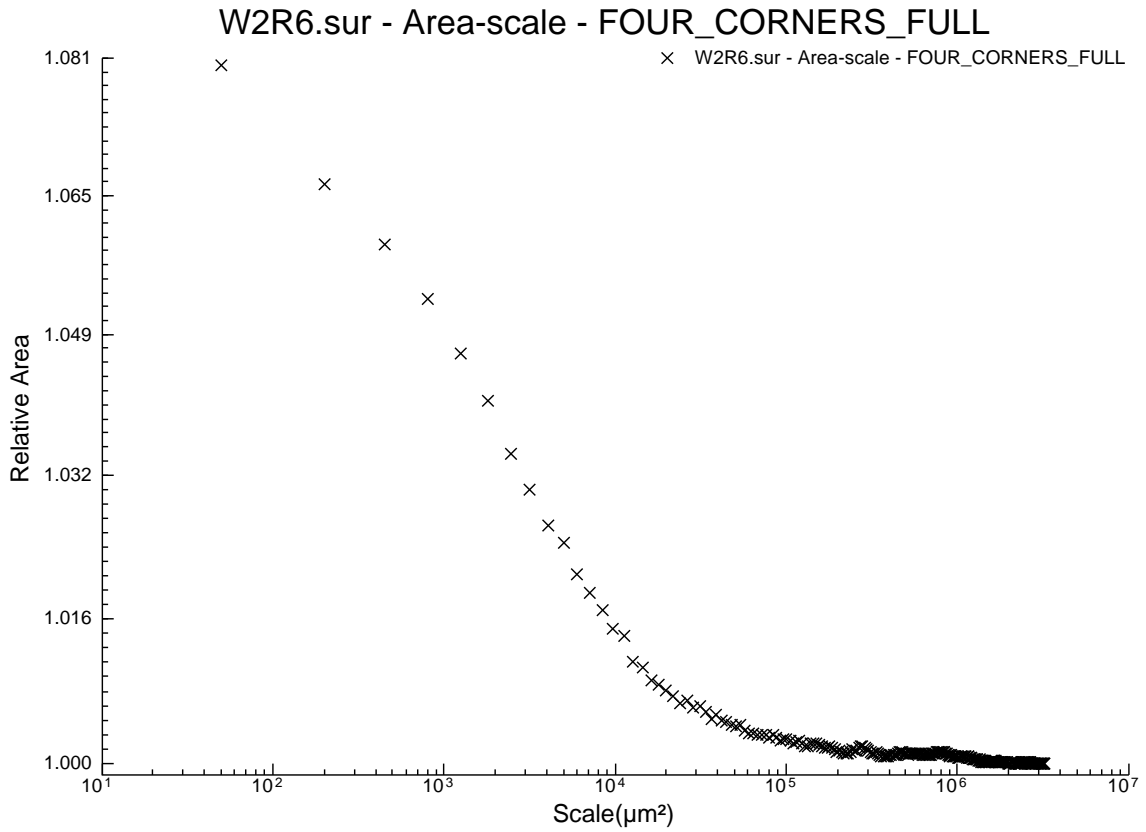
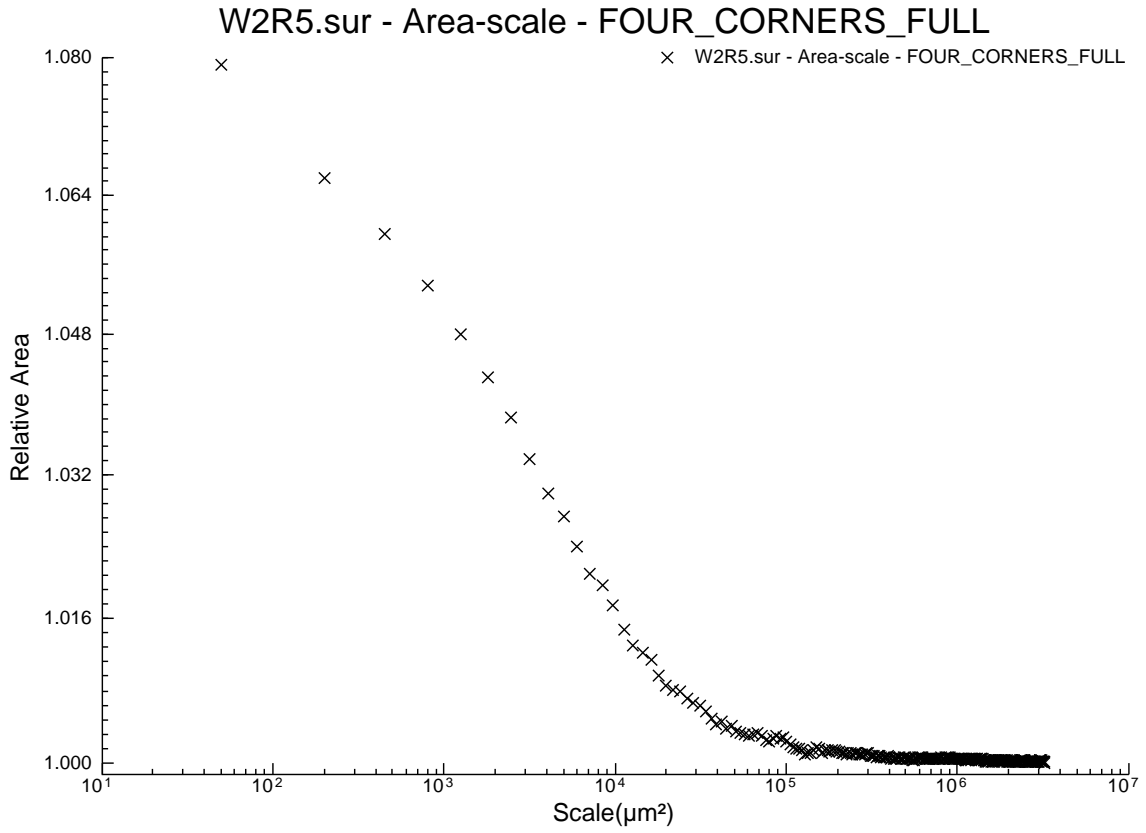


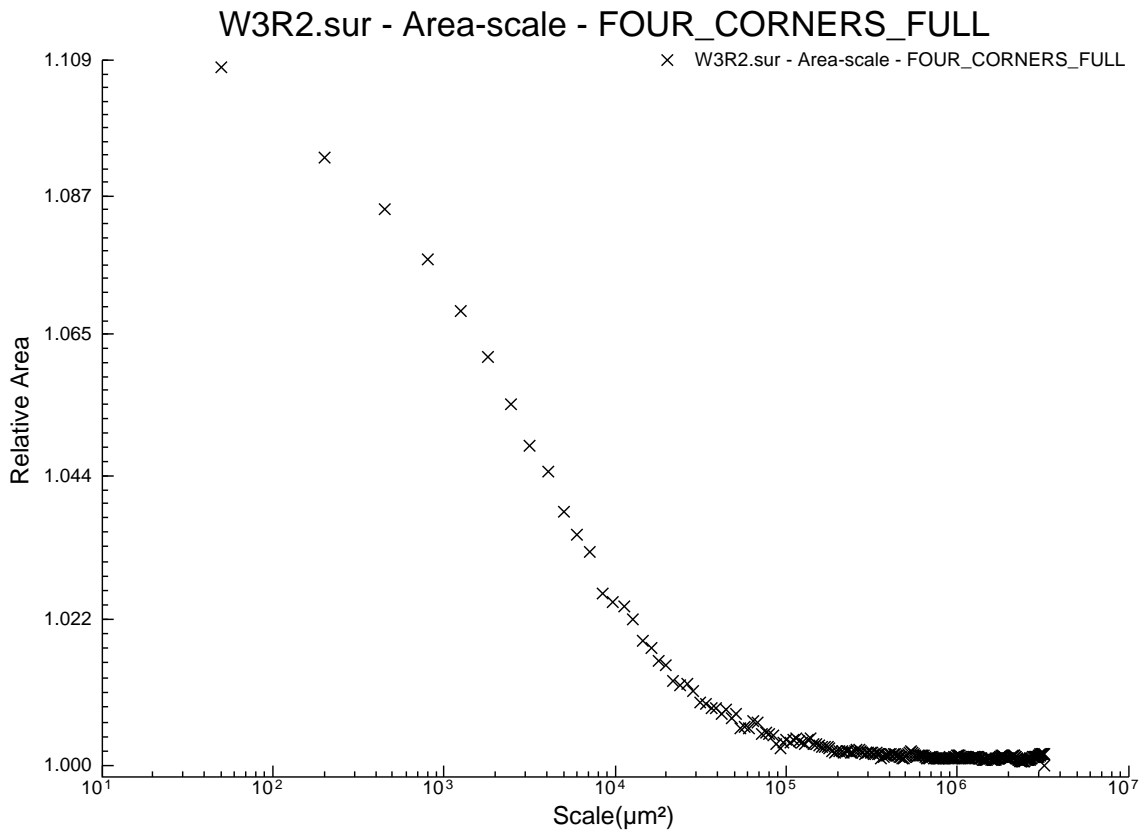
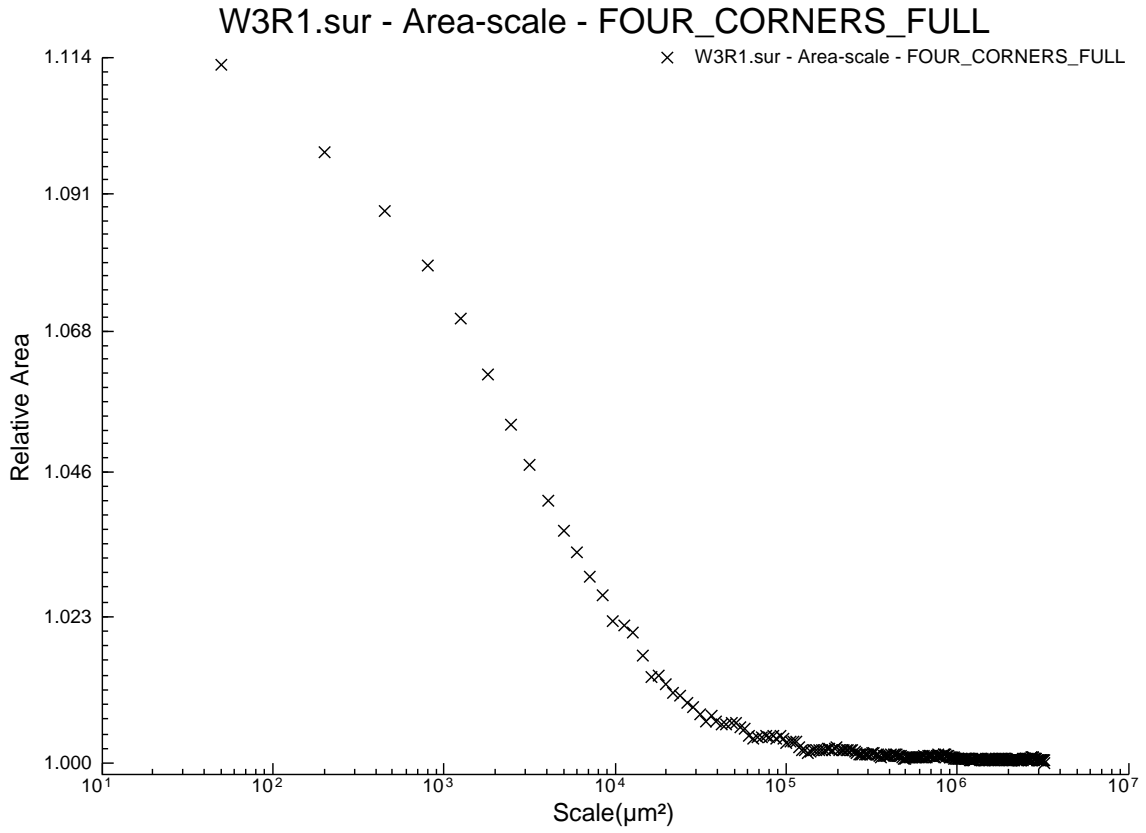


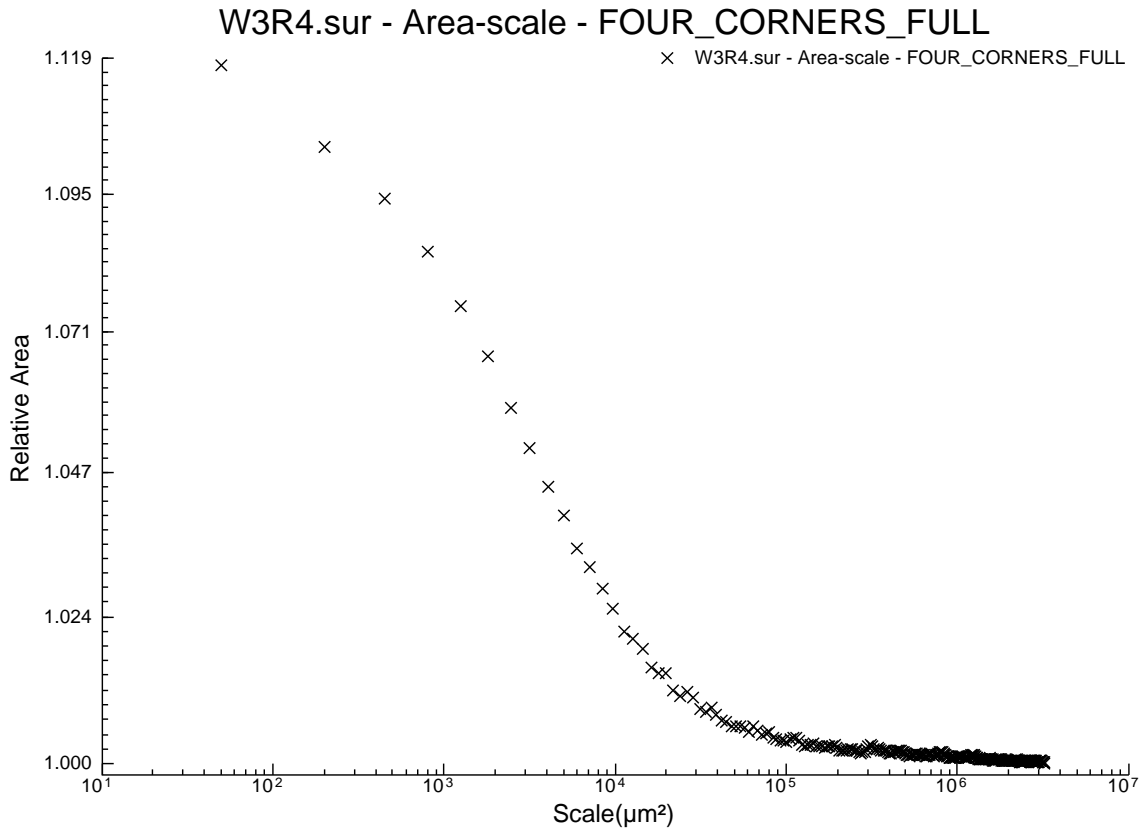
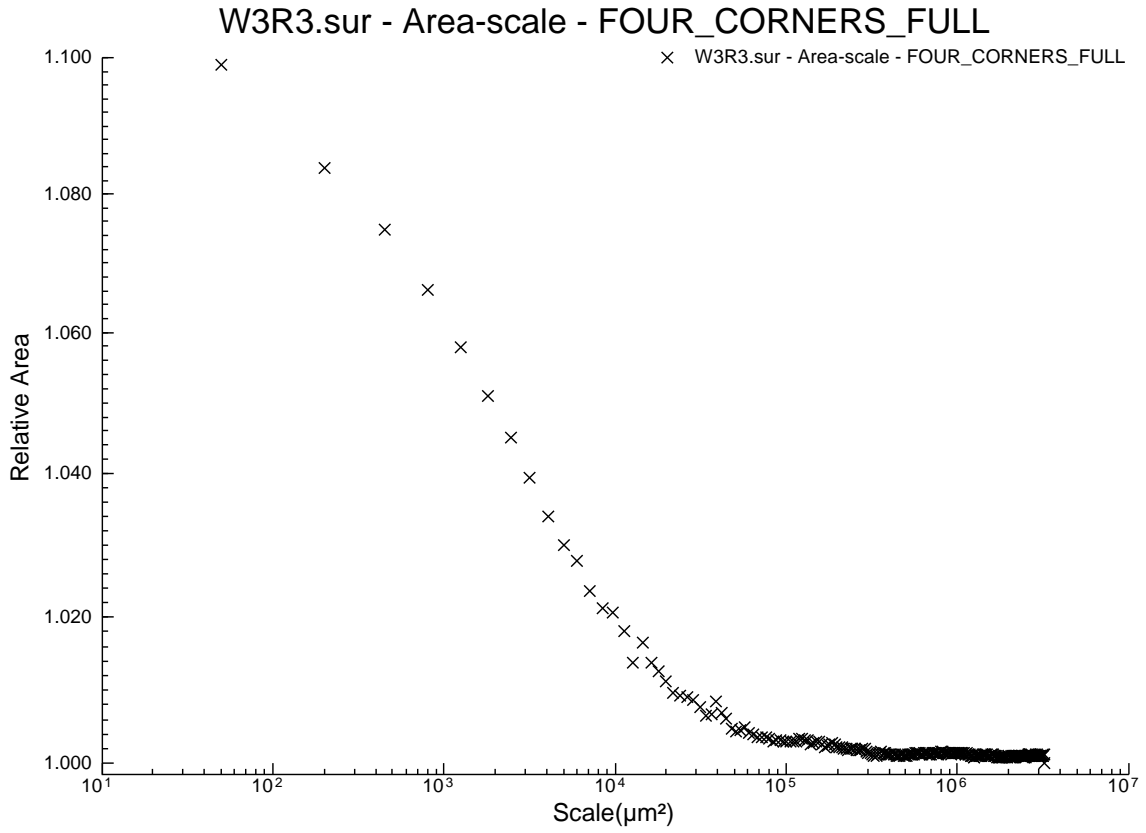


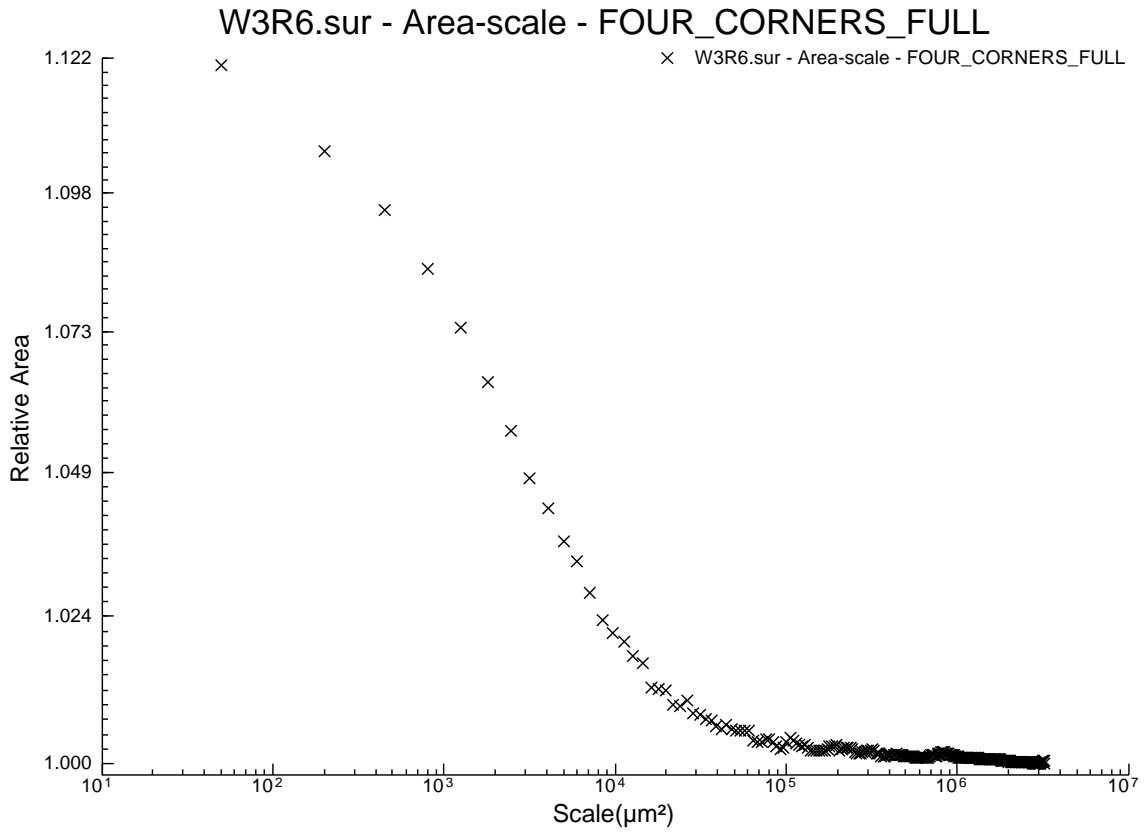
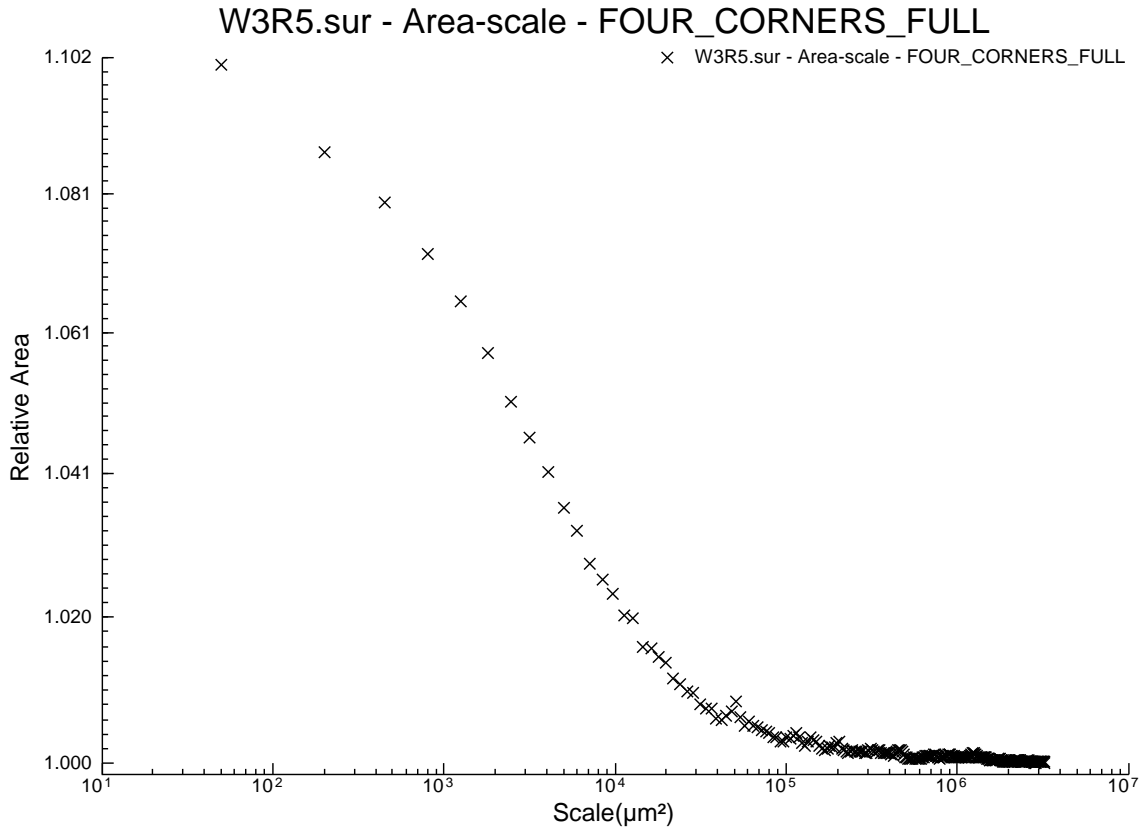






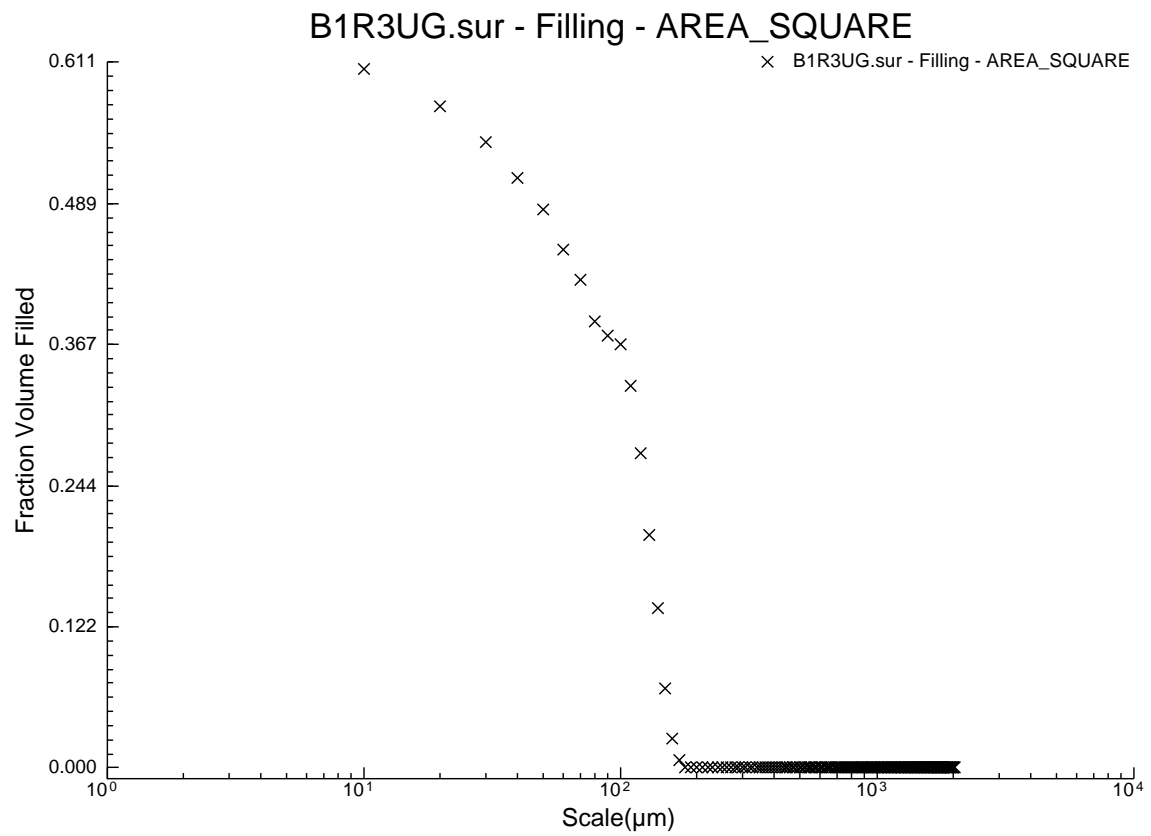
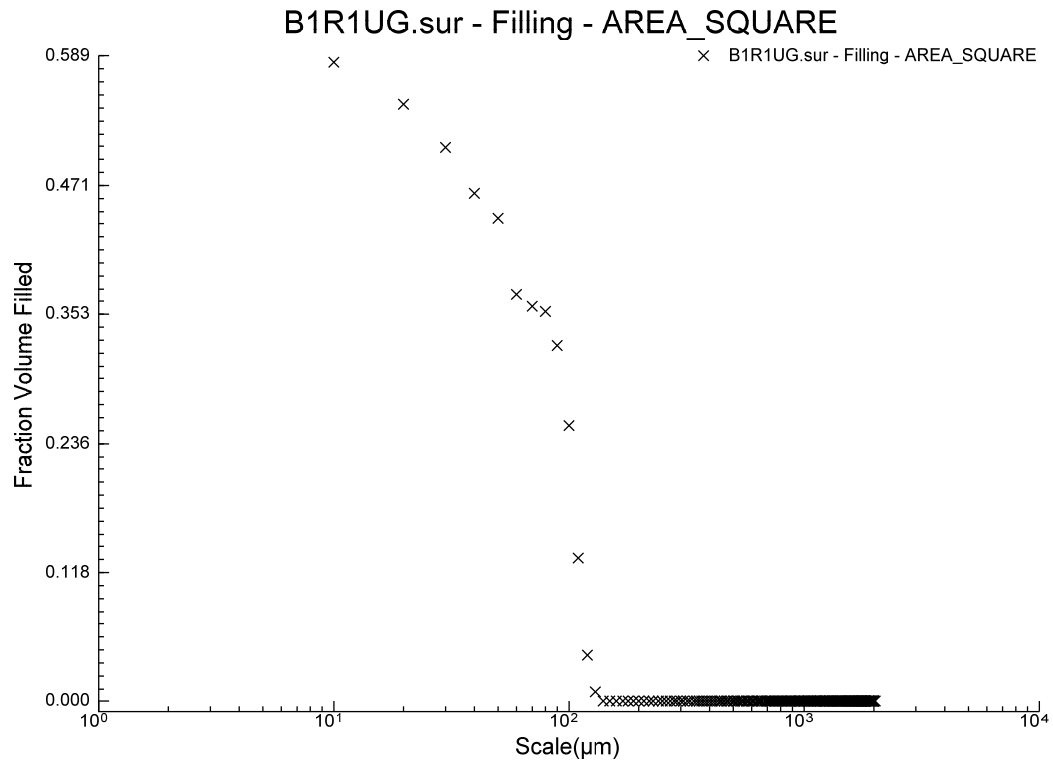




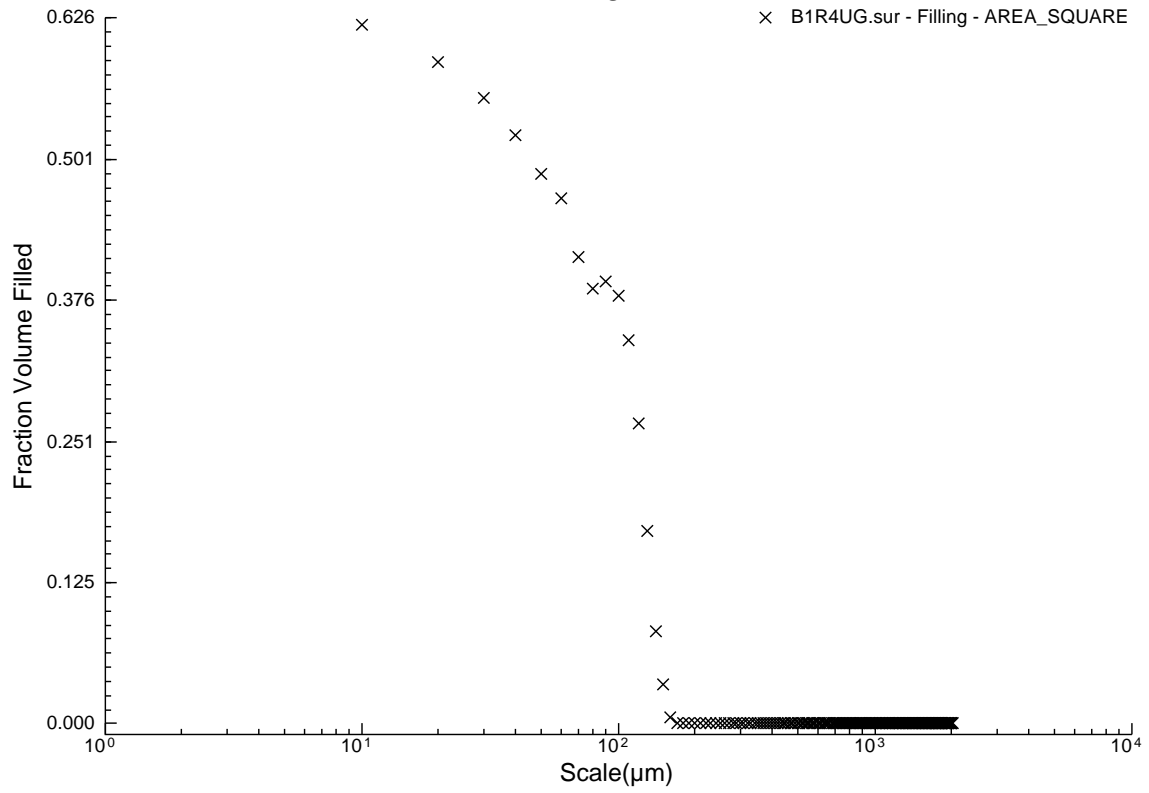


# Appendix B

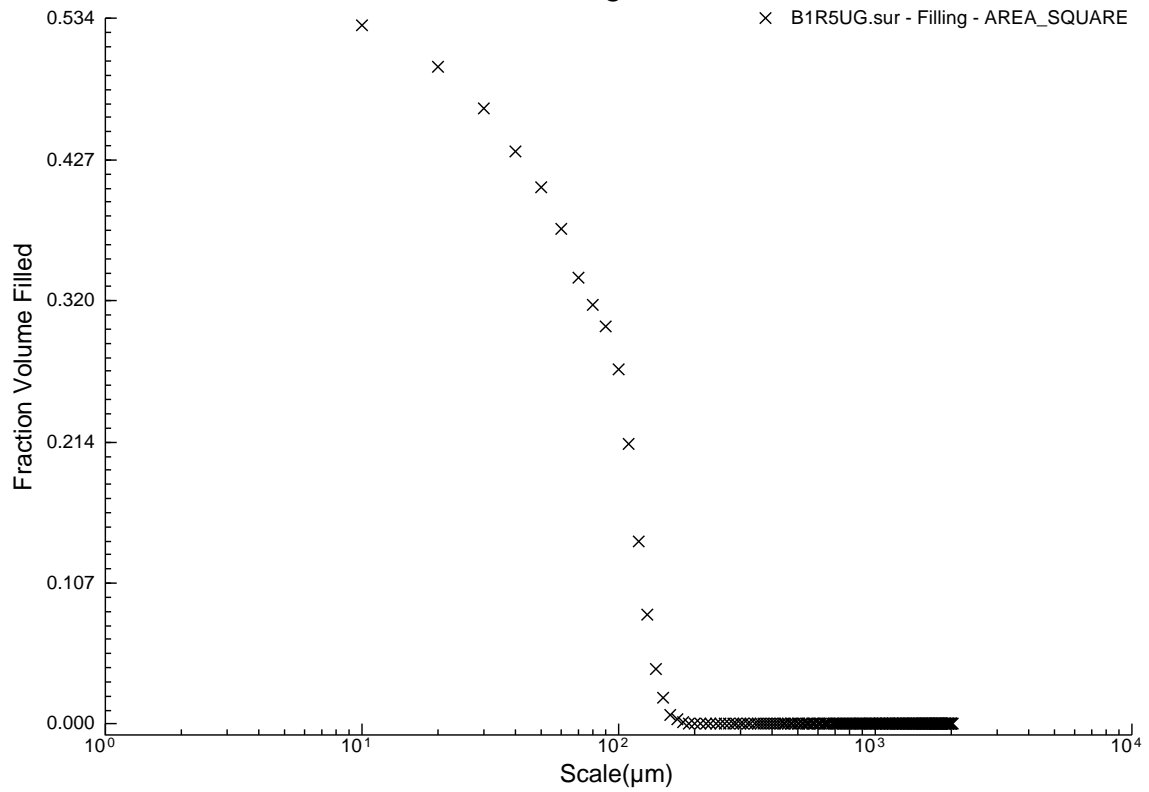
## Average texture-depth plots



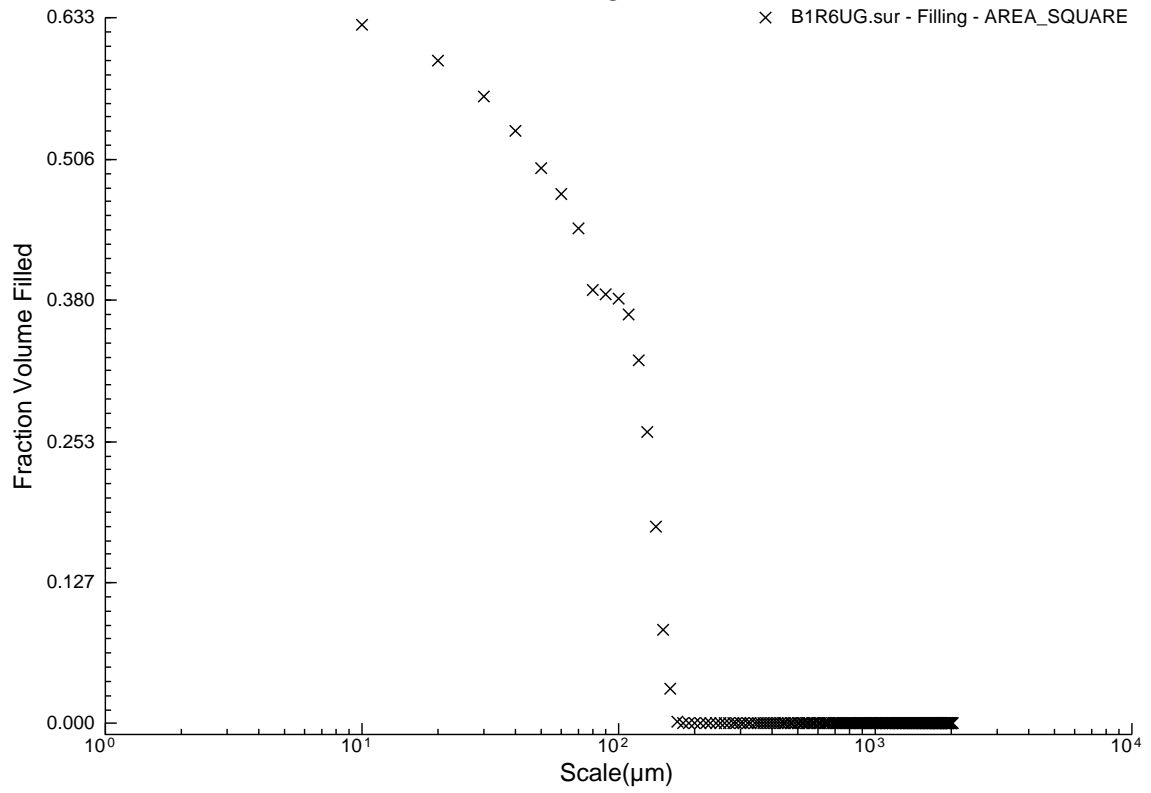
B1R4UG.sur - Filling - AREA\_SQUARE



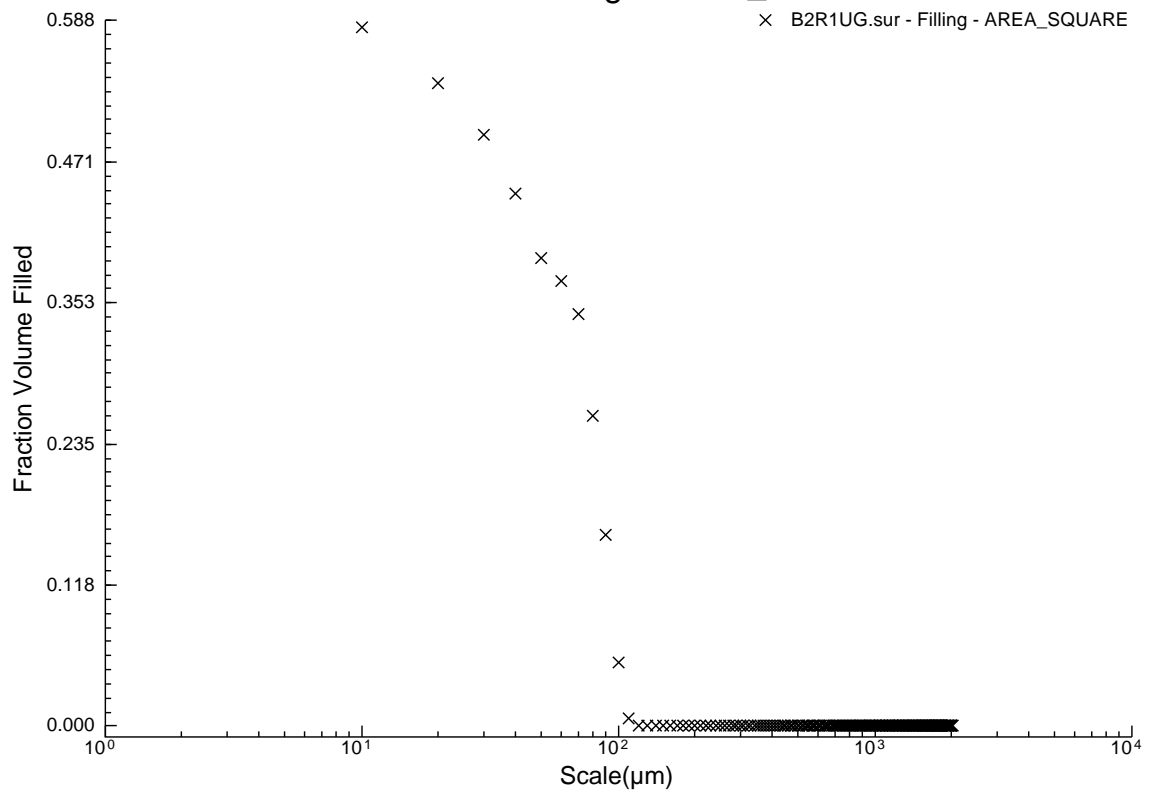
B1R5UG.sur - Filling - AREA\_SQUARE

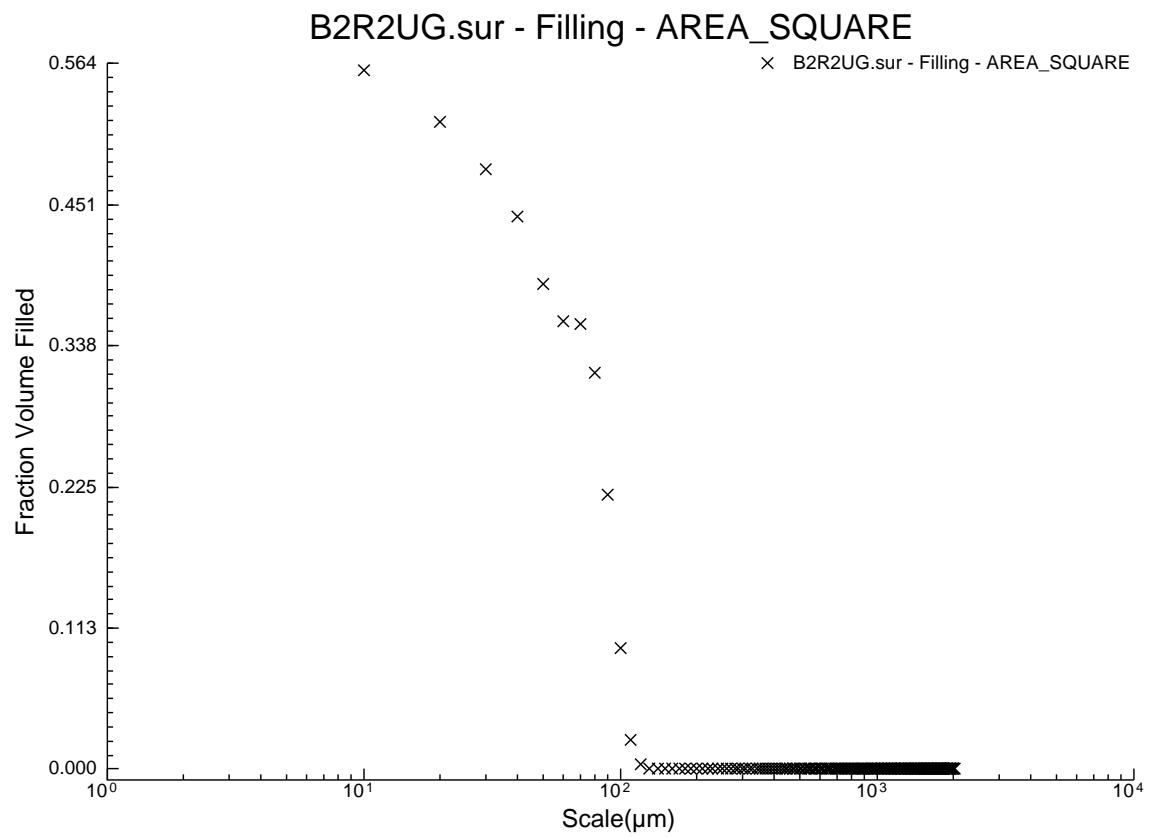
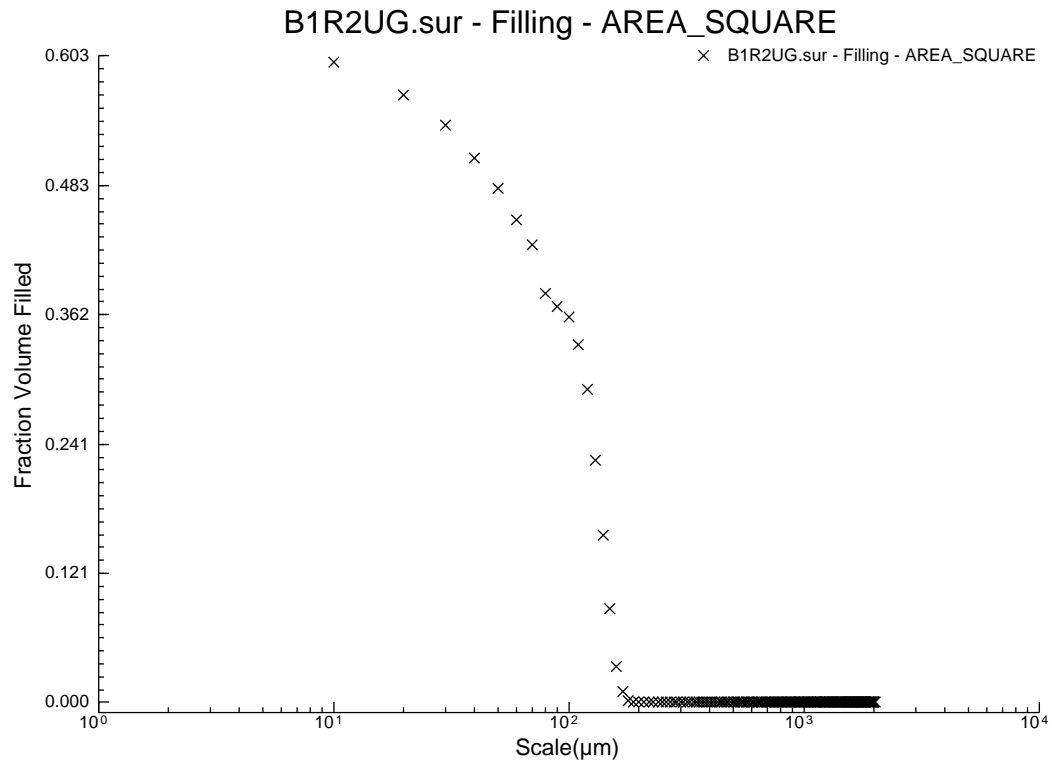


B1R6UG.sur - Filling - AREA\_SQUARE

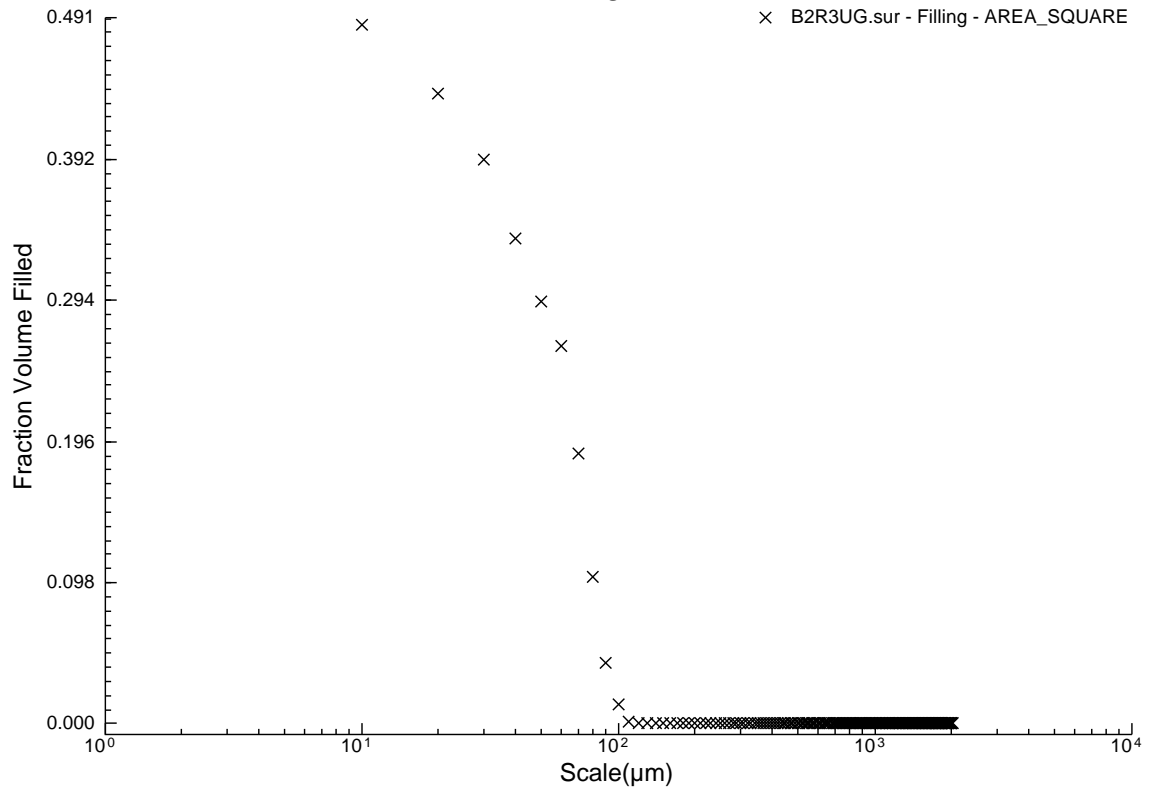


B2R1UG.sur - Filling - AREA\_SQUARE

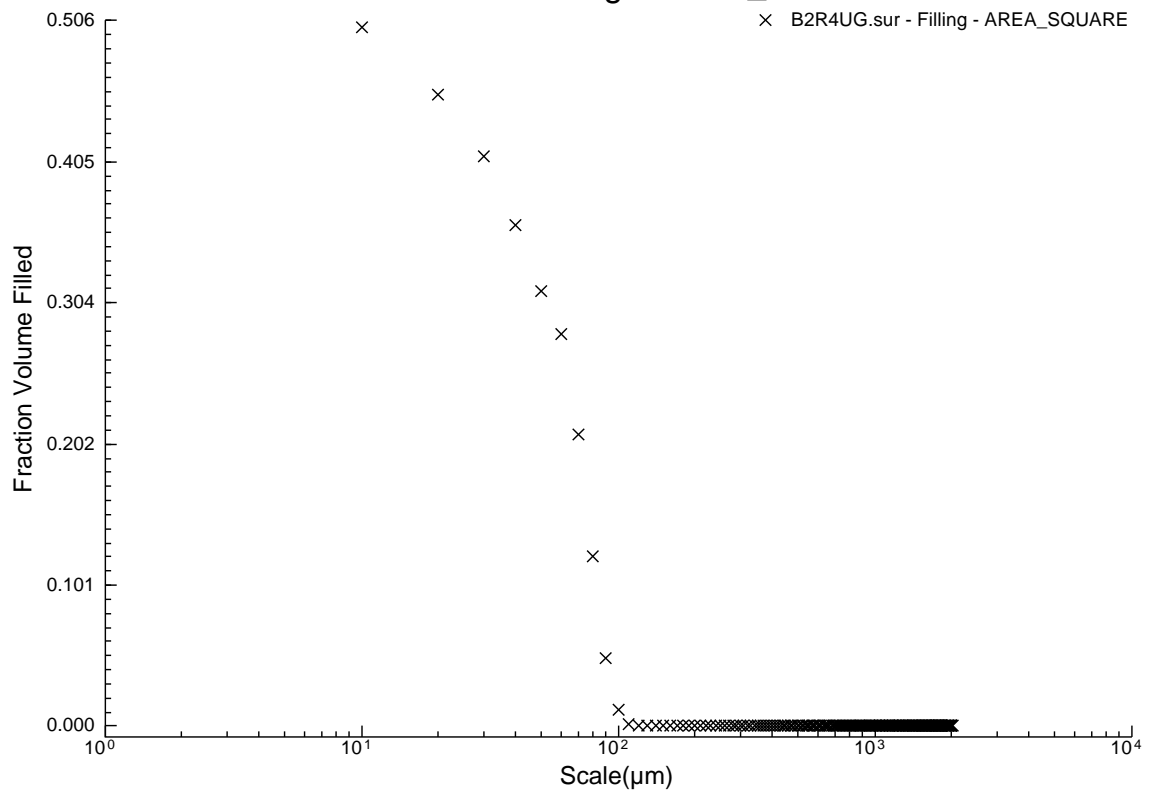




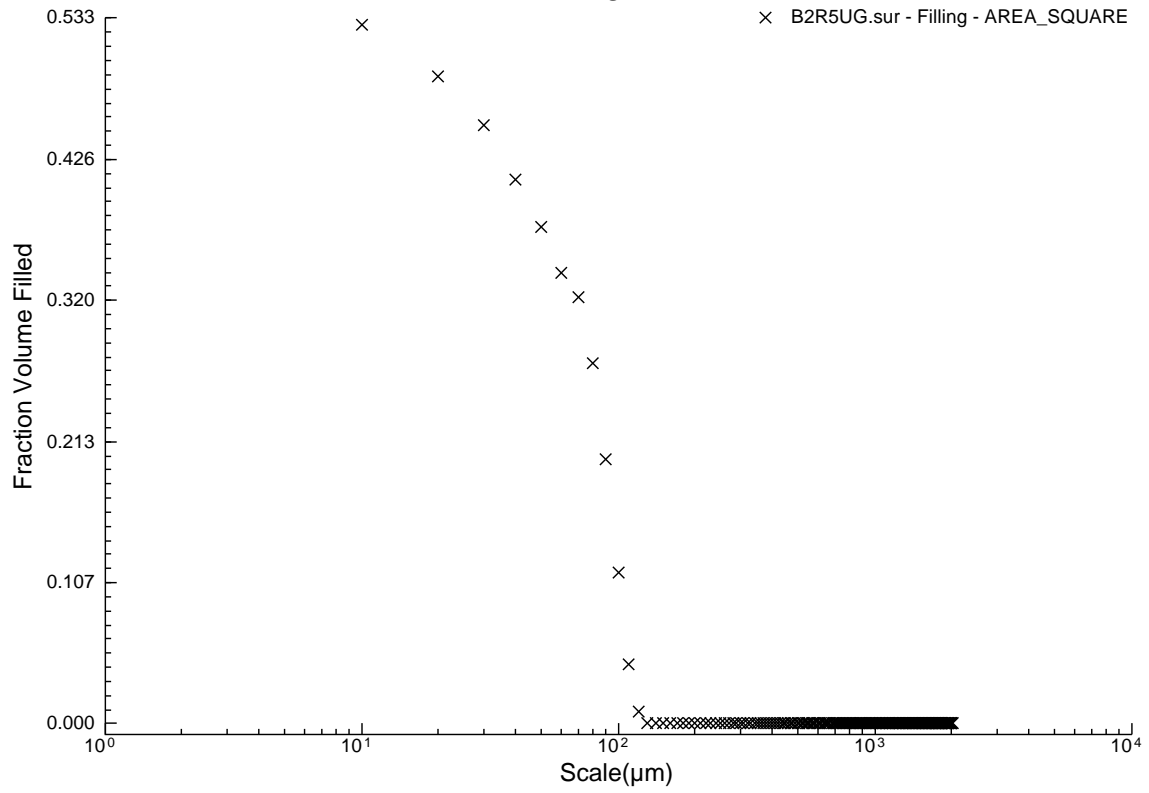
B2R3UG.sur - Filling - AREA\_SQUARE



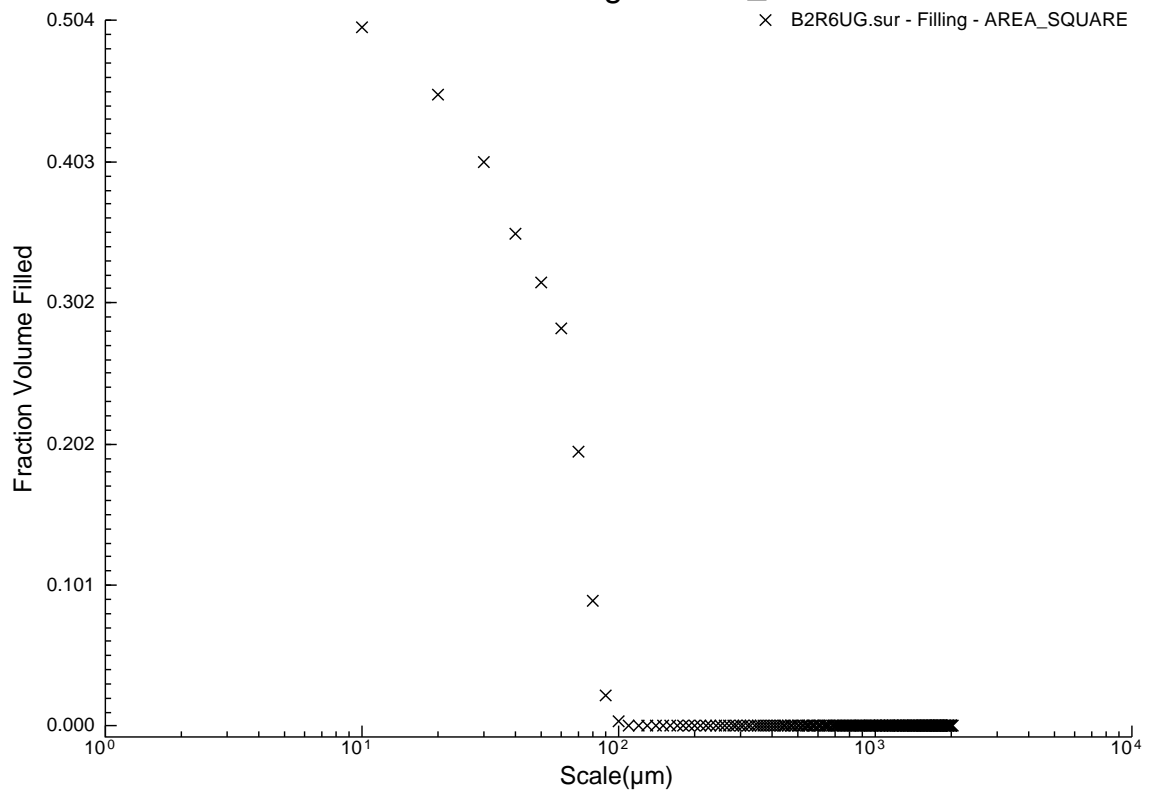
B2R4UG.sur - Filling - AREA\_SQUARE



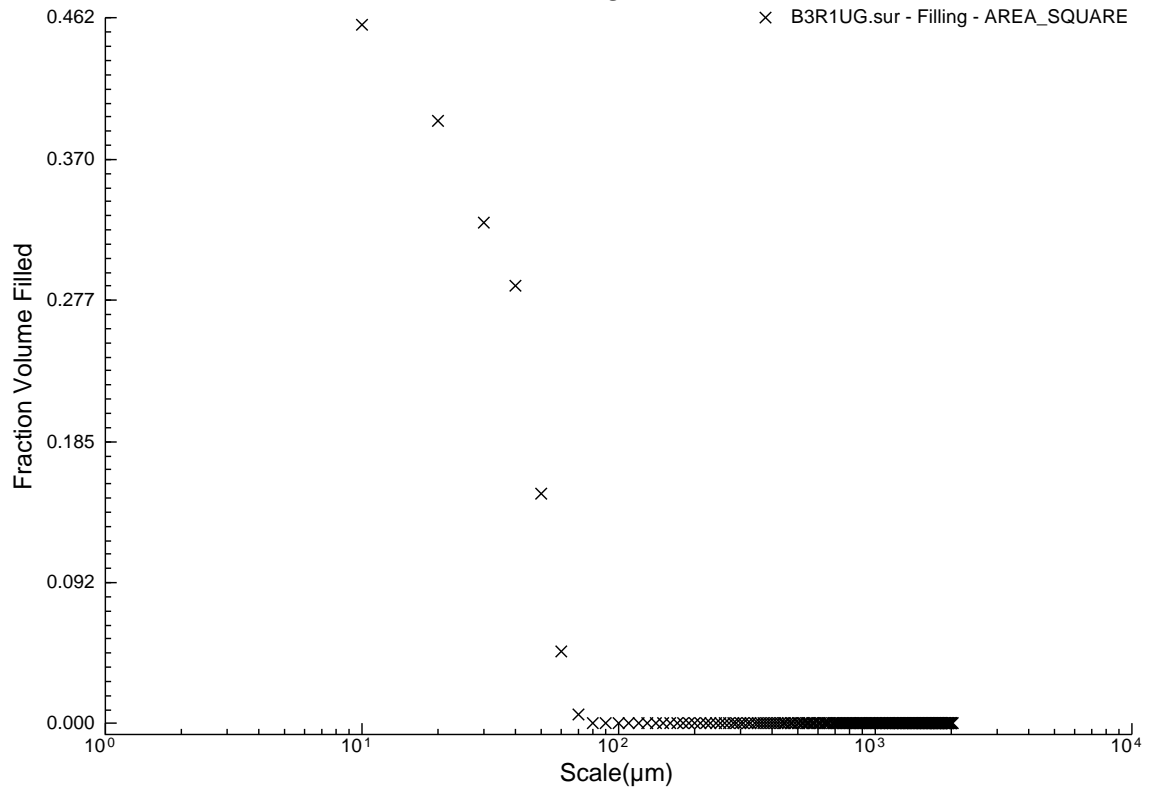
B2R5UG.sur - Filling - AREA\_SQUARE



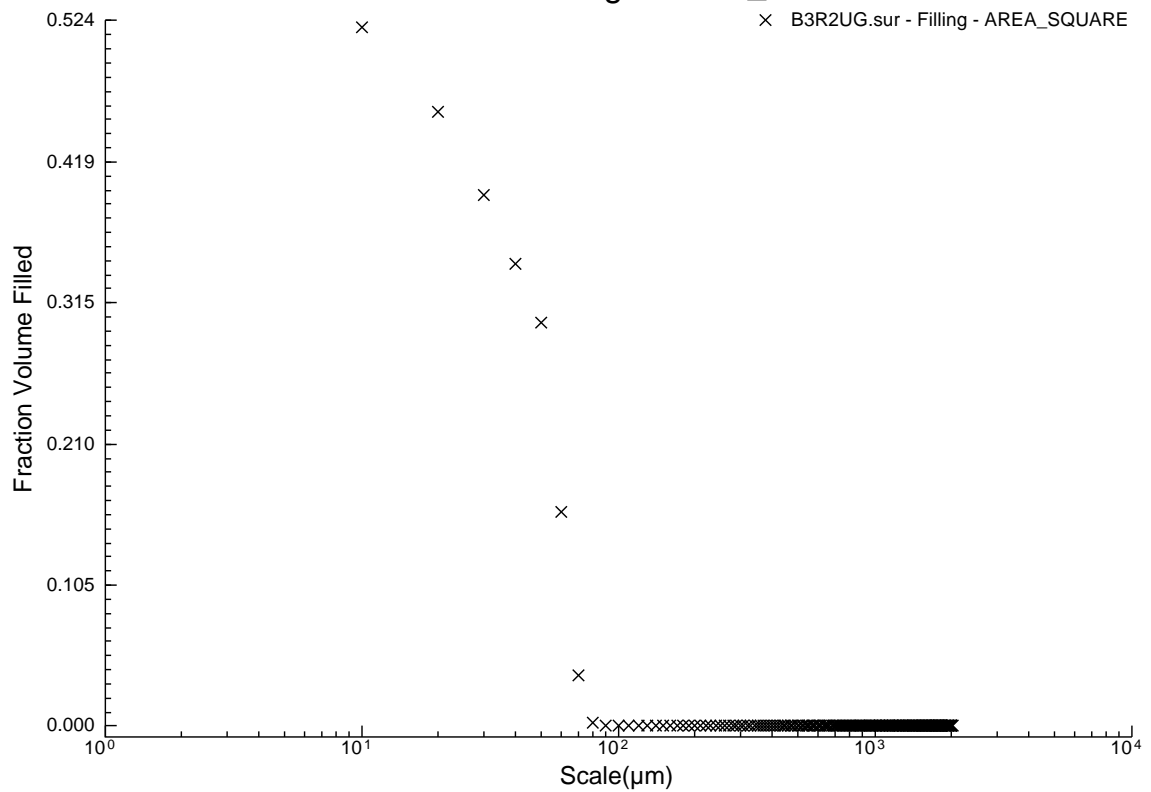
B2R6UG.sur - Filling - AREA\_SQUARE



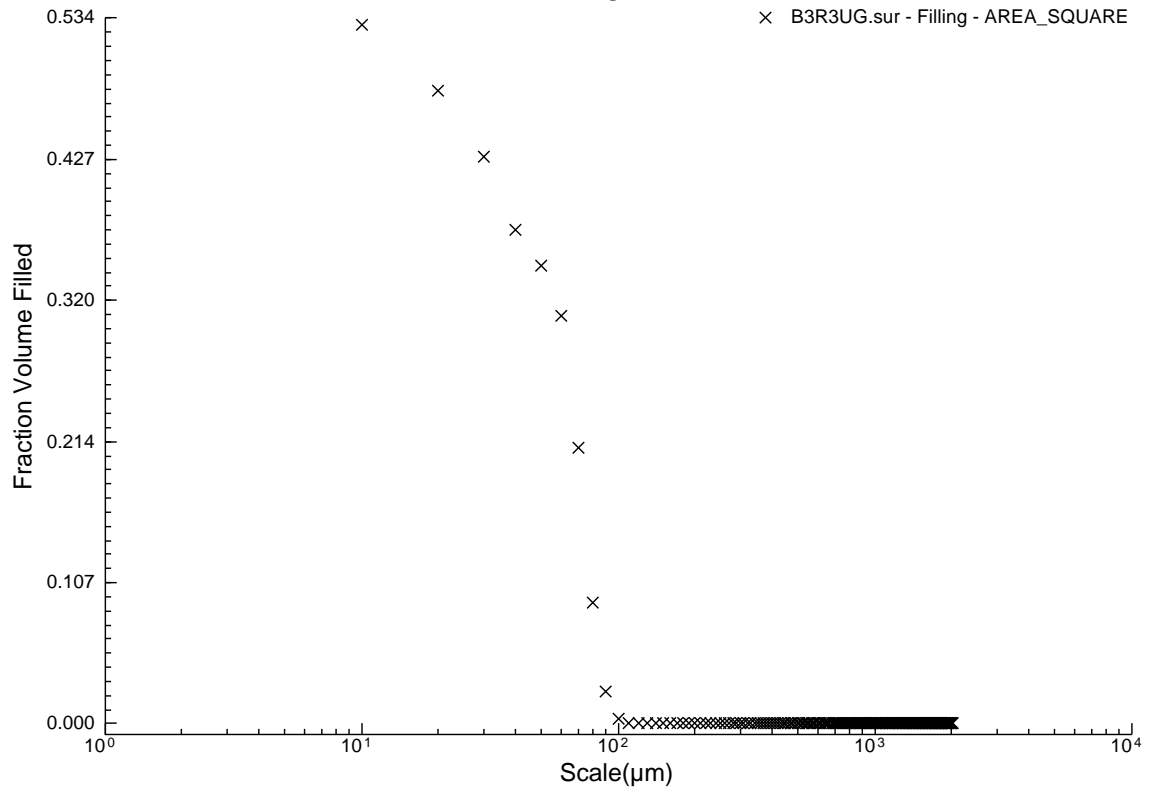
B3R1UG.sur - Filling - AREA\_SQUARE



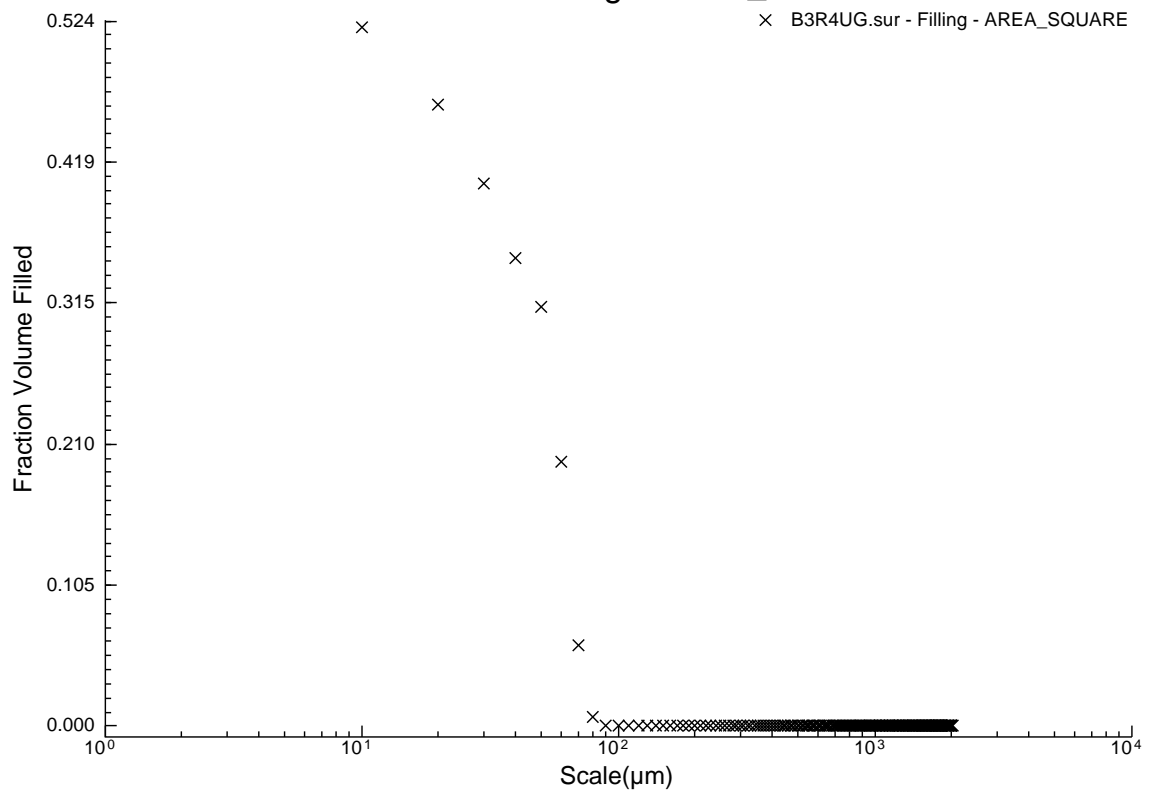
B3R2UG.sur - Filling - AREA\_SQUARE



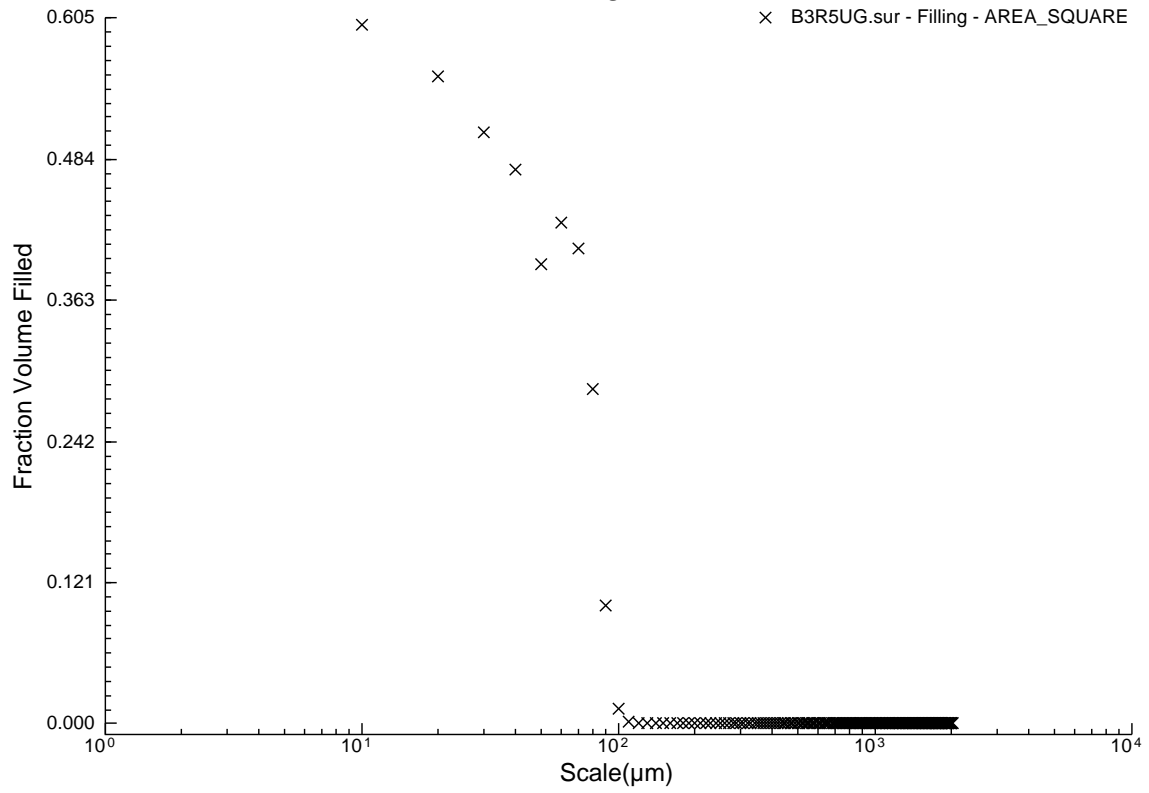
B3R3UG.sur - Filling - AREA\_SQUARE



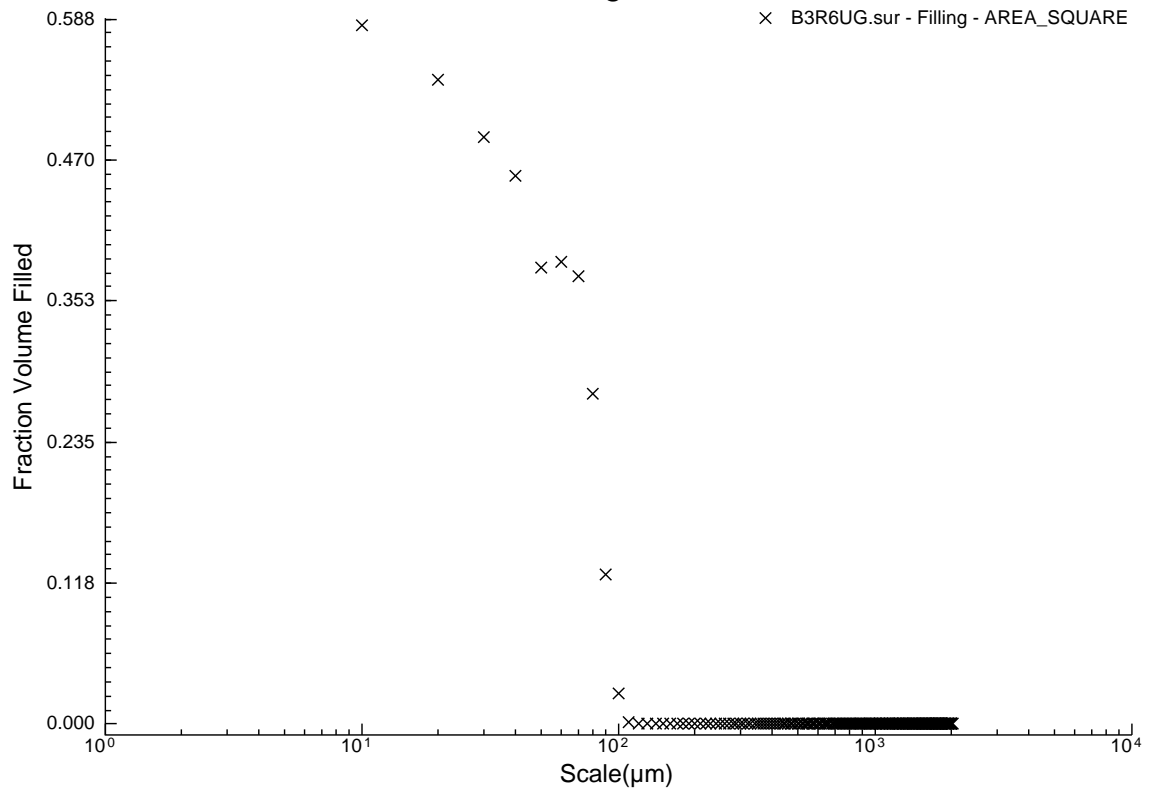
B3R4UG.sur - Filling - AREA\_SQUARE



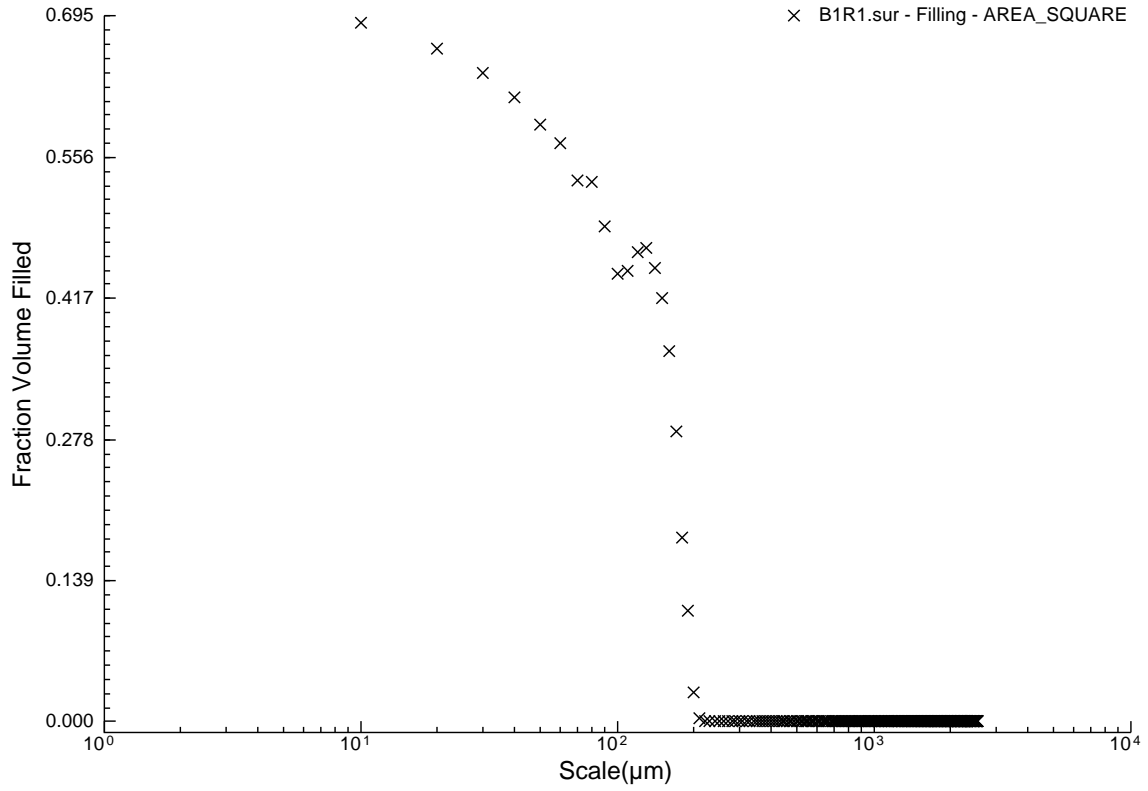
B3R5UG.sur - Filling - AREA\_SQUARE



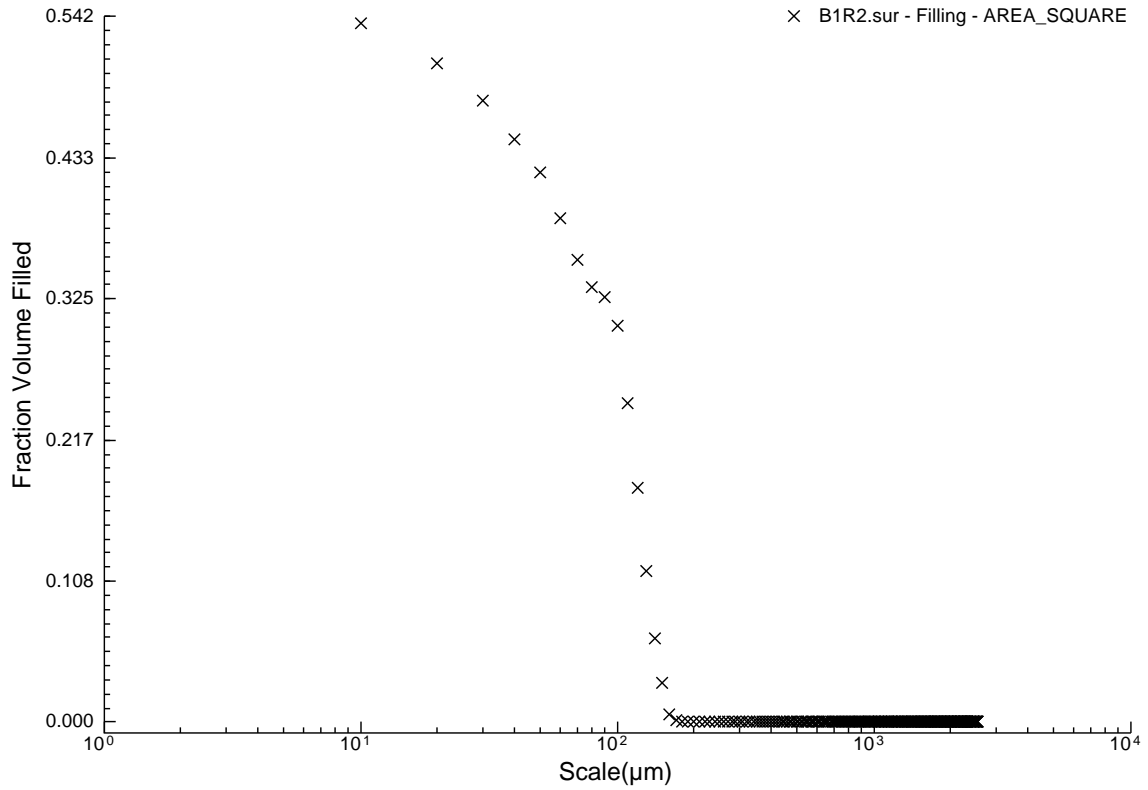
B3R6UG.sur - Filling - AREA\_SQUARE



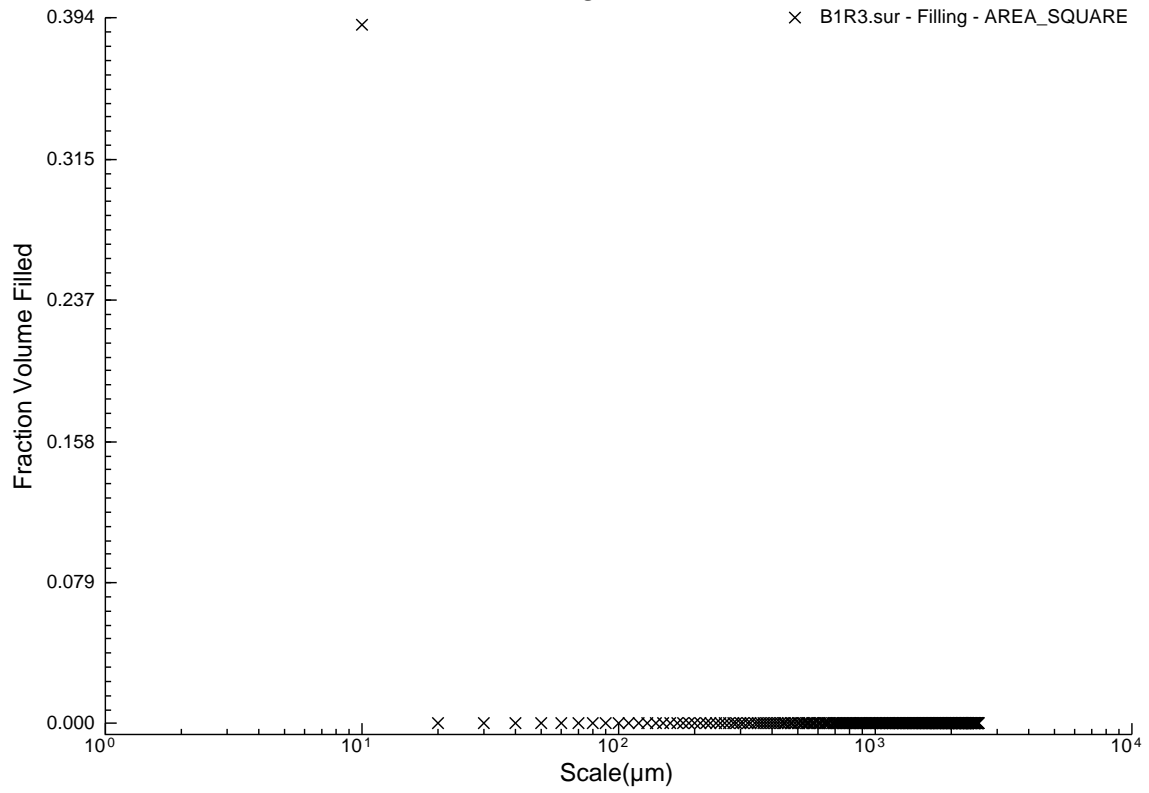
B1R1.sur - Filling - AREA\_SQUARE



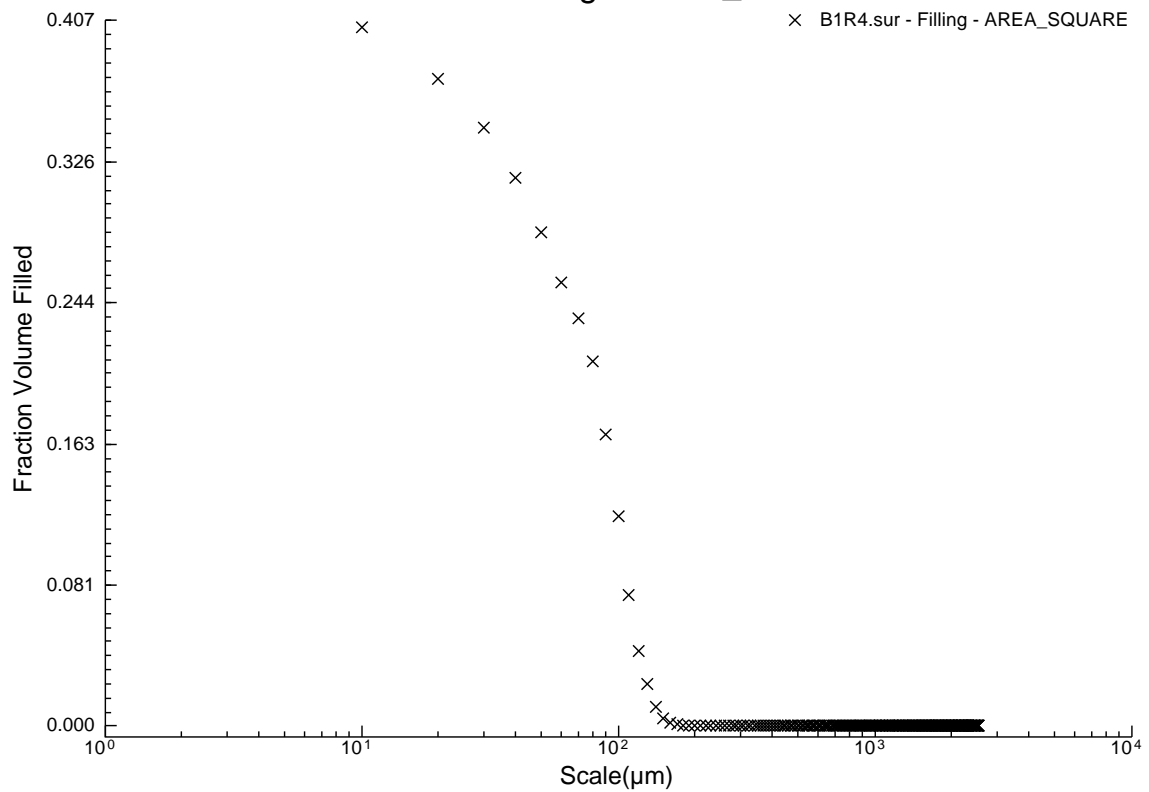
B1R2.sur - Filling - AREA\_SQUARE



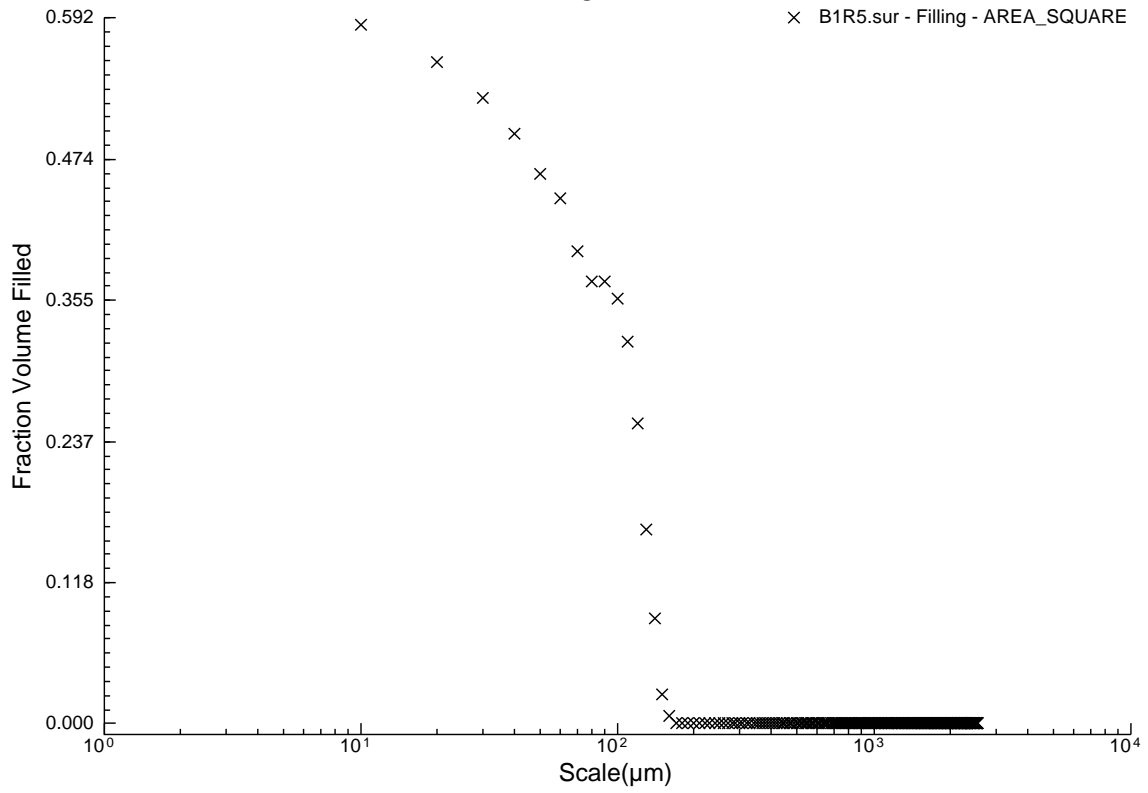
B1R3.sur - Filling - AREA\_SQUARE



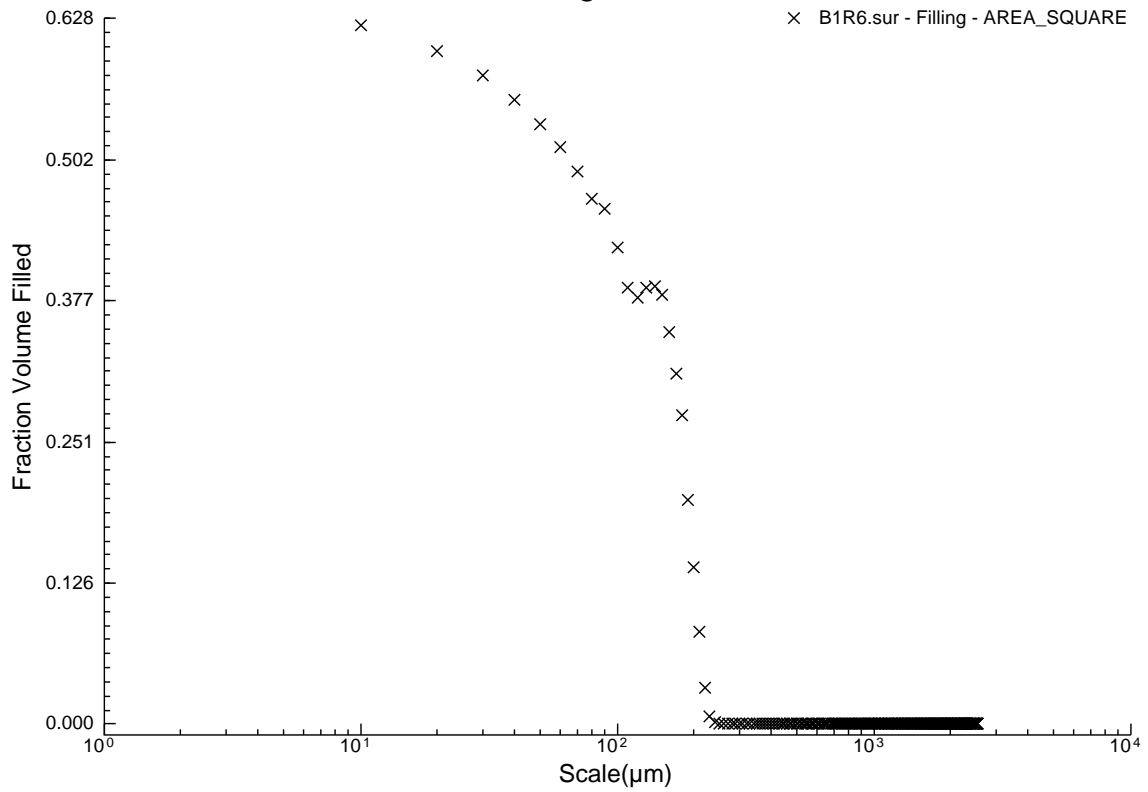
B1R4.sur - Filling - AREA\_SQUARE



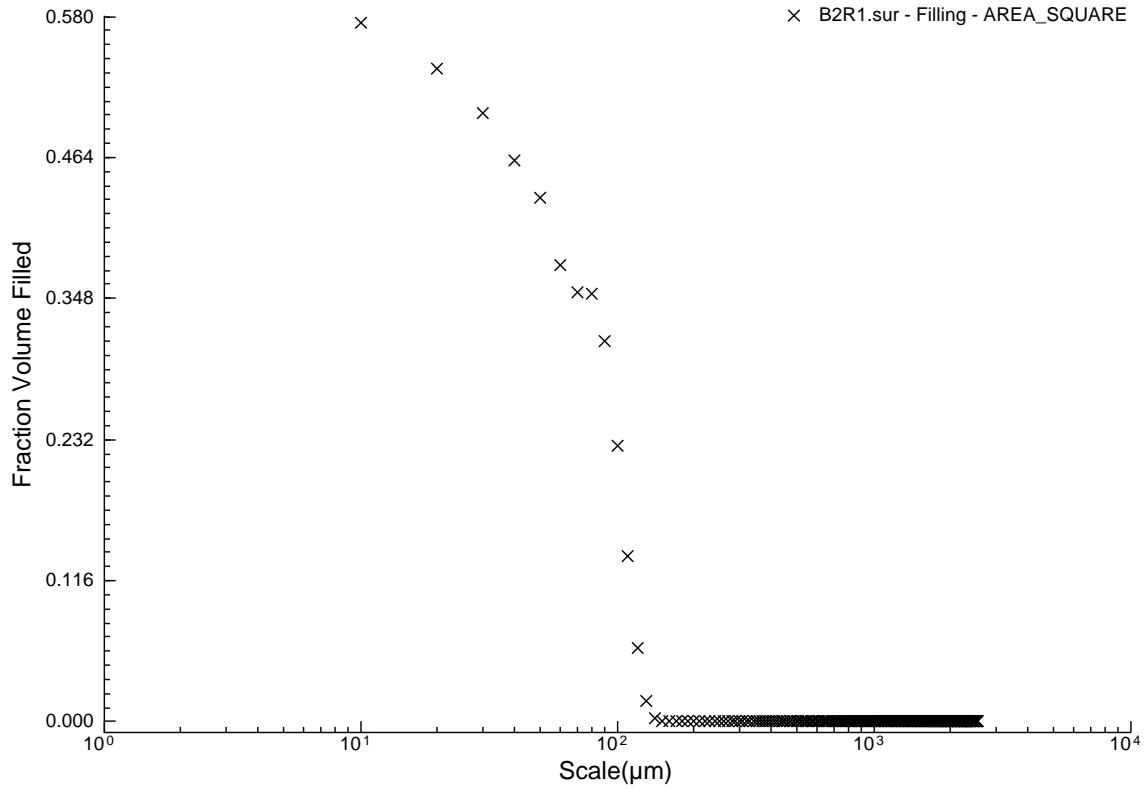
B1R5.sur - Filling - AREA\_SQUARE



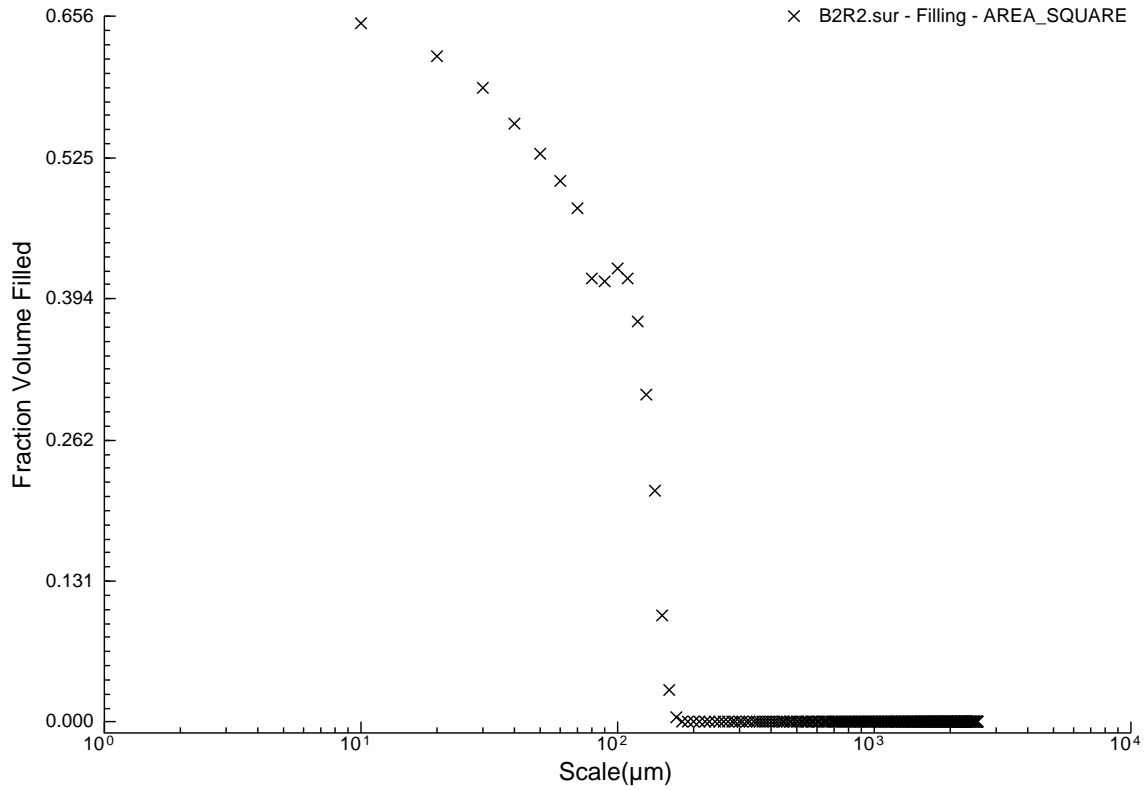
B1R6.sur - Filling - AREA\_SQUARE



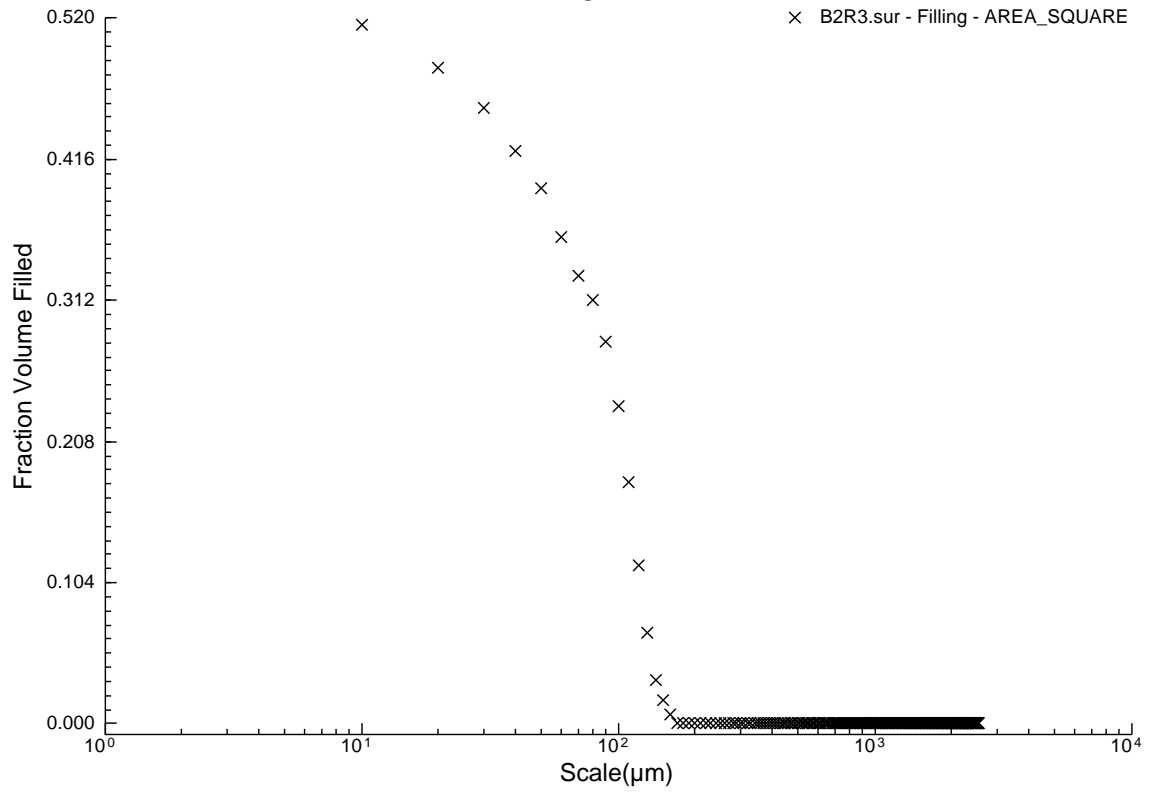
B2R1.sur - Filling - AREA\_SQUARE



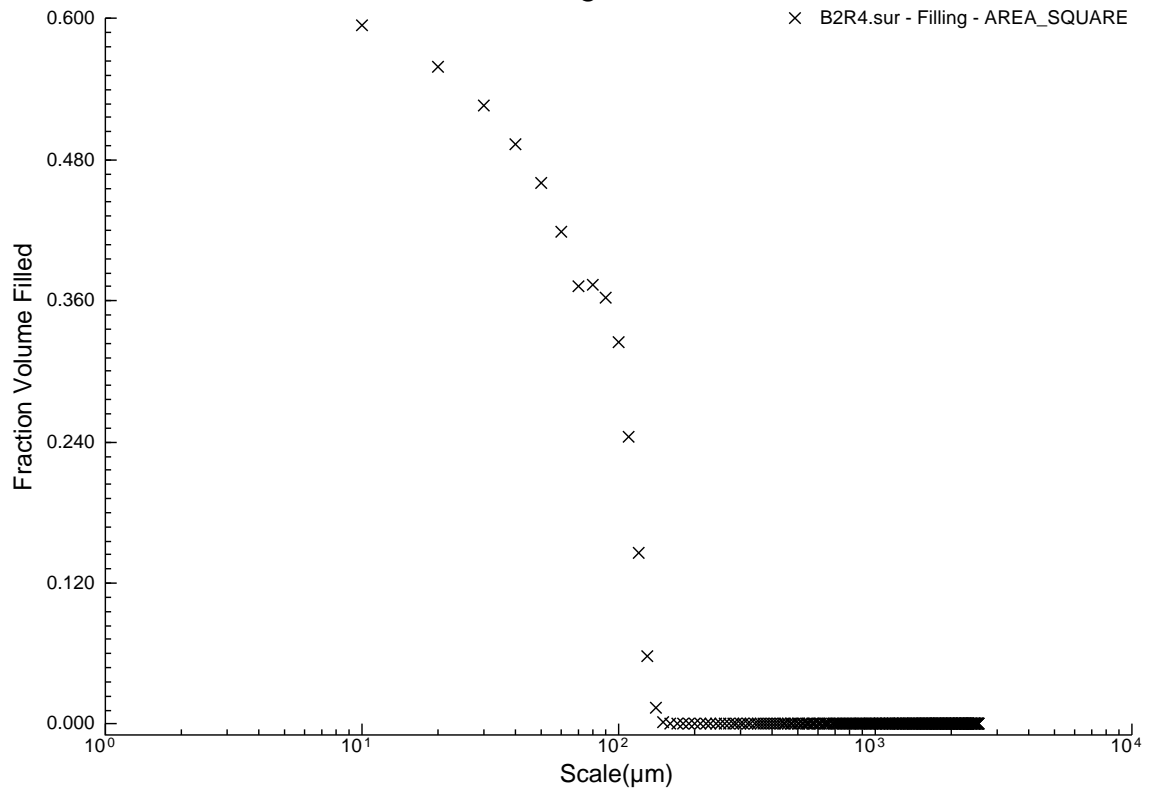
B2R2.sur - Filling - AREA\_SQUARE



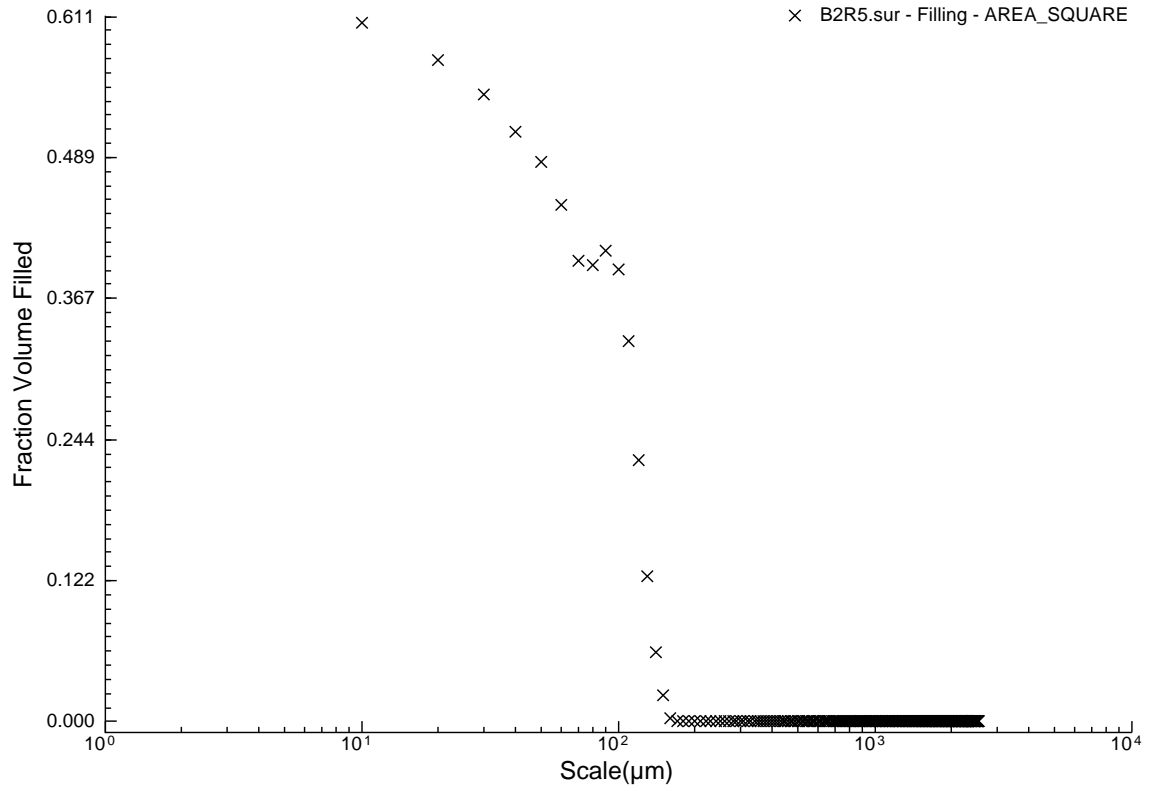
B2R3.sur - Filling - AREA\_SQUARE



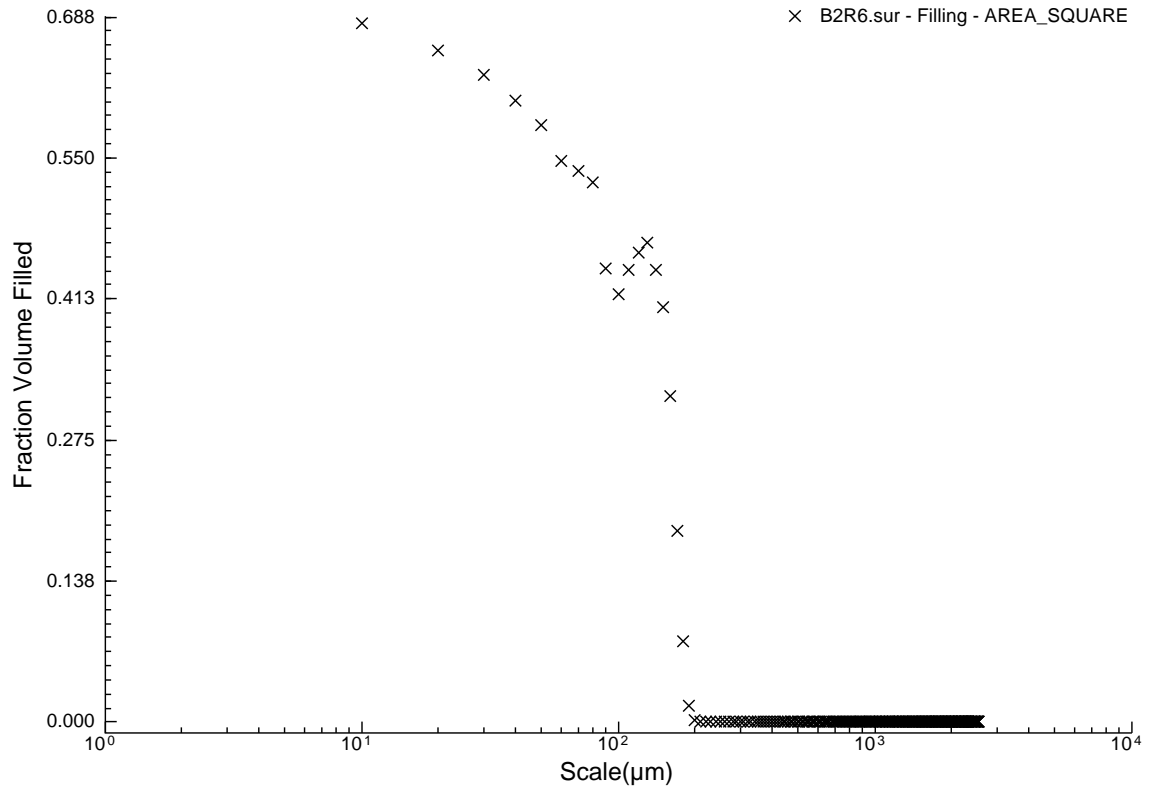
B2R4.sur - Filling - AREA\_SQUARE

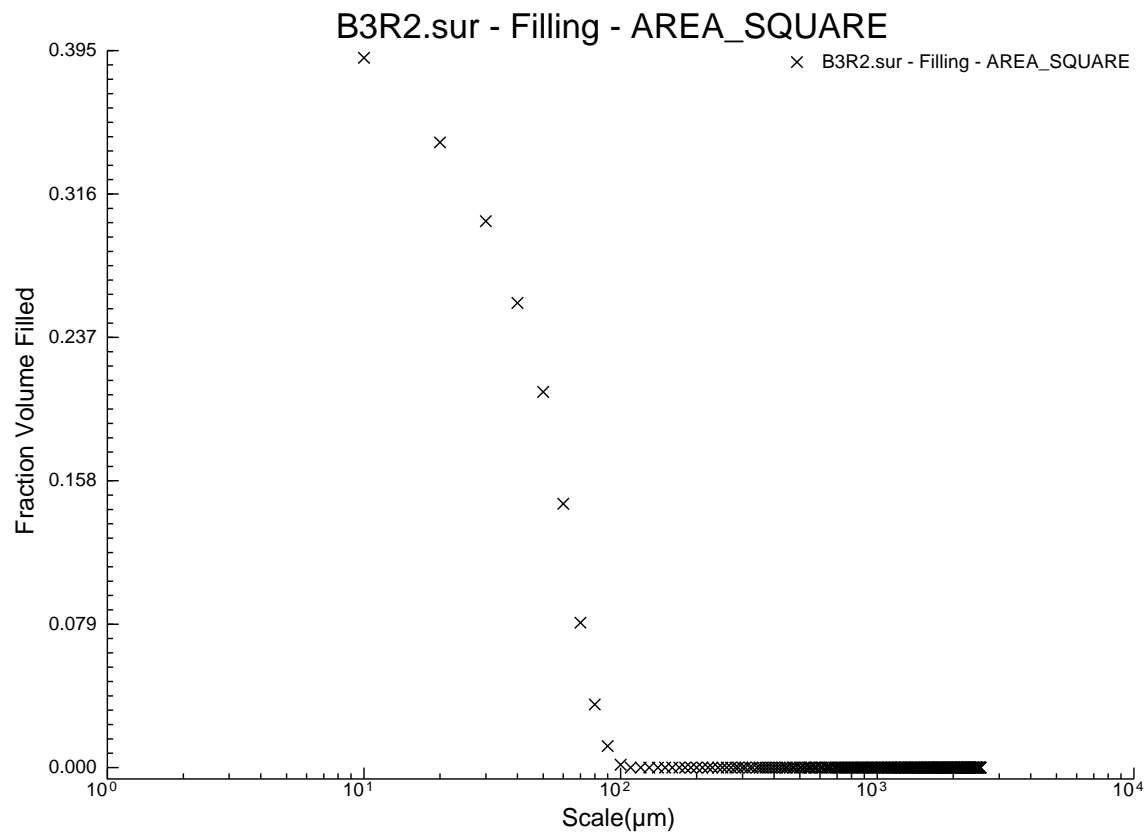
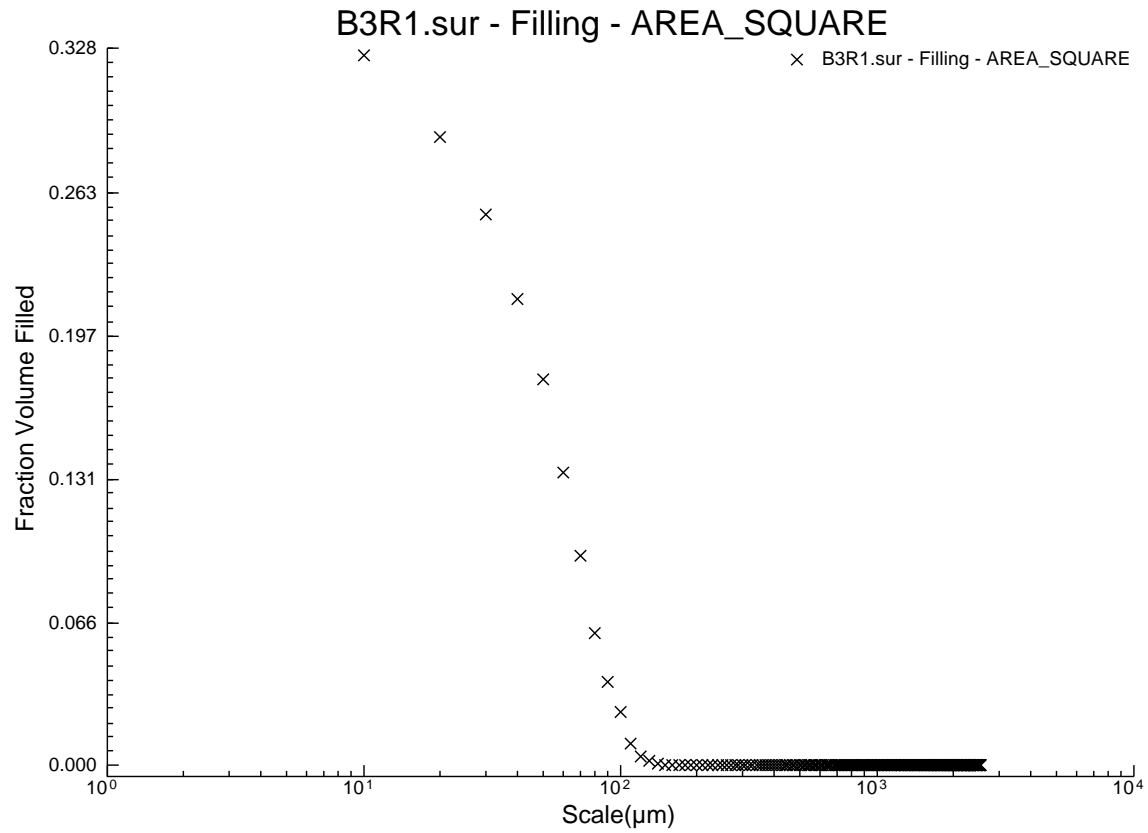


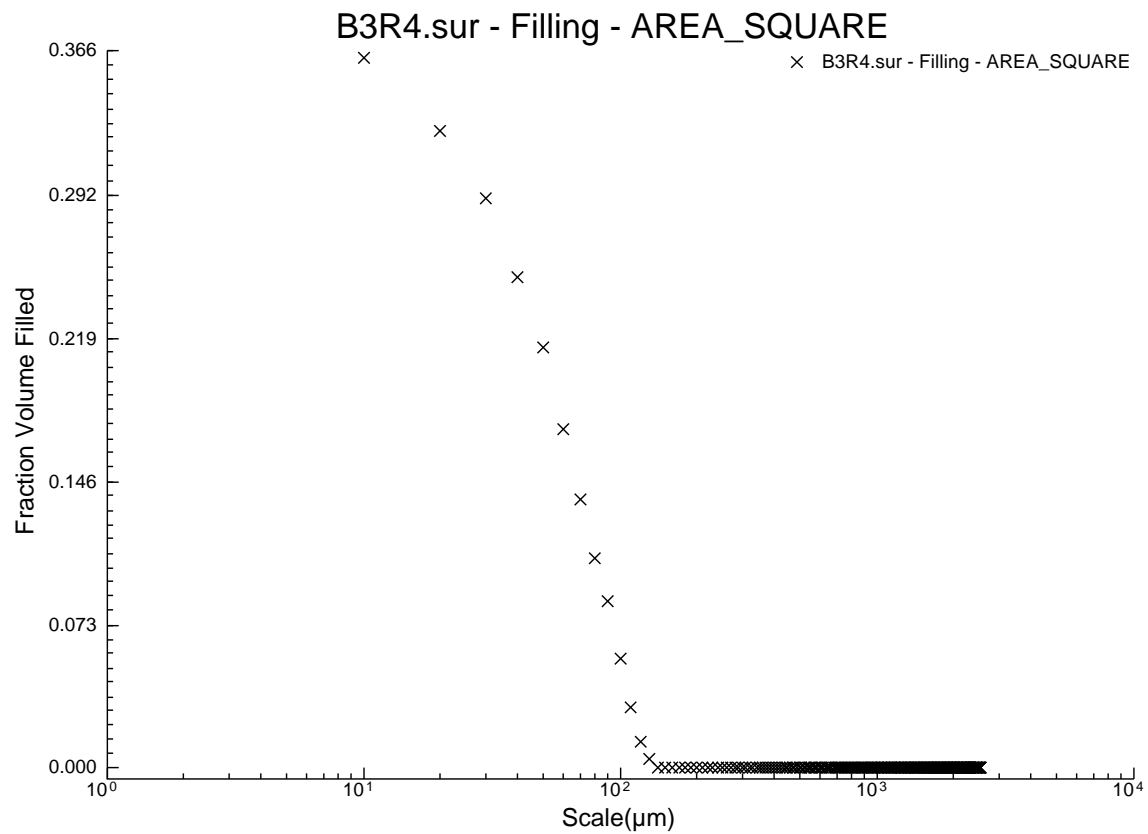
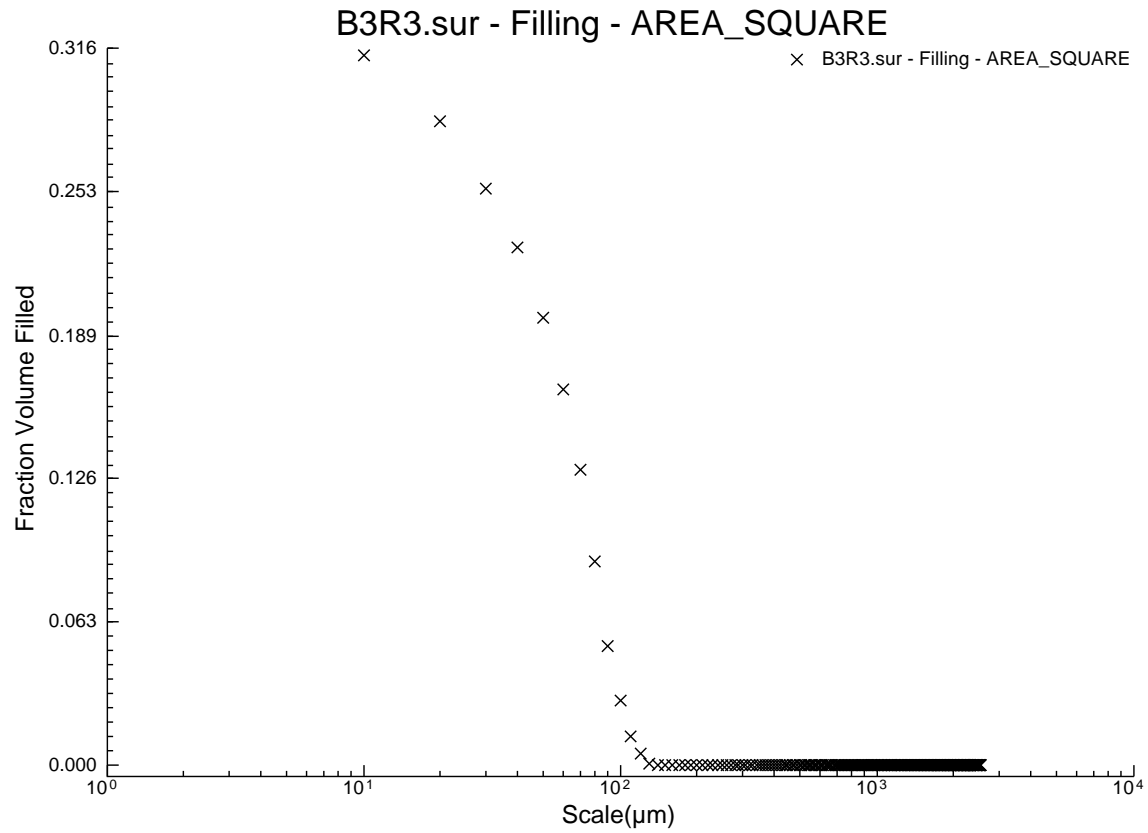
B2R5.sur - Filling - AREA\_SQUARE



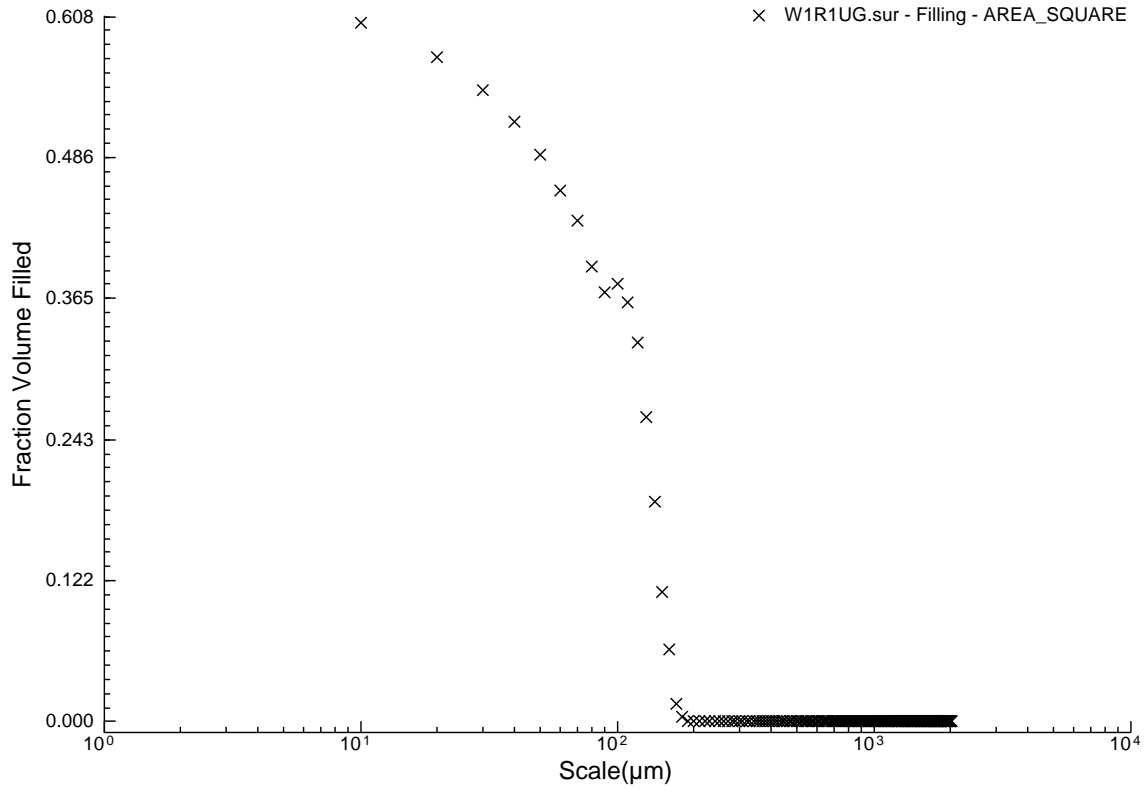
B2R6.sur - Filling - AREA\_SQUARE



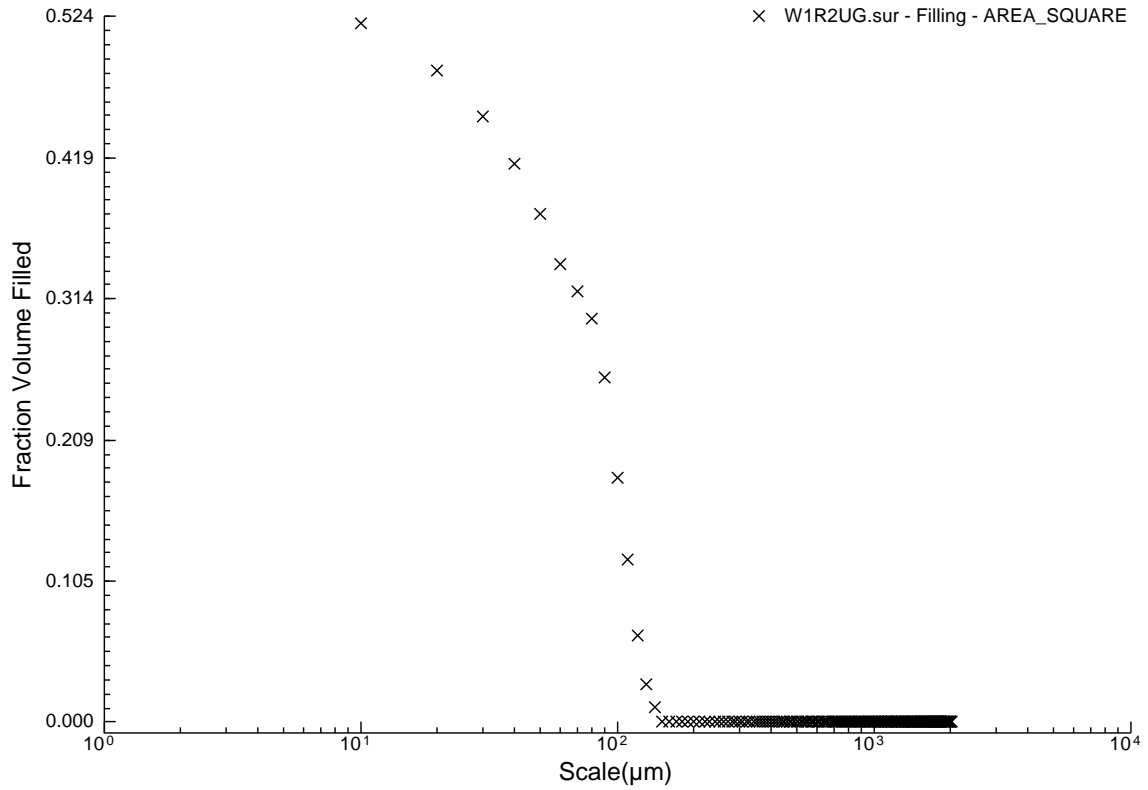




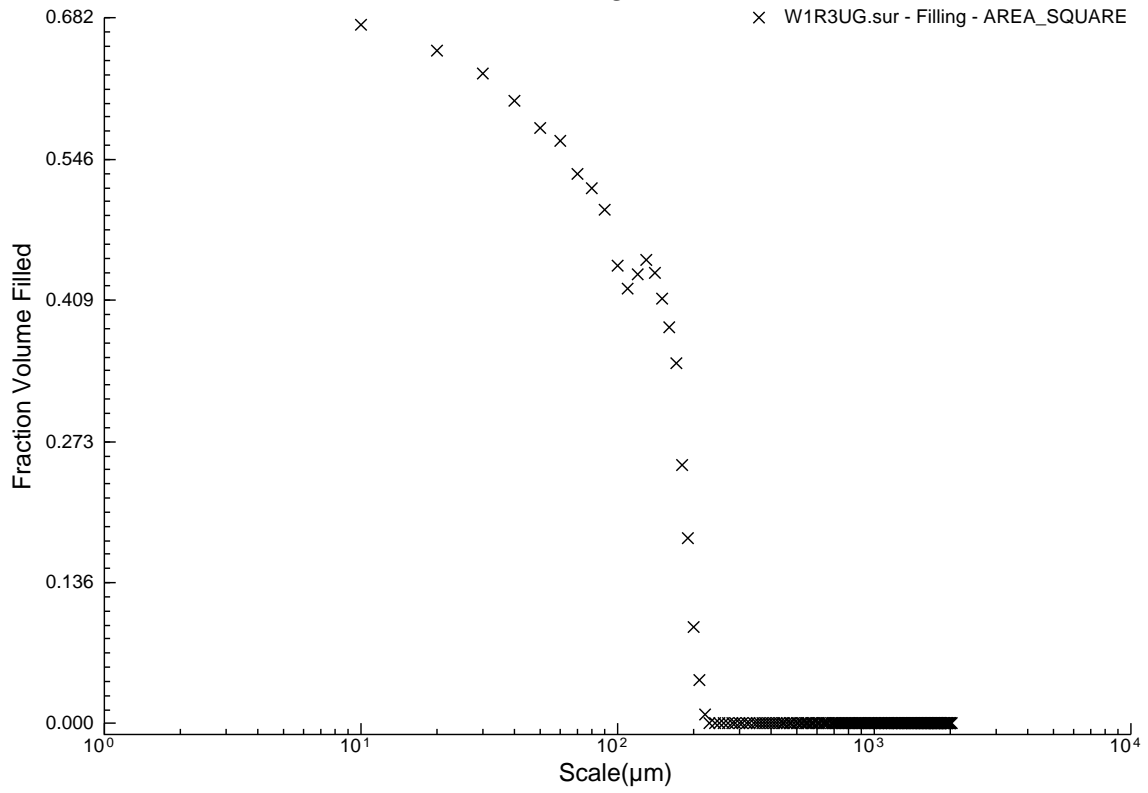
W1R1UG.sur - Filling - AREA\_SQUARE



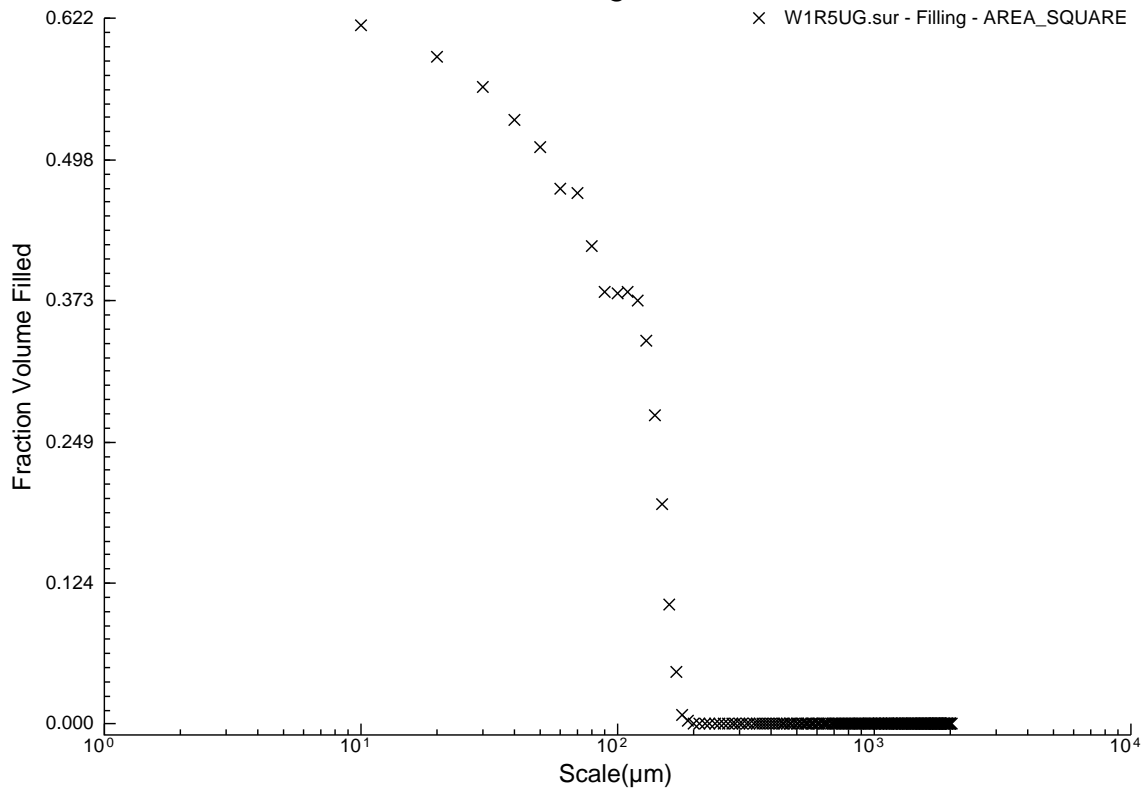
W1R2UG.sur - Filling - AREA\_SQUARE



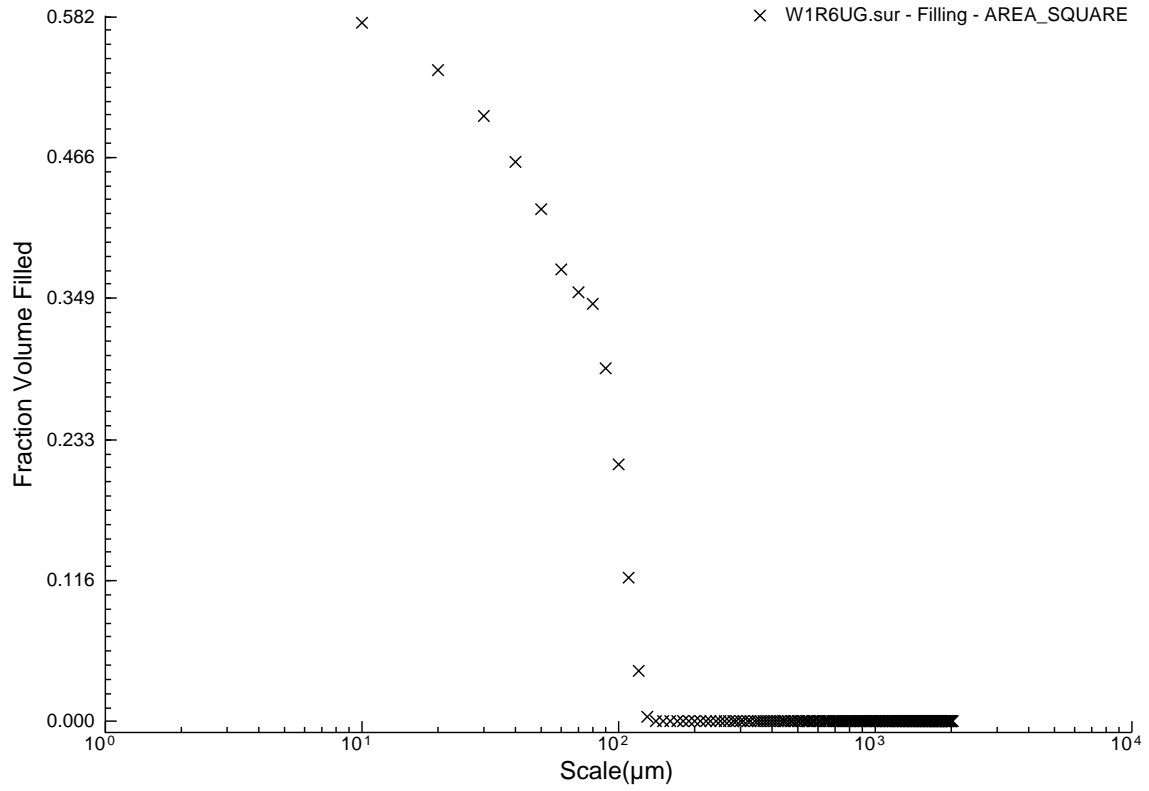
W1R3UG.sur - Filling - AREA\_SQUARE



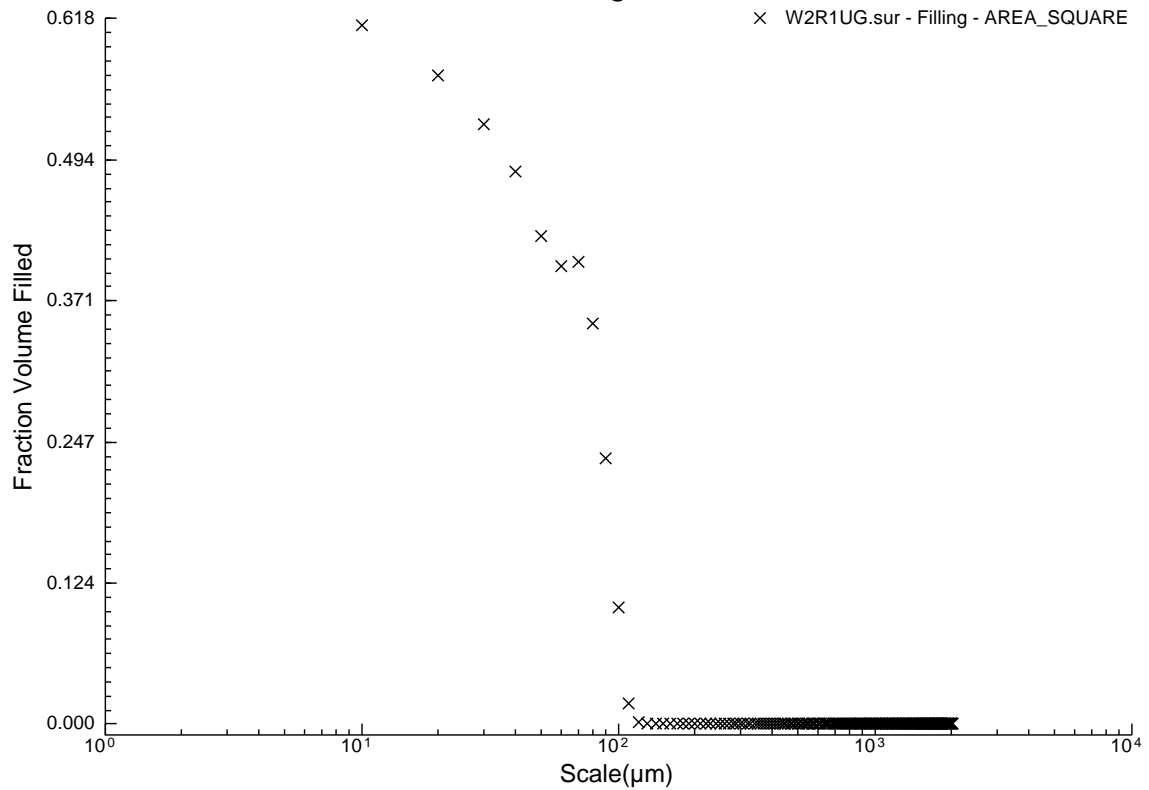
W1R5UG.sur - Filling - AREA\_SQUARE



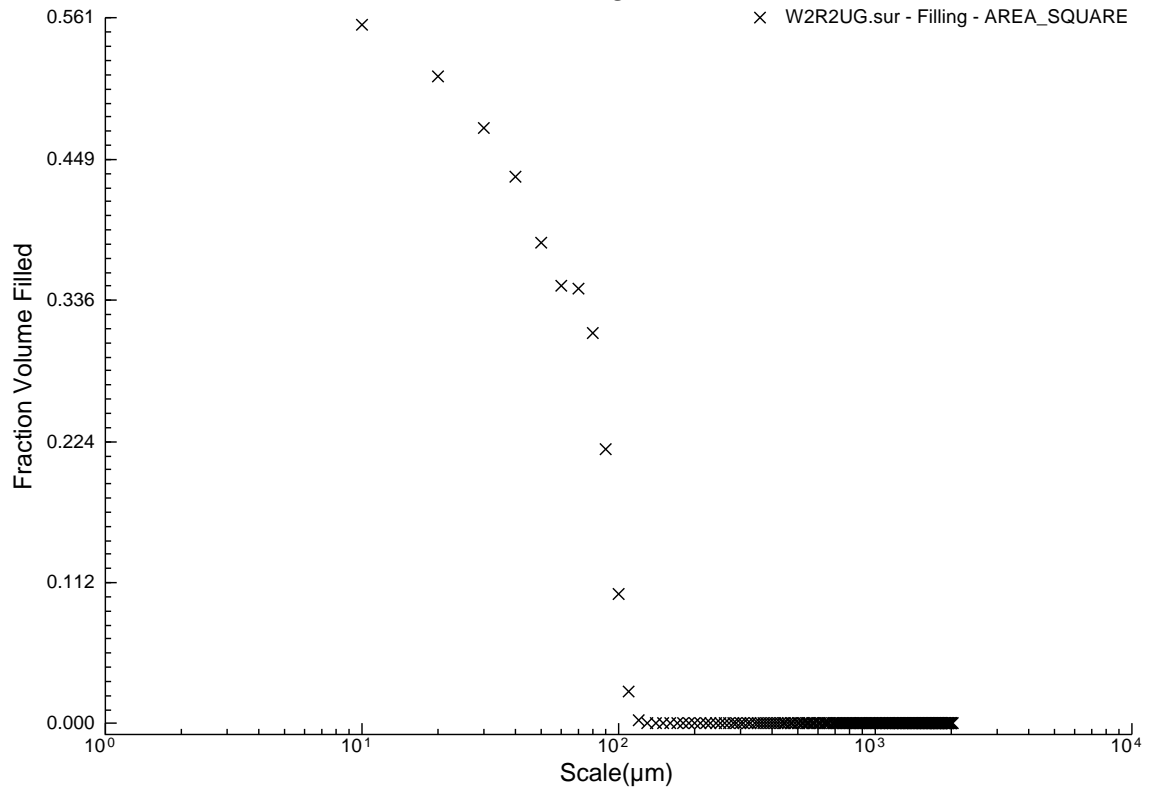
W1R6UG.sur - Filling - AREA\_SQUARE



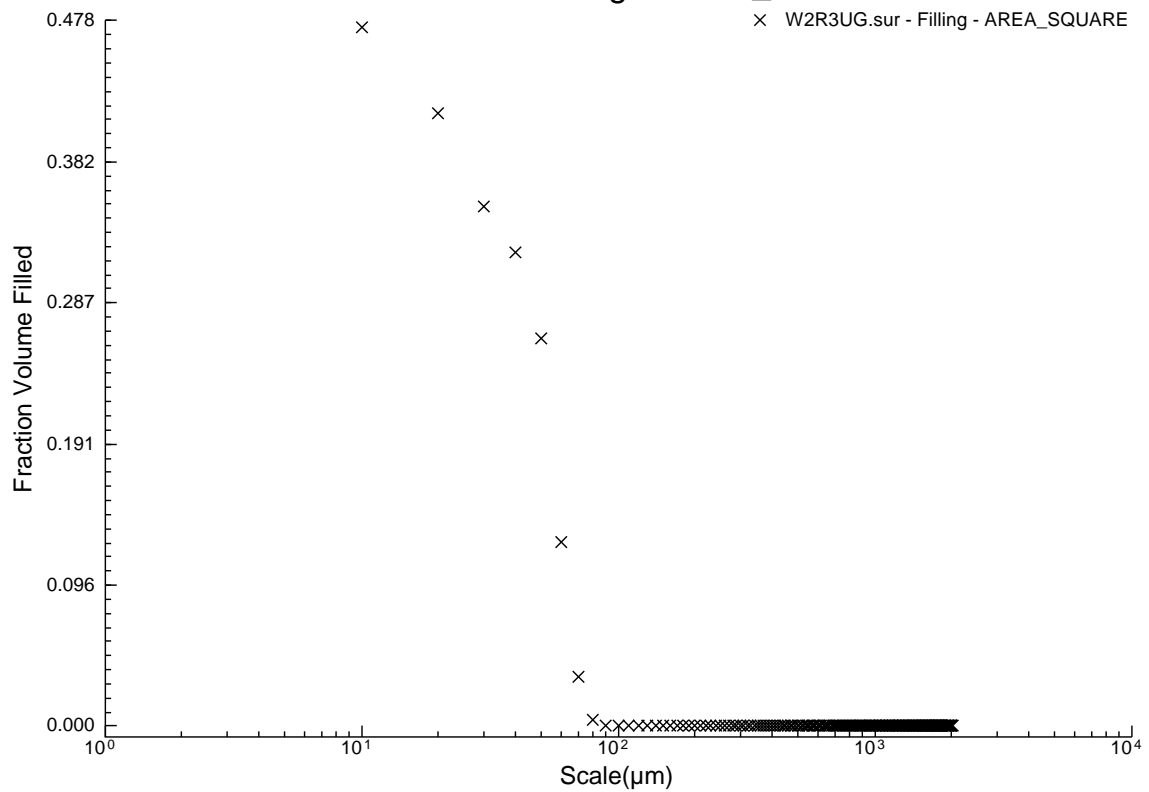
W2R1UG.sur - Filling - AREA\_SQUARE



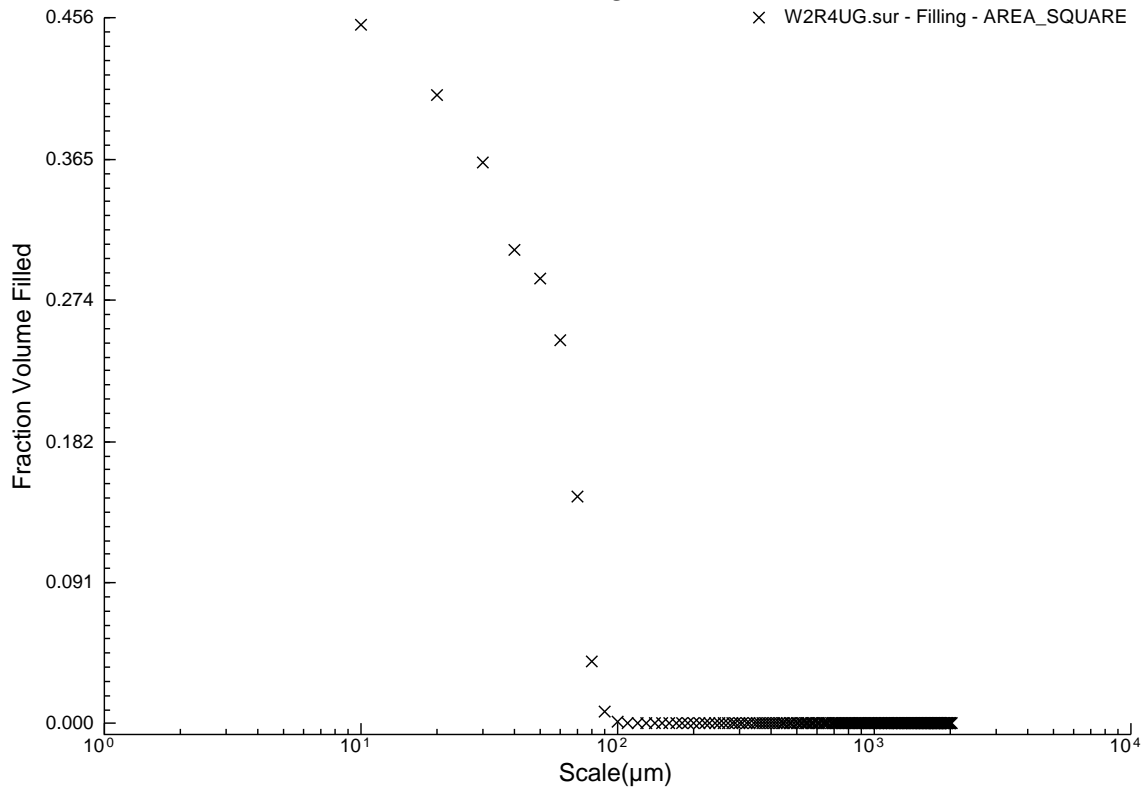
W2R2UG.sur - Filling - AREA\_SQUARE



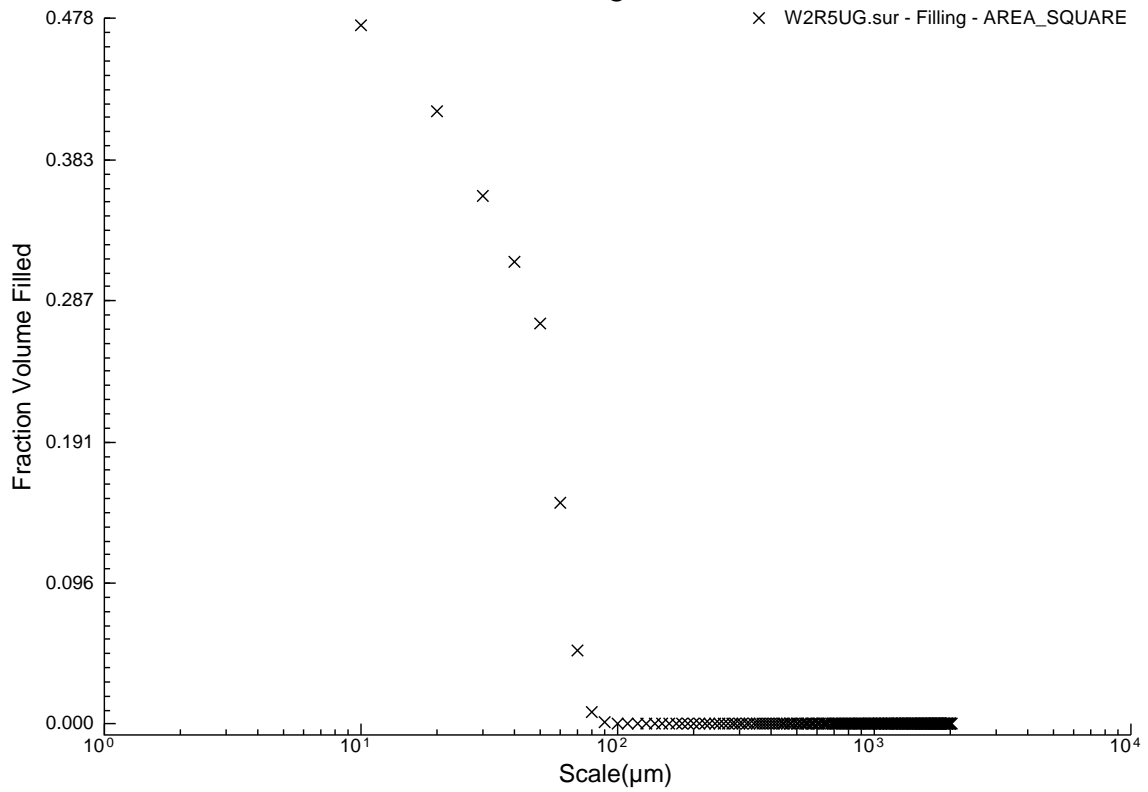
W2R3UG.sur - Filling - AREA\_SQUARE



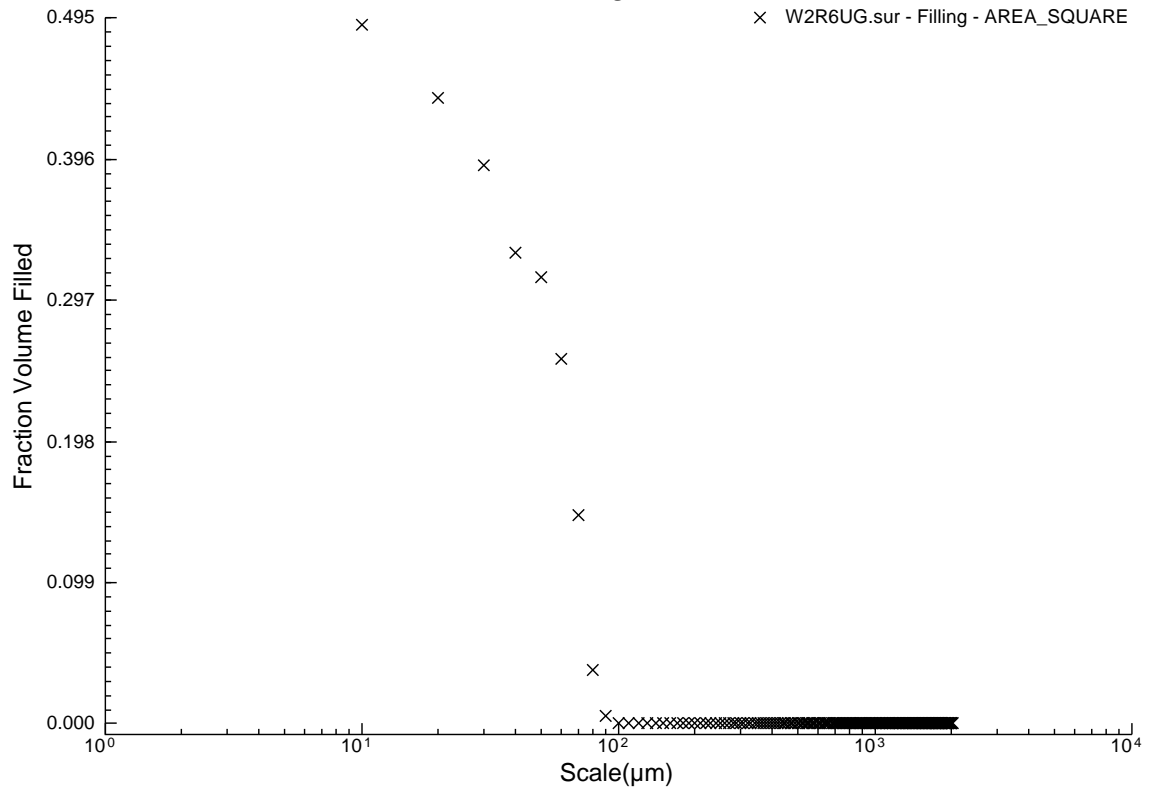
W2R4UG.sur - Filling - AREA\_SQUARE



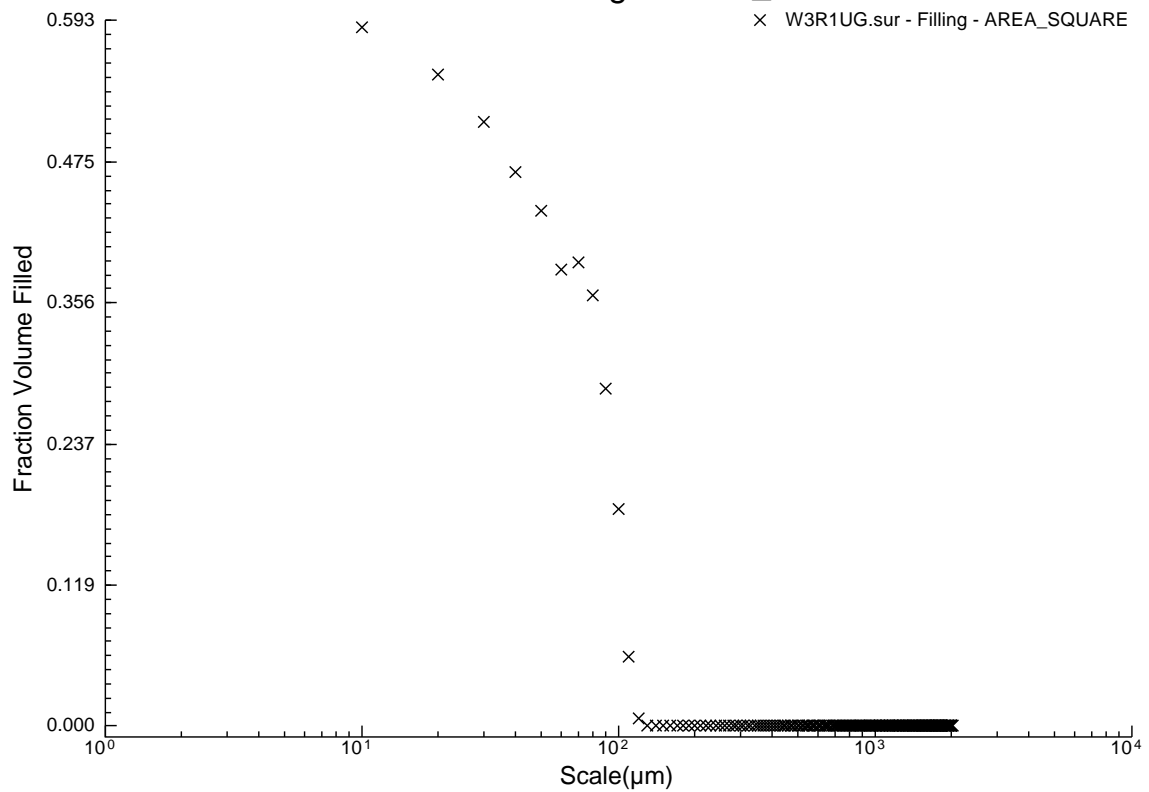
W2R5UG.sur - Filling - AREA\_SQUARE



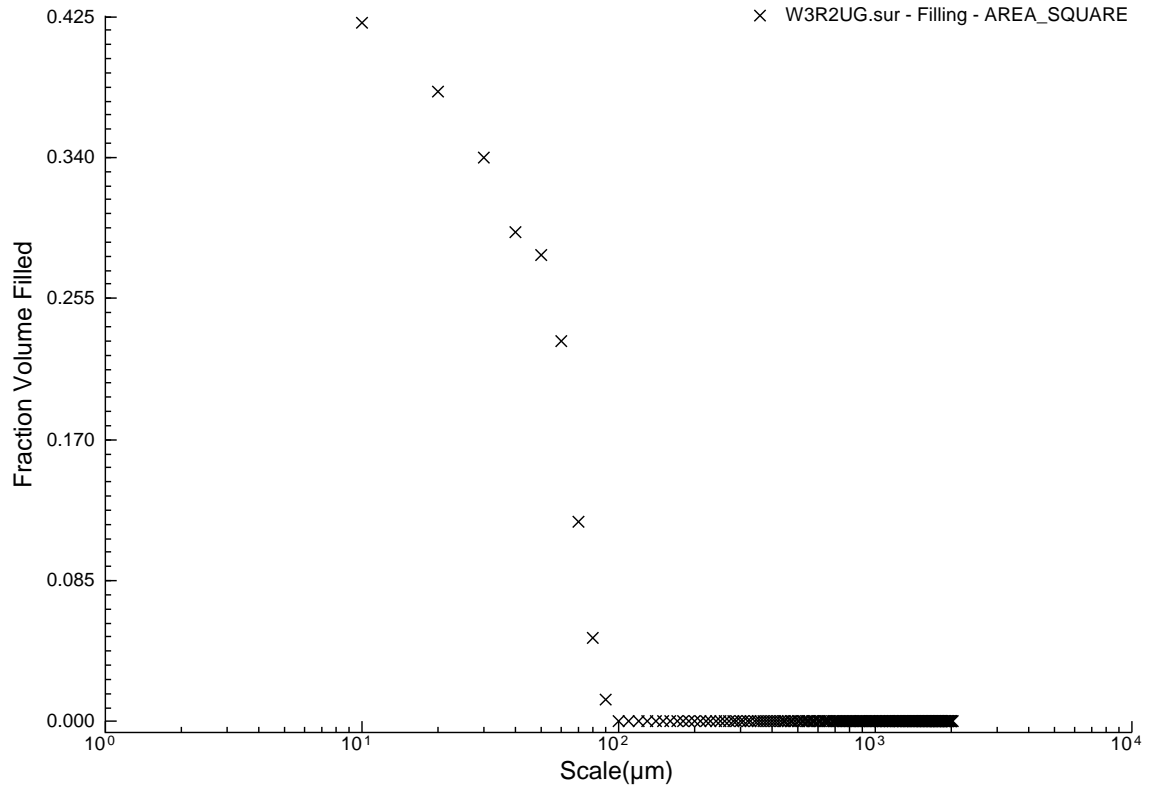
W2R6UG.sur - Filling - AREA\_SQUARE



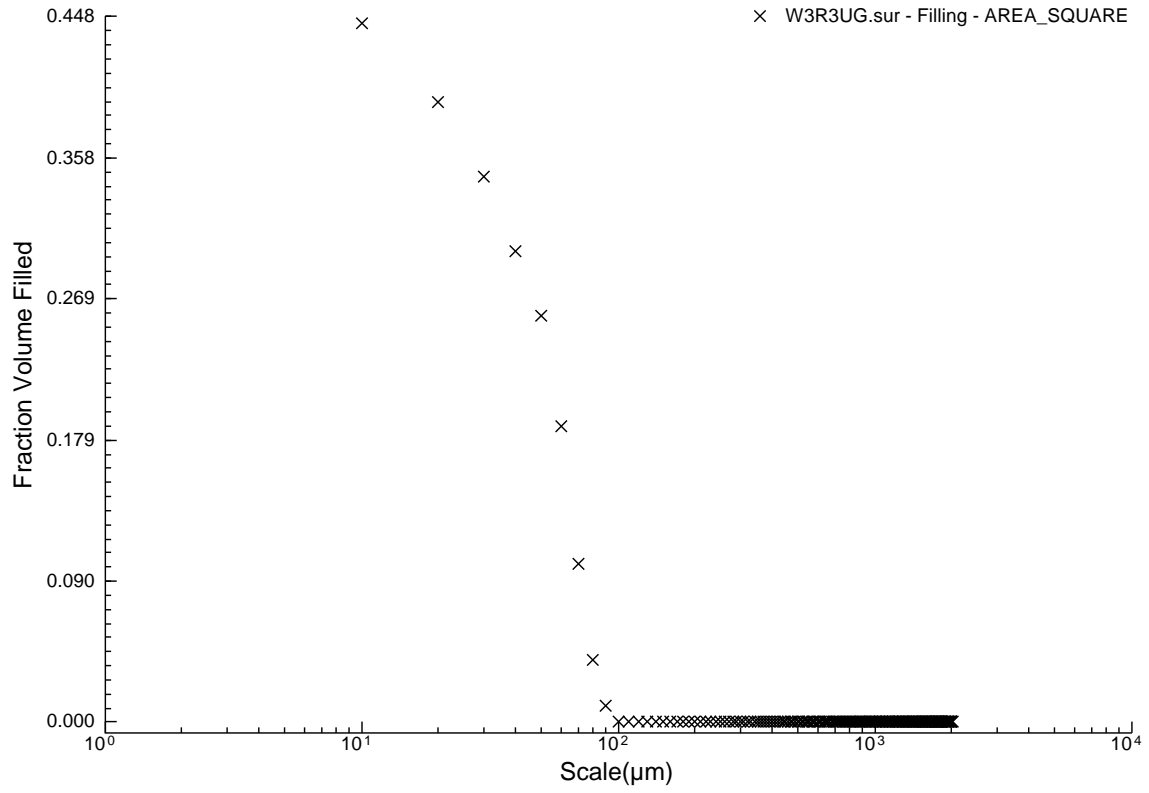
W3R1UG.sur - Filling - AREA\_SQUARE



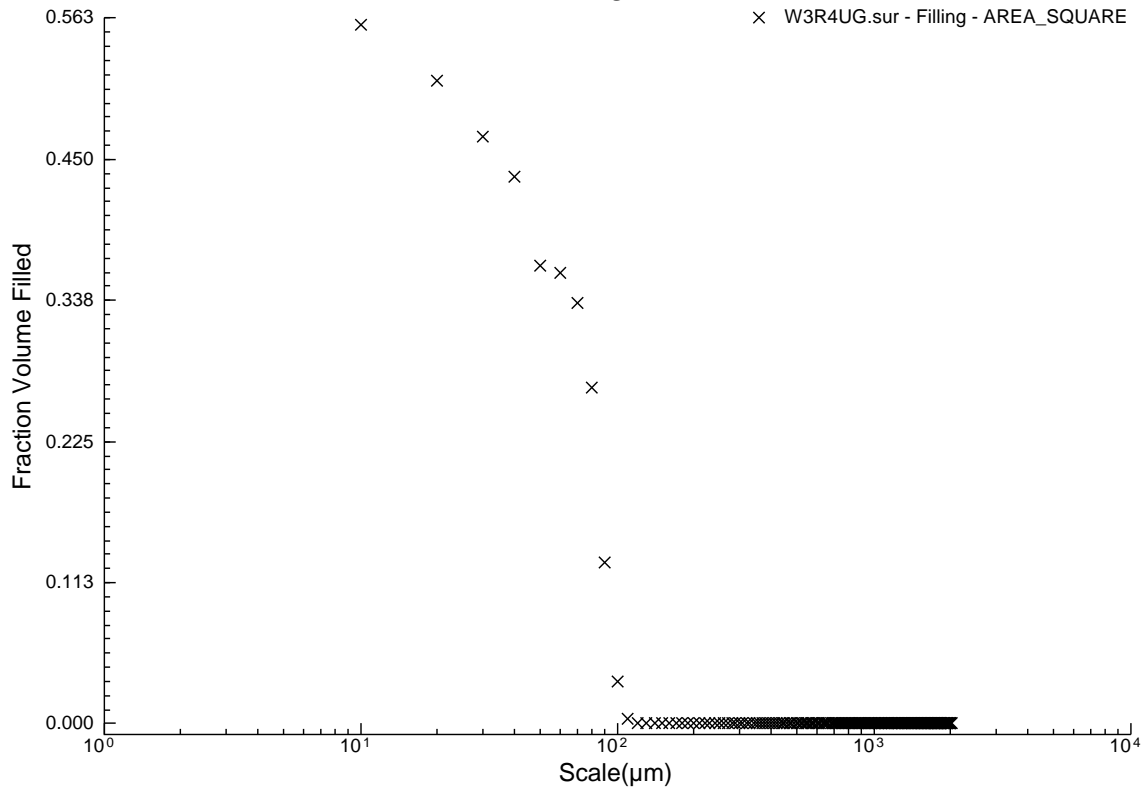
W3R2UG.sur - Filling - AREA\_SQUARE



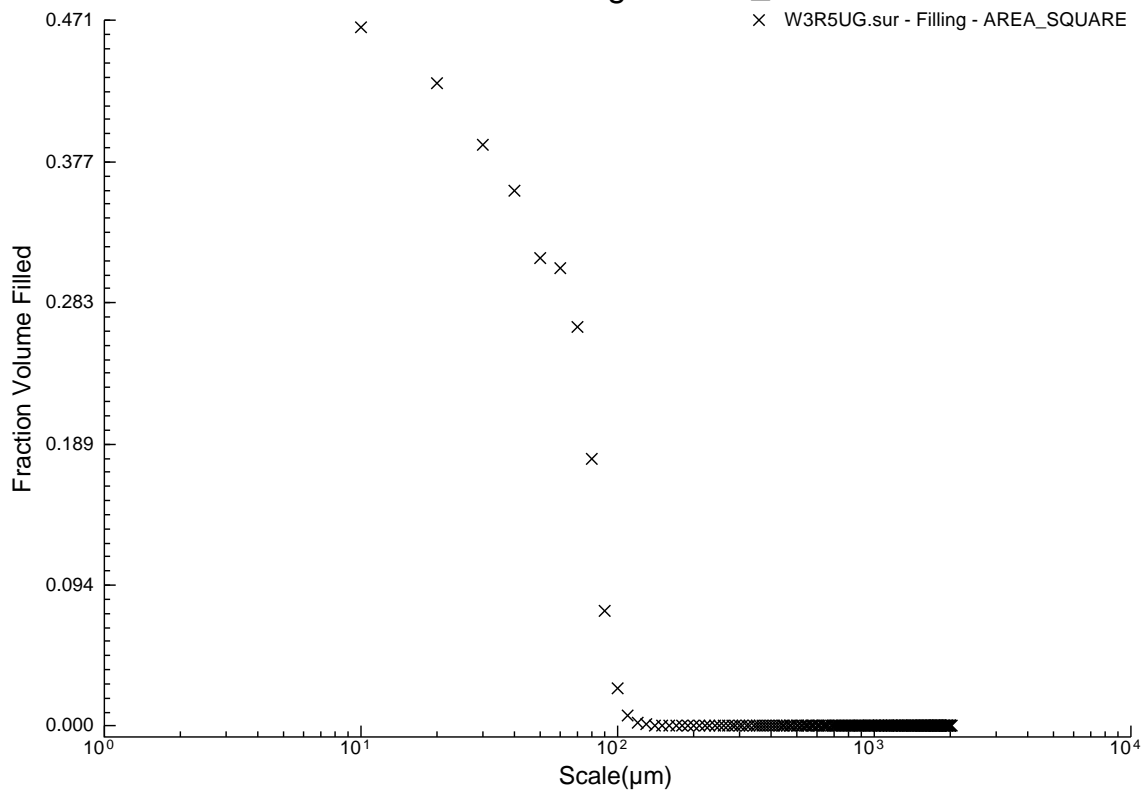
W3R3UG.sur - Filling - AREA\_SQUARE



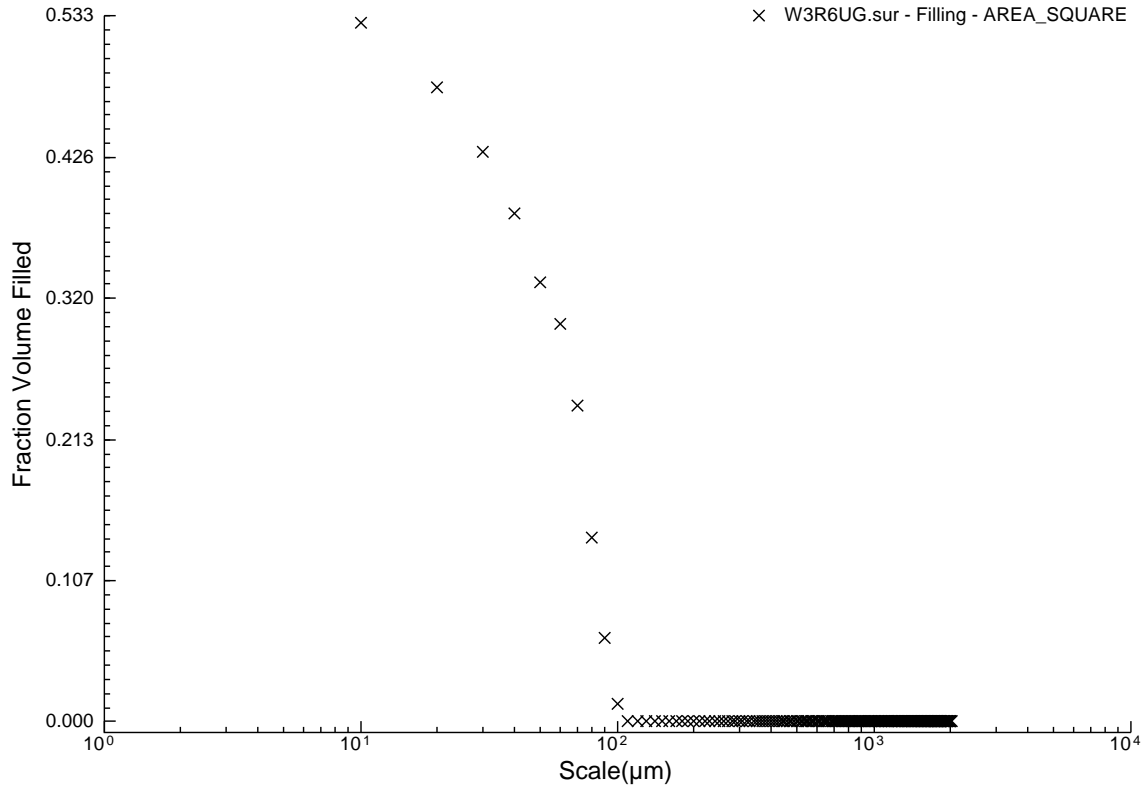
W3R4UG.sur - Filling - AREA\_SQUARE



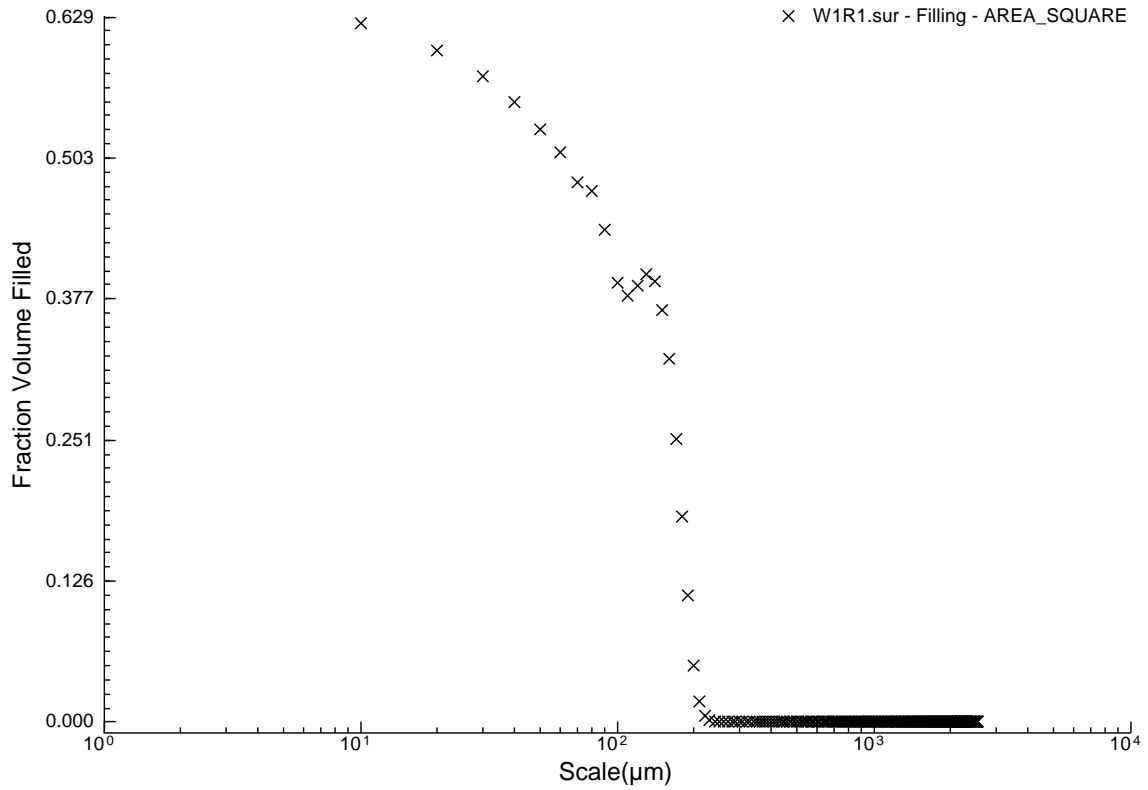
W3R5UG.sur - Filling - AREA\_SQUARE



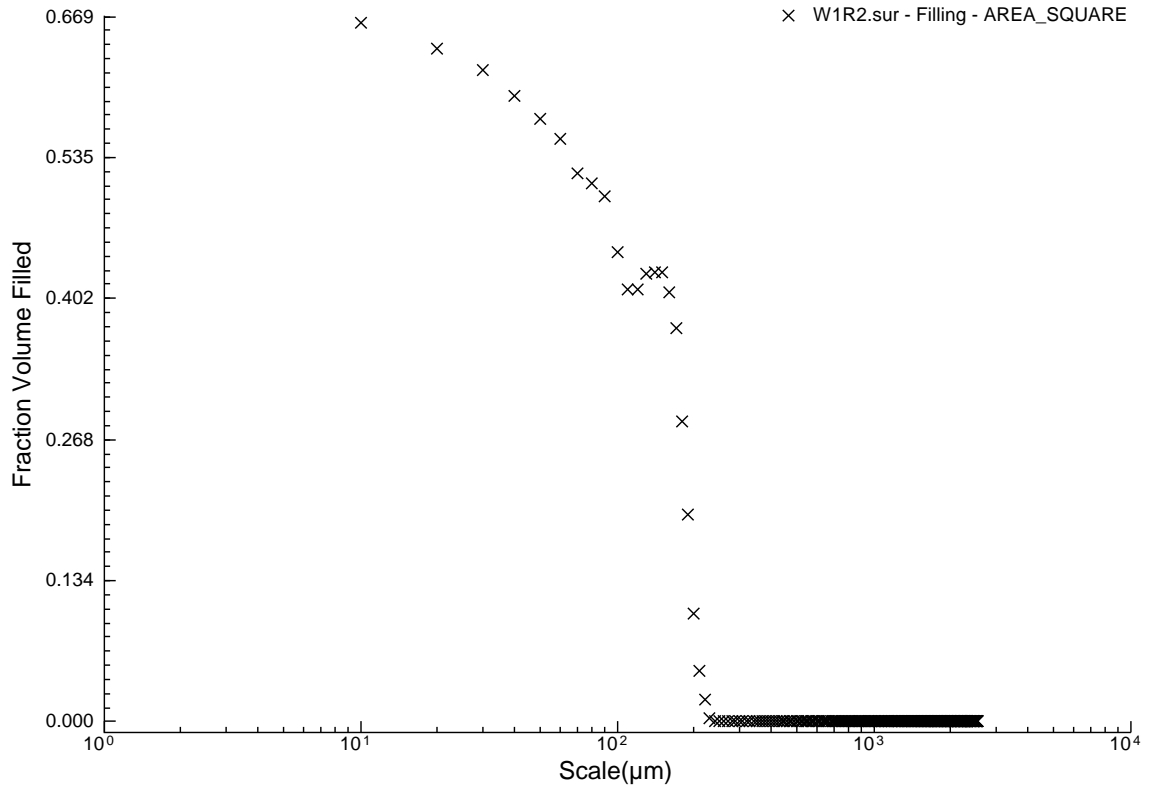
W3R6UG.sur - Filling - AREA\_SQUARE



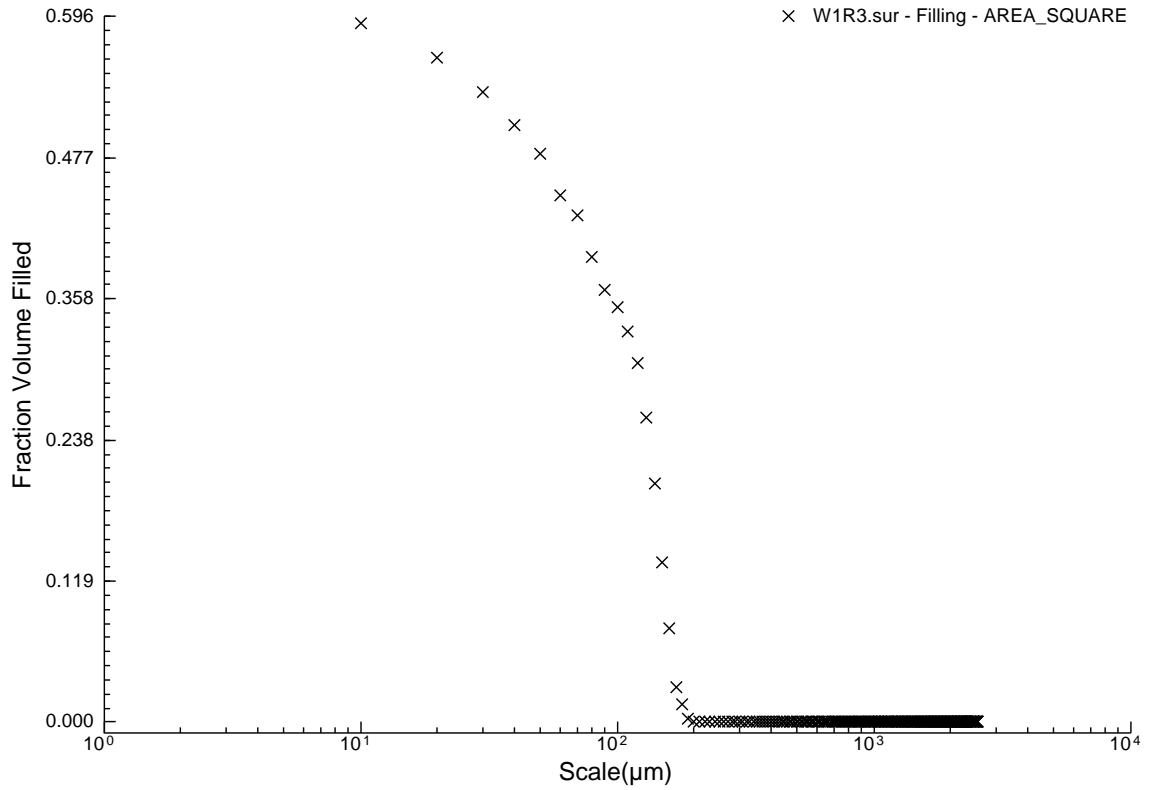
W1R1.sur - Filling - AREA\_SQUARE



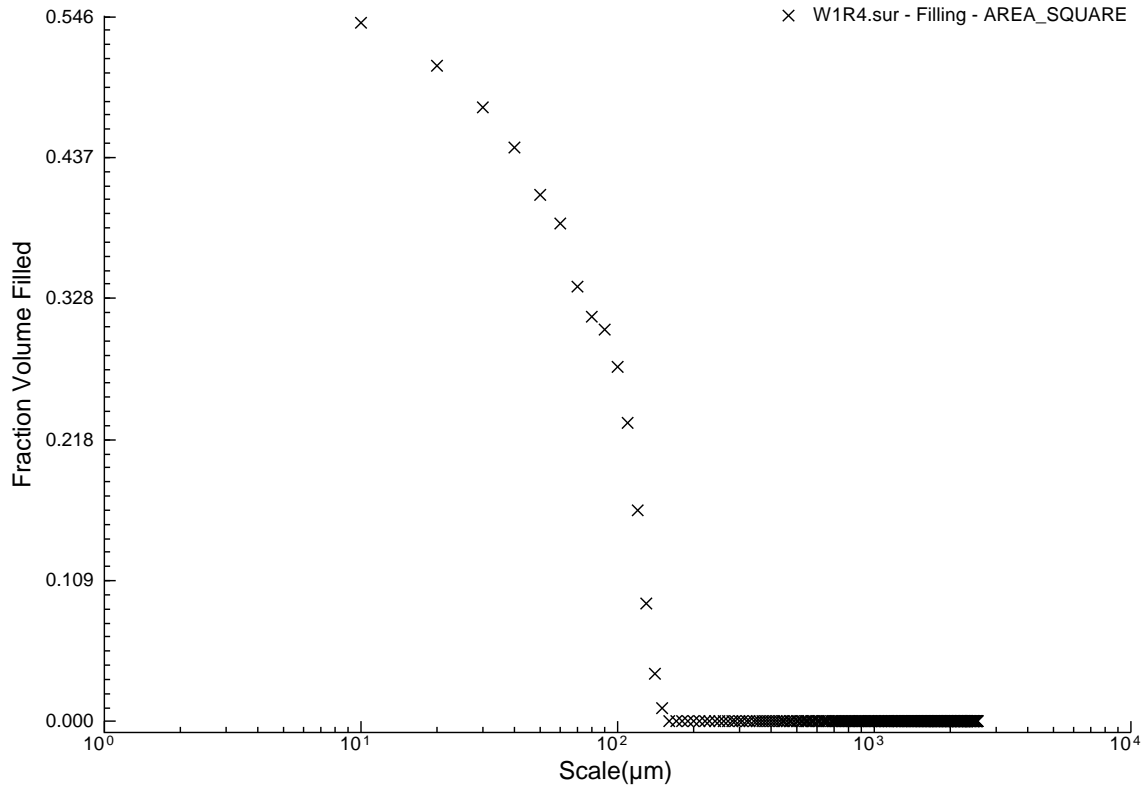
W1R2.sur - Filling - AREA\_SQUARE



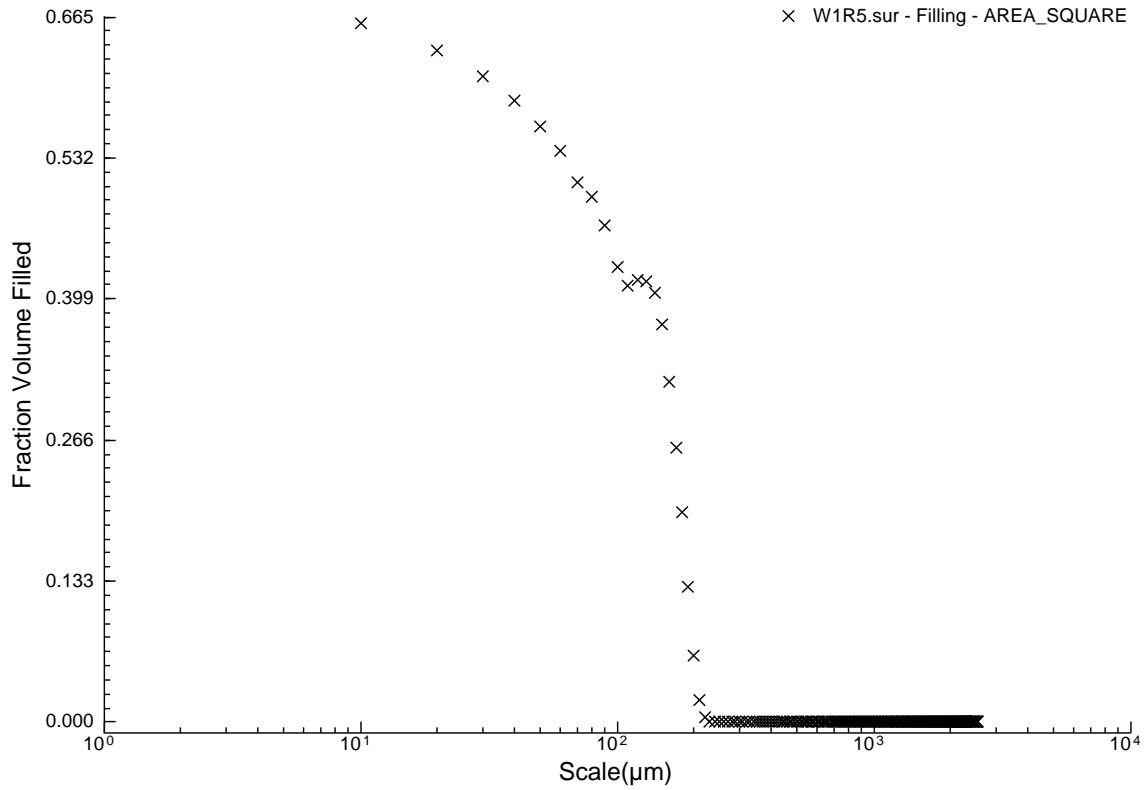
W1R3.sur - Filling - AREA\_SQUARE



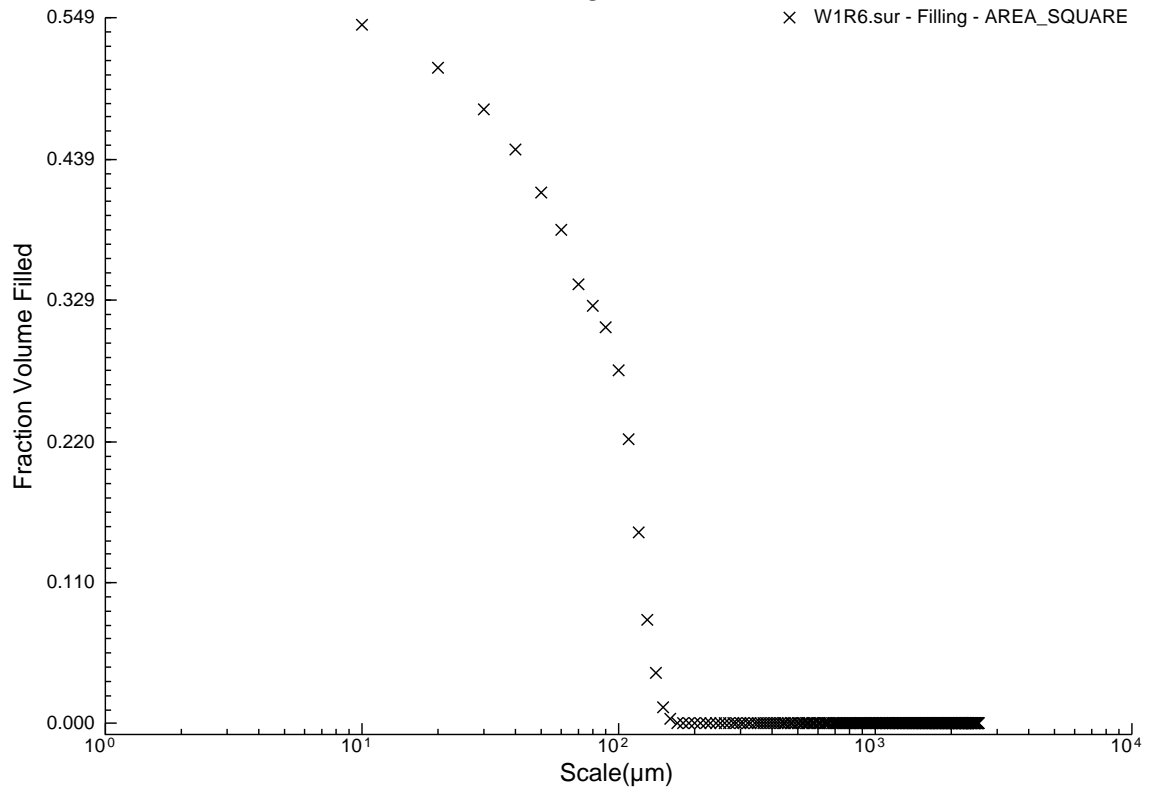
W1R4.sur - Filling - AREA\_SQUARE



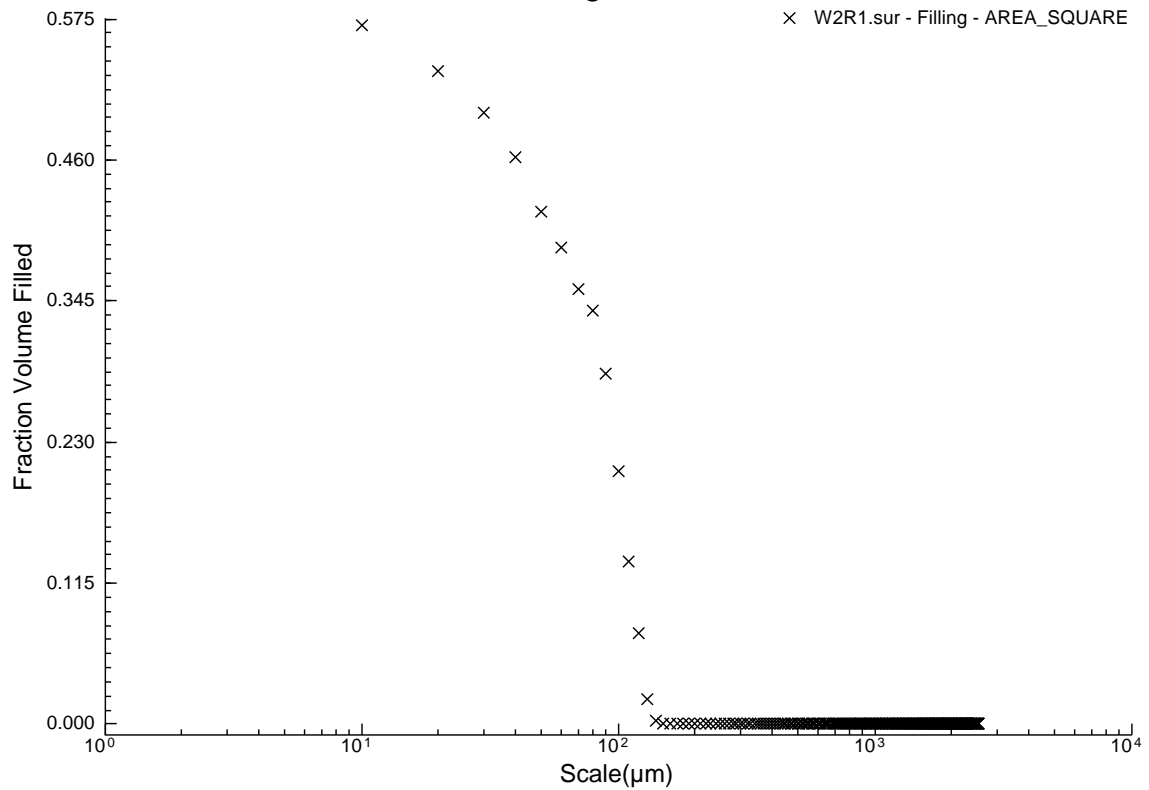
W1R5.sur - Filling - AREA\_SQUARE



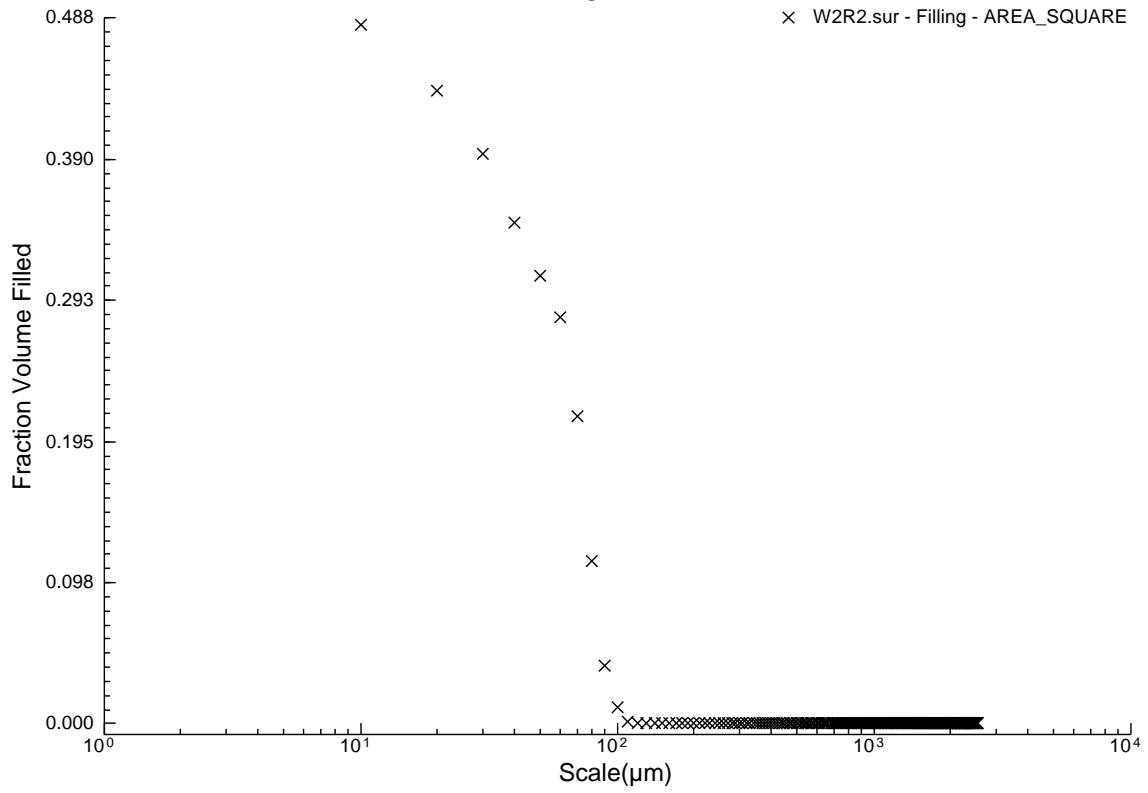
W1R6.sur - Filling - AREA\_SQUARE



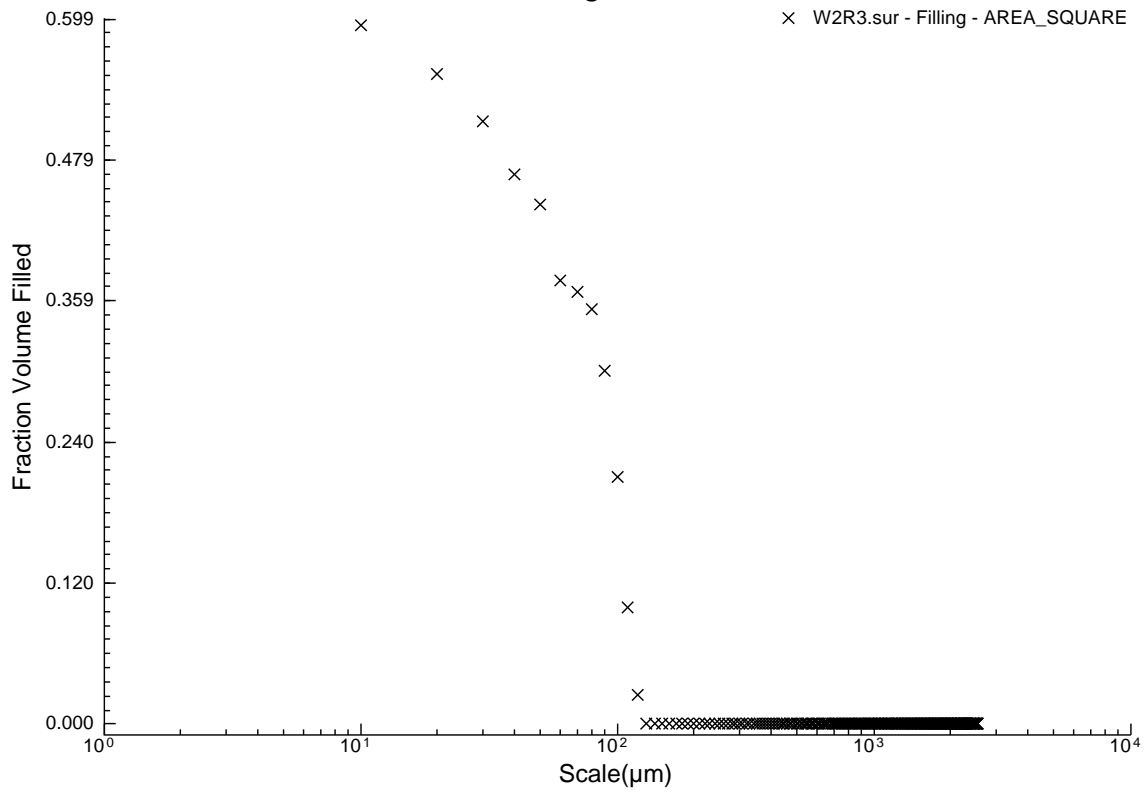
W2R1.sur - Filling - AREA\_SQUARE



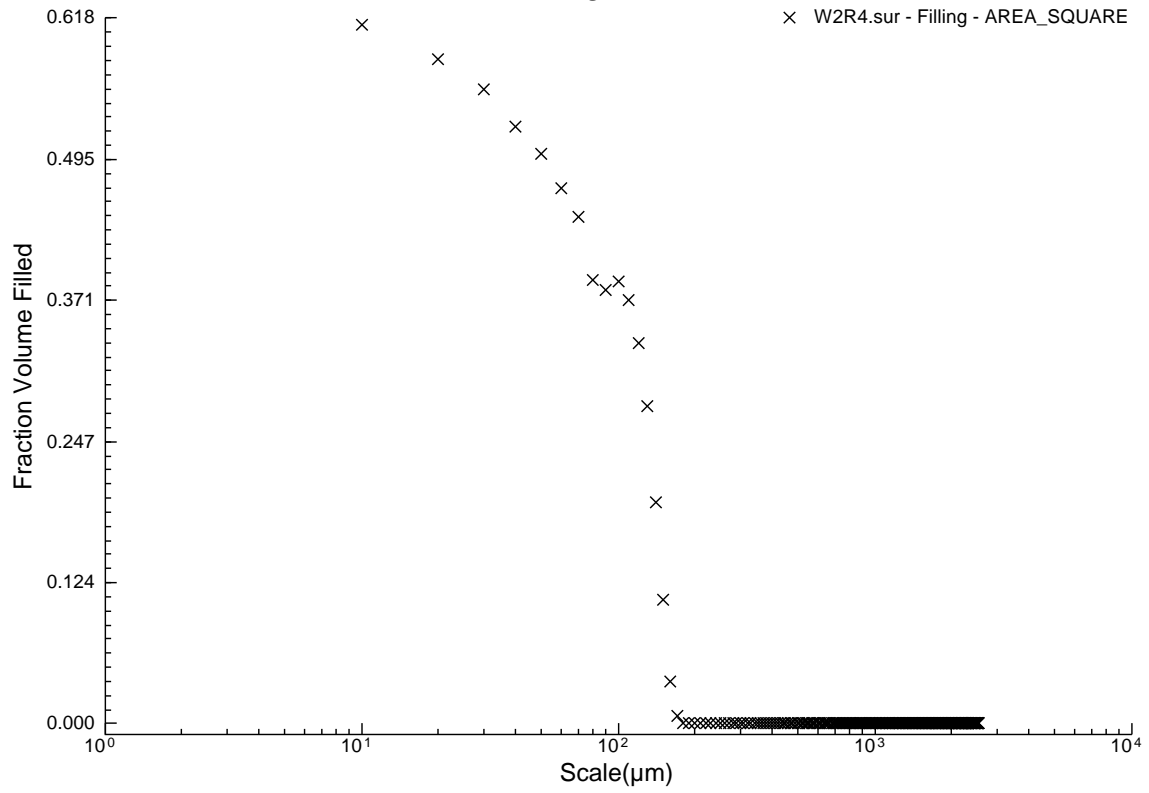
W2R2.sur - Filling - AREA\_SQUARE



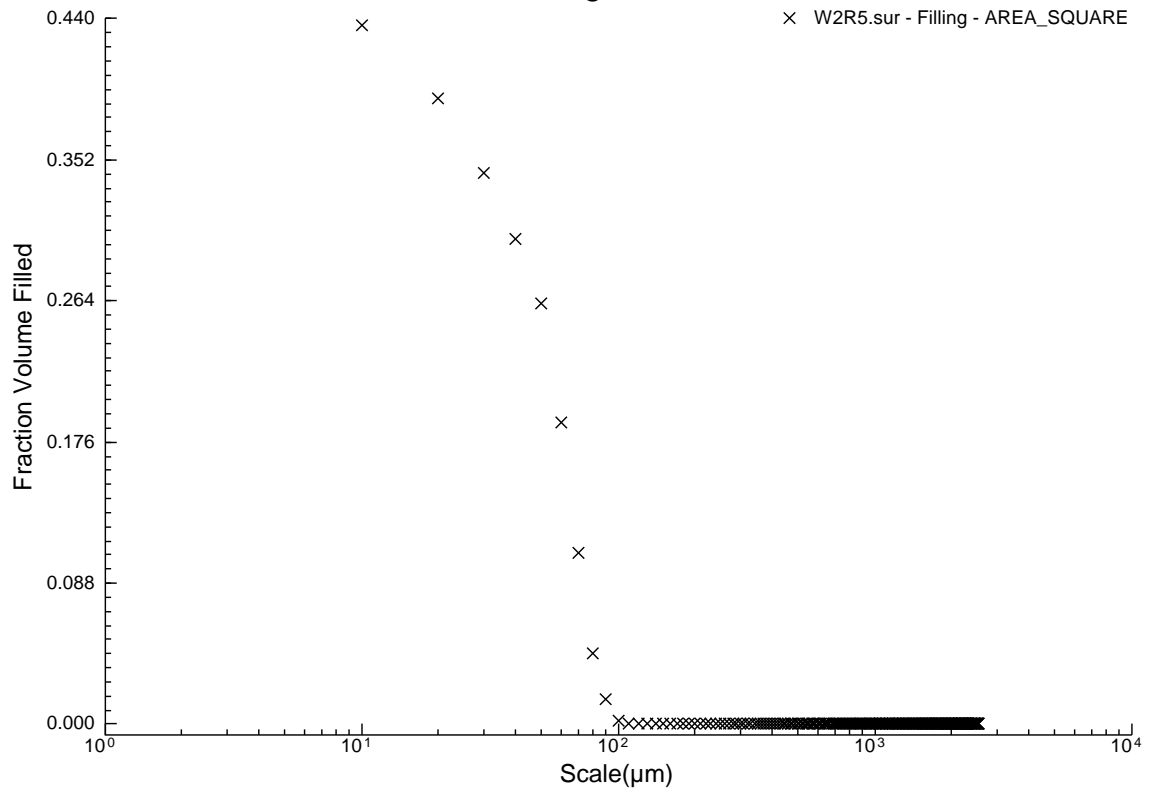
W2R3.sur - Filling - AREA\_SQUARE



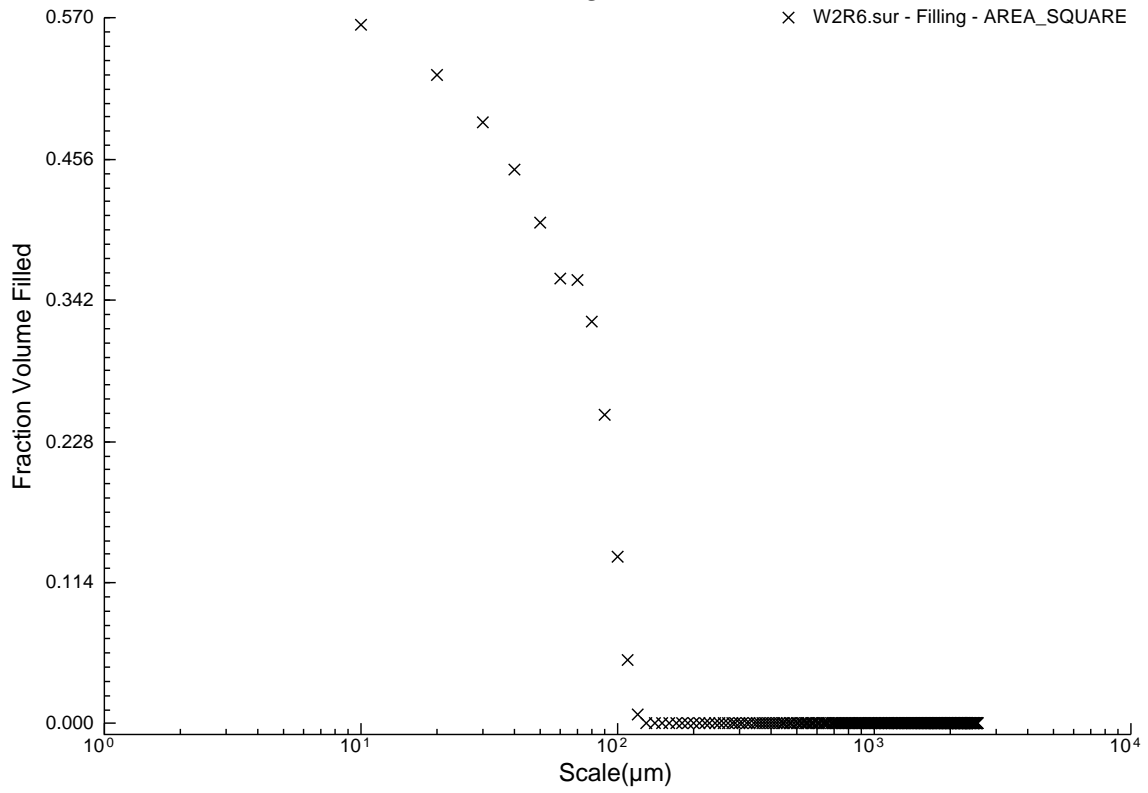
W2R4.sur - Filling - AREA\_SQUARE



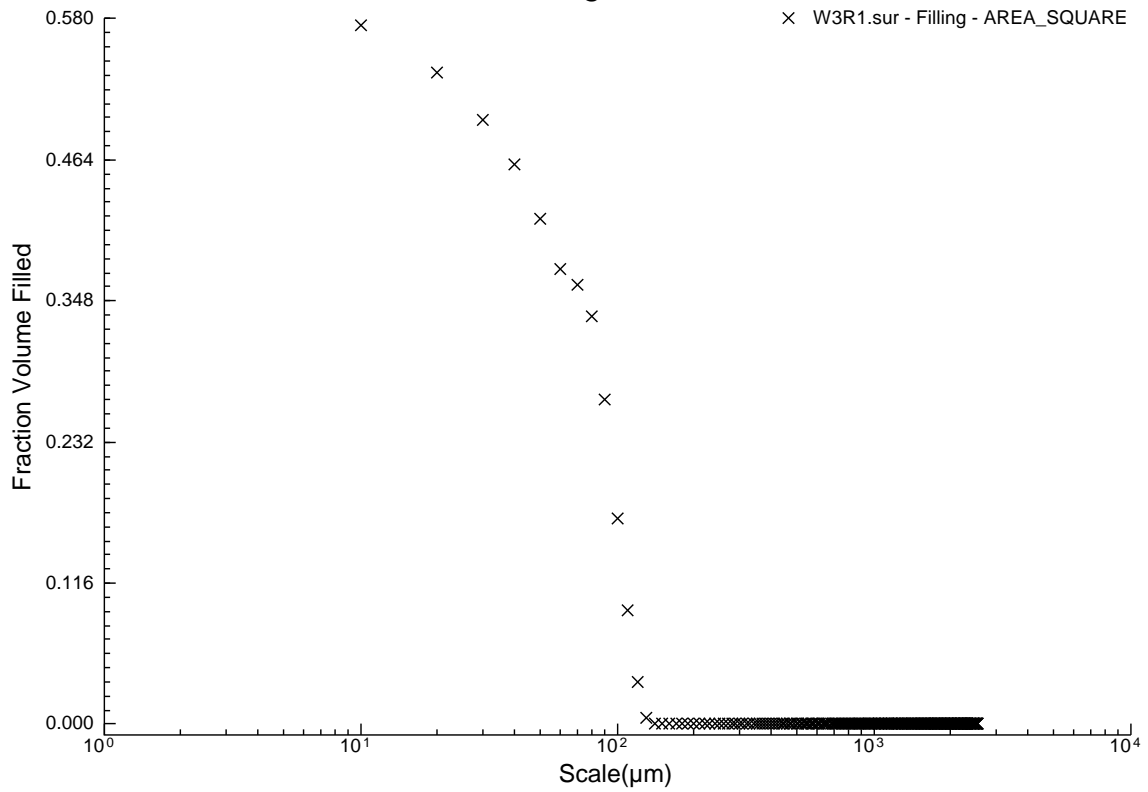
W2R5.sur - Filling - AREA\_SQUARE



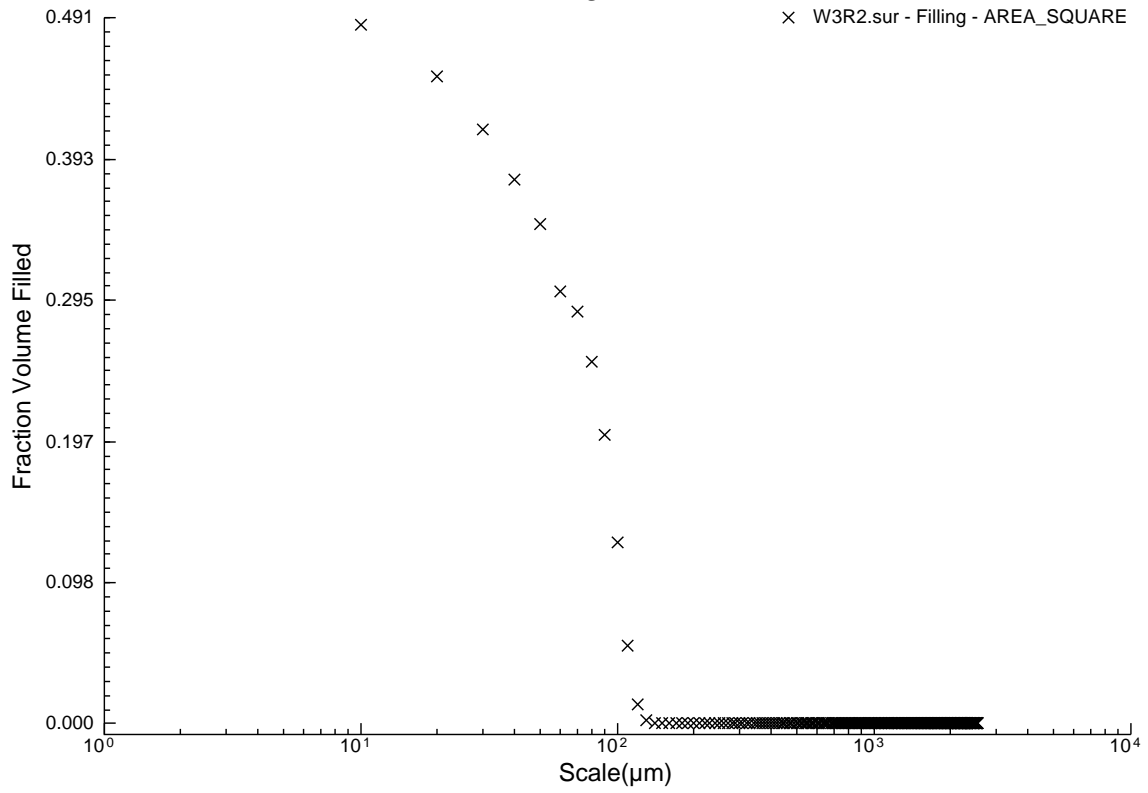
W2R6.sur - Filling - AREA\_SQUARE



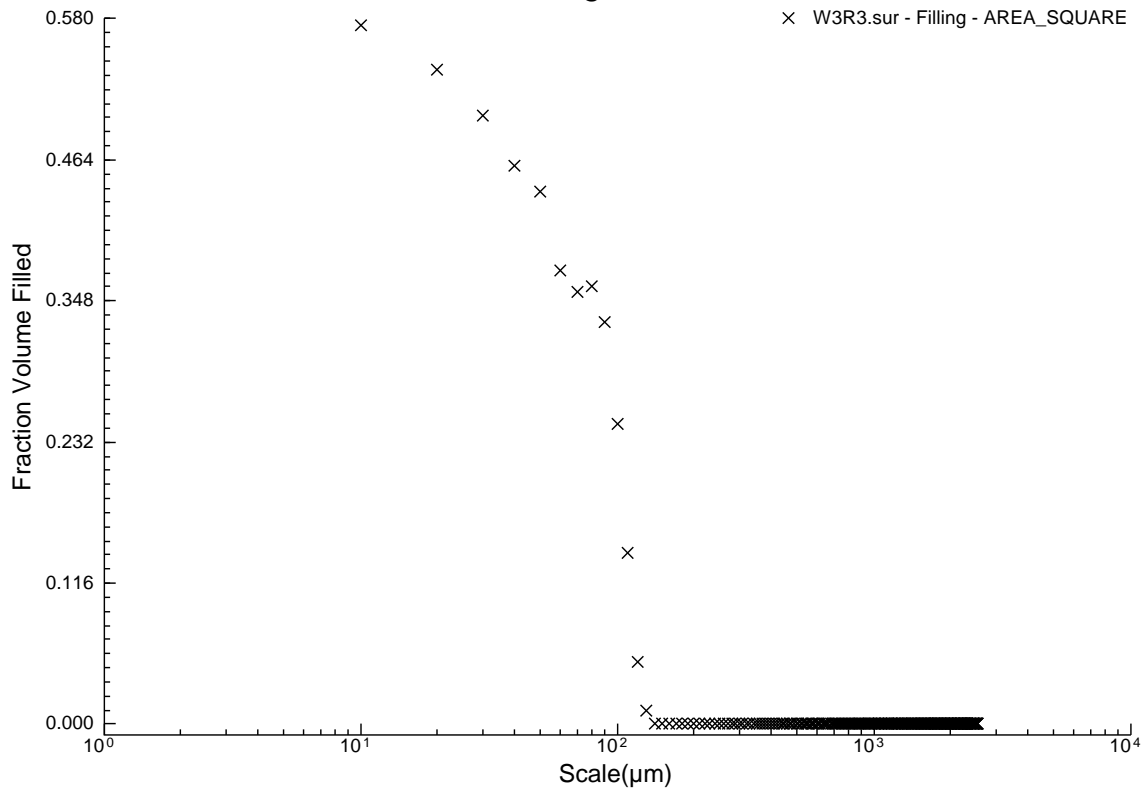
W3R1.sur - Filling - AREA\_SQUARE



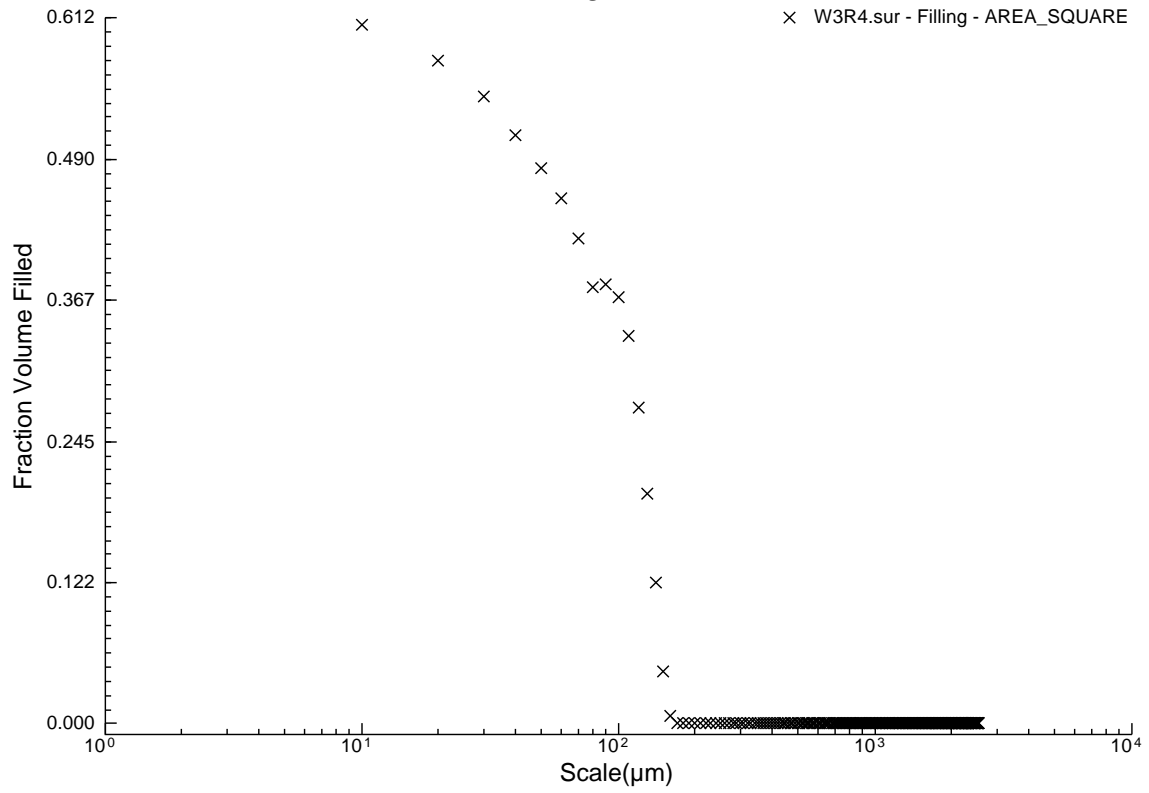
W3R2.sur - Filling - AREA\_SQUARE



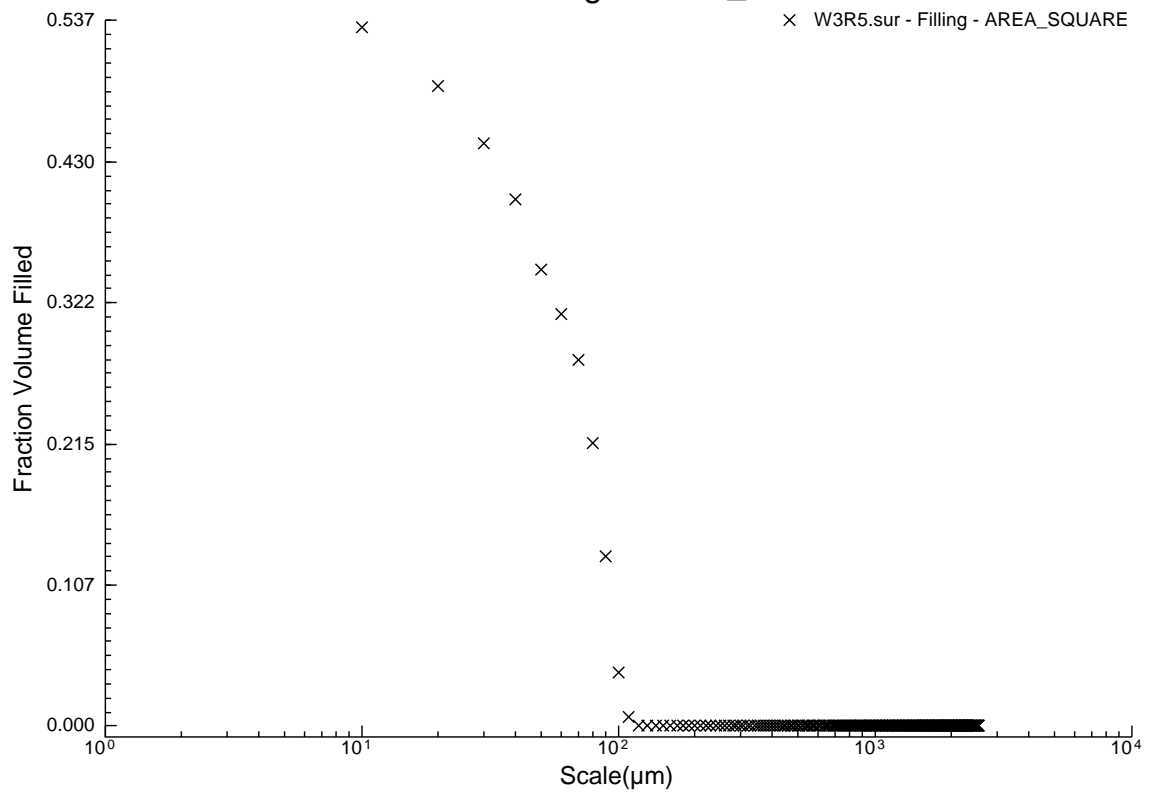
W3R3.sur - Filling - AREA\_SQUARE



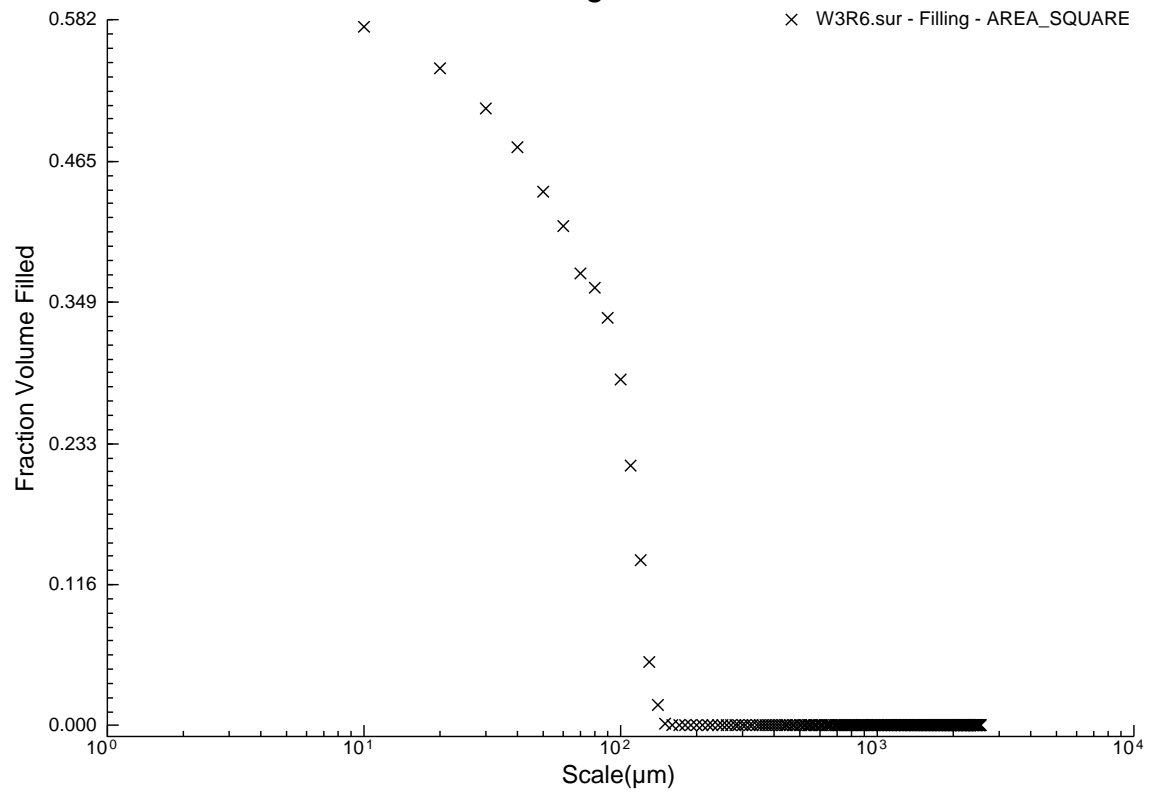
W3R4.sur - Filling - AREA\_SQUARE



W3R5.sur - Filling - AREA\_SQUARE



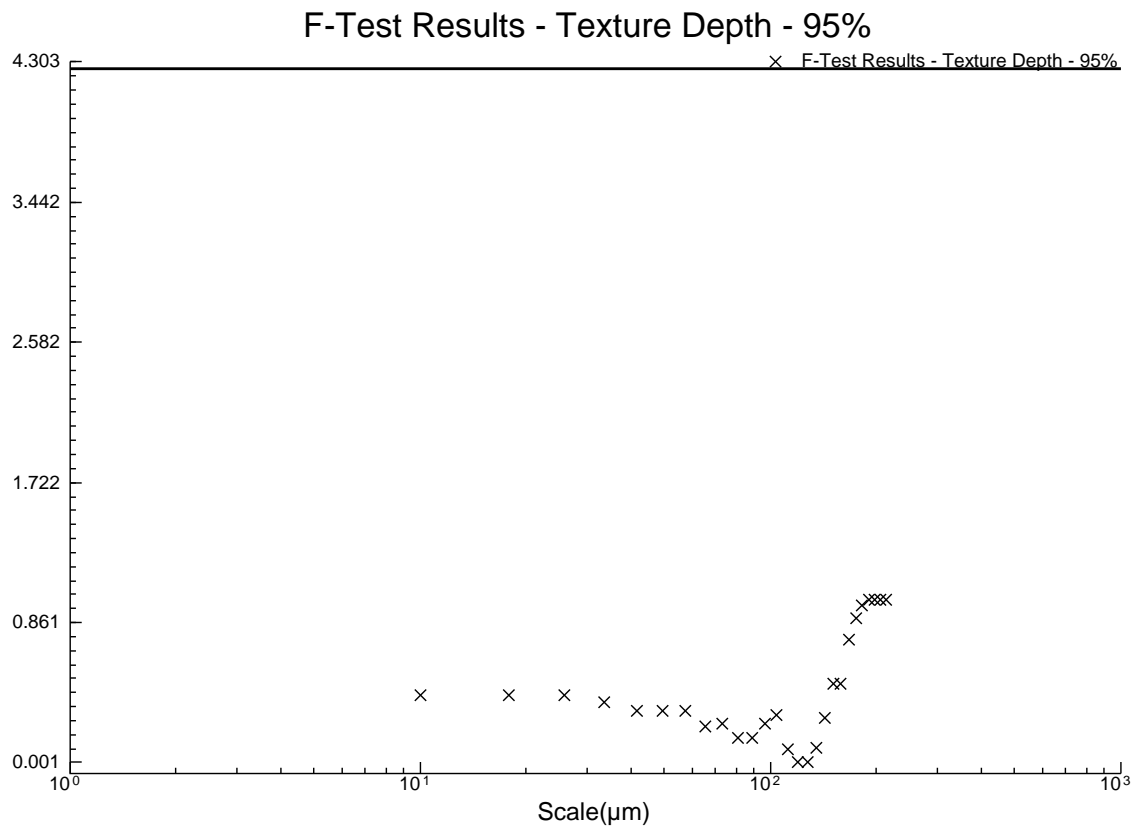
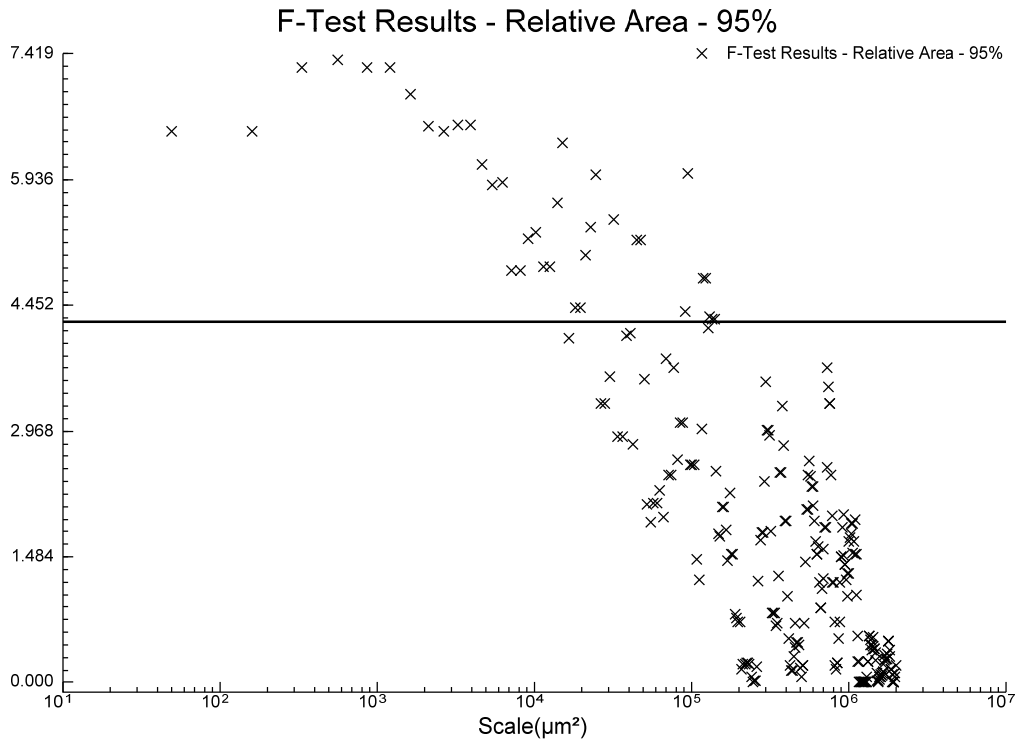
# W3R6.sur - Filling - AREA\_SQUARE



# Appendix C

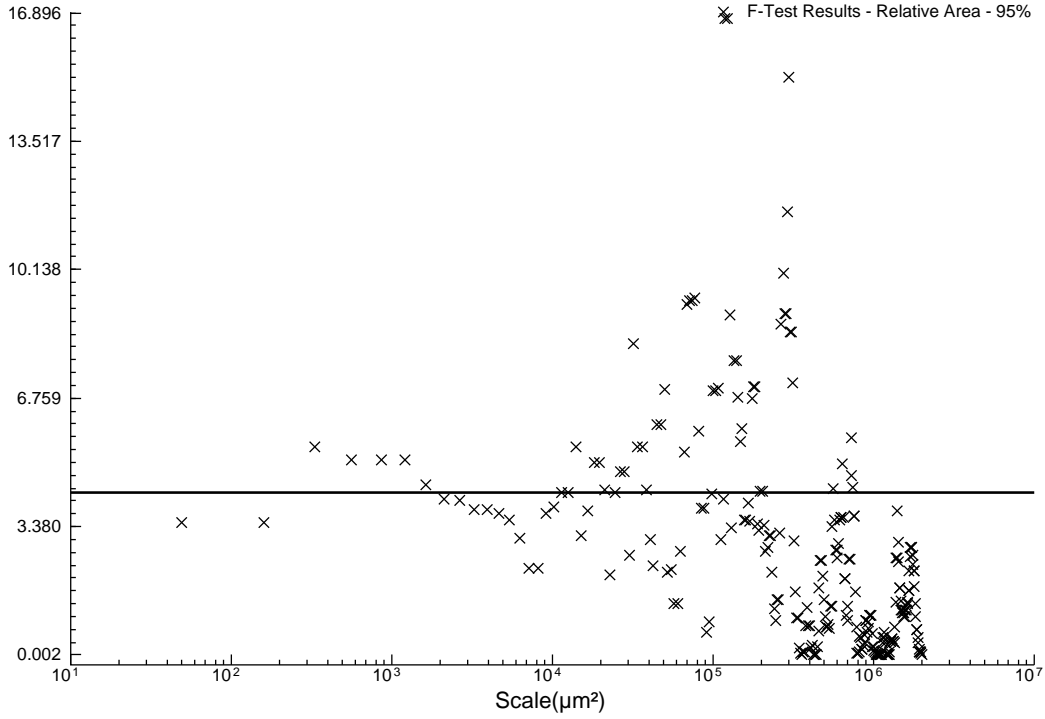
## F-test Plots

B1DVSB1U

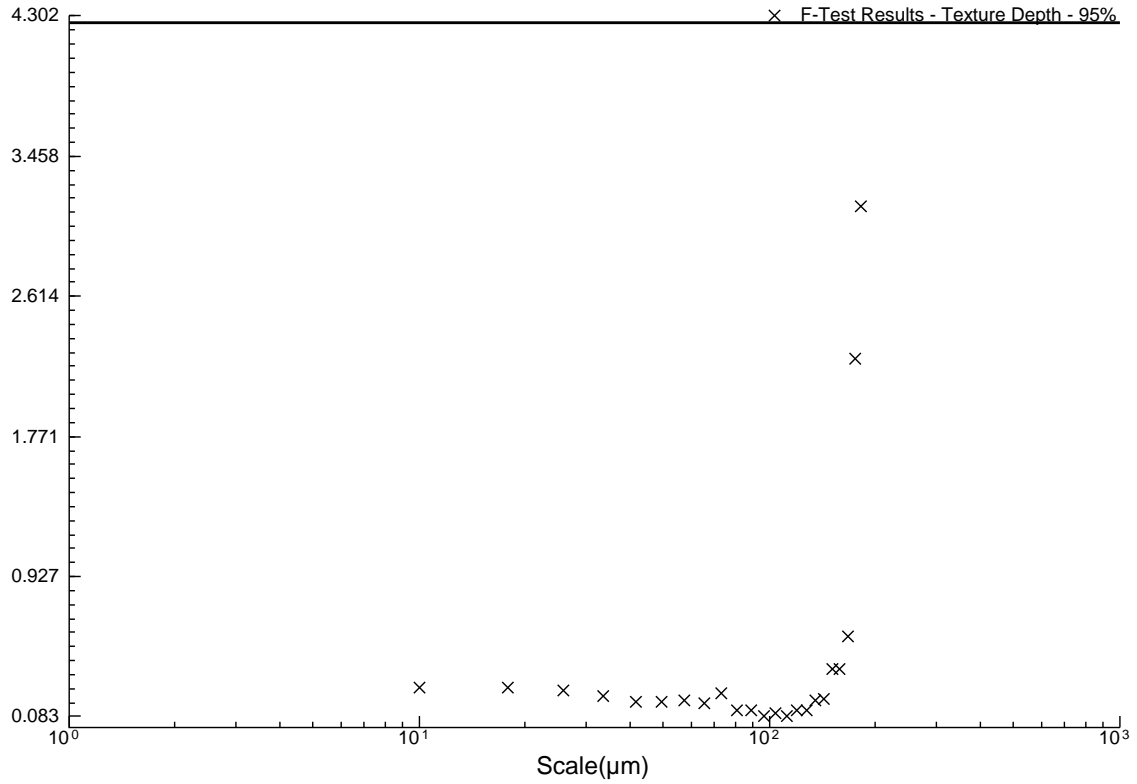


B1DVSB2U

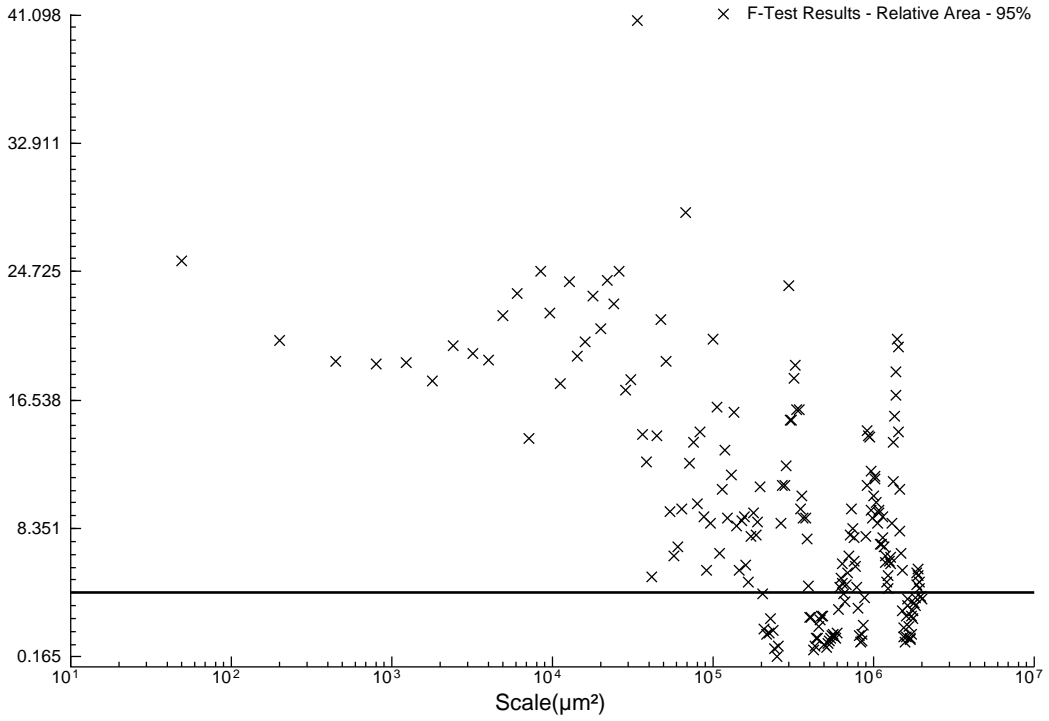
### F-Test Results - Relative Area - 95%



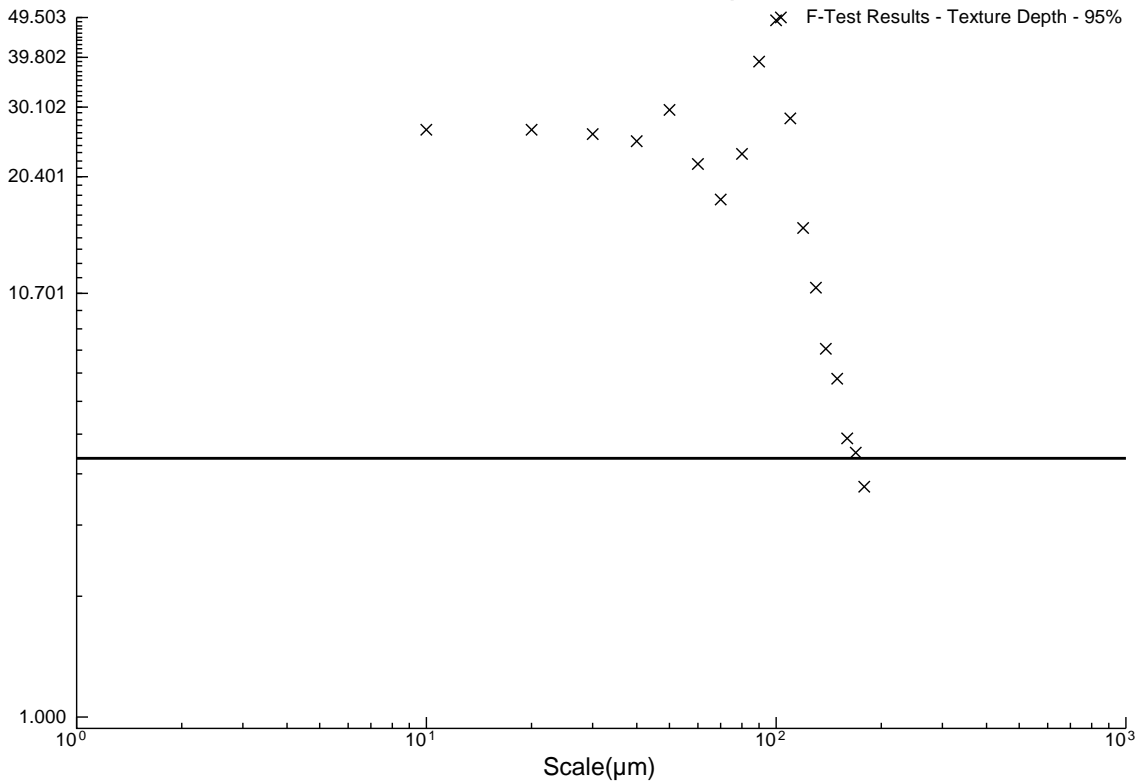
### F-Test Results - Texture Depth - 95%



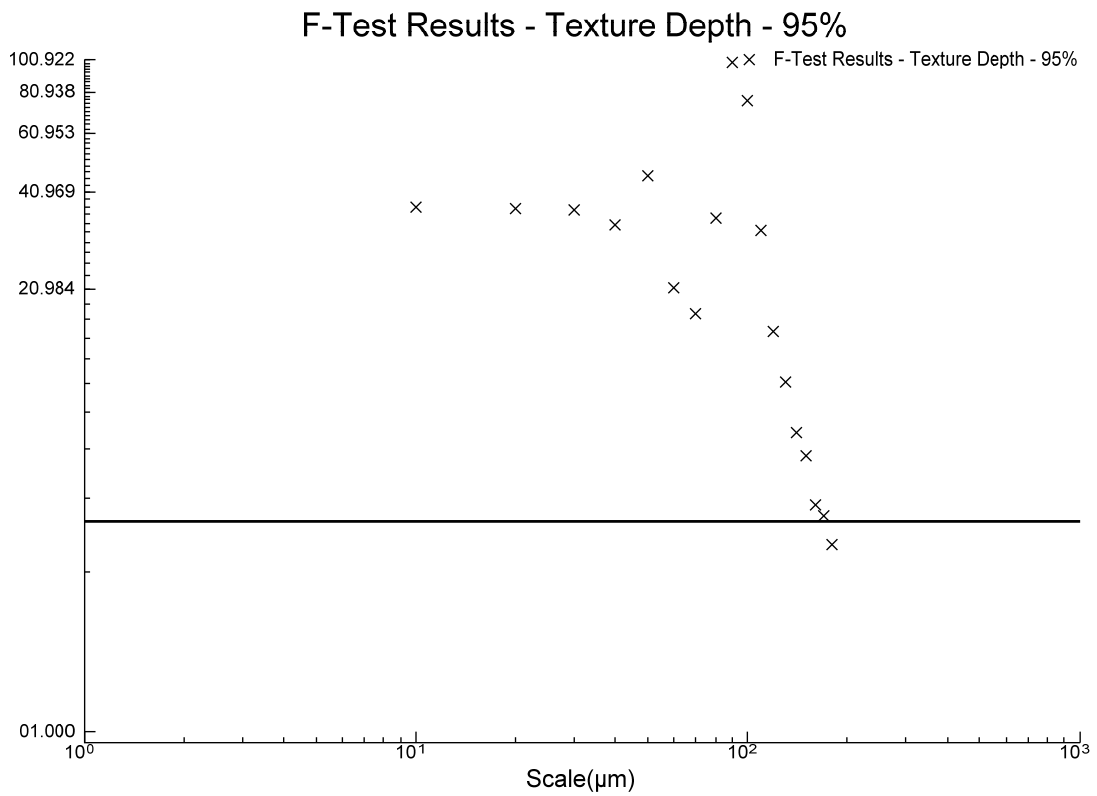
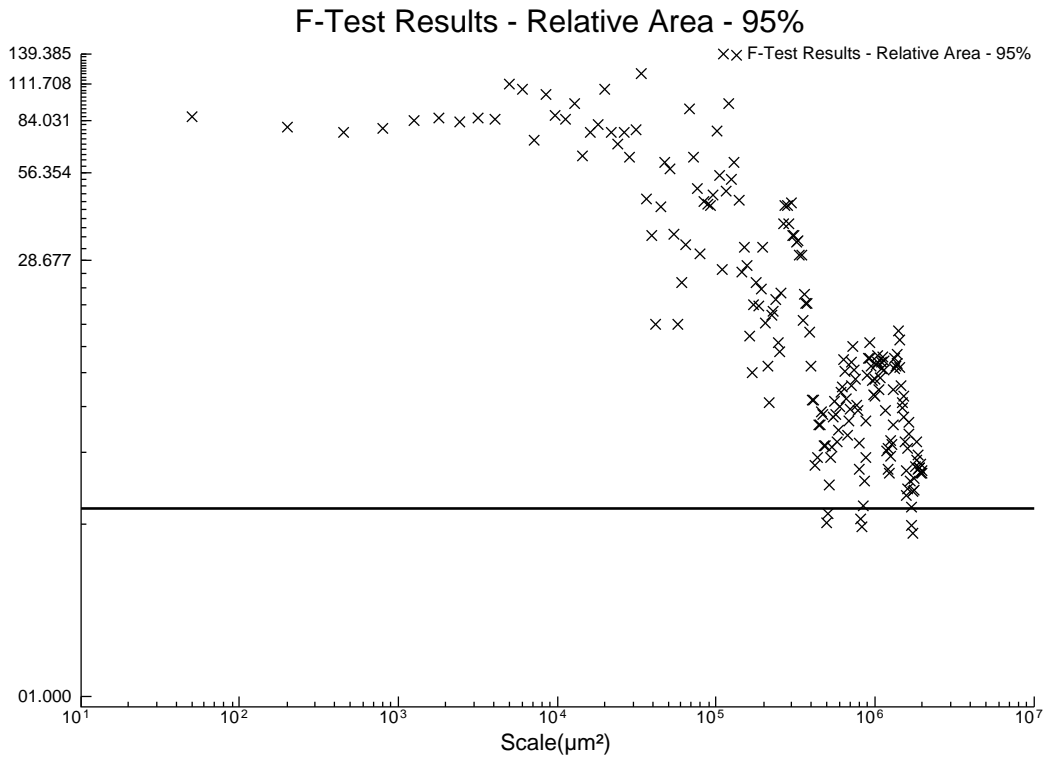
### F-Test Results - Relative Area - 95%



### F-Test Results - Texture Depth - 95%

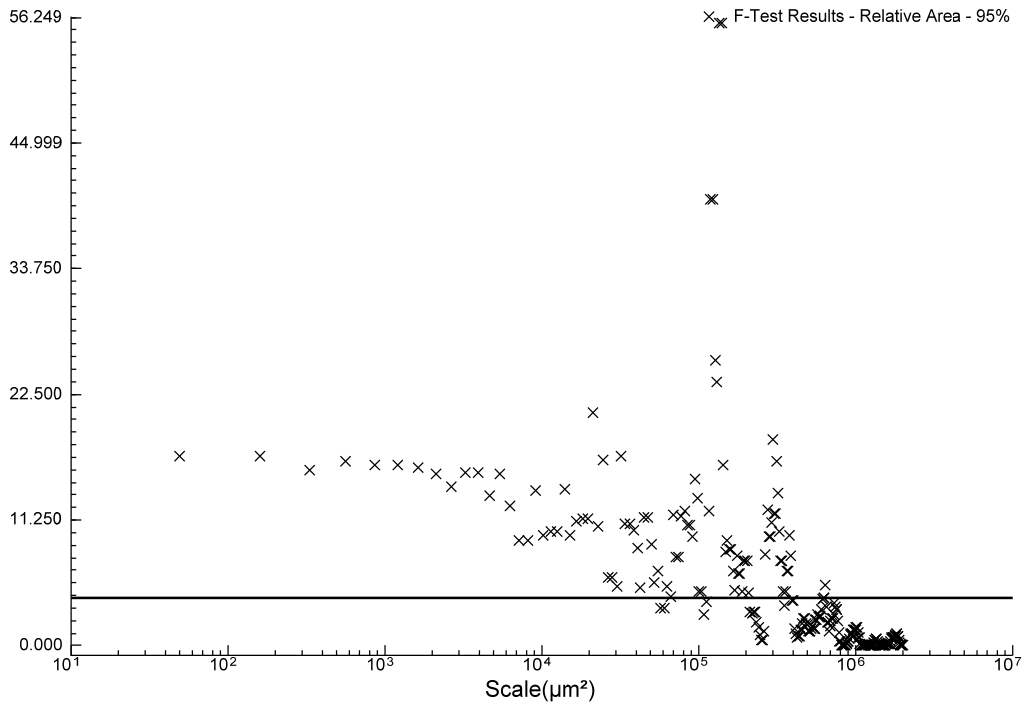


B1DVSB3D

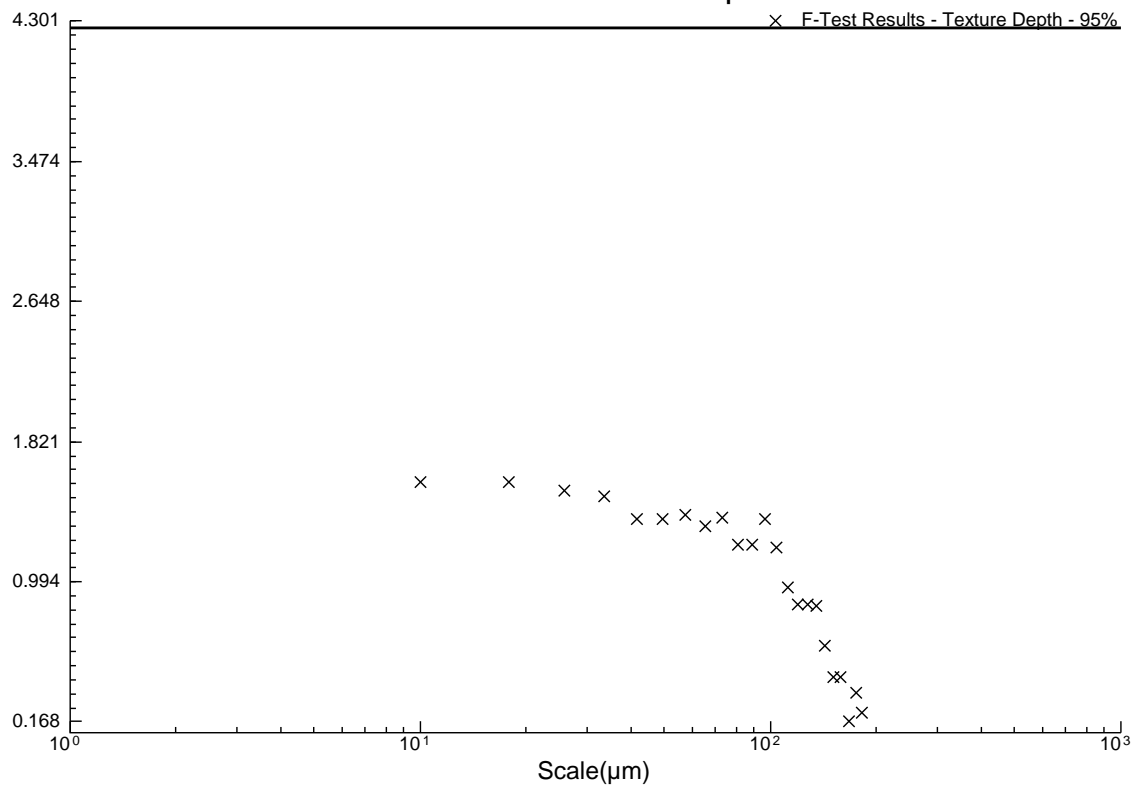


B1DVSB3U

F-Test Results - Relative Area - 95%

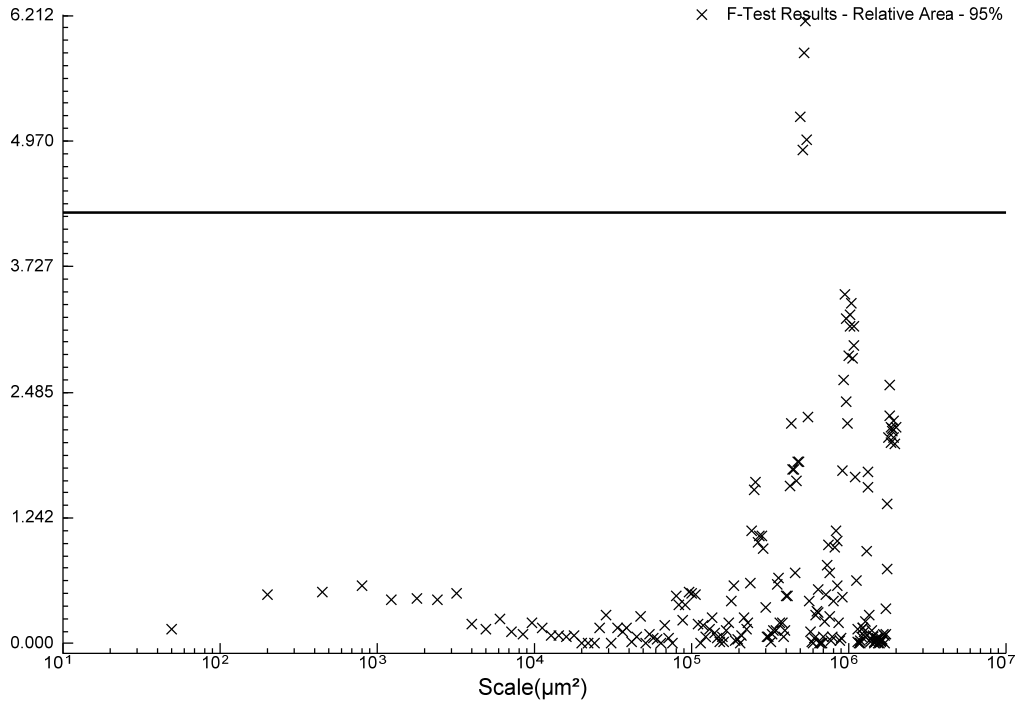


F-Test Results - Texture Depth - 95%

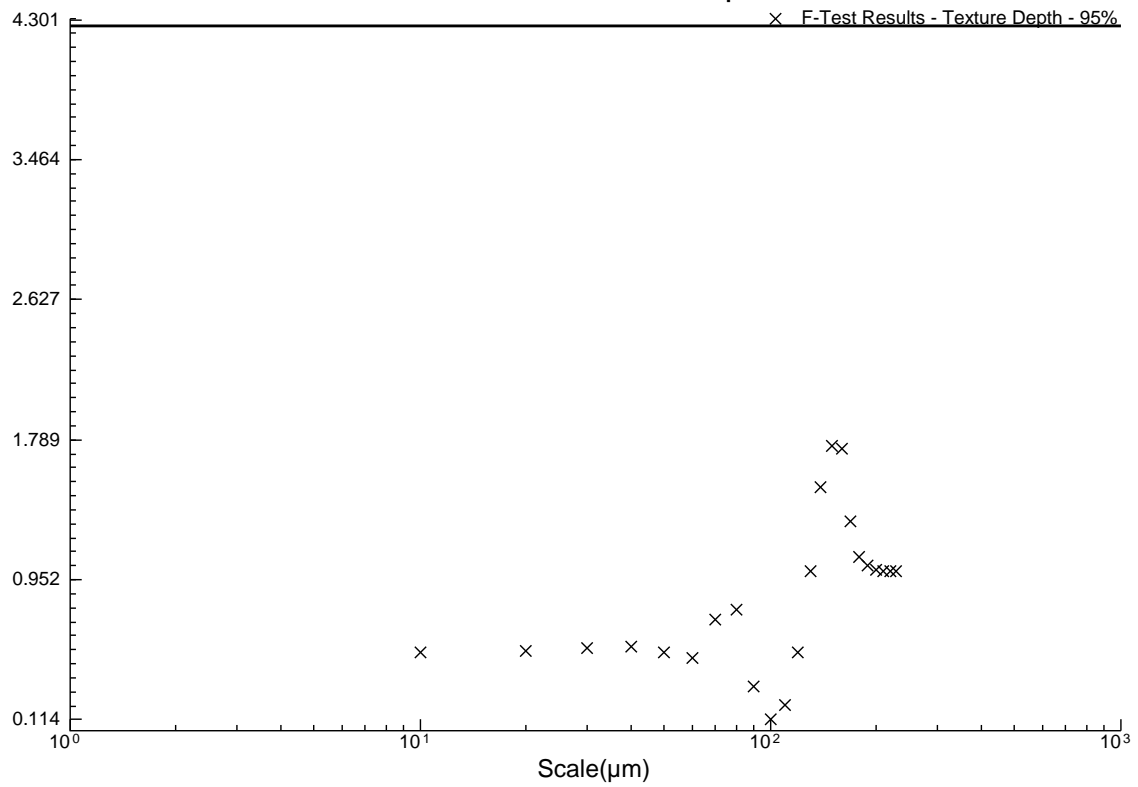


B1DVSW1D

### F-Test Results - Relative Area - 95%

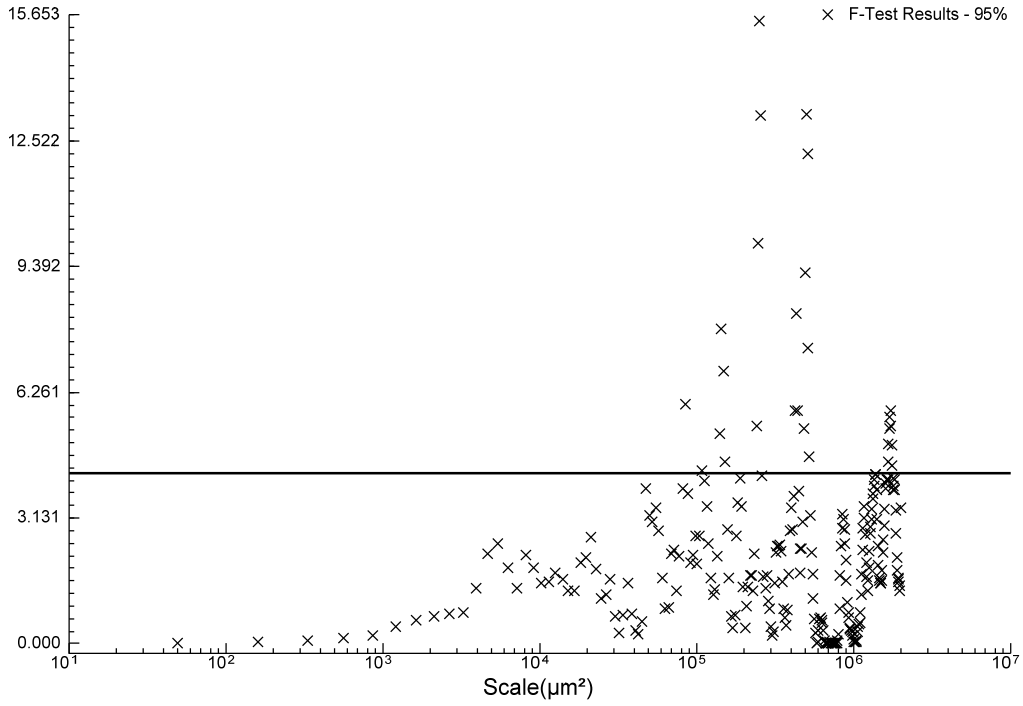


### F-Test Results - Texture Depth - 95%

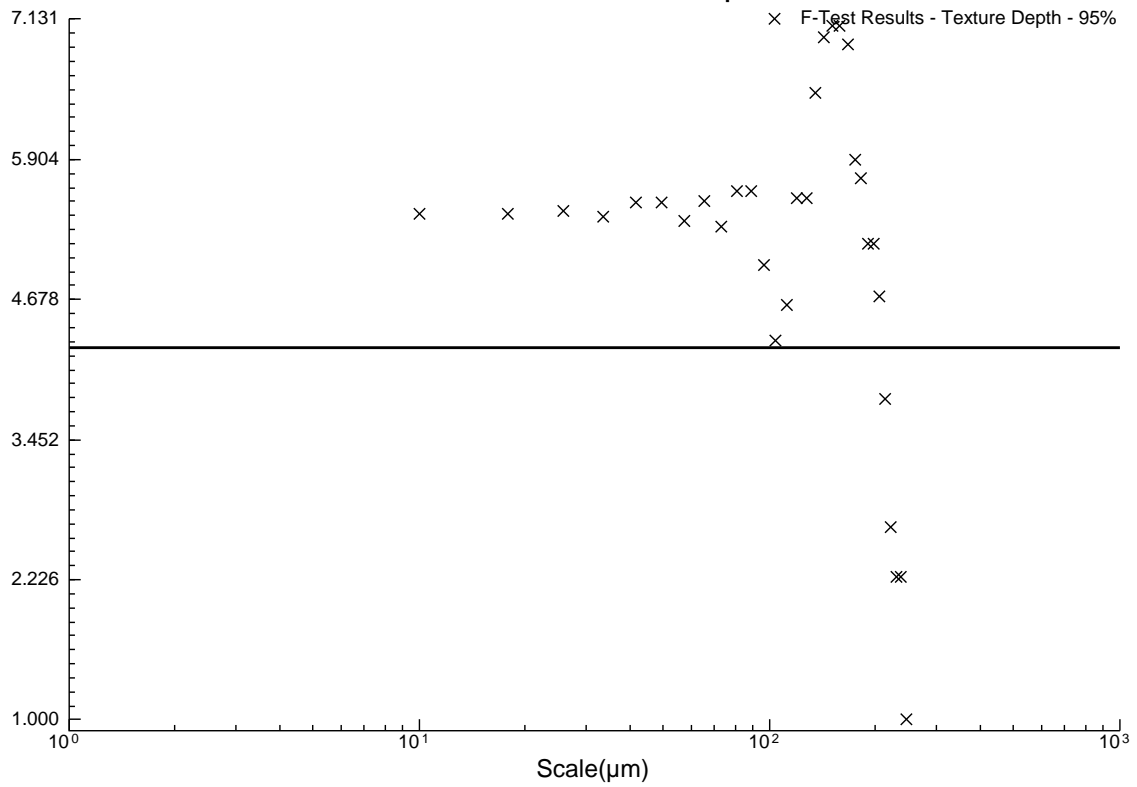


B1DVSW1U

### F-Test Results - 95%

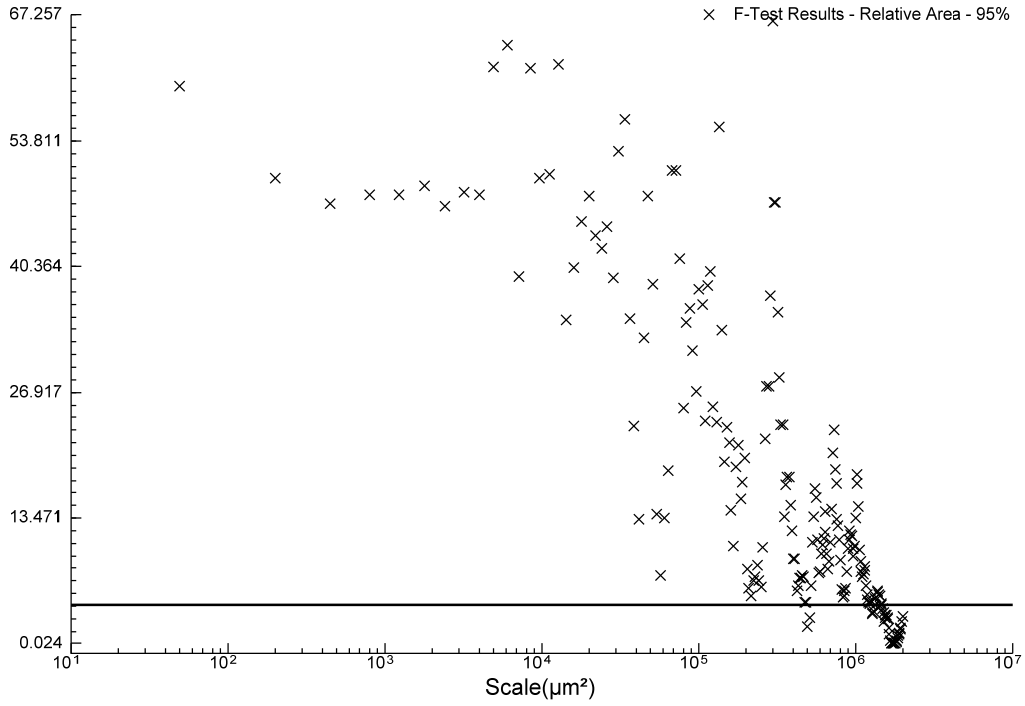


### F-Test Results - Texture Depth - 95%

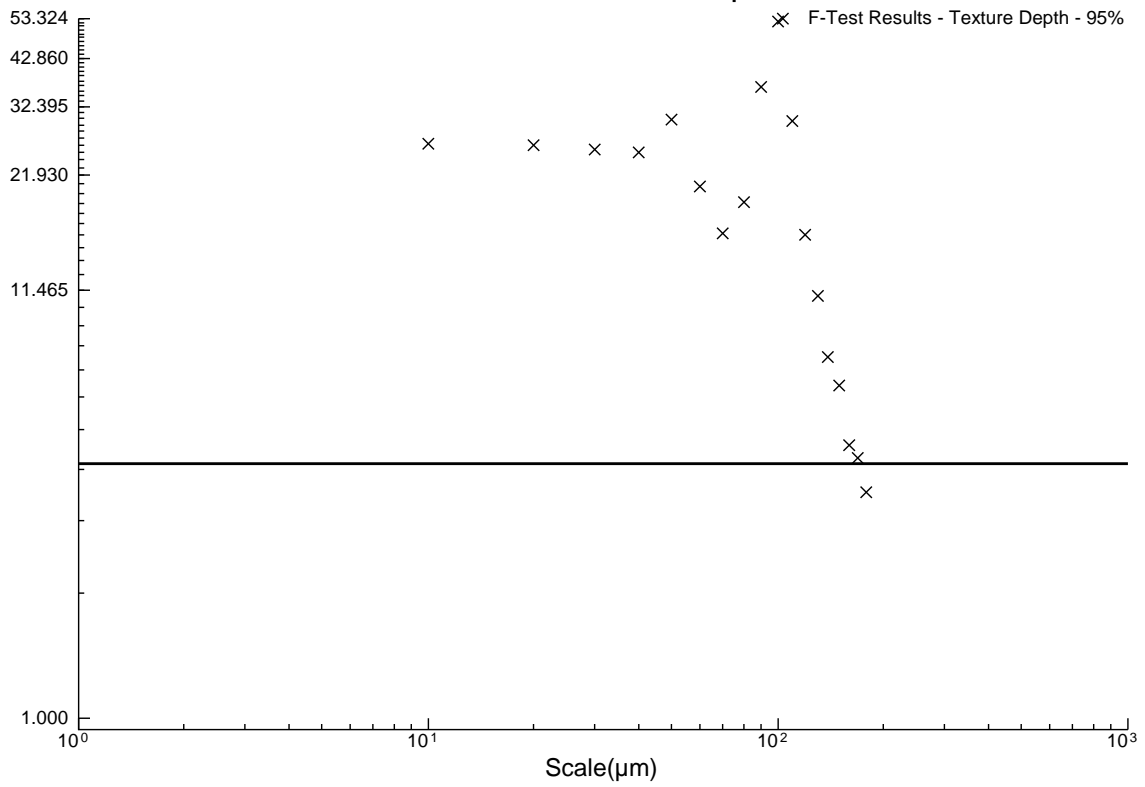


B1DVSW2D

### F-Test Results - Relative Area - 95%

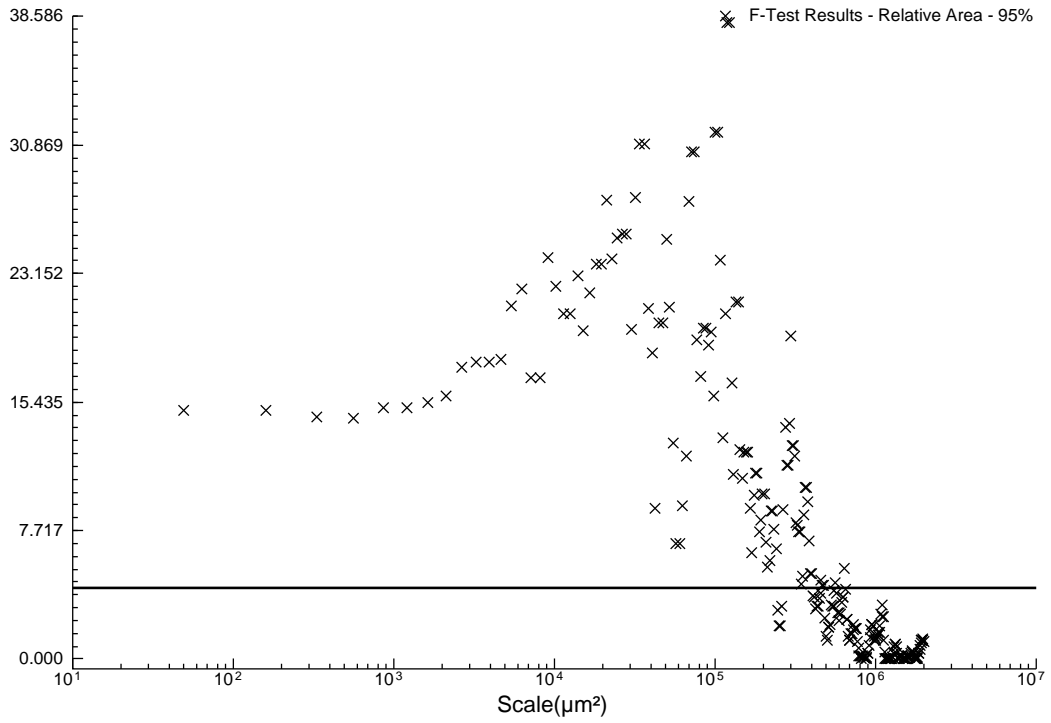


### F-Test Results - Texture Depth - 95%

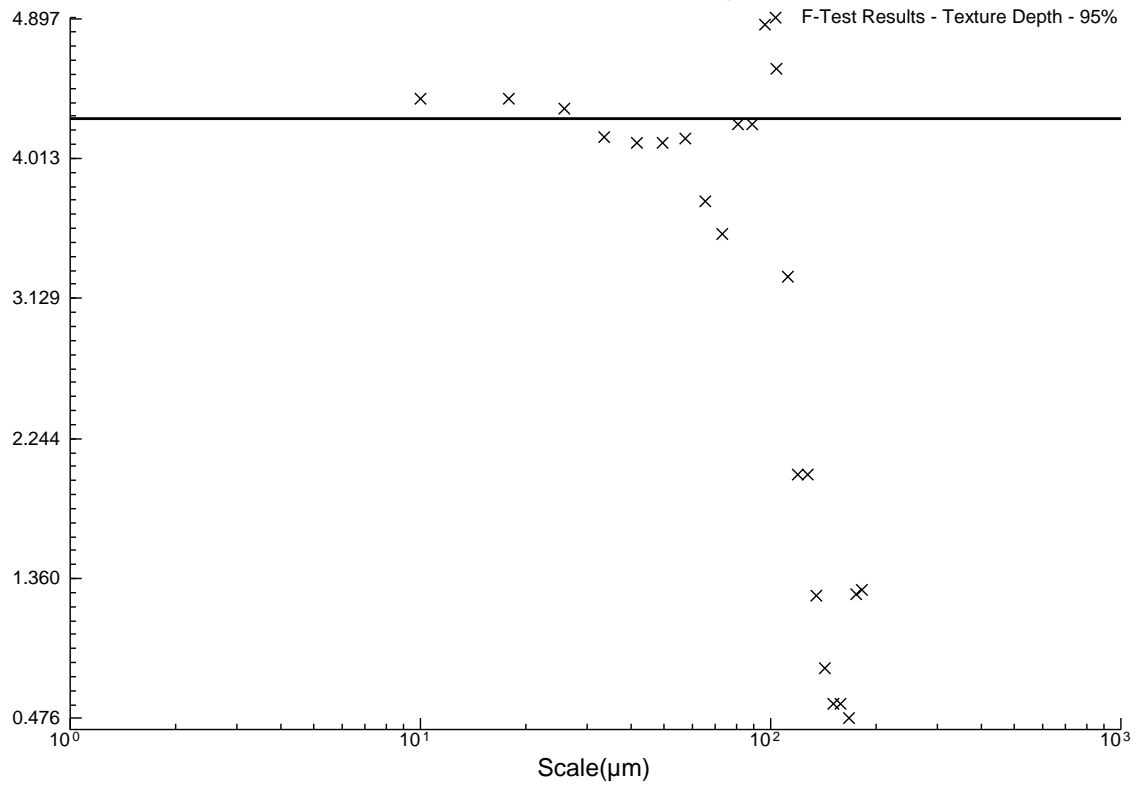


B1DVSW2U

### F-Test Results - Relative Area - 95%

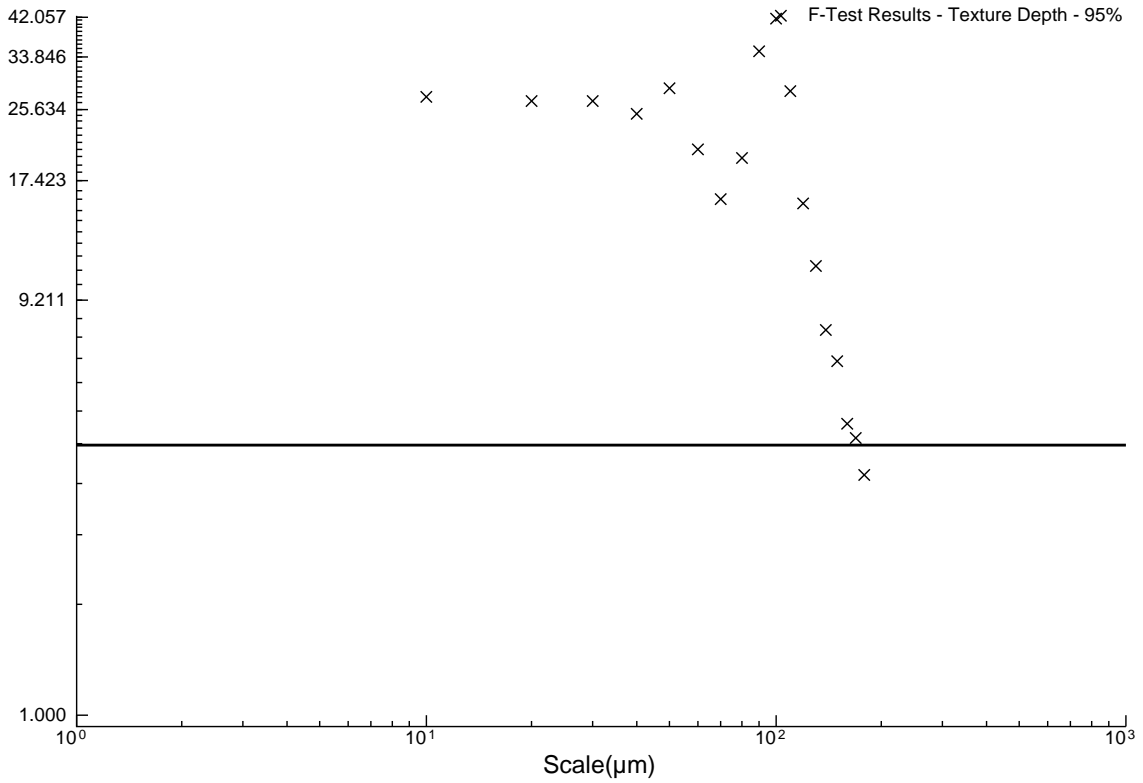


### F-Test Results - Texture Depth - 95%

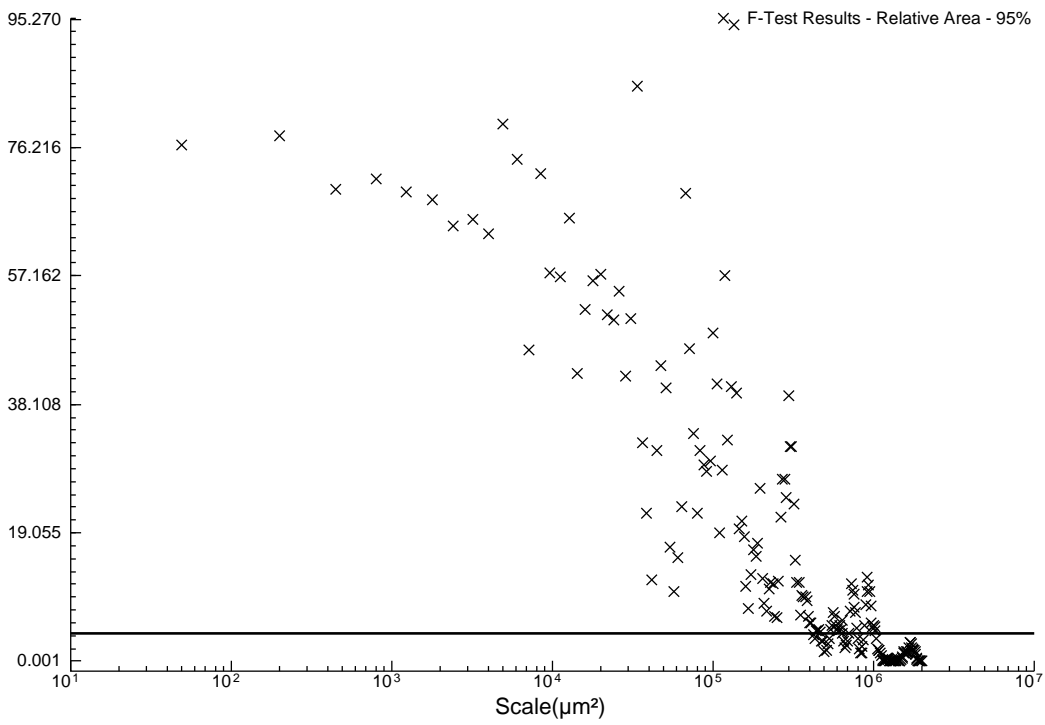


B1DVSW3D

### F-Test Results - Texture Depth - 95%

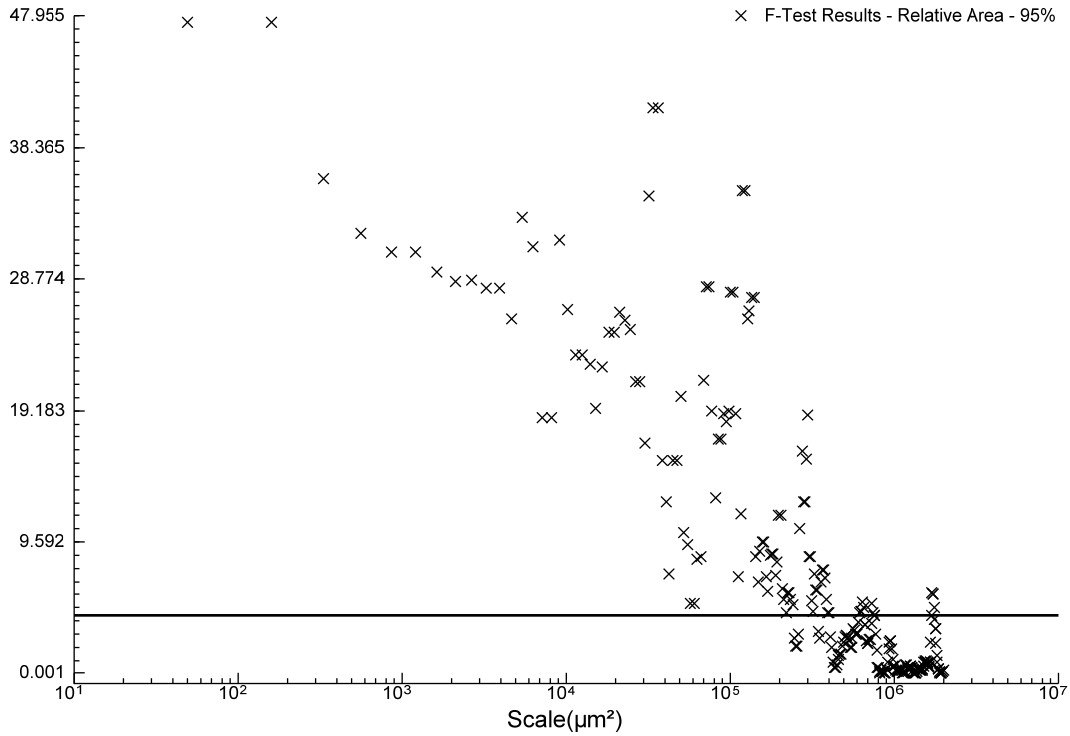


### F-Test Results - Relative Area - 95%

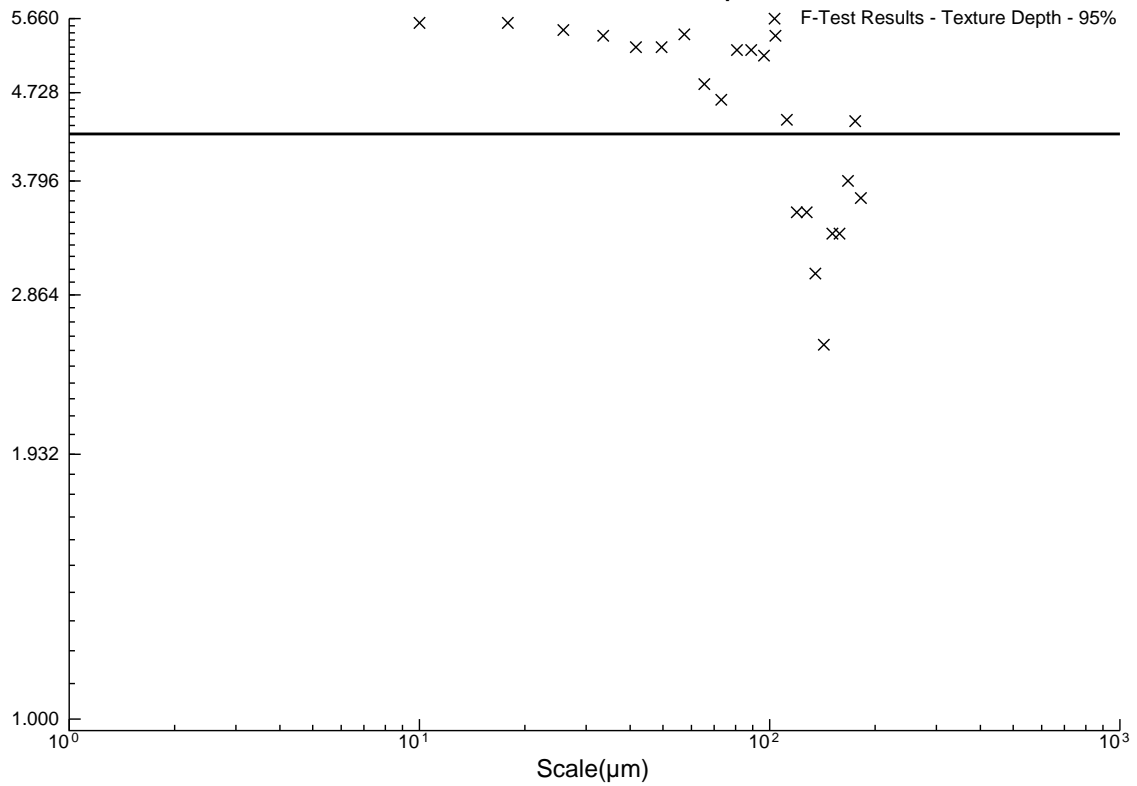


B1DVSW3U

### F-Test Results - Relative Area - 95%

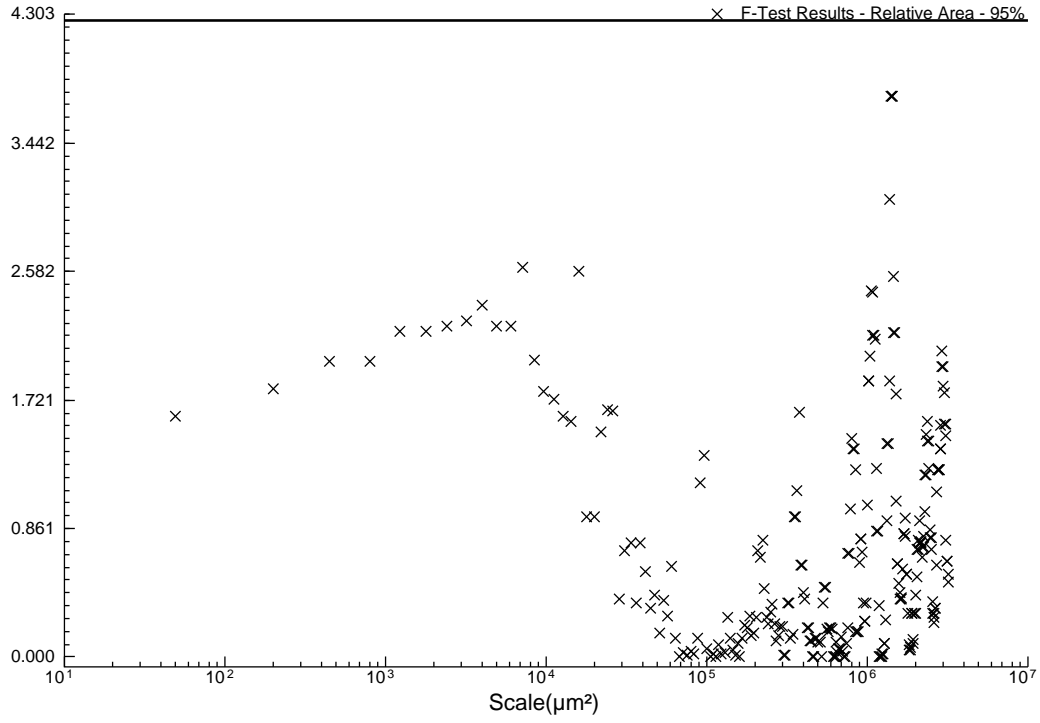


### F-Test Results - Texture Depth - 95%

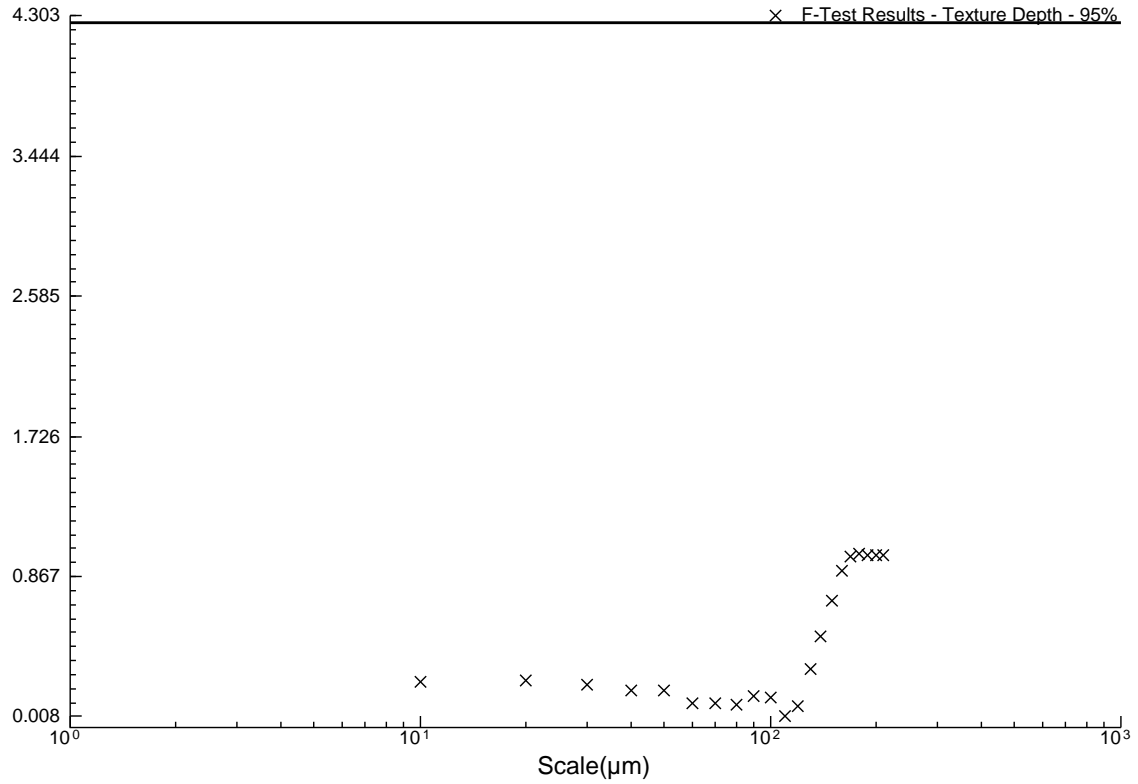


B1UVSB2U

F-Test Results - Relative Area - 95%

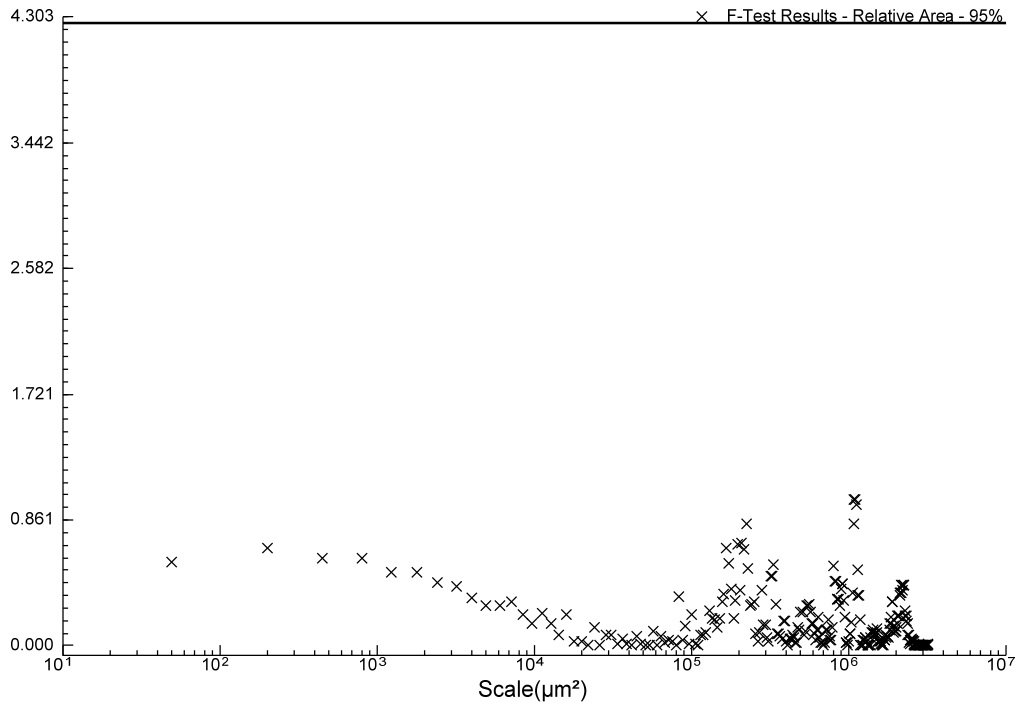


F-Test Results - Texture Depth - 95%

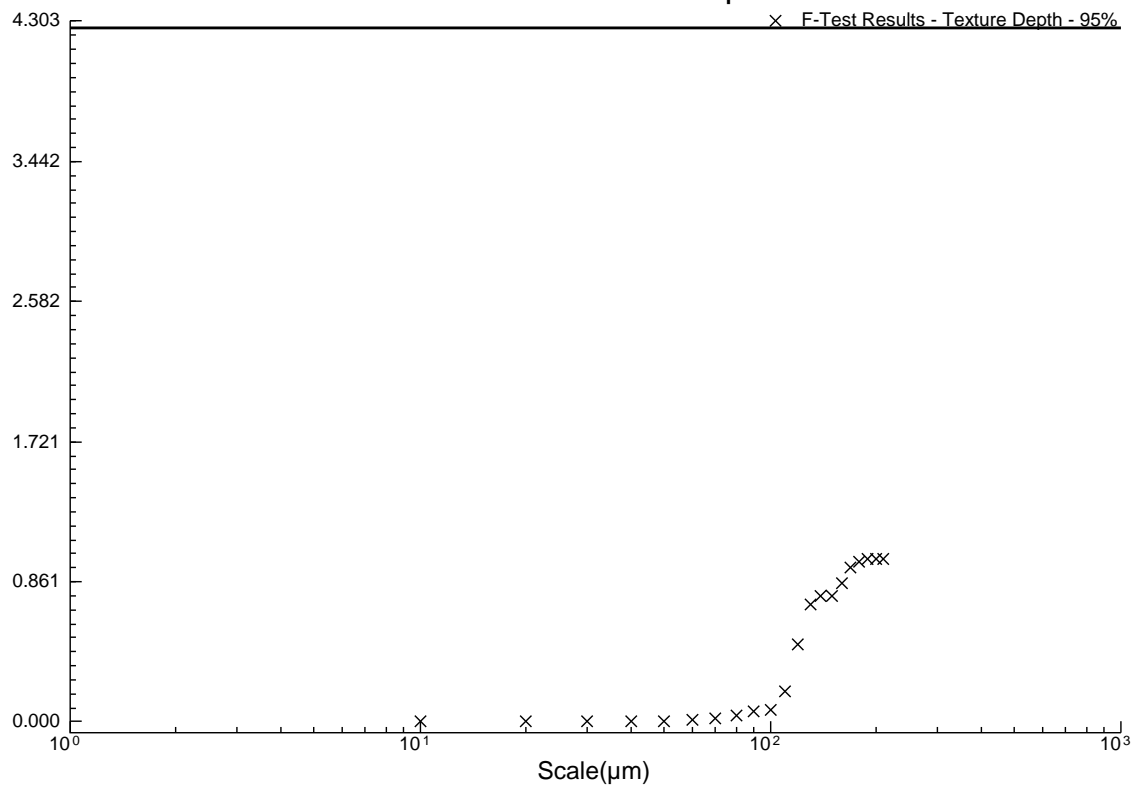


B1UVSB3U

### F-Test Results - Relative Area - 95%

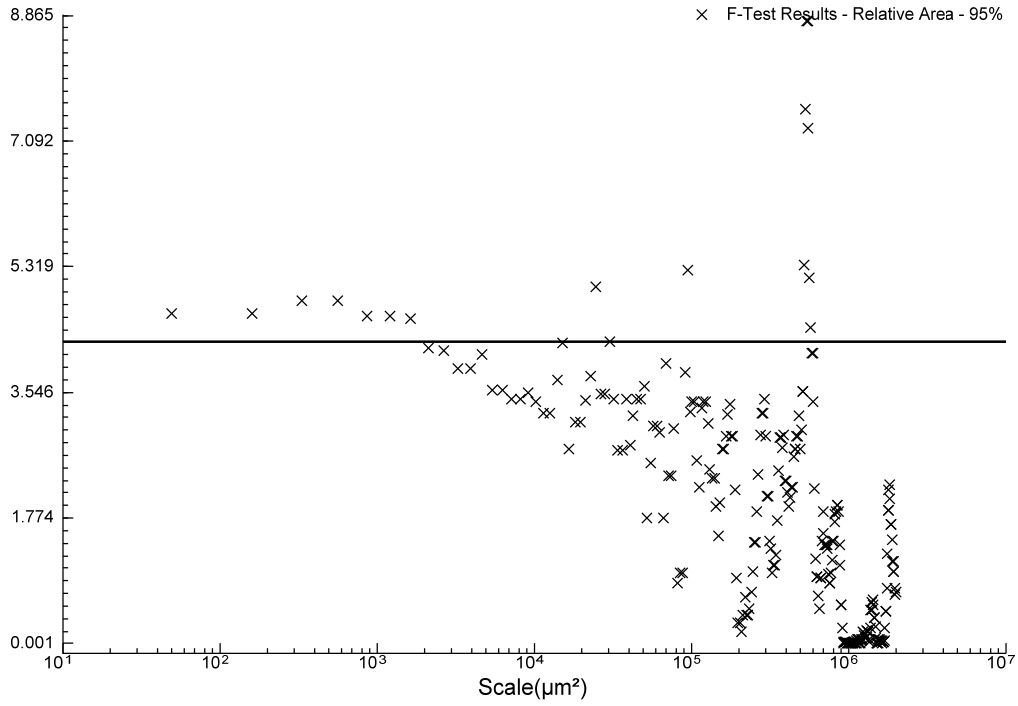


### F-Test Results - Texture Depth - 95%

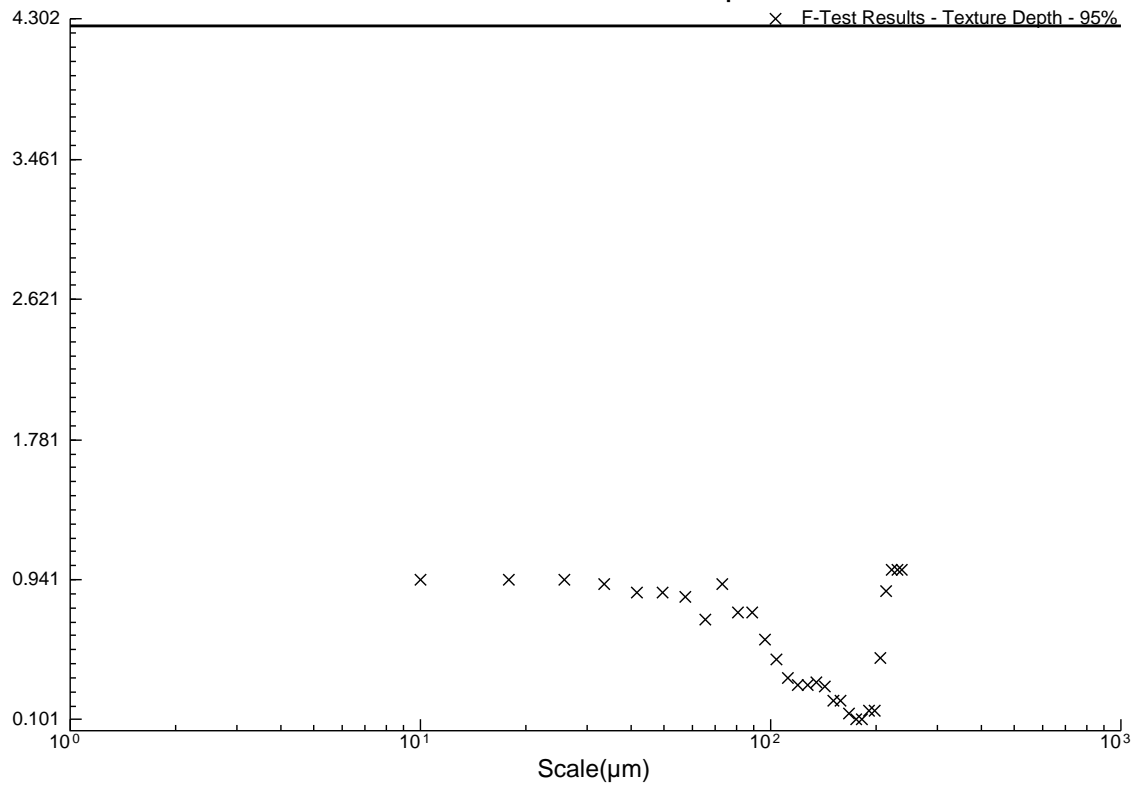


B1UVSW1D

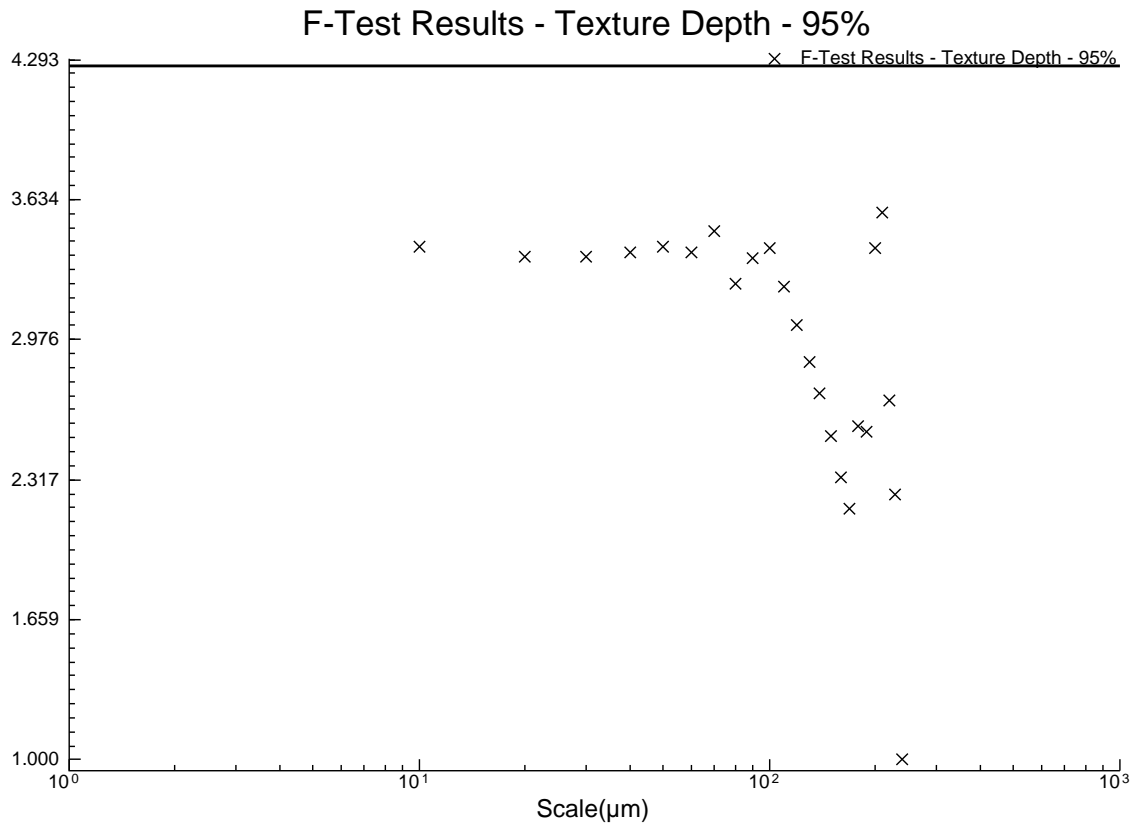
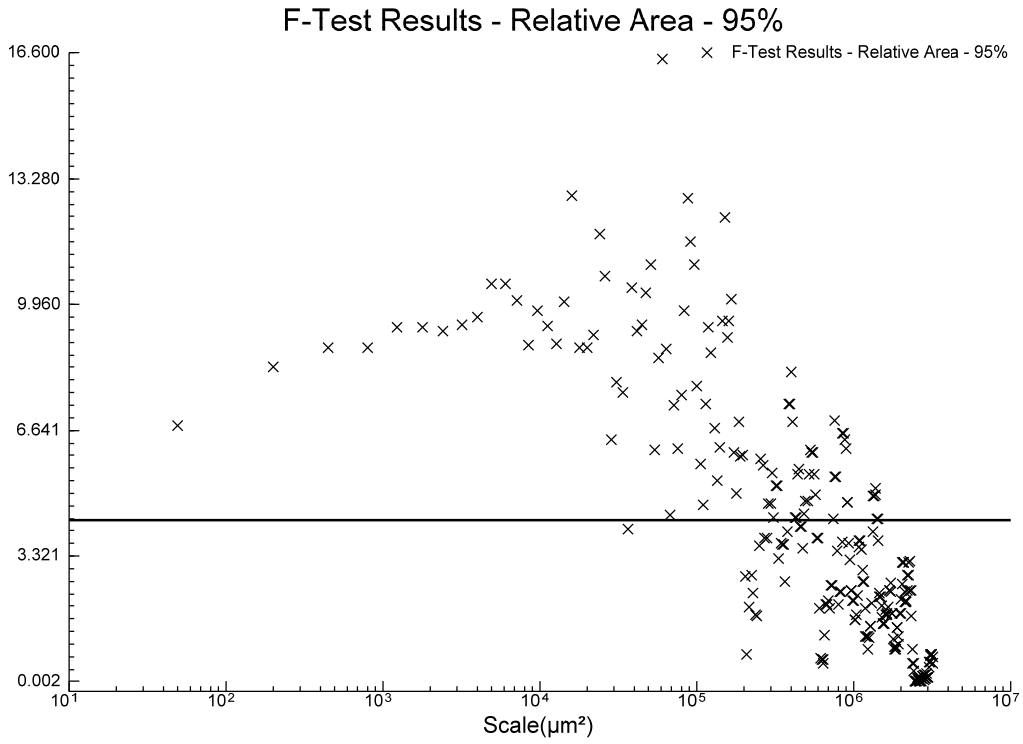
### F-Test Results - Relative Area - 95%



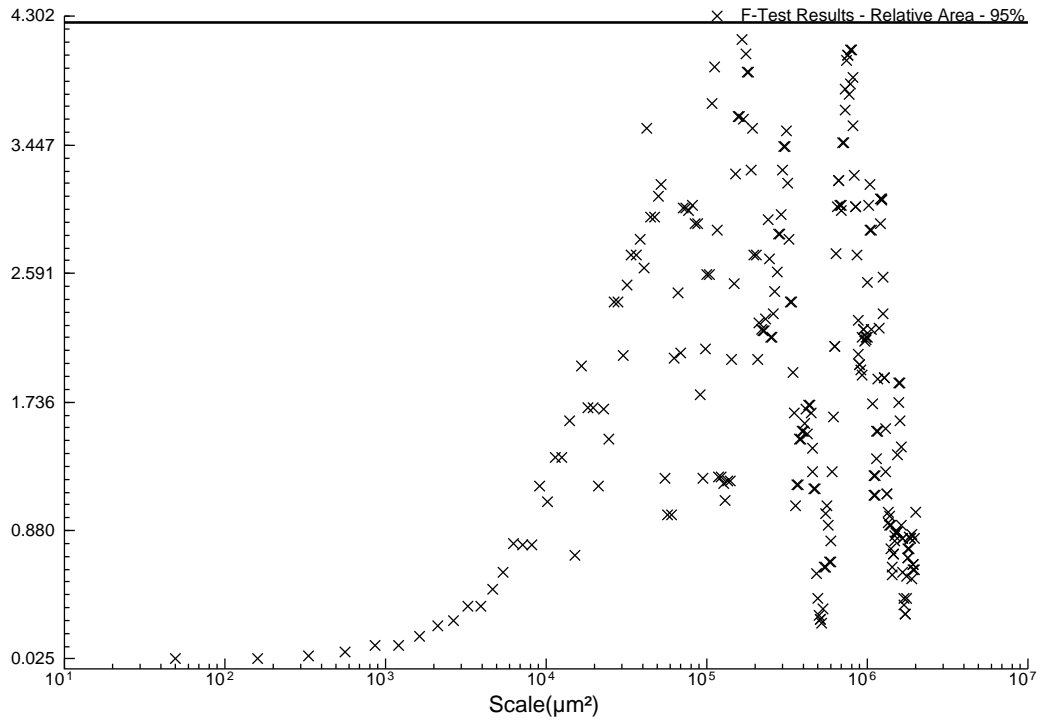
### F-Test Results - Texture Depth - 95%



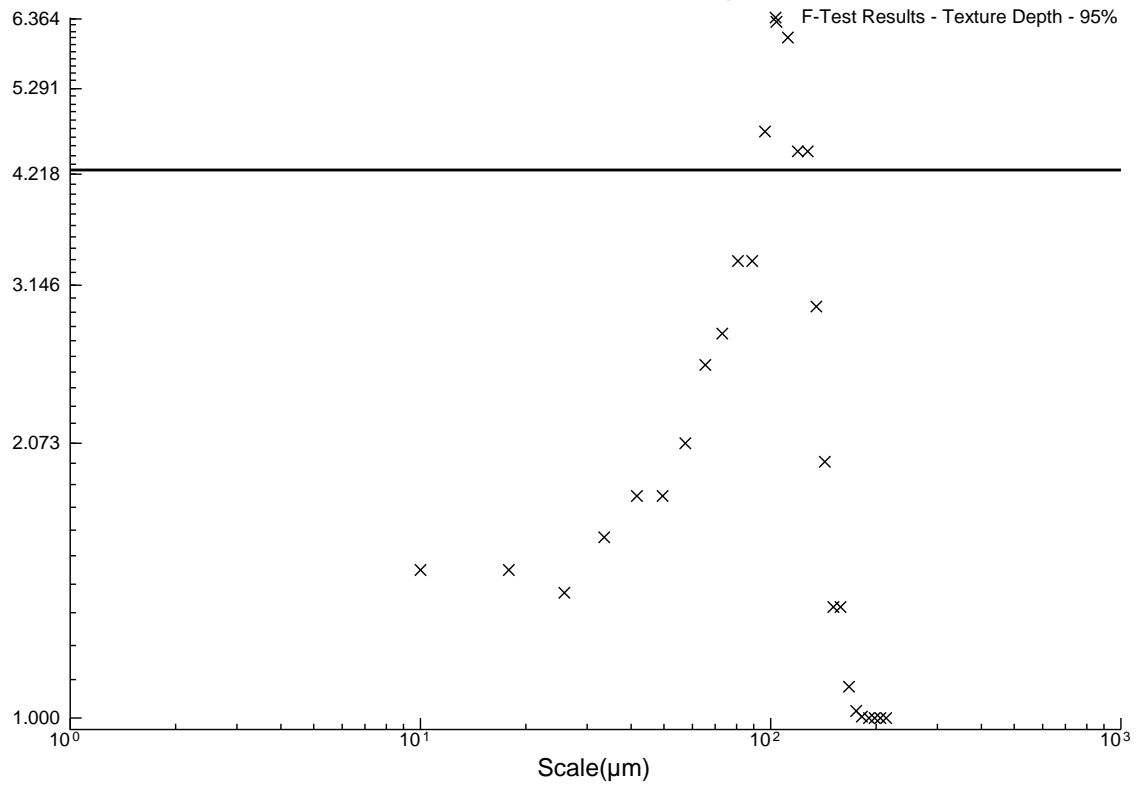
B1UVSW1U



F-Test Results - Relative Area - 95%

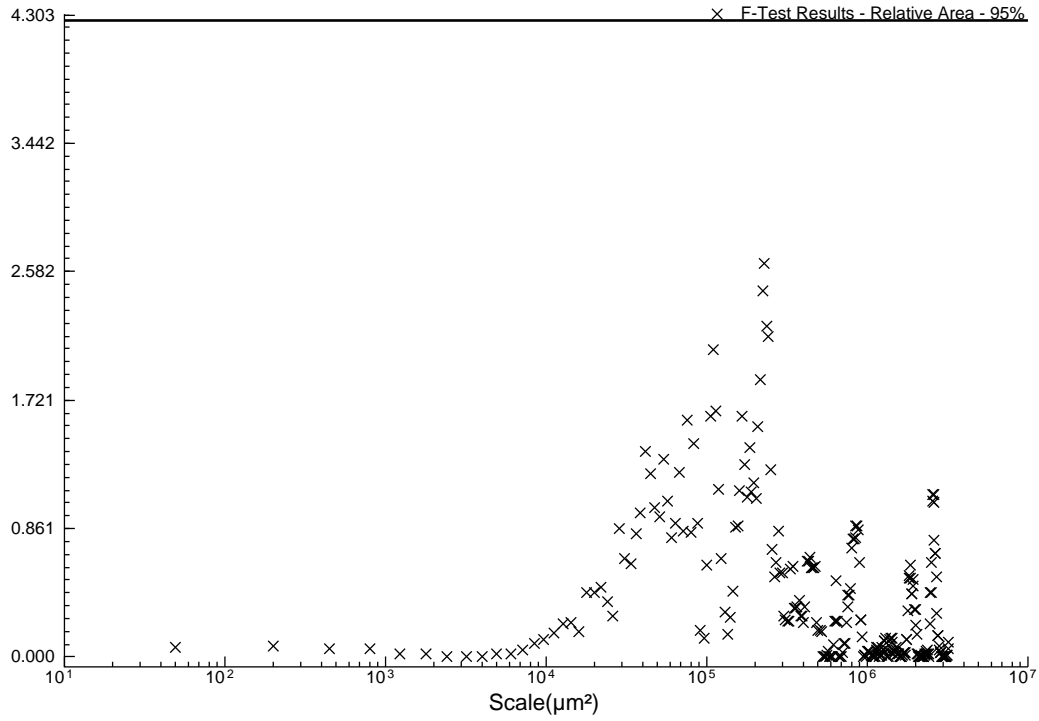


F-Test Results - Texture Depth - 95%

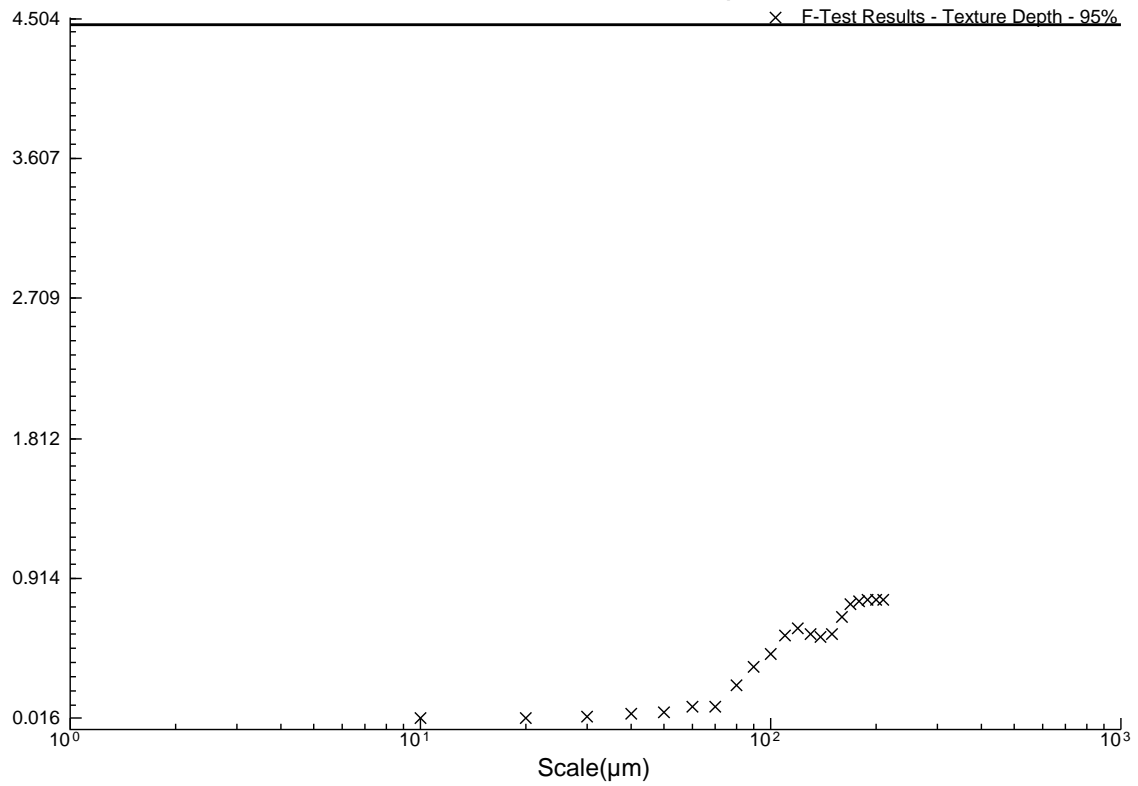


B1UVSW2U

### F-Test Results - Relative Area - 95%

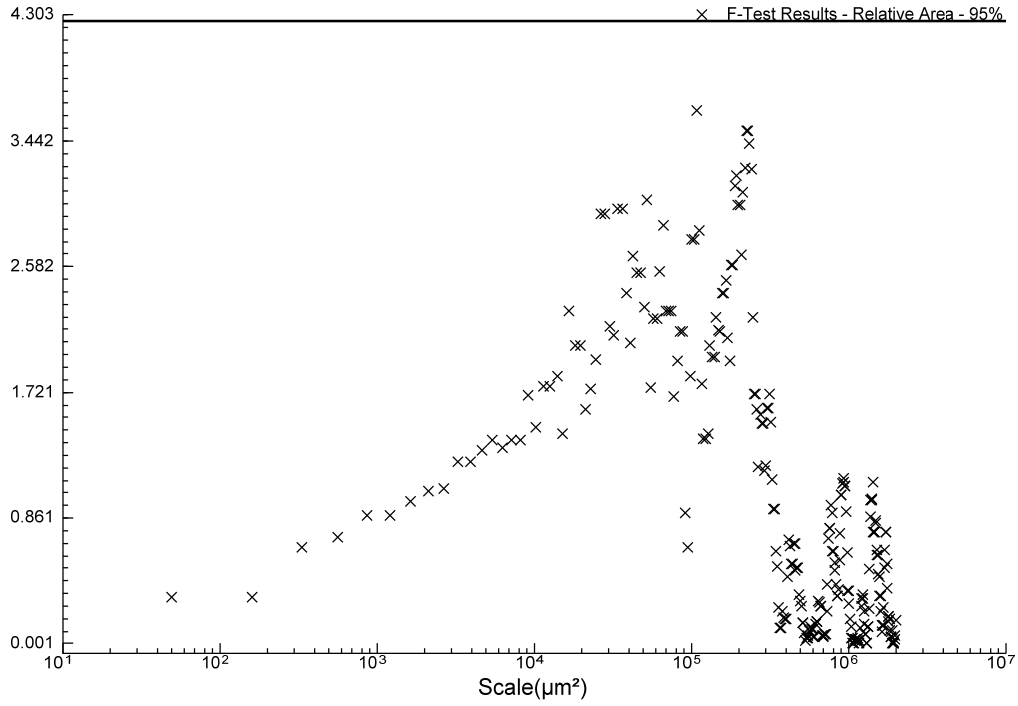


### F-Test Results - Texture Depth - 95%

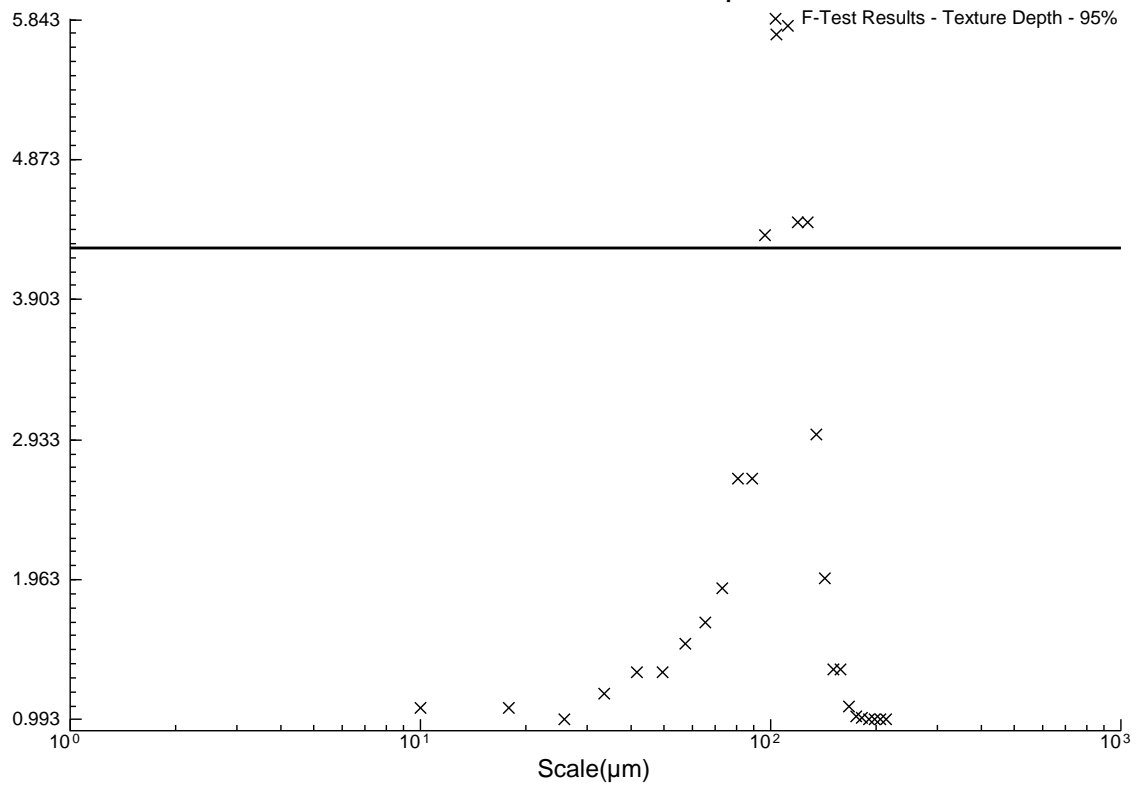


B1UVSW3D

### F-Test Results - Relative Area - 95%

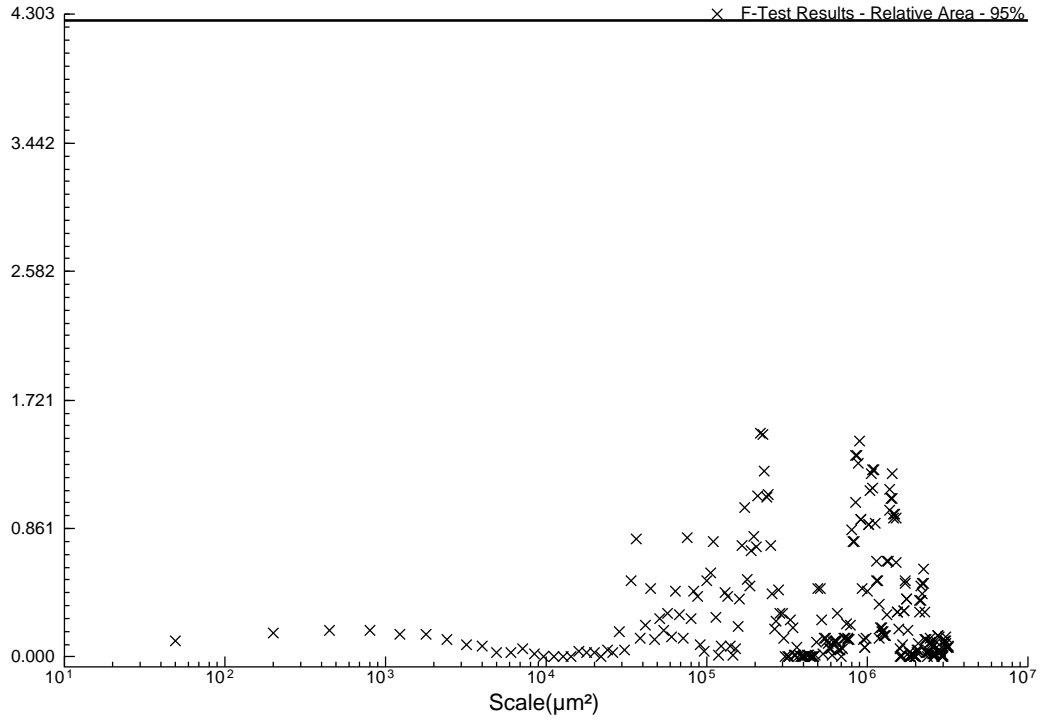


### F-Test Results - Texture Depth - 95%

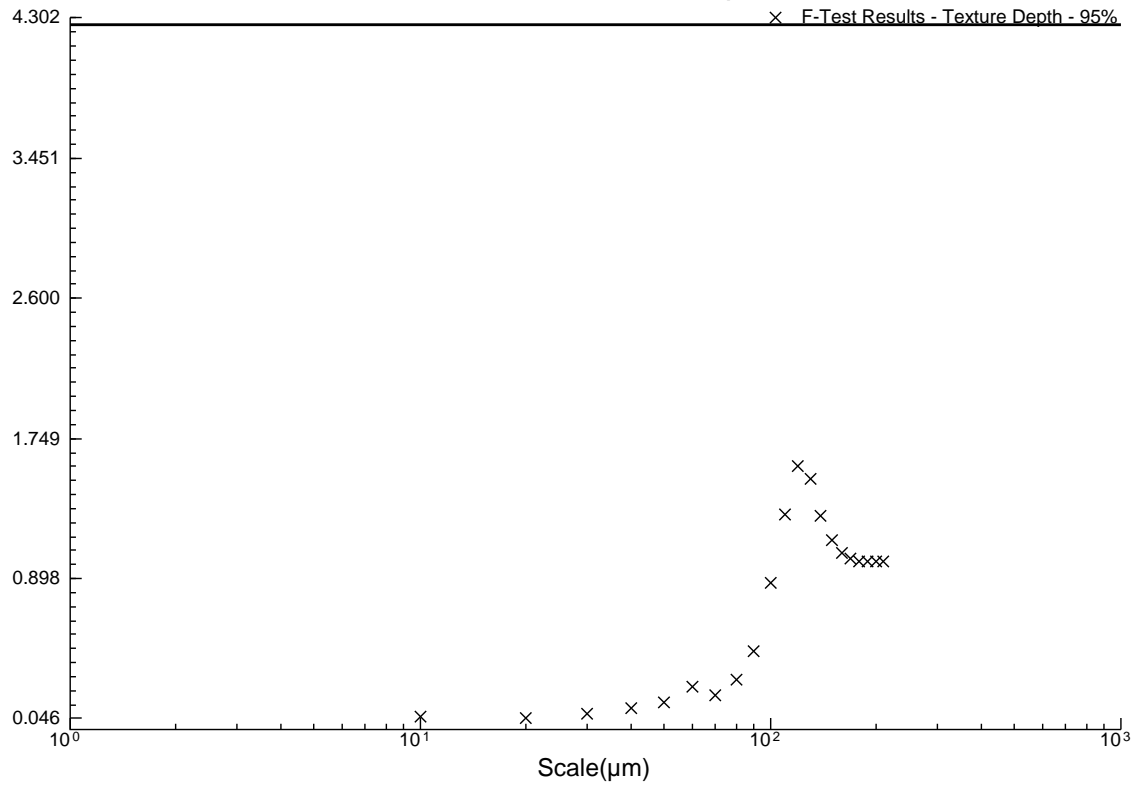


B1UVSW3U

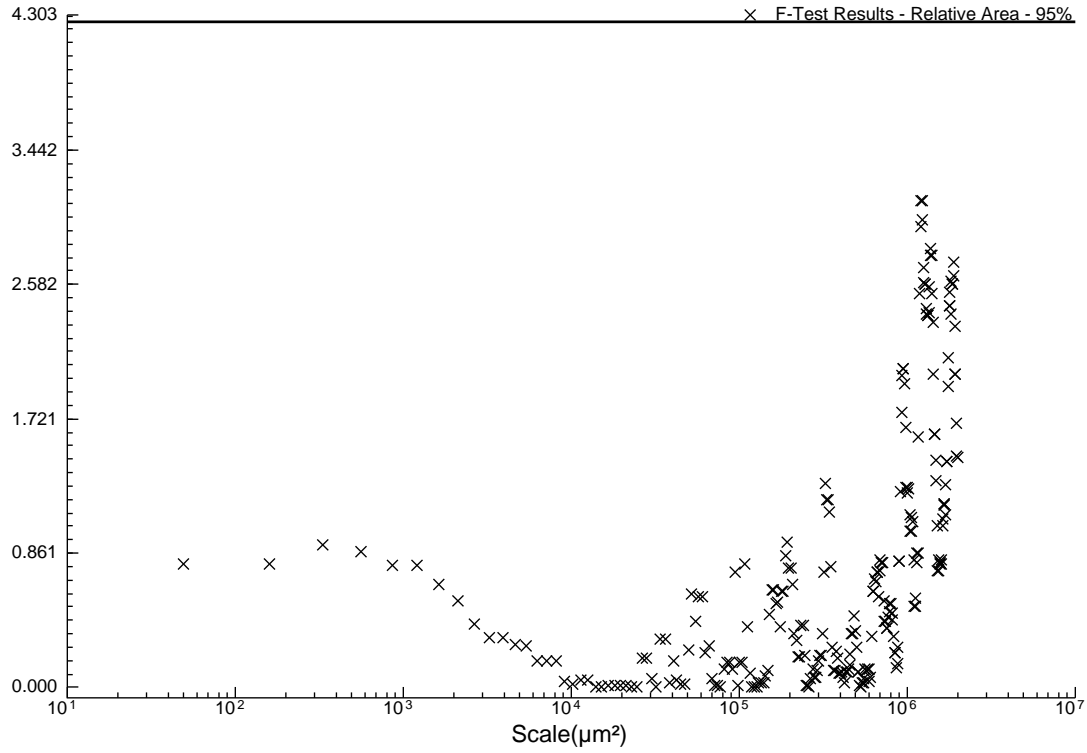
F-Test Results - Relative Area - 95%



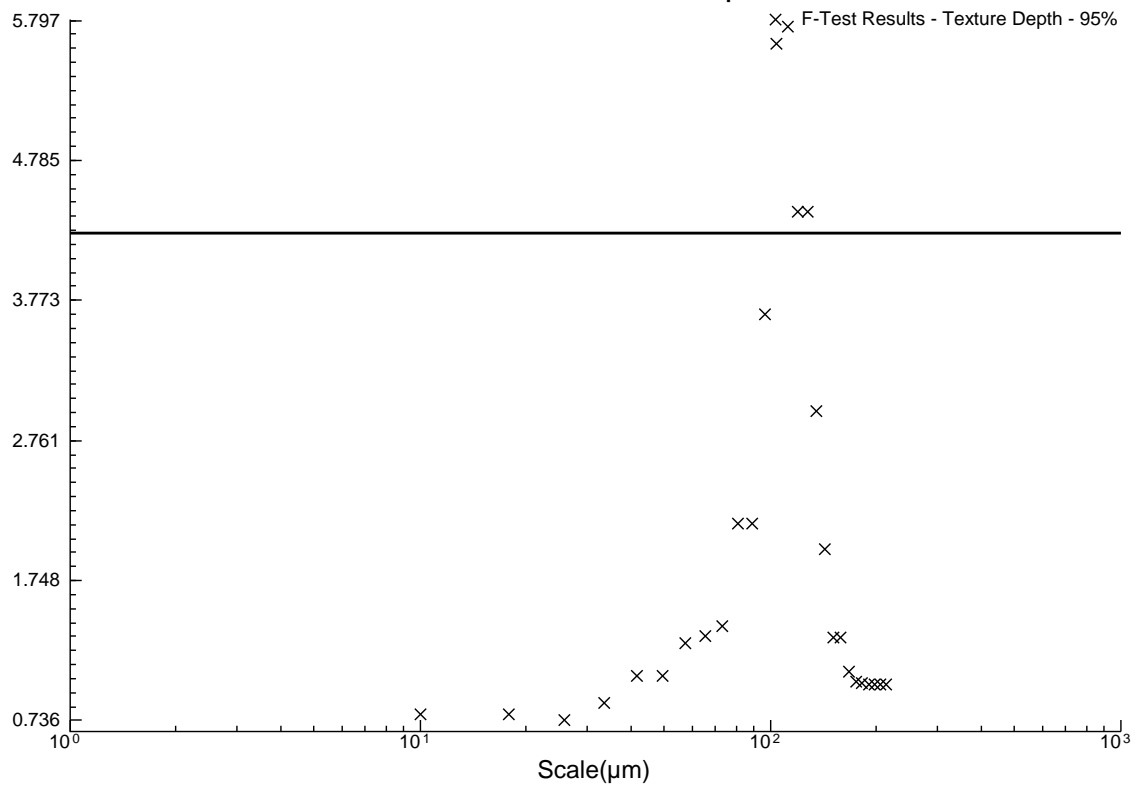
F-Test Results - Texture Depth - 95%



F-Test Results - Relative Area - 95%

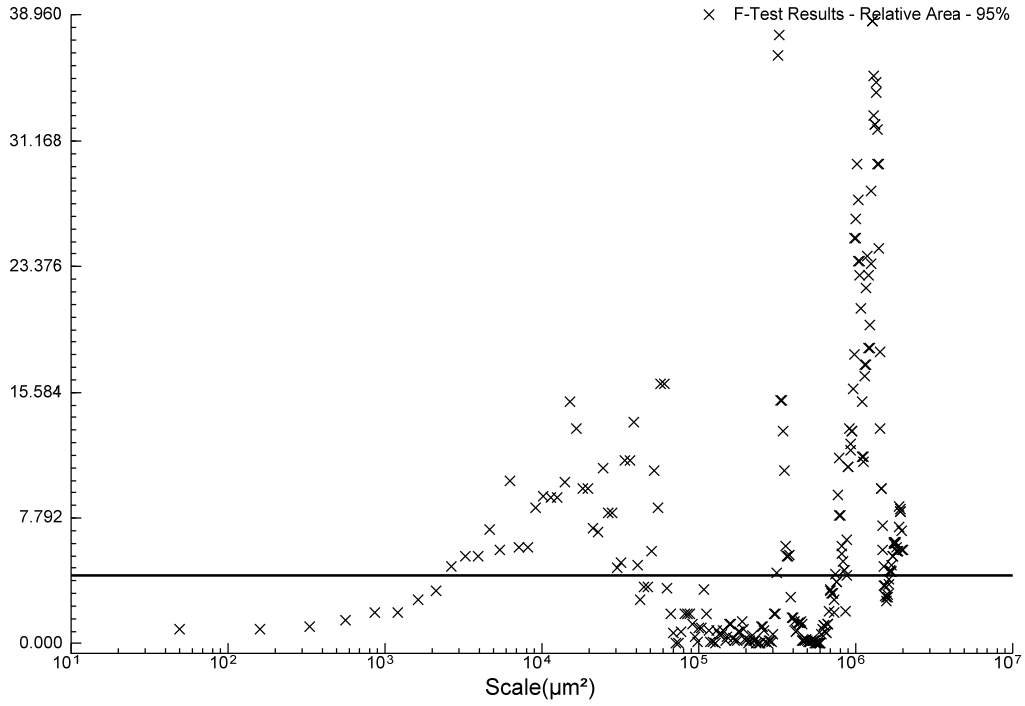


F-Test Results - Texture Depth - 95%

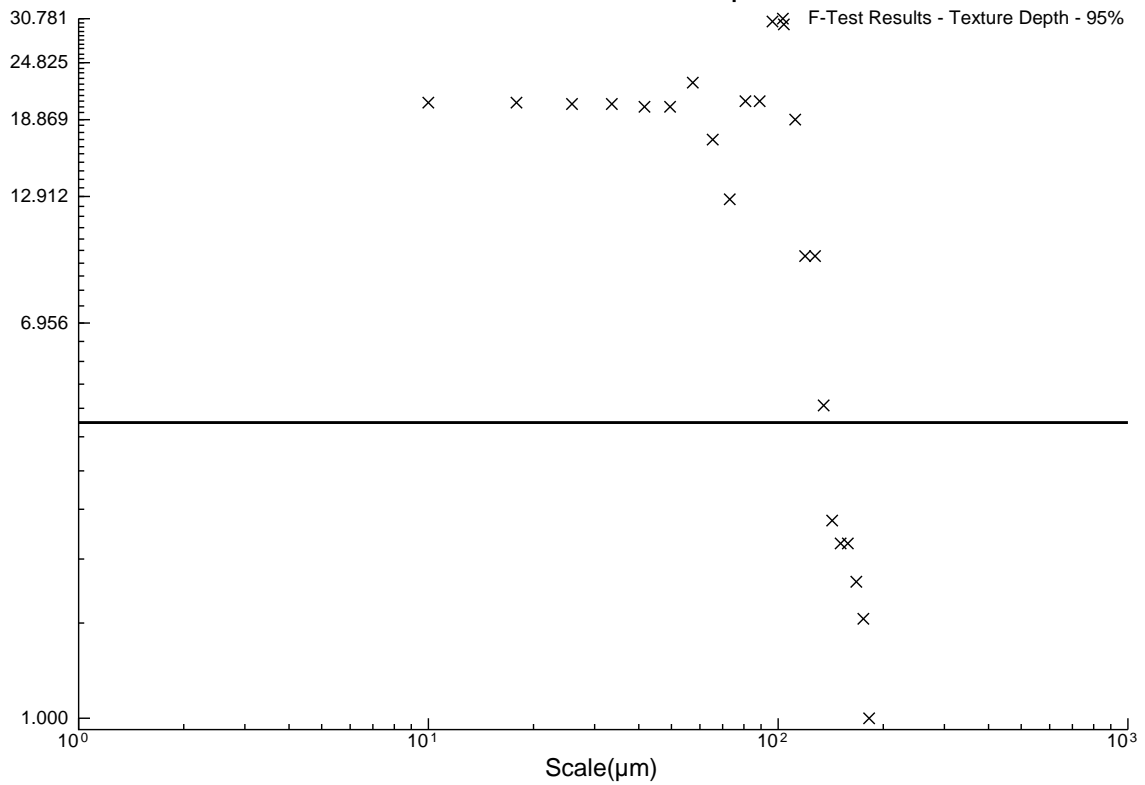


B2DVSB2U

### F-Test Results - Relative Area - 95%

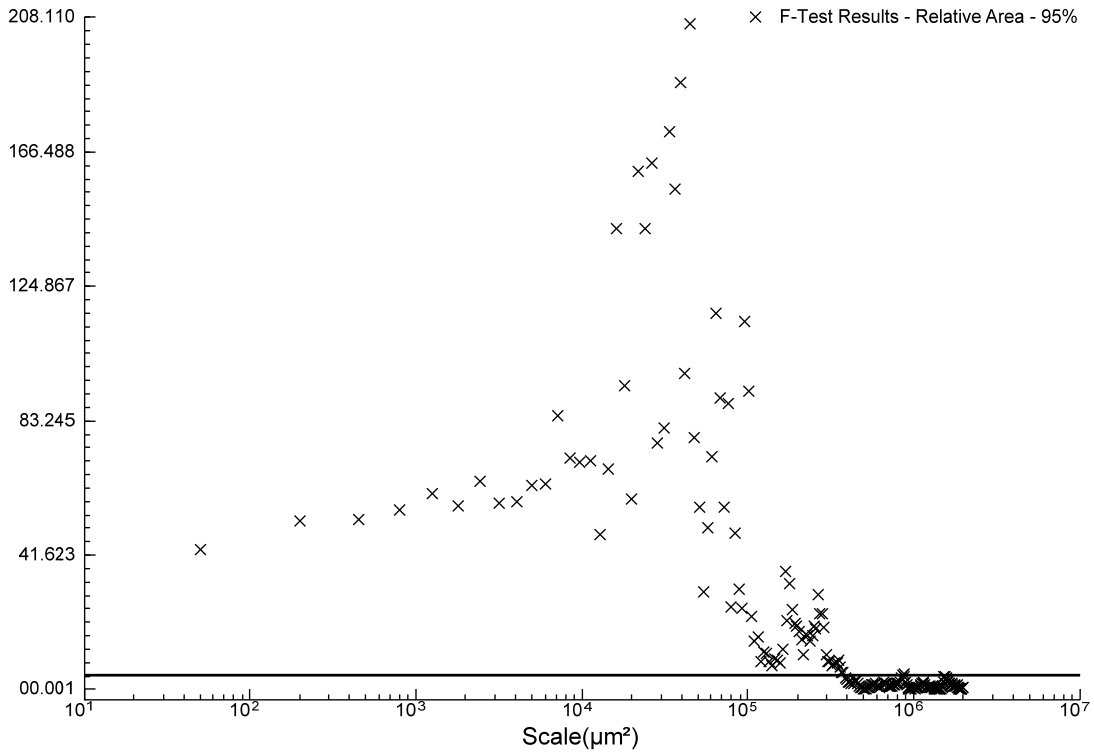


### F-Test Results - Texture Depth - 95%

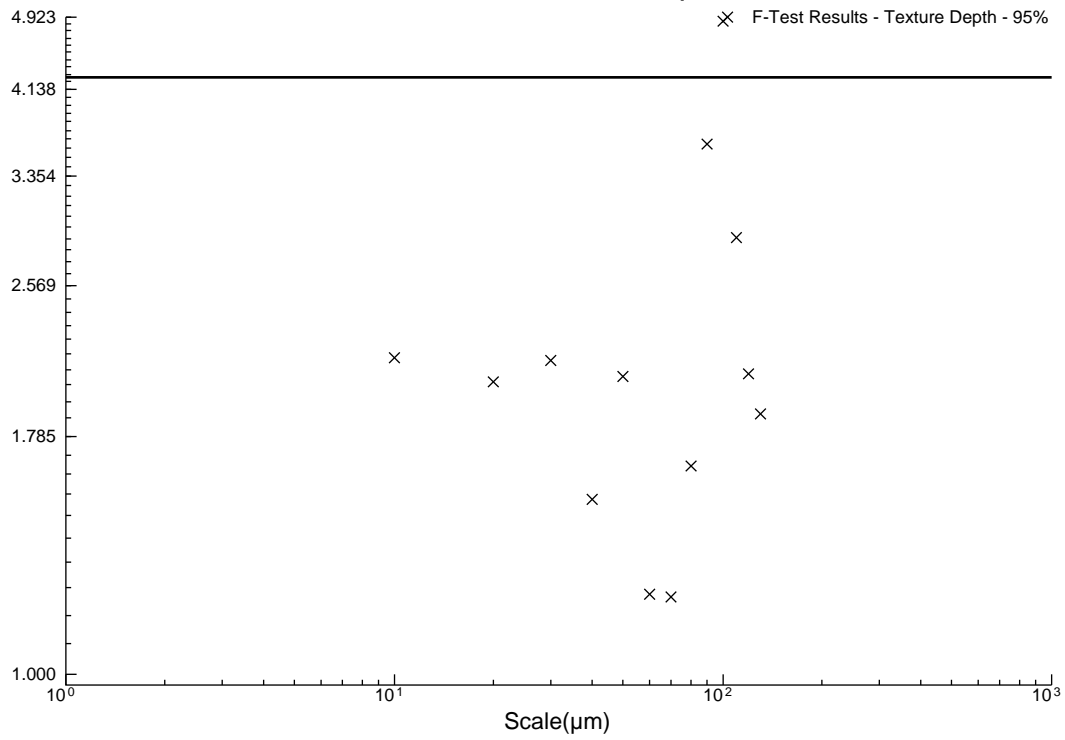


B2DVSB3D

### F-Test Results - Relative Area - 95%

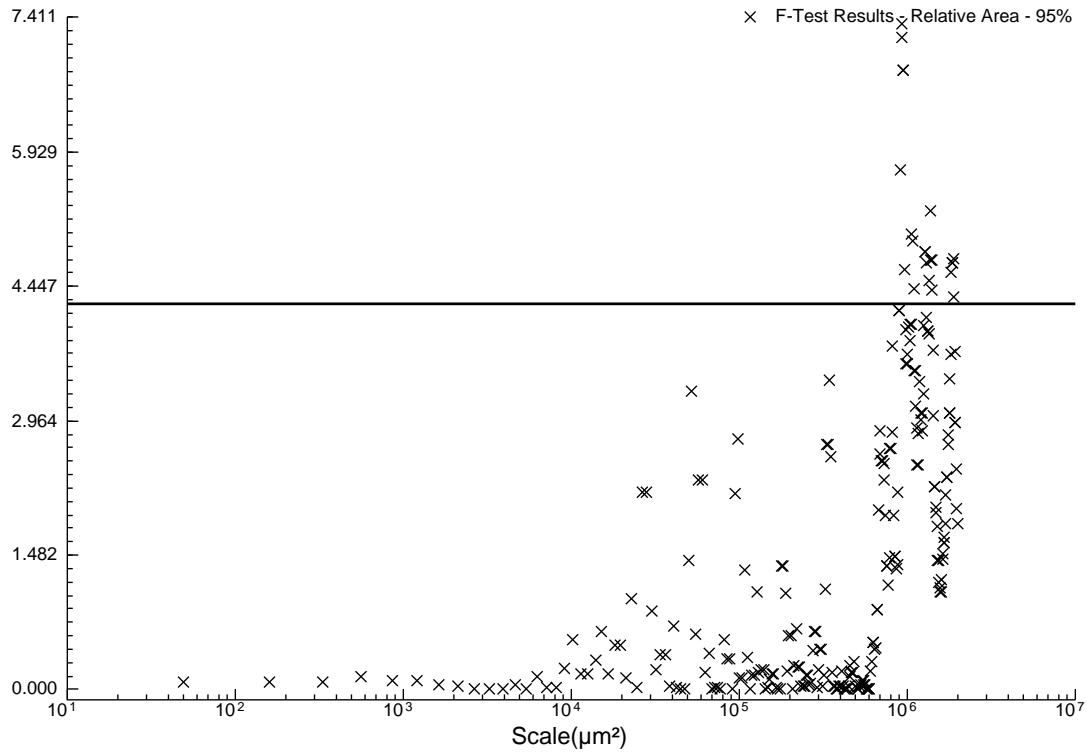


### F-Test Results - Texture Depth - 95%

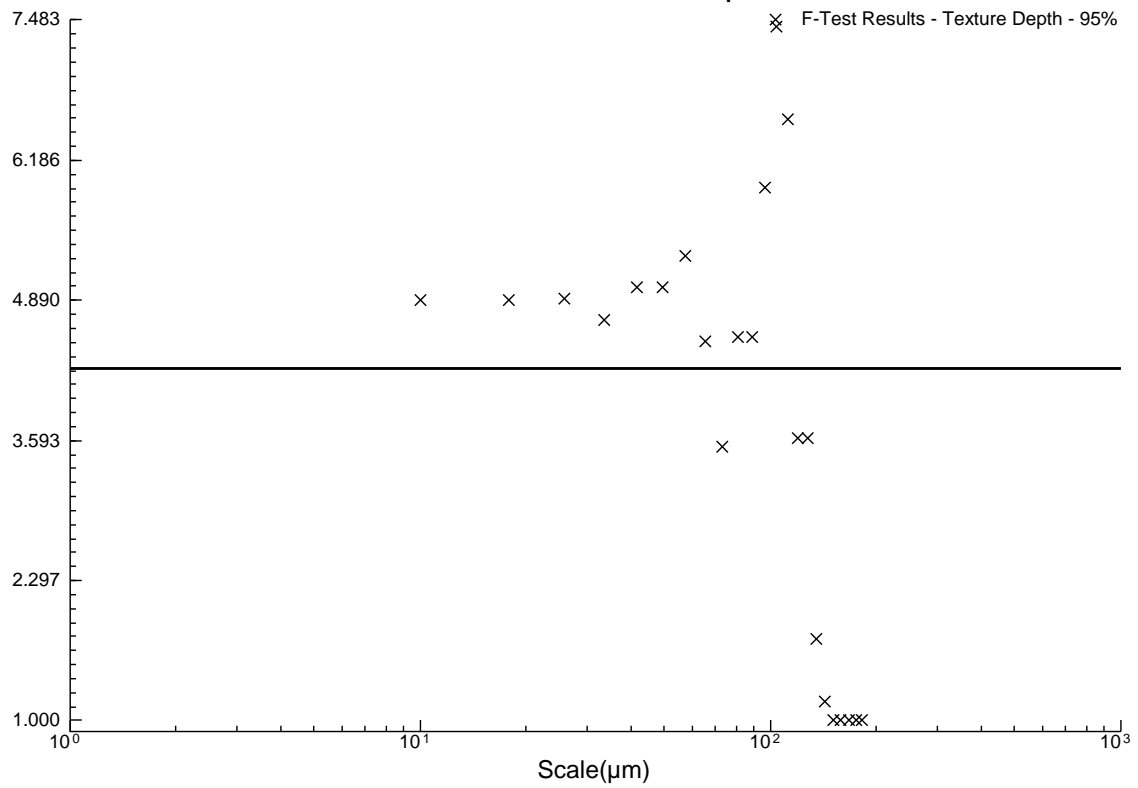


B2DVSB3U

### F-Test Results - Relative Area - 95%

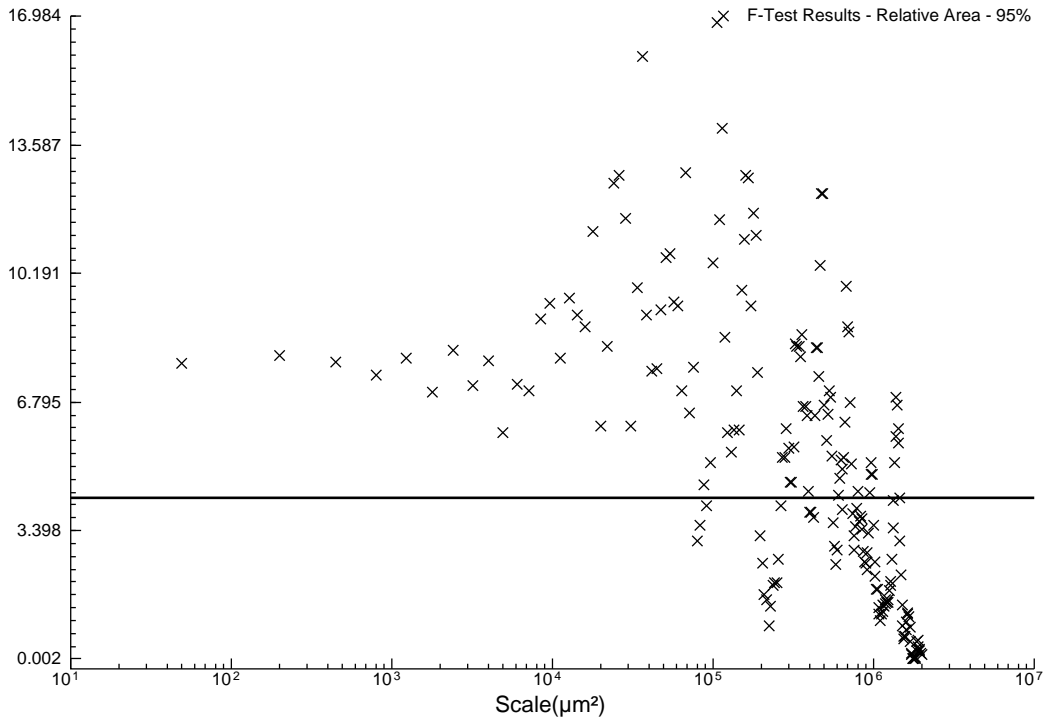


### F-Test Results - Texture Depth - 95%

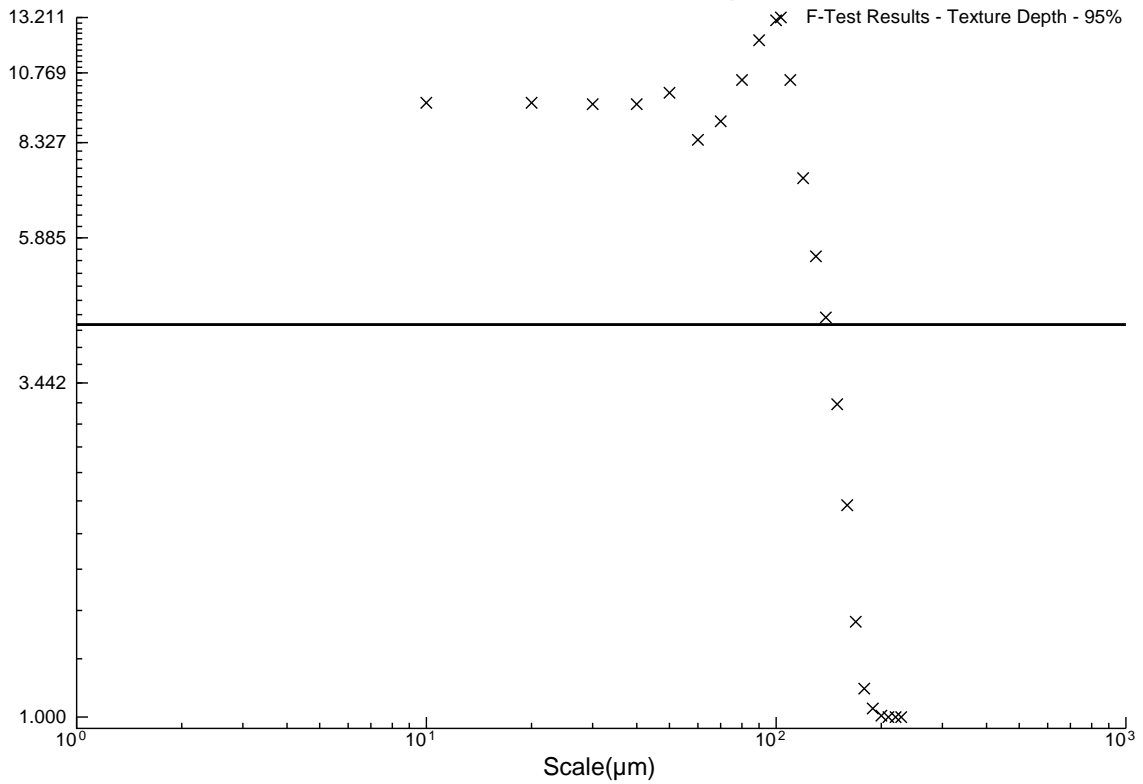


B2DVSW1D

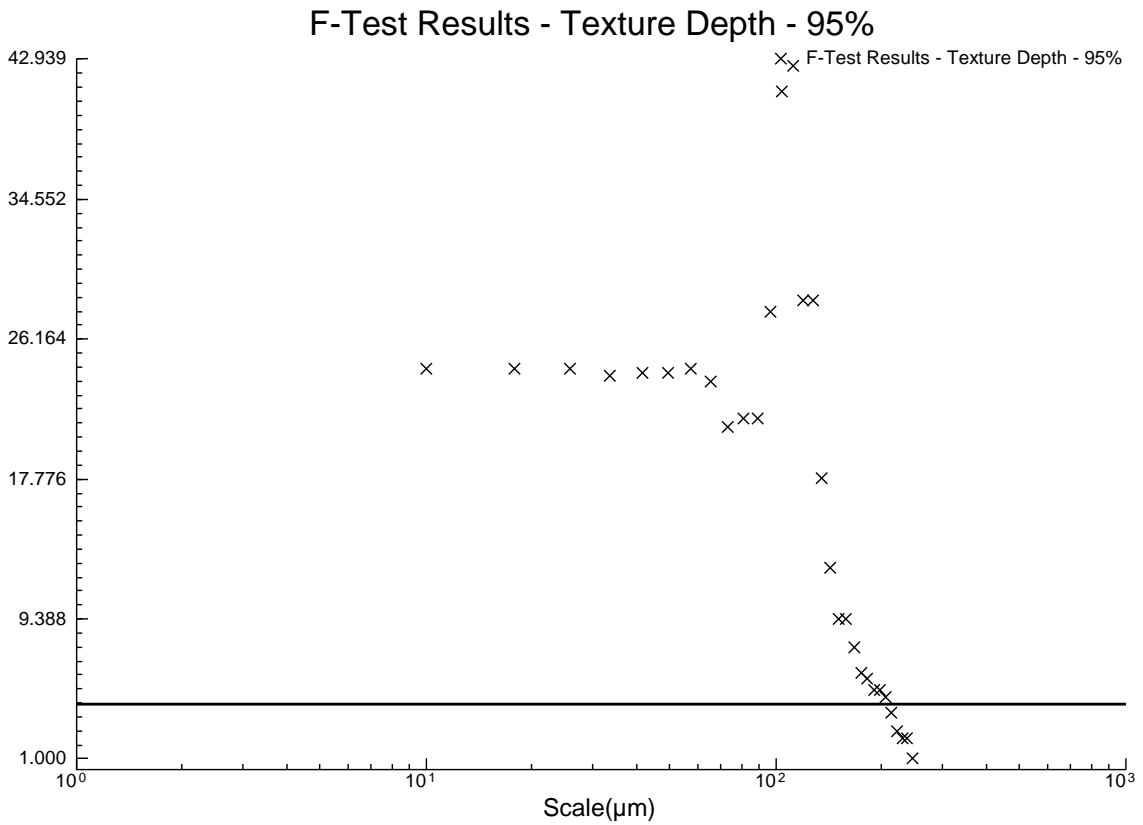
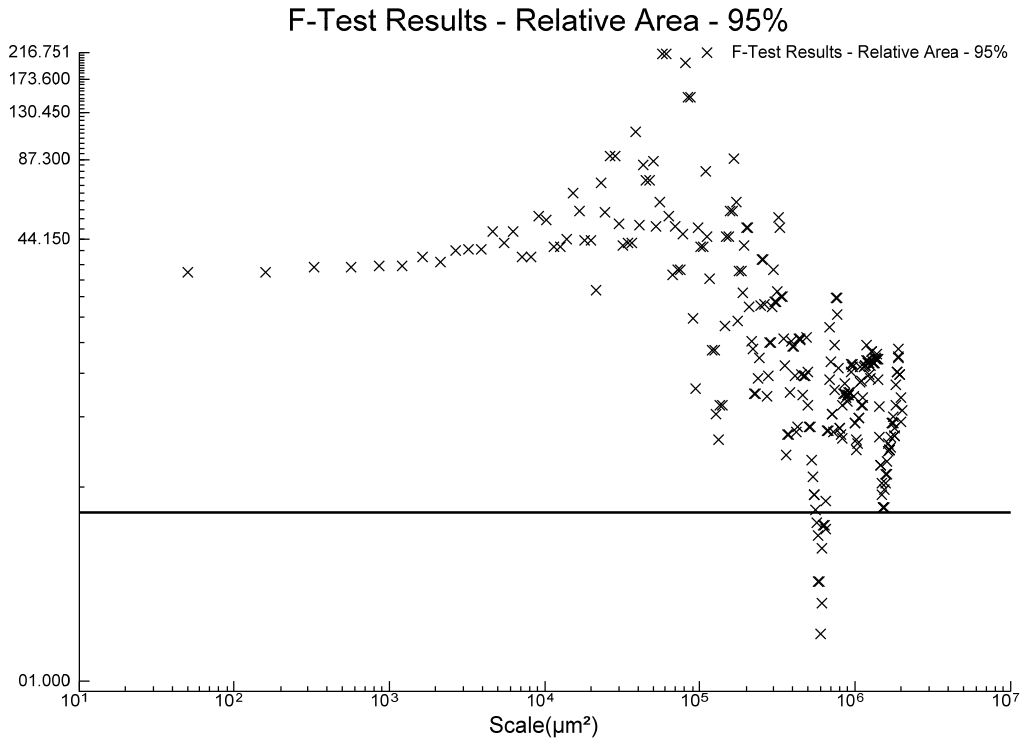
### F-Test Results - Relative Area - 95%



### F-Test Results - Texture Depth - 95%

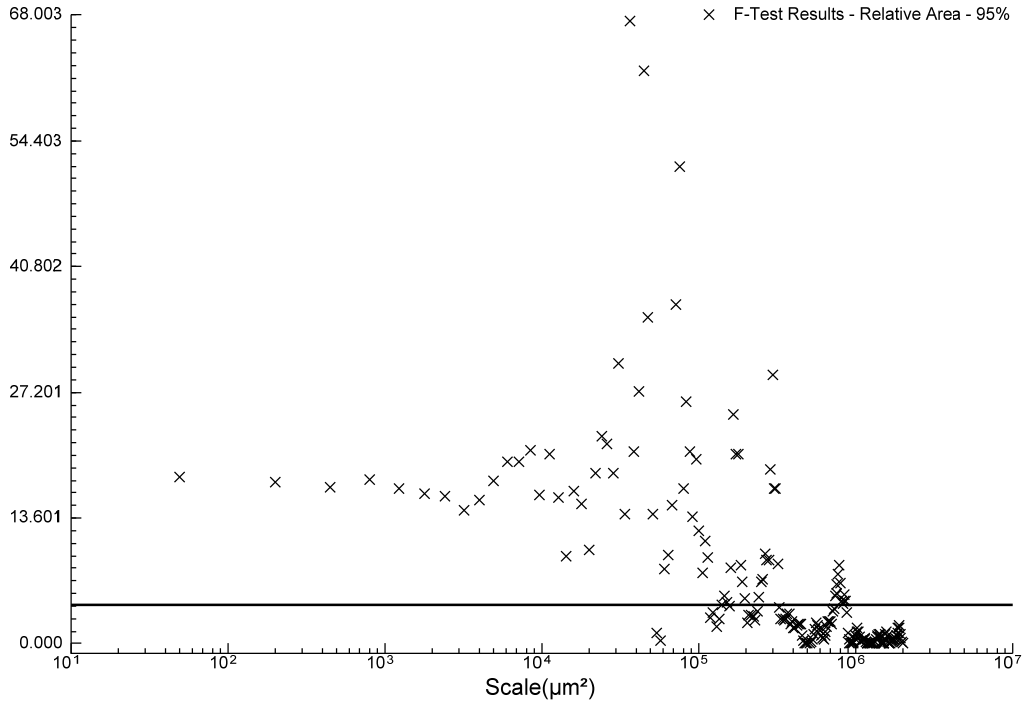


B2DVSW1U

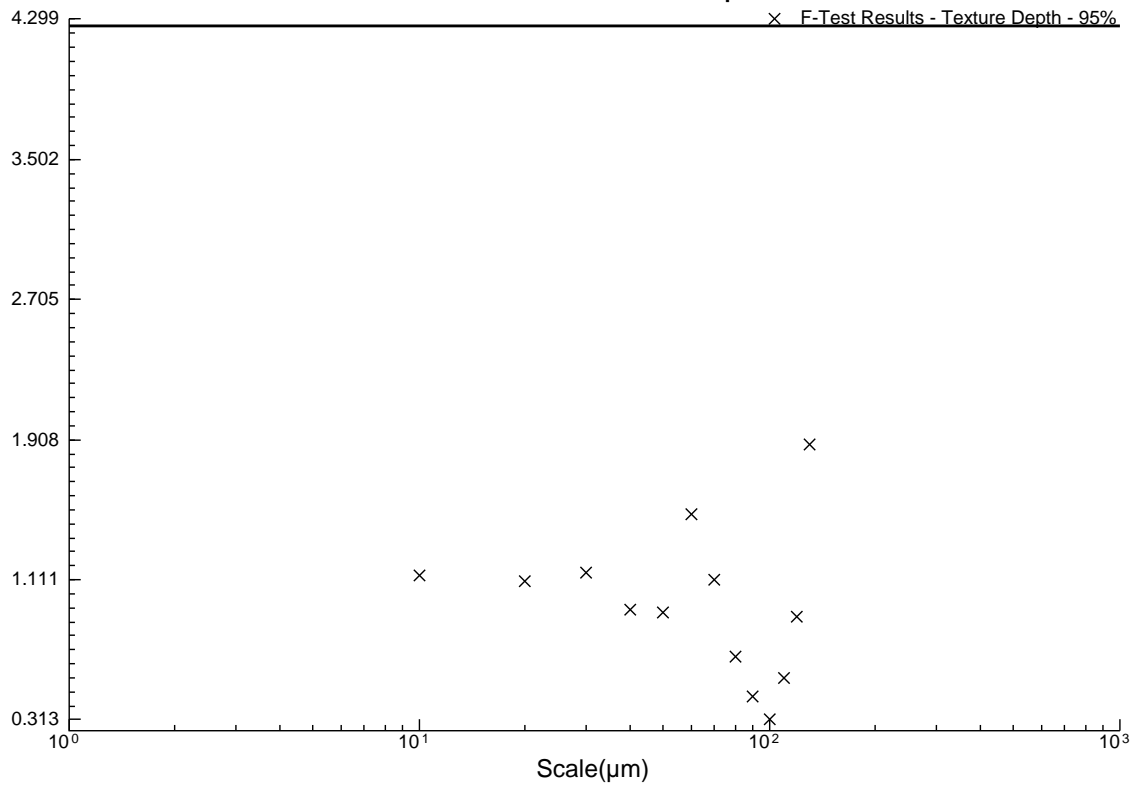


B2DVSW2D

### F-Test Results - Relative Area - 95%

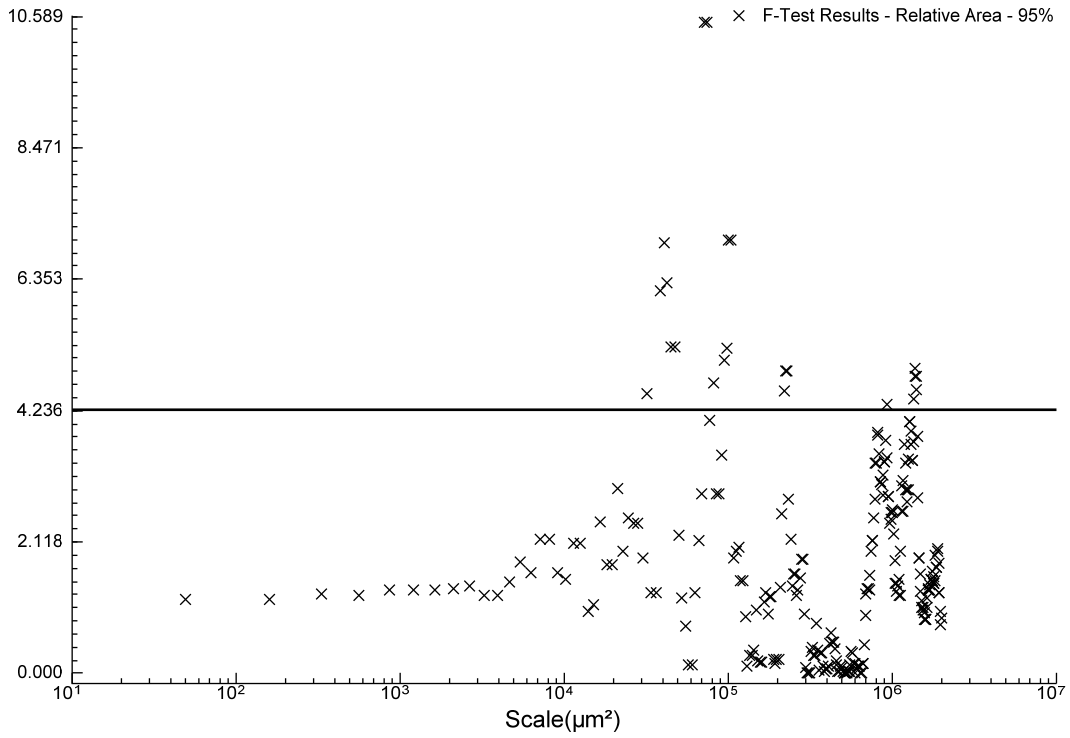


### F-Test Results - Texture Depth - 95%

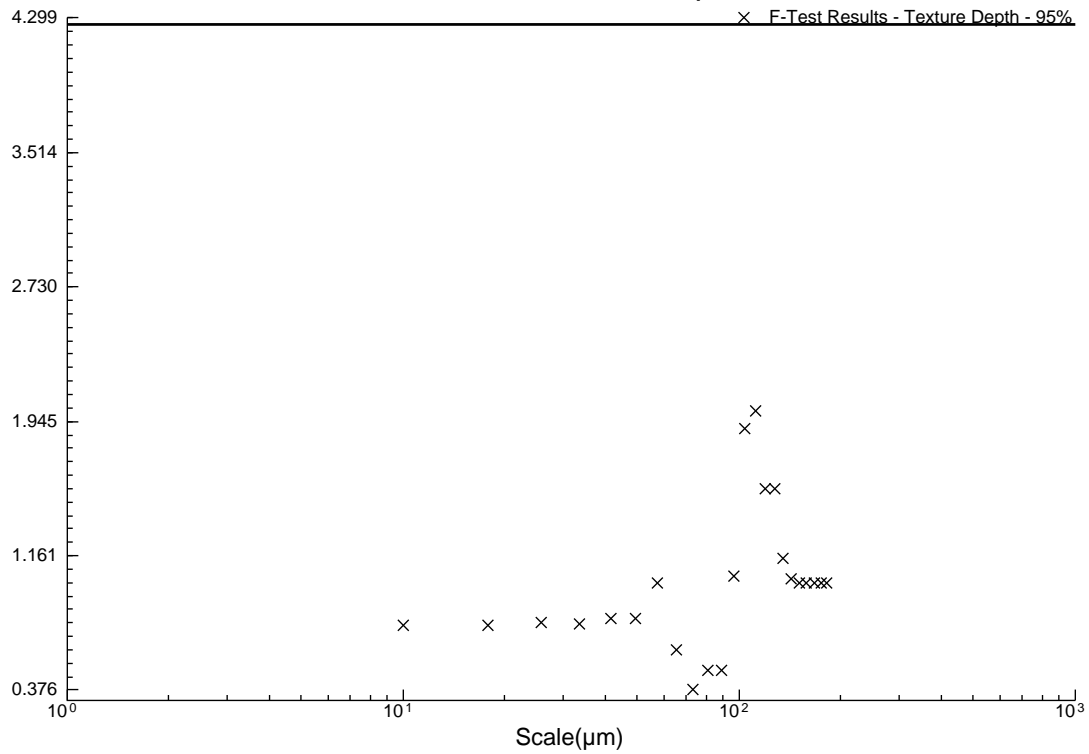


B2DVSW2U

### F-Test Results - Relative Area - 95%

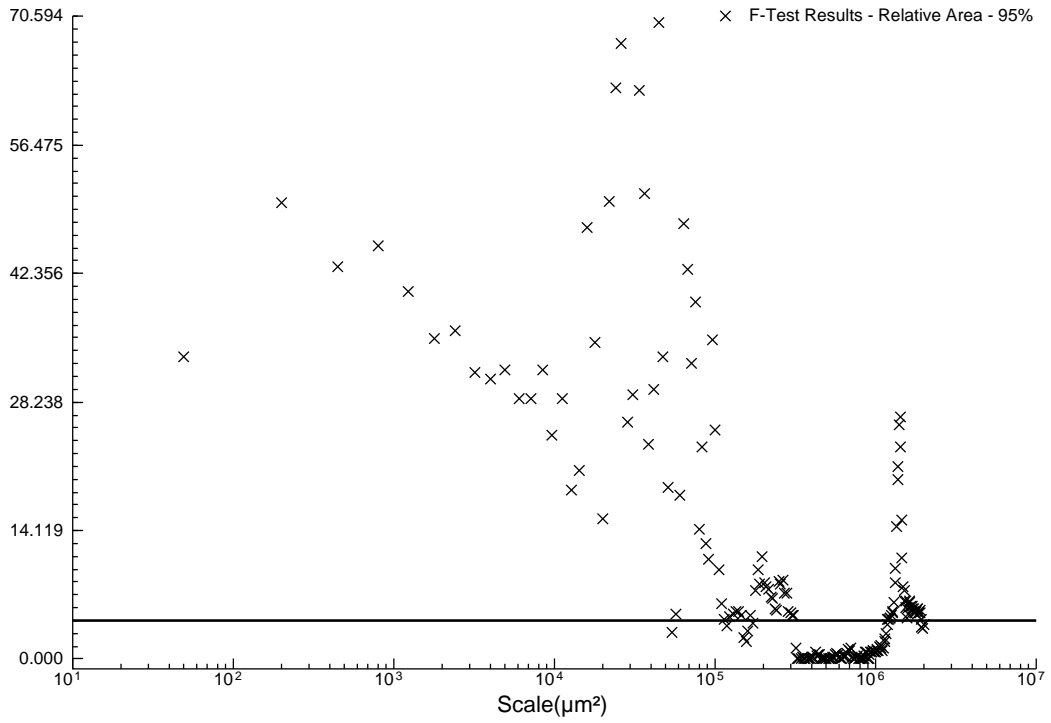


### F-Test Results - Texture Depth - 95%

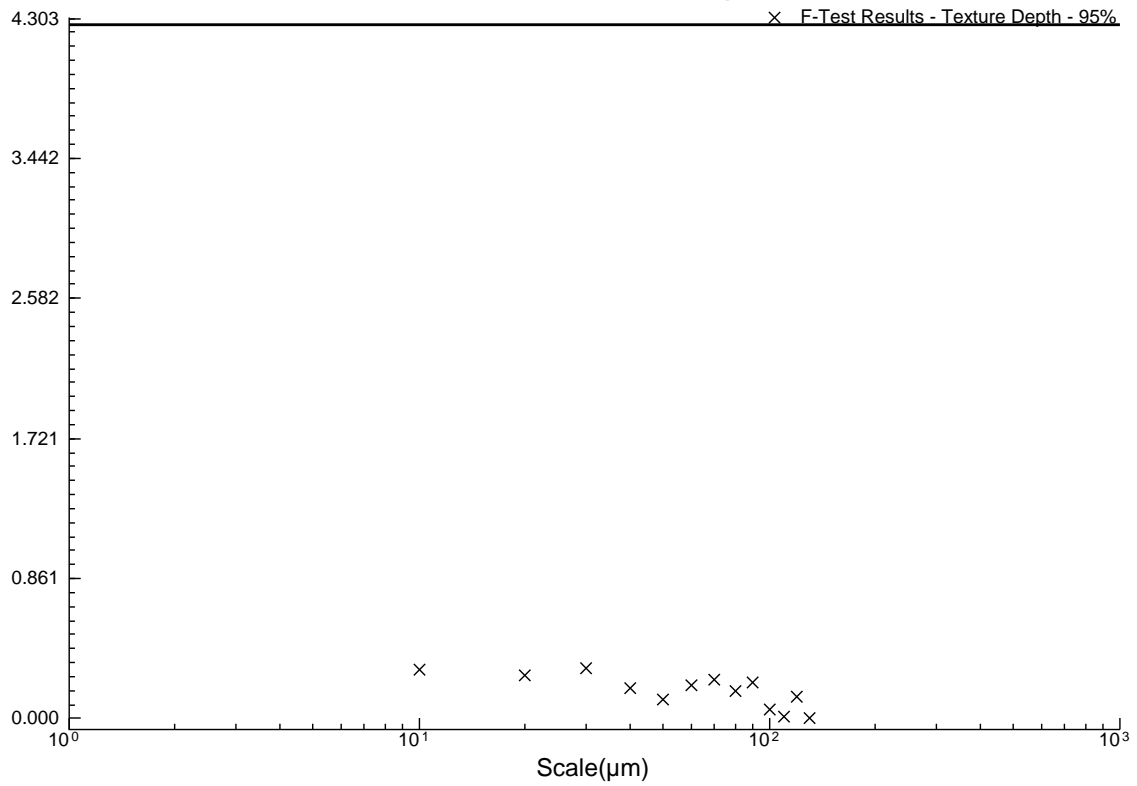


B2DVSW3D

### F-Test Results - Relative Area - 95%

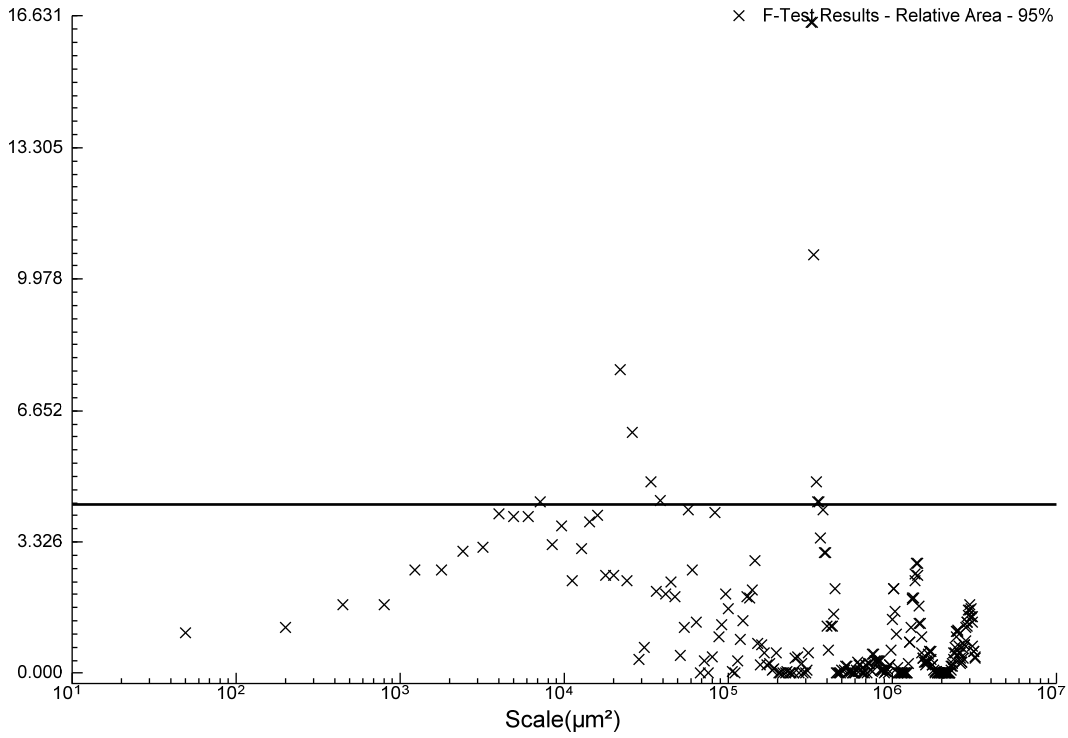


### F-Test Results - Texture Depth - 95%

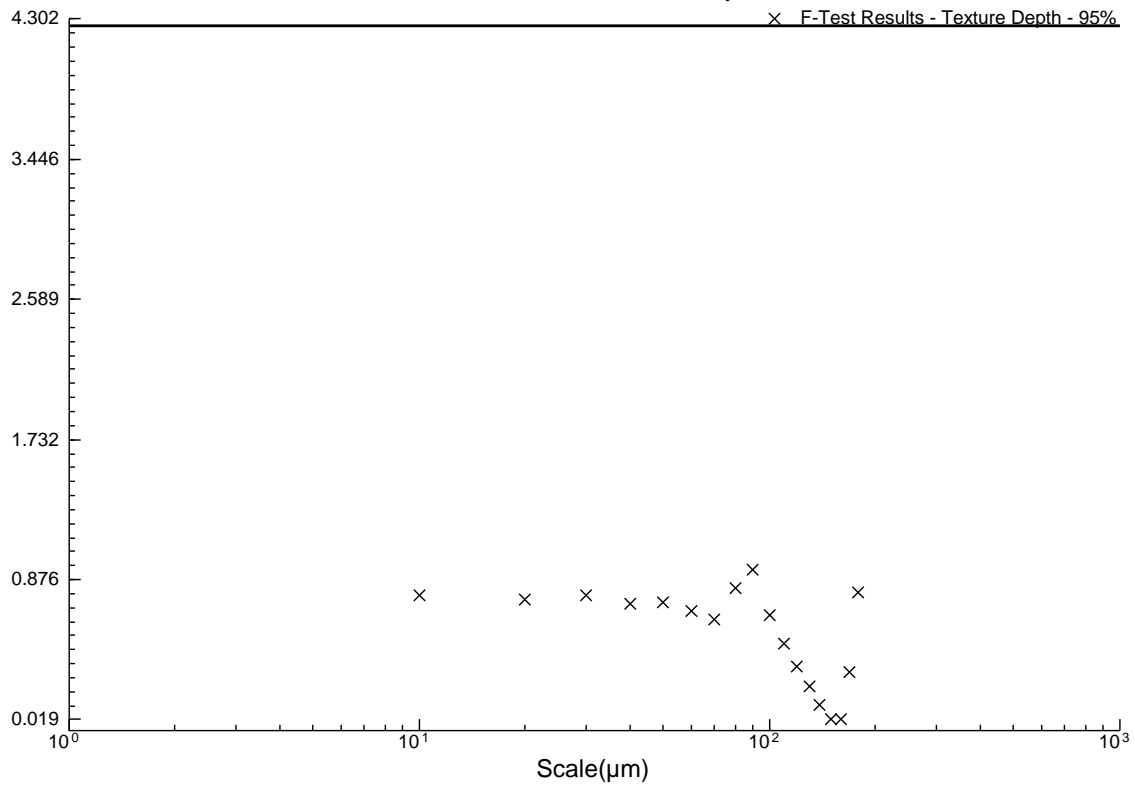


B2UVSB3U

### F-Test Results - Relative Area - 95%

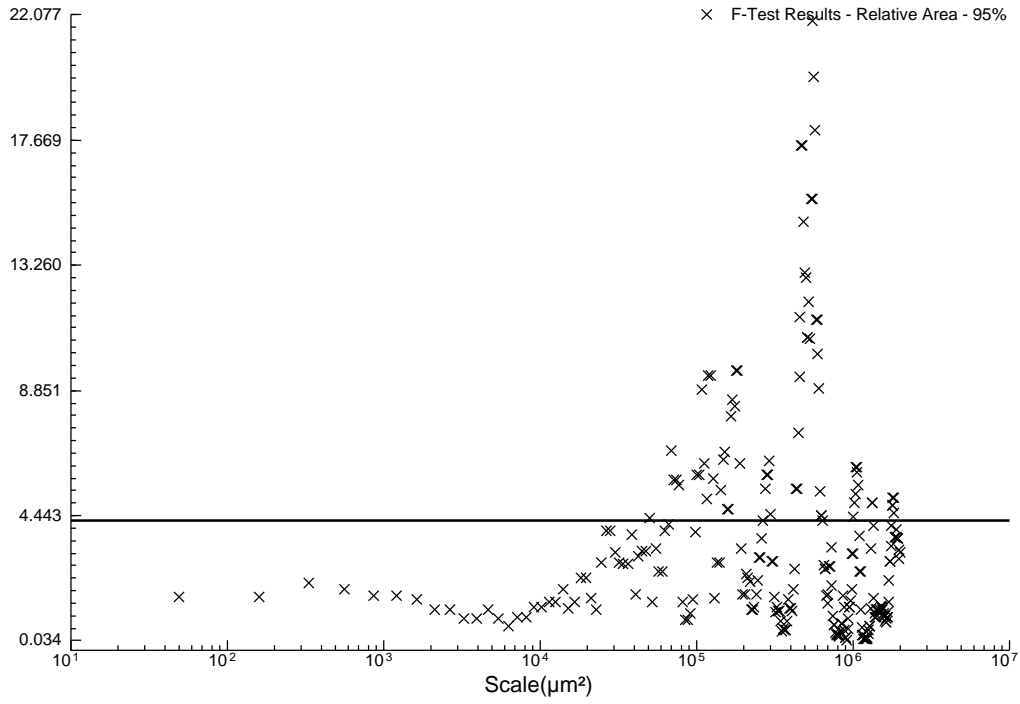


### F-Test Results - Texture Depth - 95%

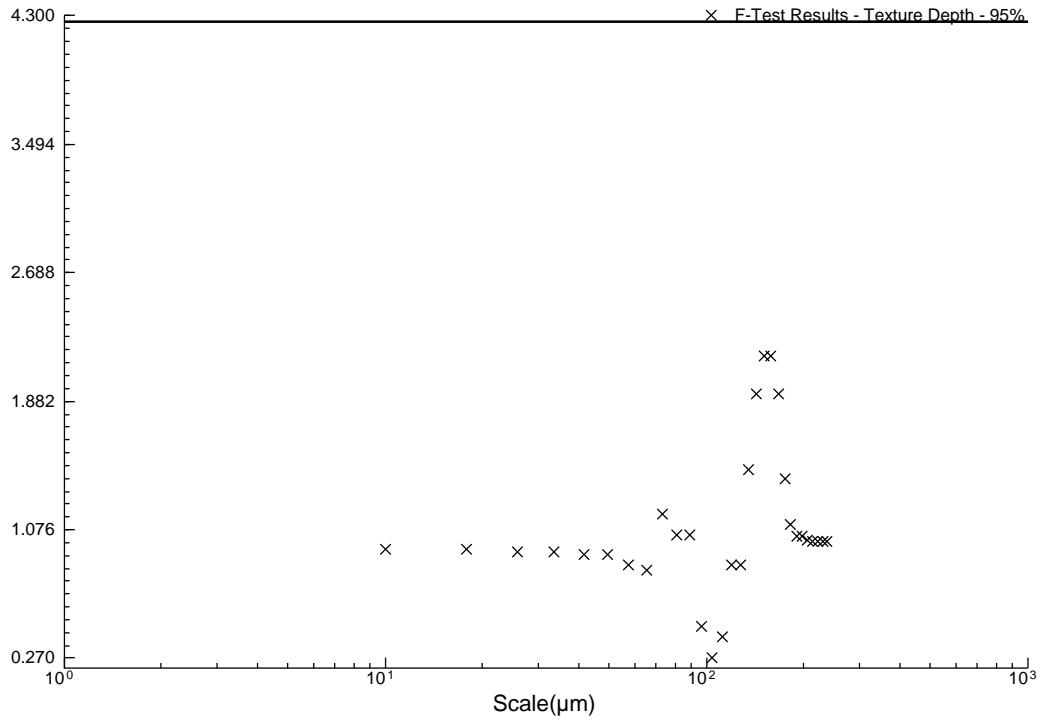


B2UVSW1D

### F-Test Results - Relative Area - 95%

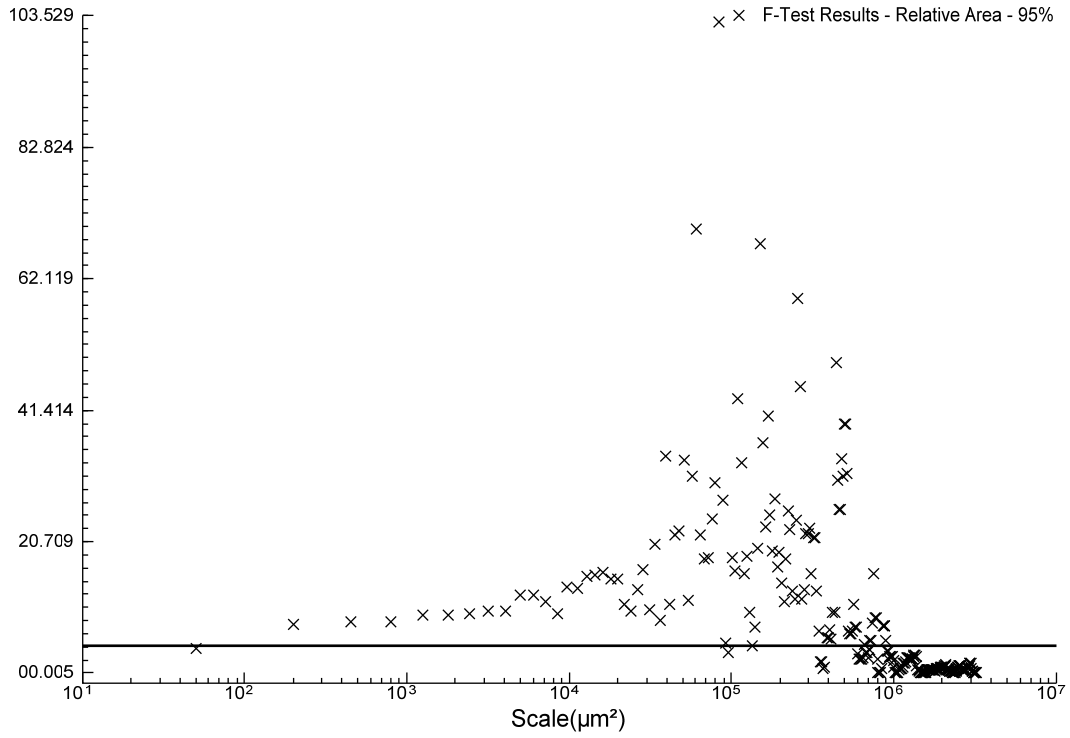


### F-Test Results - Texture Depth - 95%

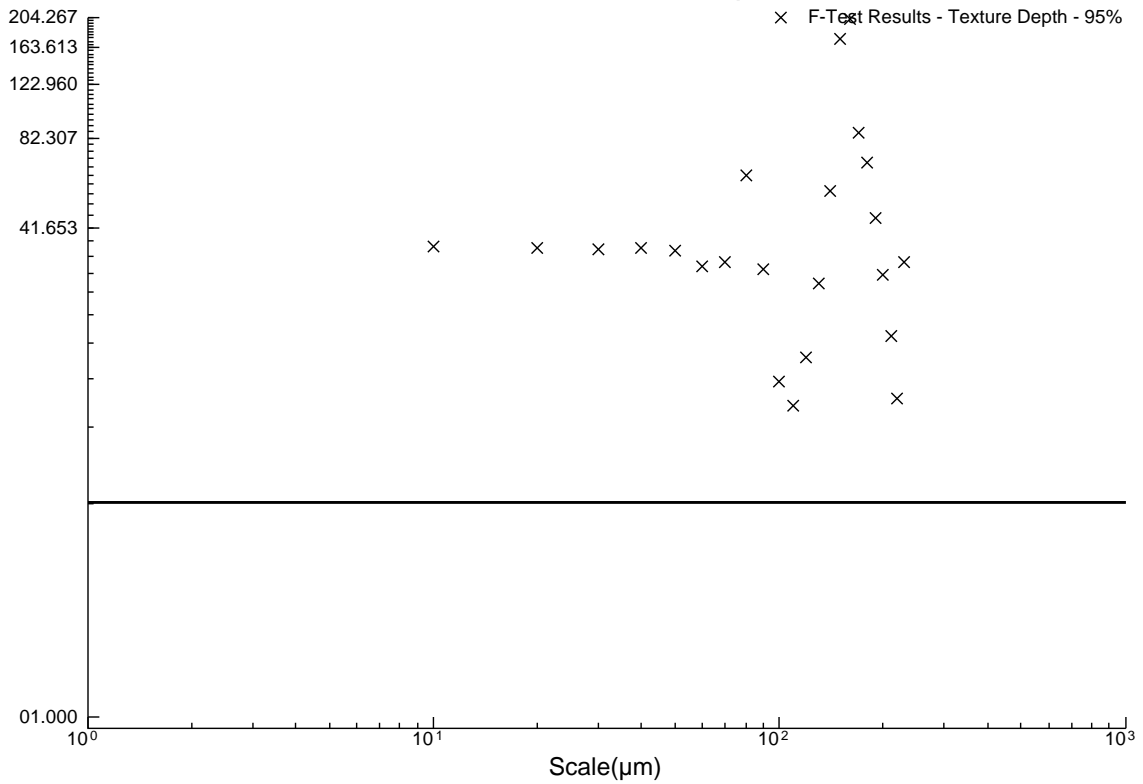


B2UVSW1U

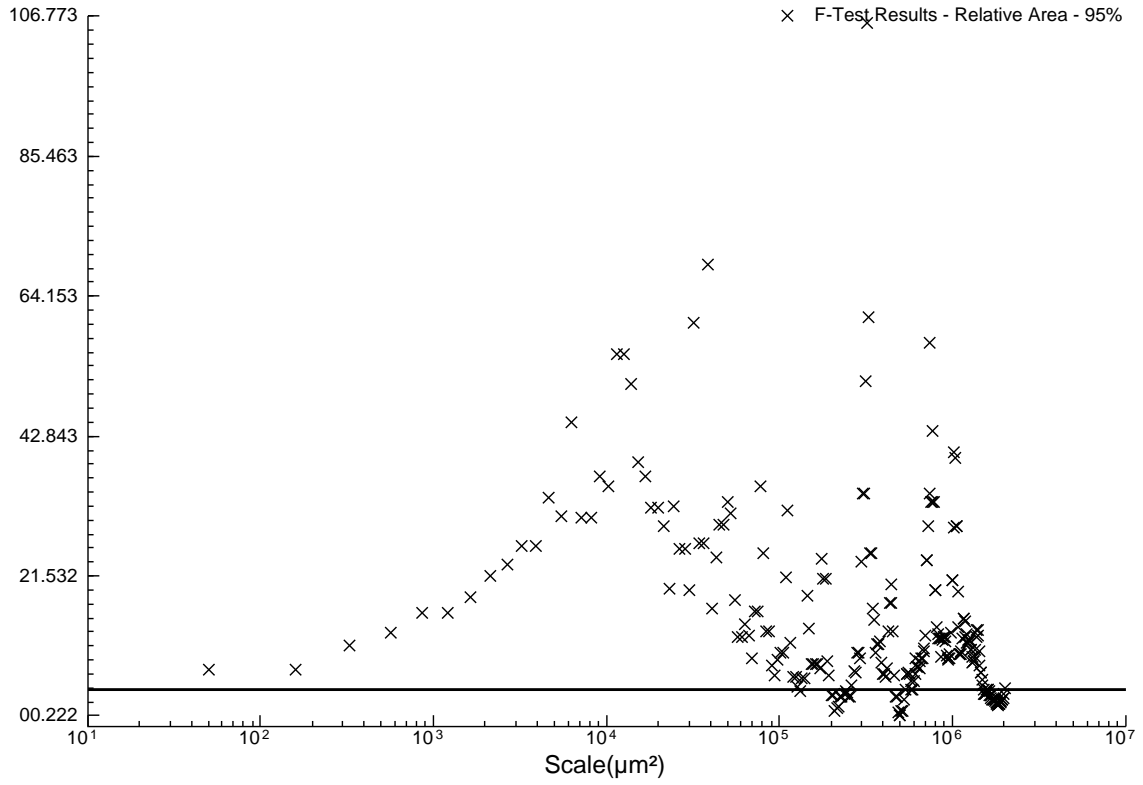
### F-Test Results - Relative Area - 95%



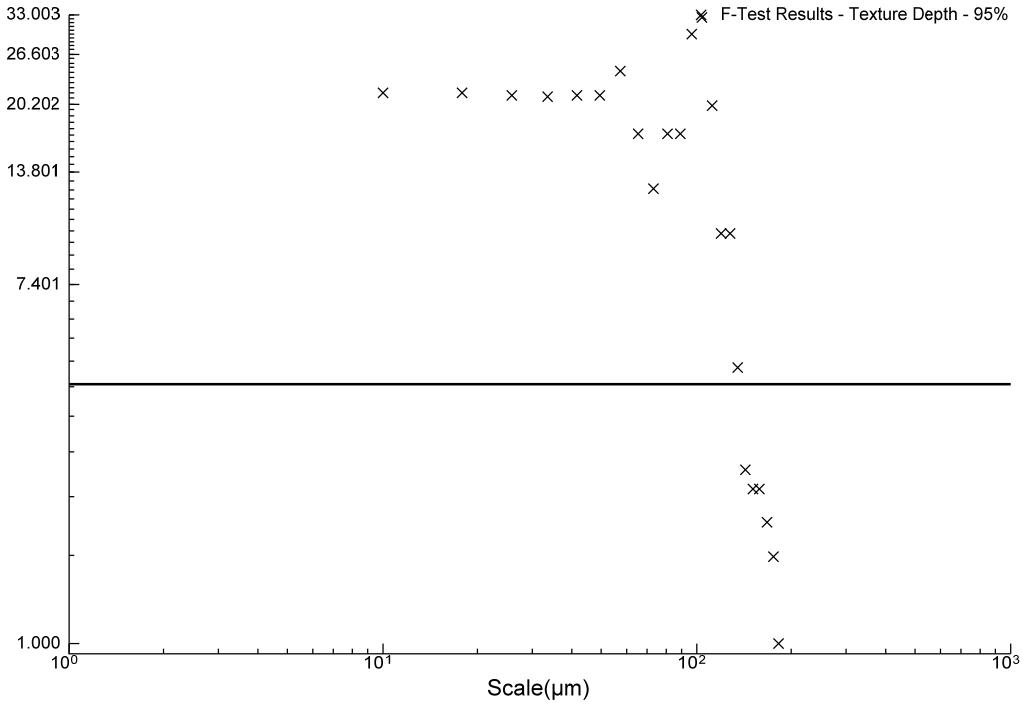
### F-Test Results - Texture Depth - 95%



### F-Test Results - Relative Area - 95%

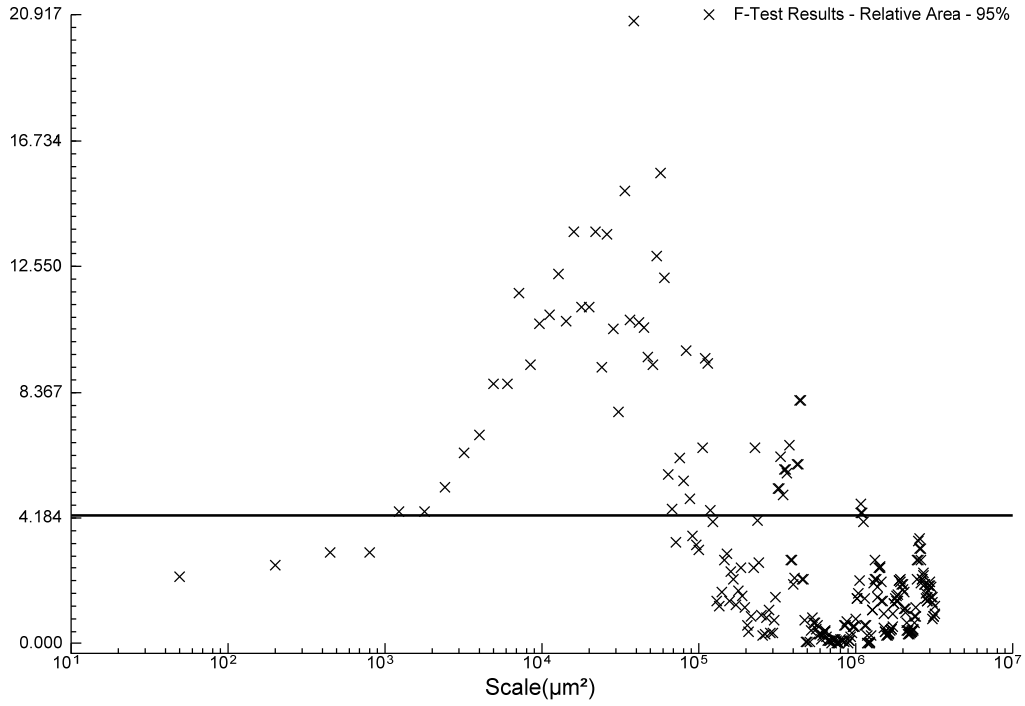


### F-Test Results - Texture Depth - 95%

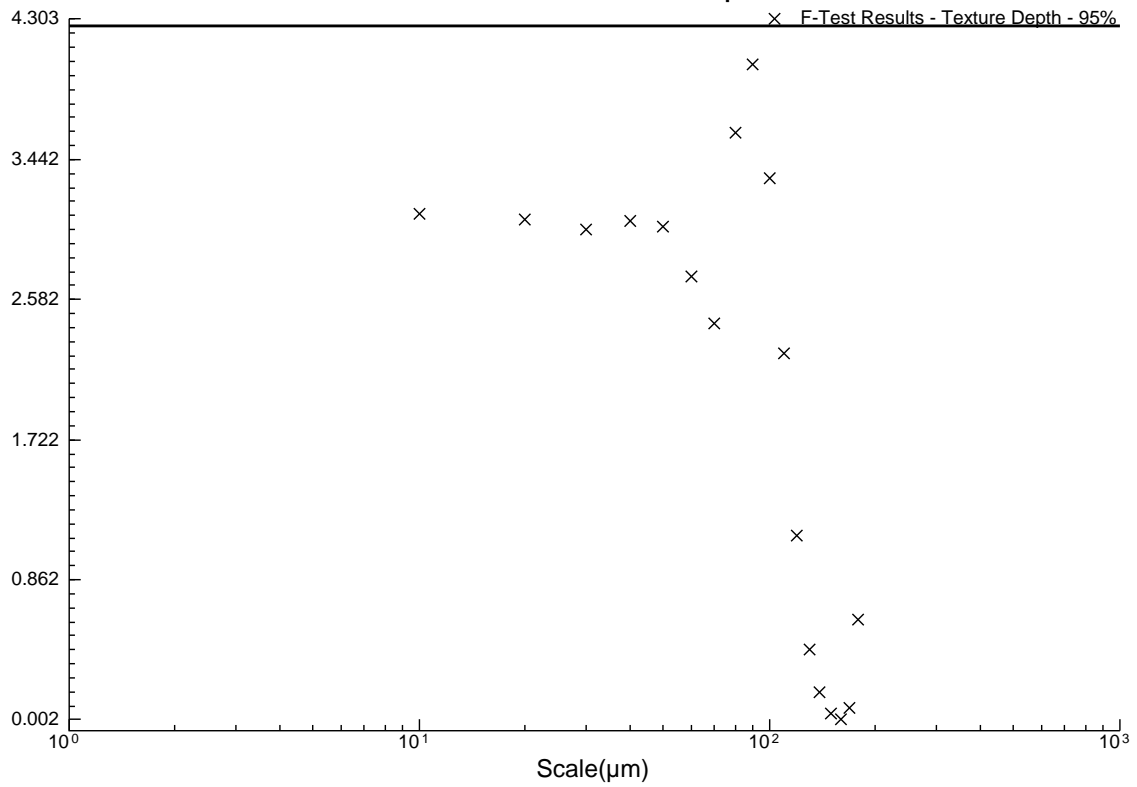


B2UVSW2U

### F-Test Results - Relative Area - 95%

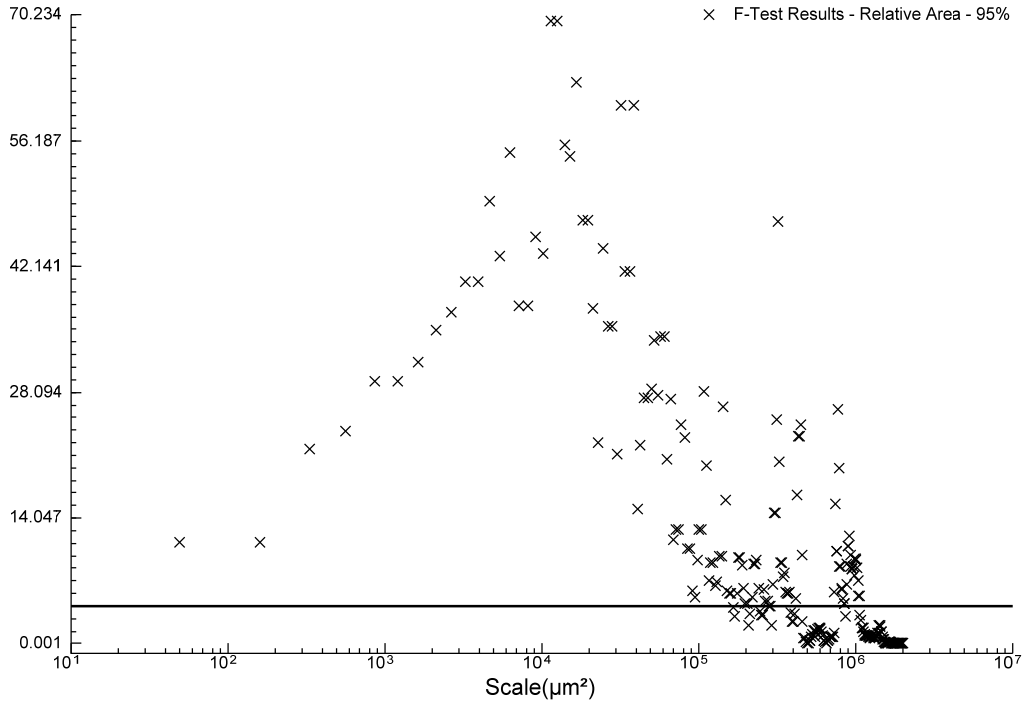


### F-Test Results - Texture Depth - 95%

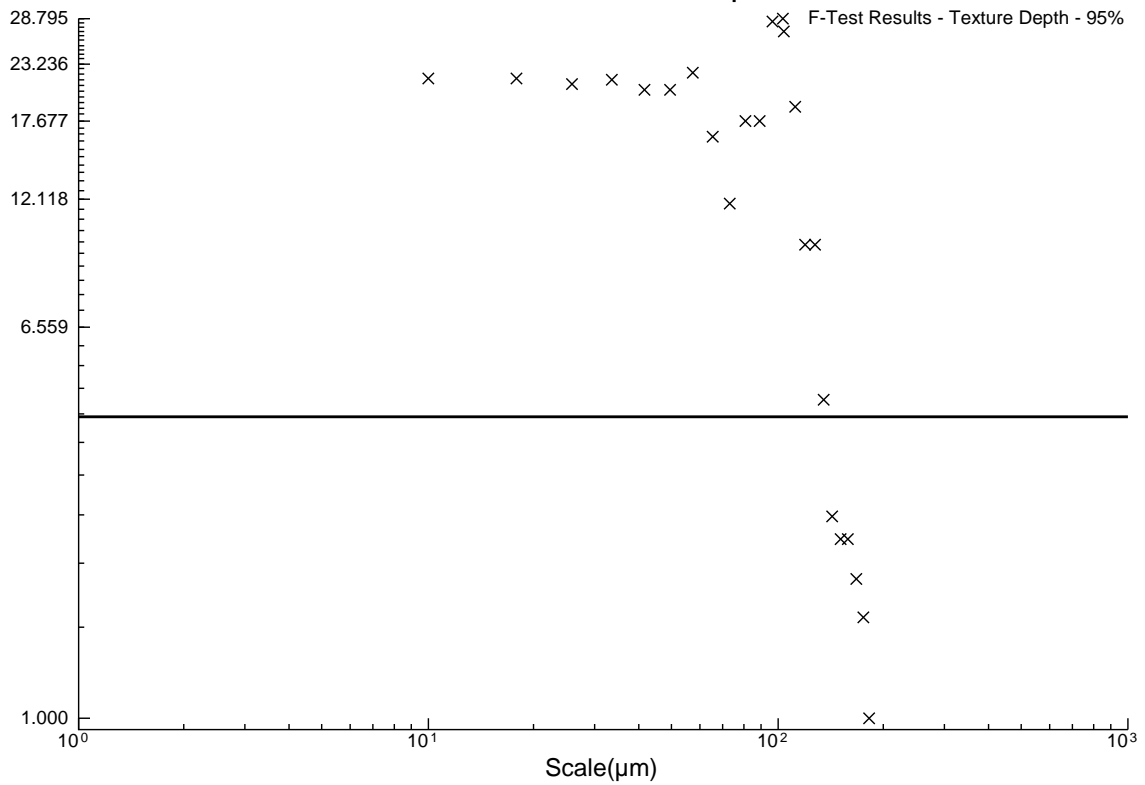


B2UVSW3D

### F-Test Results - Relative Area - 95%

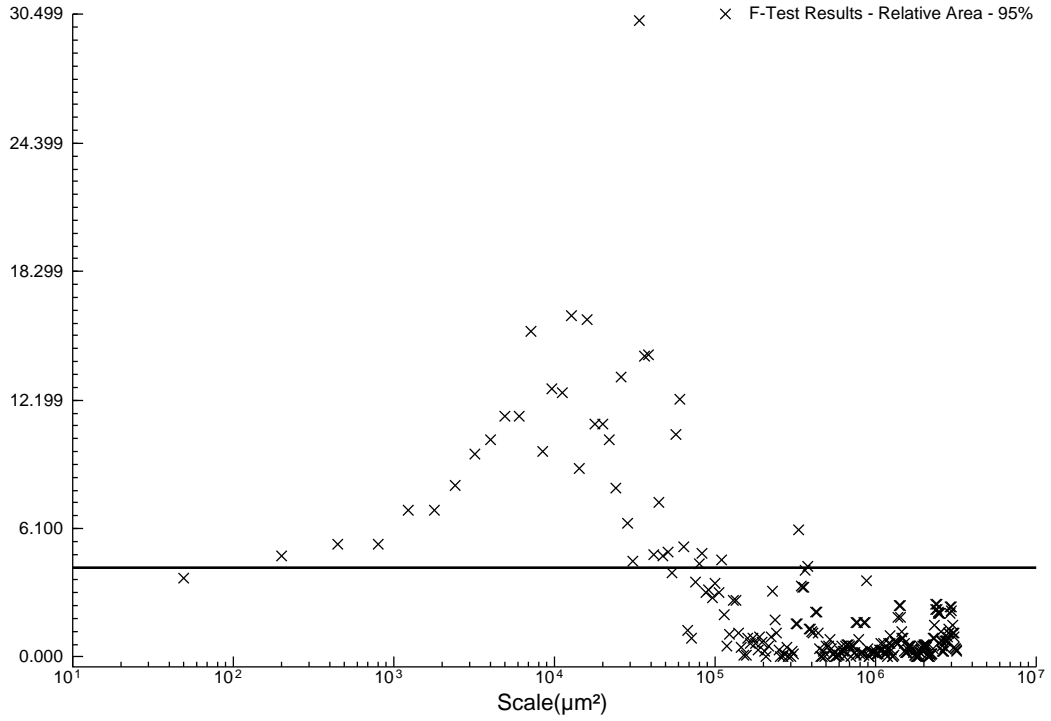


### F-Test Results - Texture Depth - 95%

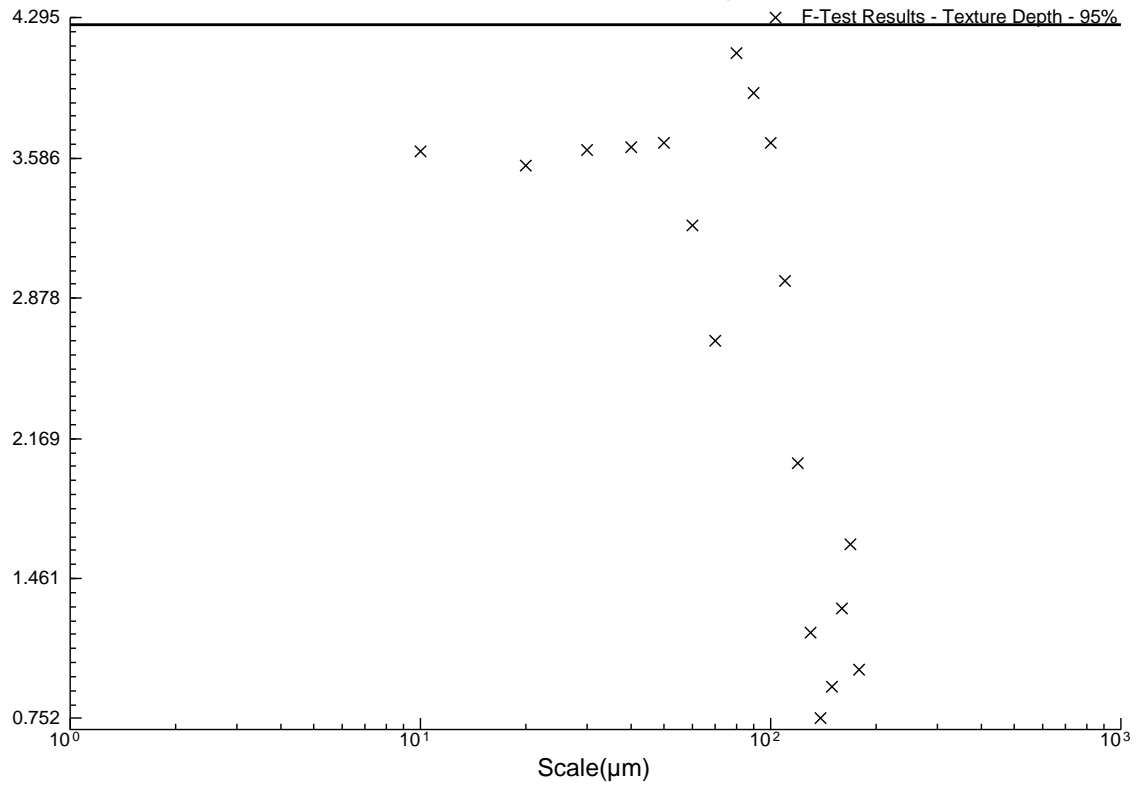


B2UVSW3U

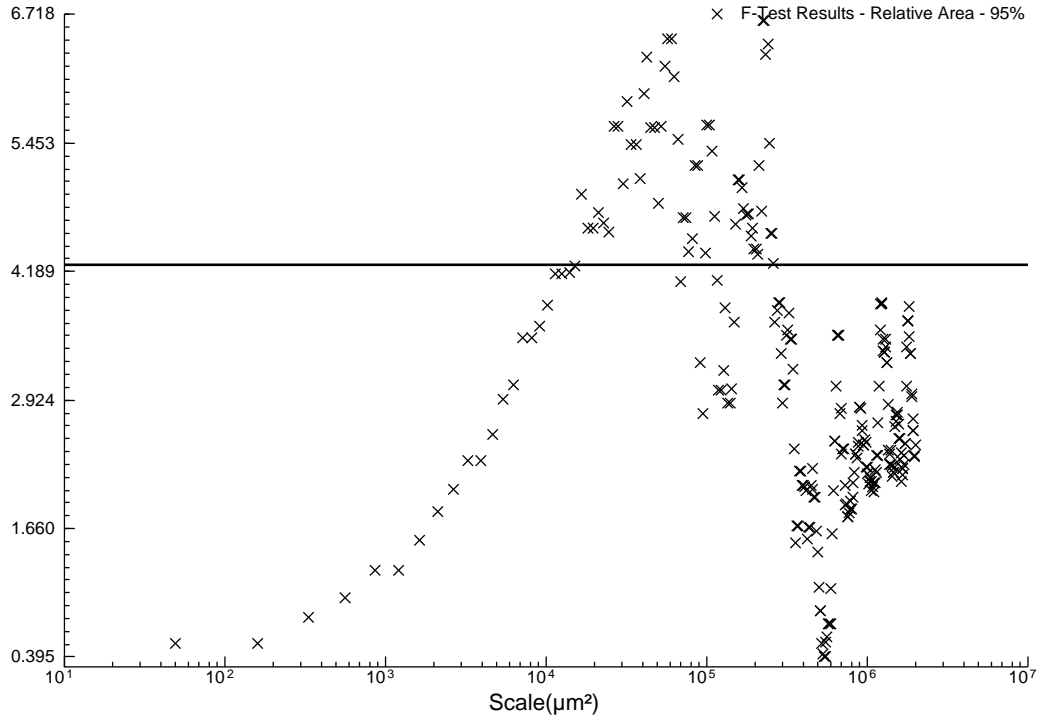
### F-Test Results - Relative Area - 95%



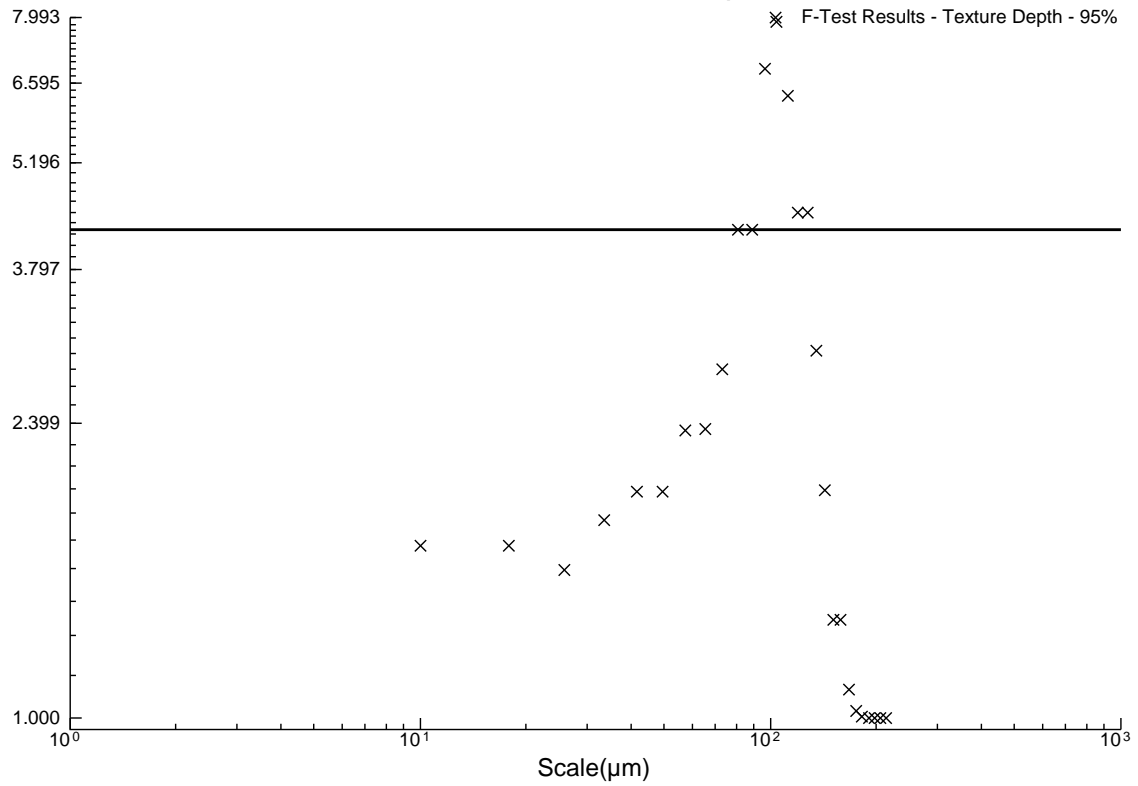
### F-Test Results - Texture Depth - 95%

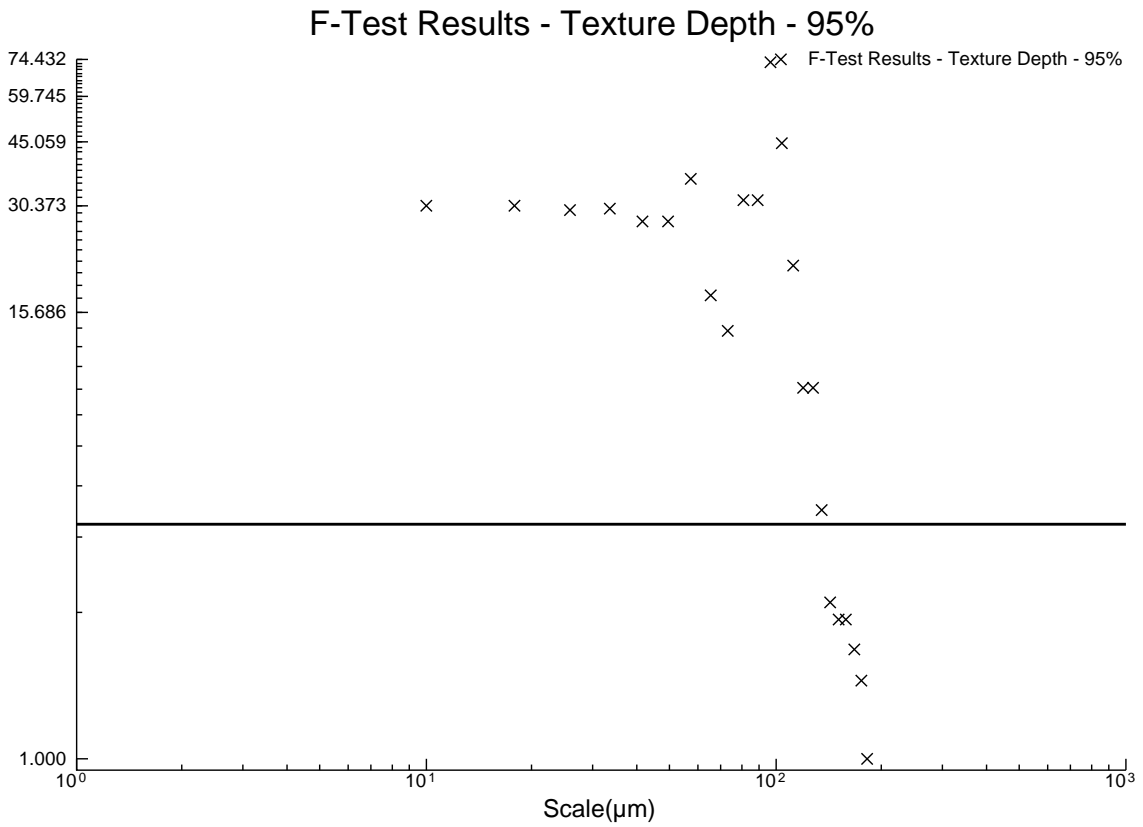
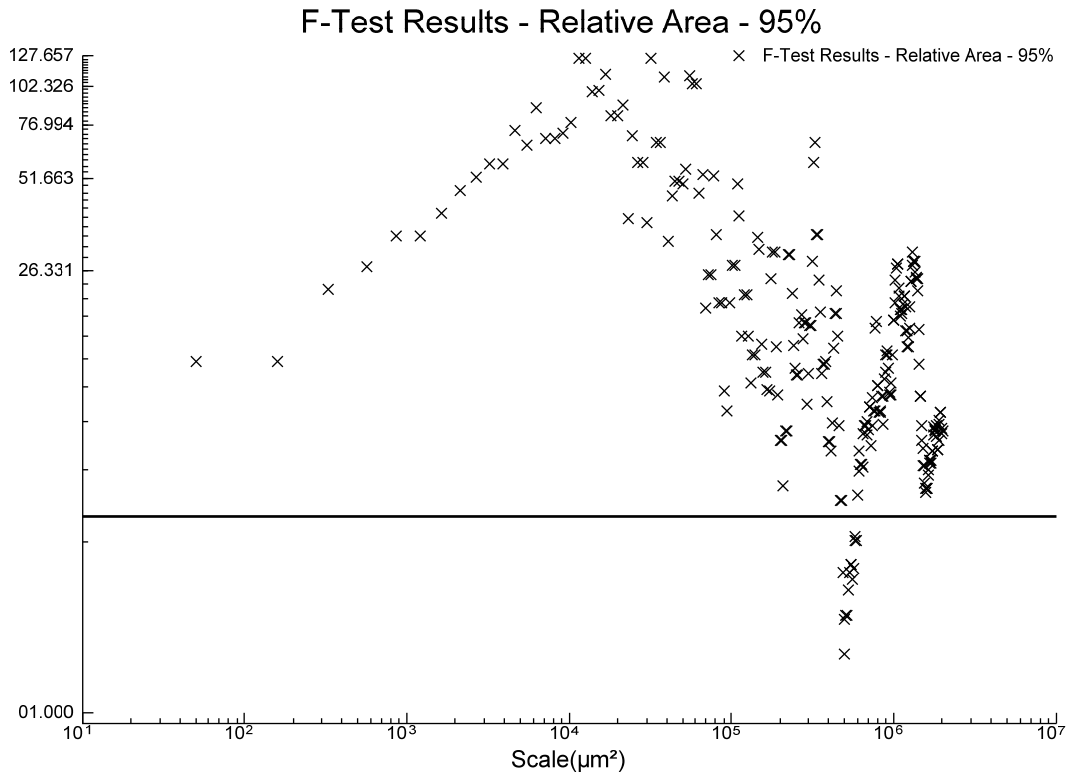


### F-Test Results - Relative Area - 95%



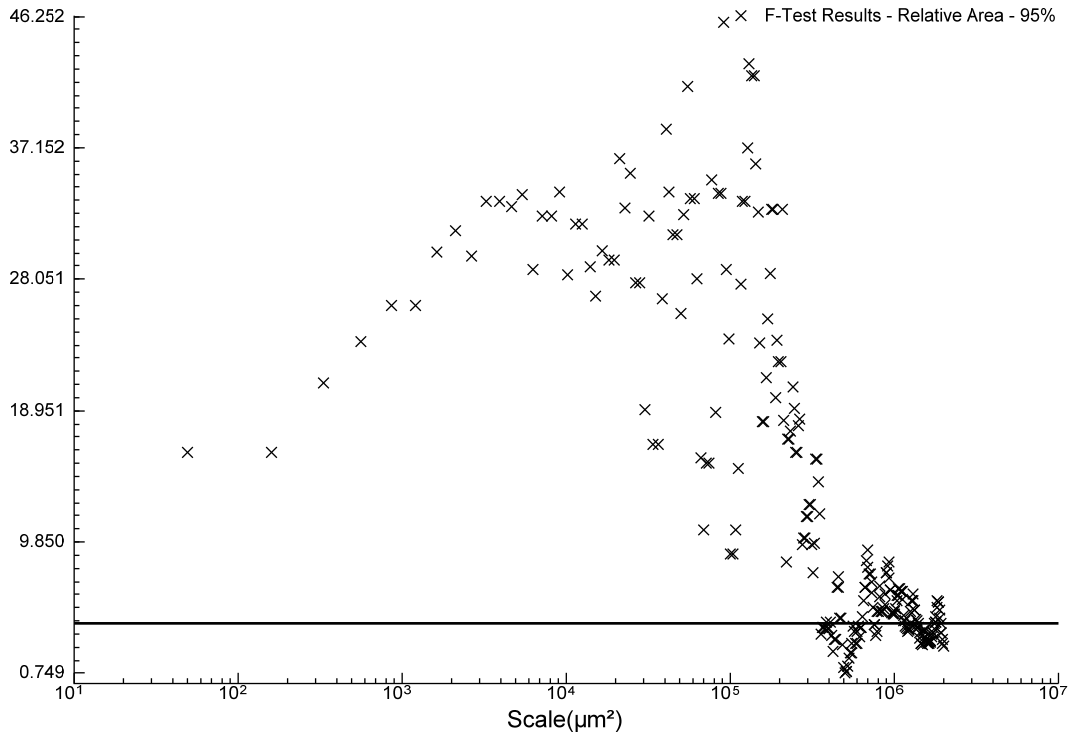
### F-Test Results - Texture Depth - 95%



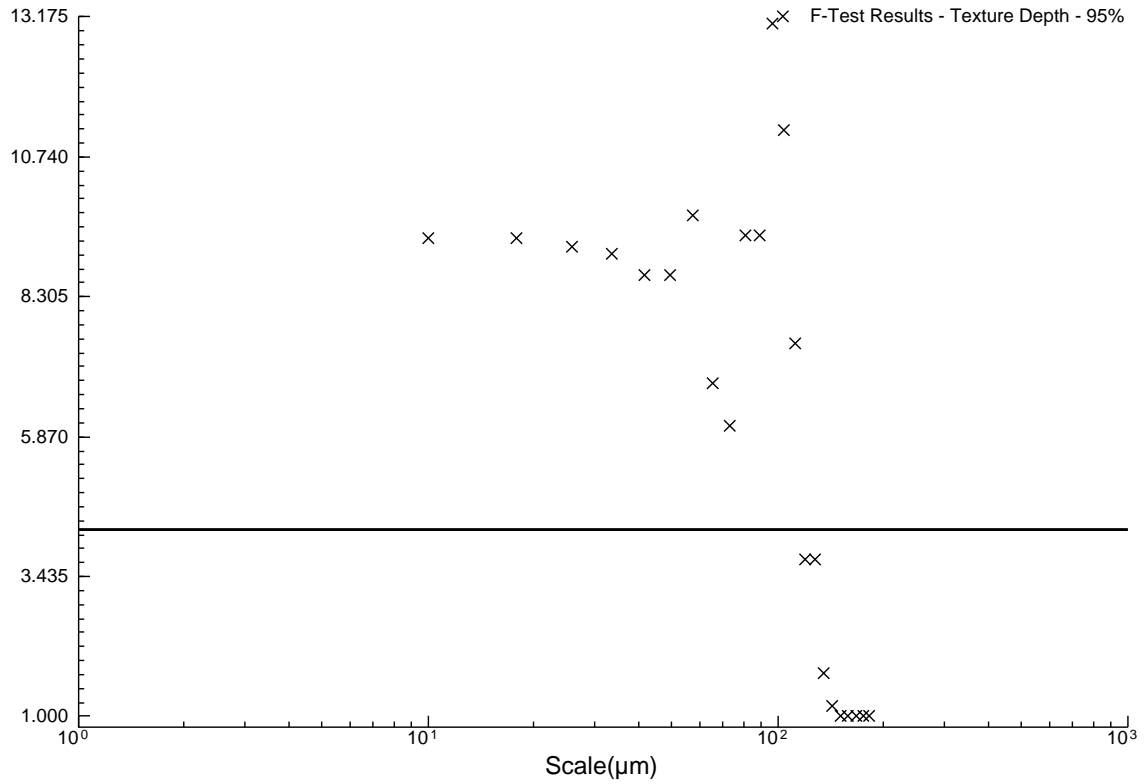


B3DVSB3U

### F-Test Results - Relative Area - 95%

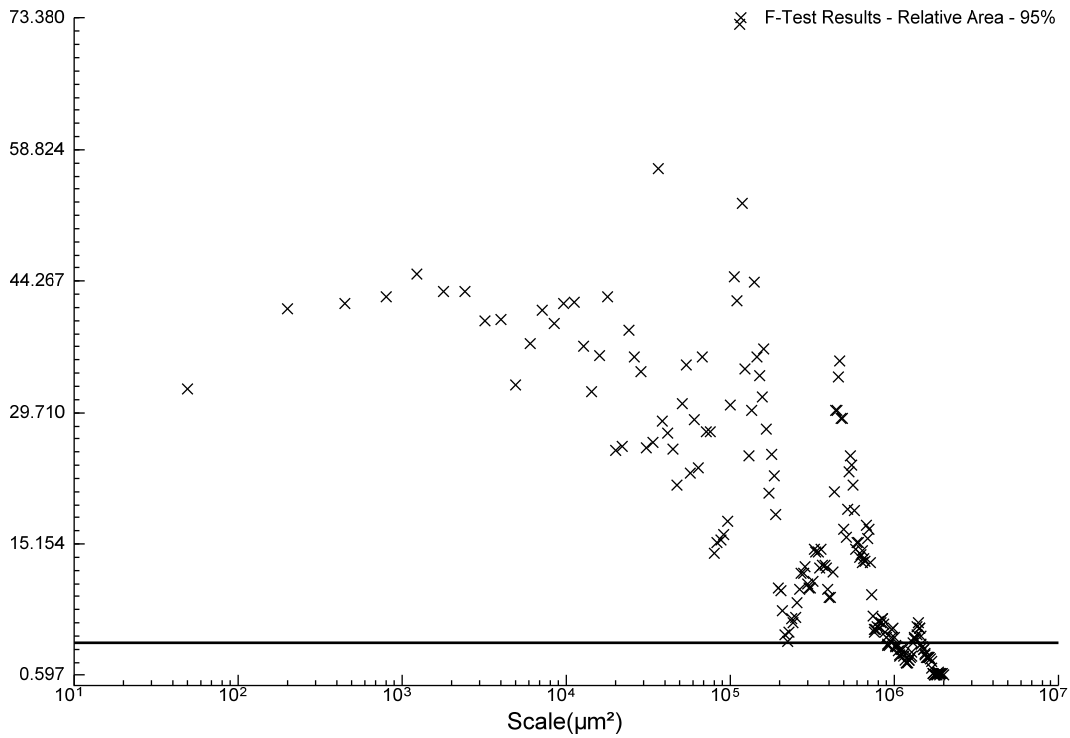


### F-Test Results - Texture Depth - 95%

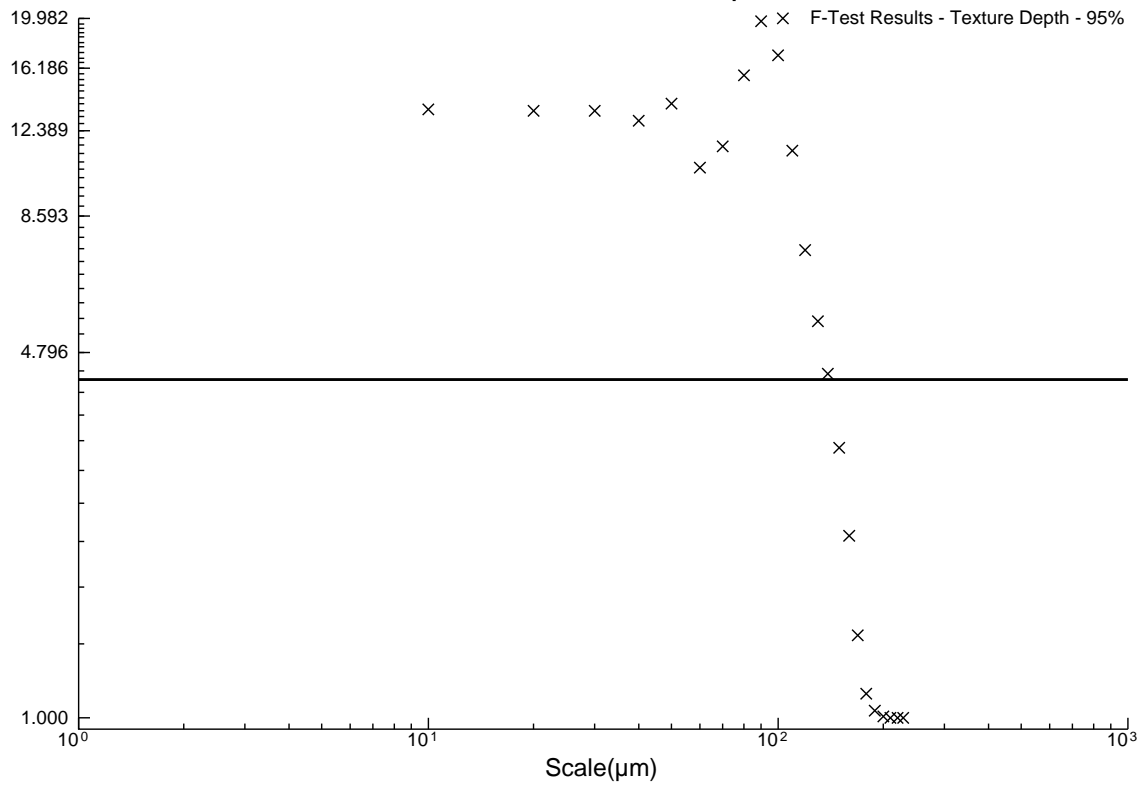


B3DVSWID

### F-Test Results - Relative Area - 95%

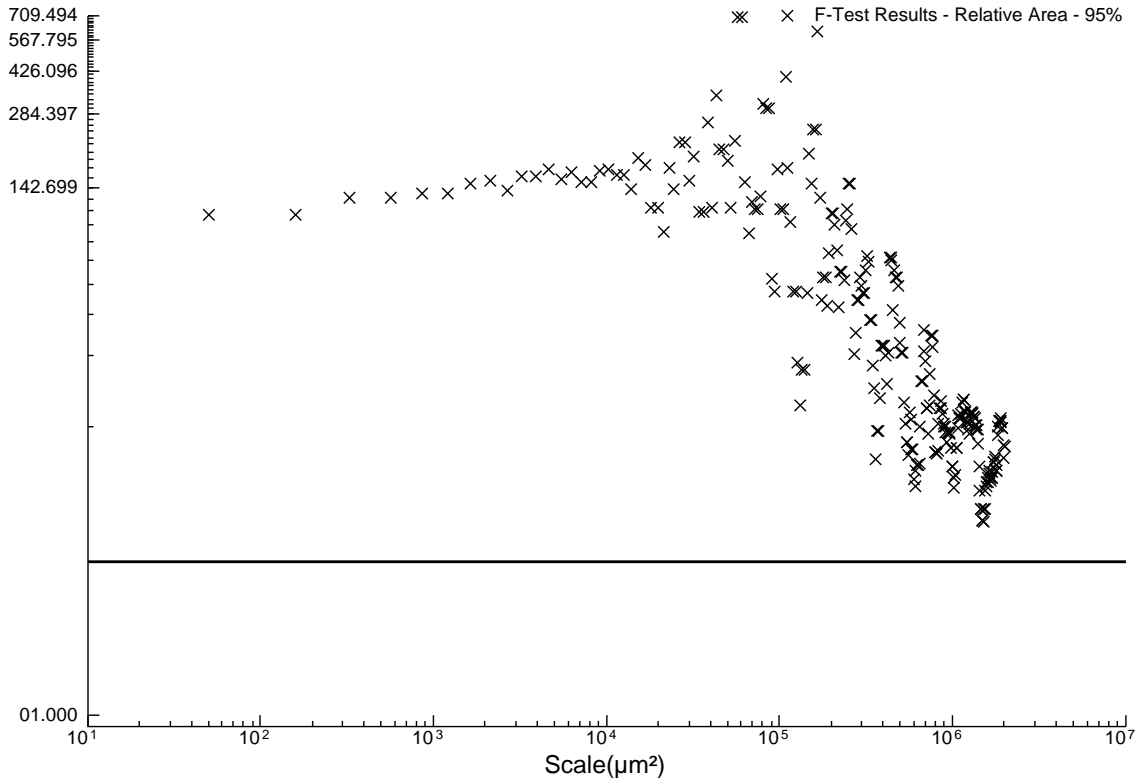


### F-Test Results - Texture Depth - 95%

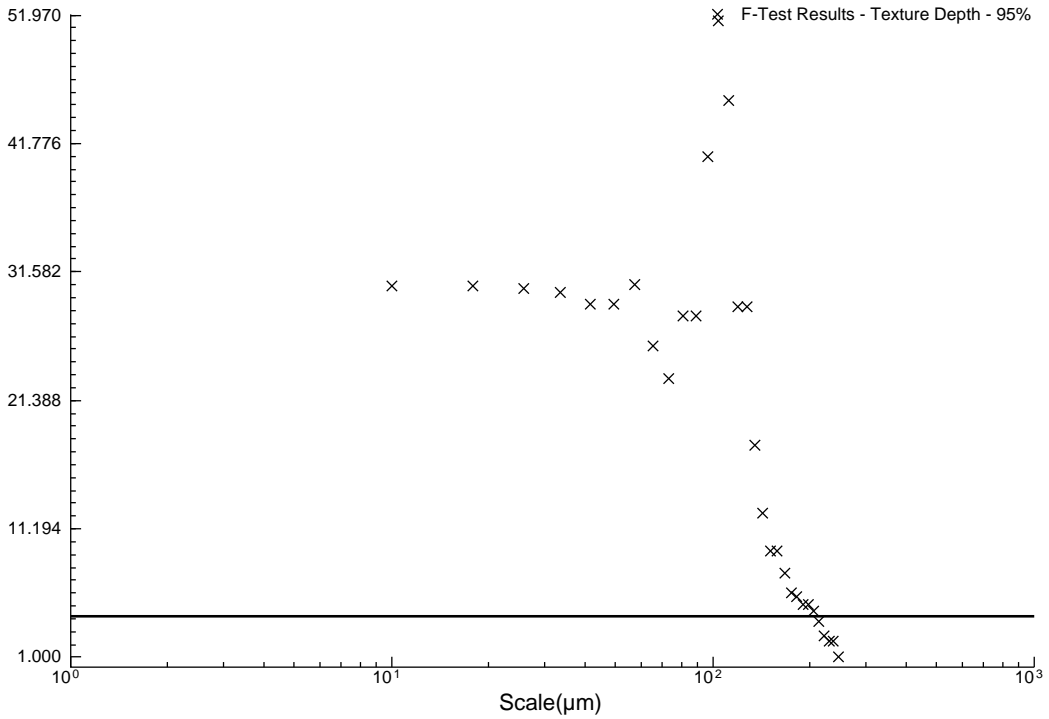


B3DVSW1U

### F-Test Results - Relative Area - 95%

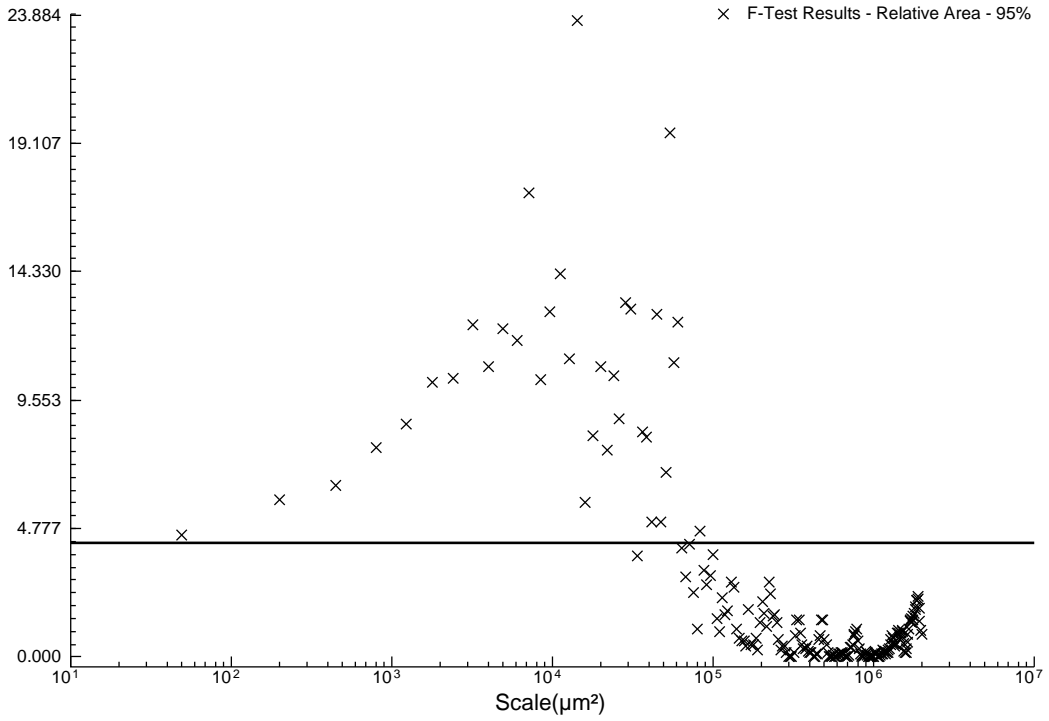


### F-Test Results - Texture Depth - 95%

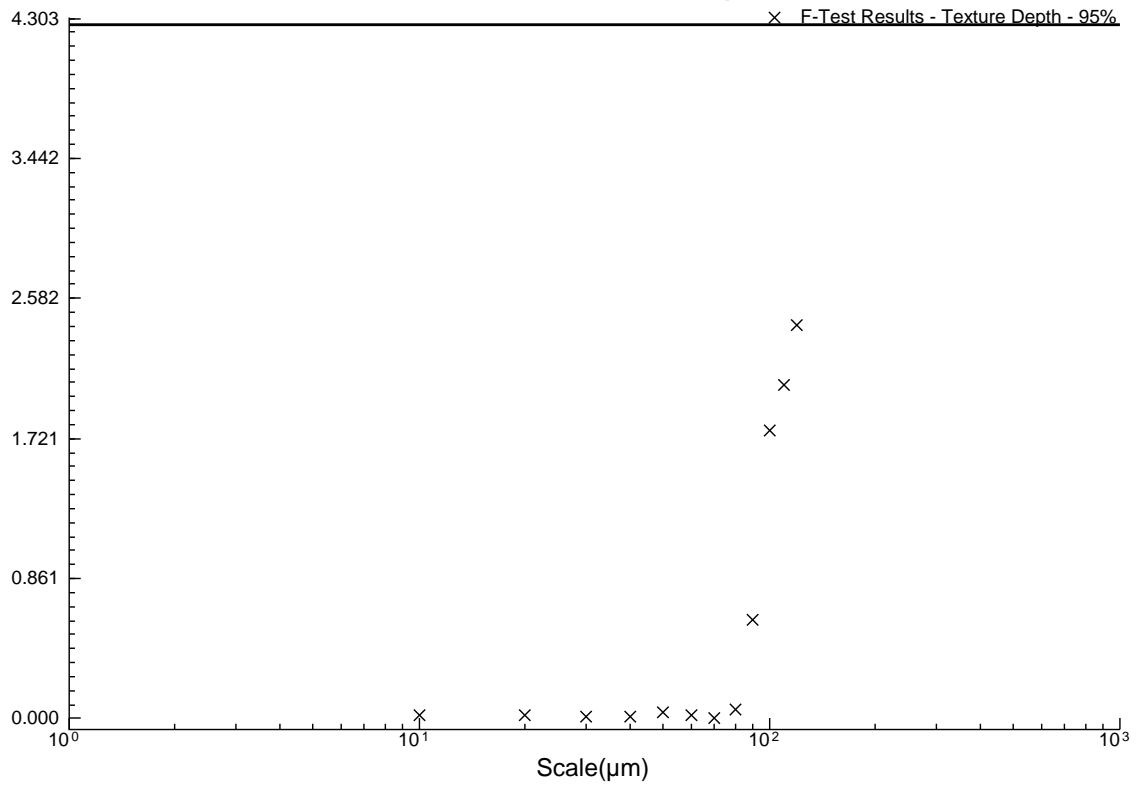


B3DVSW2D

### F-Test Results - Relative Area - 95%

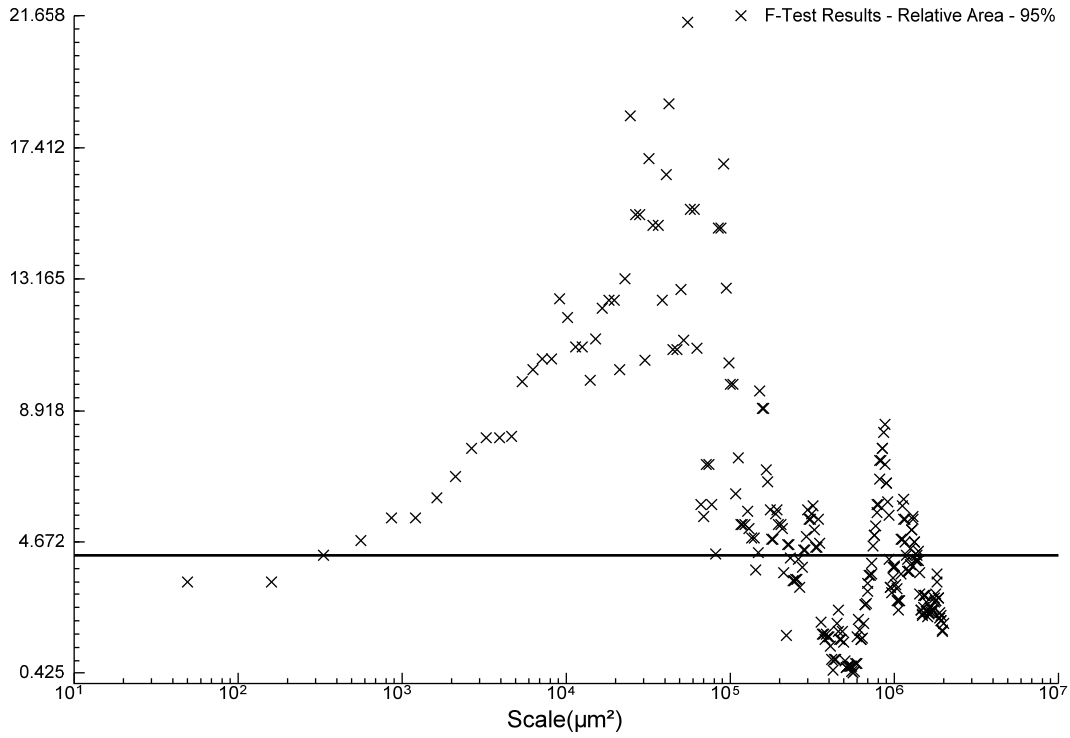


### F-Test Results - Texture Depth - 95%

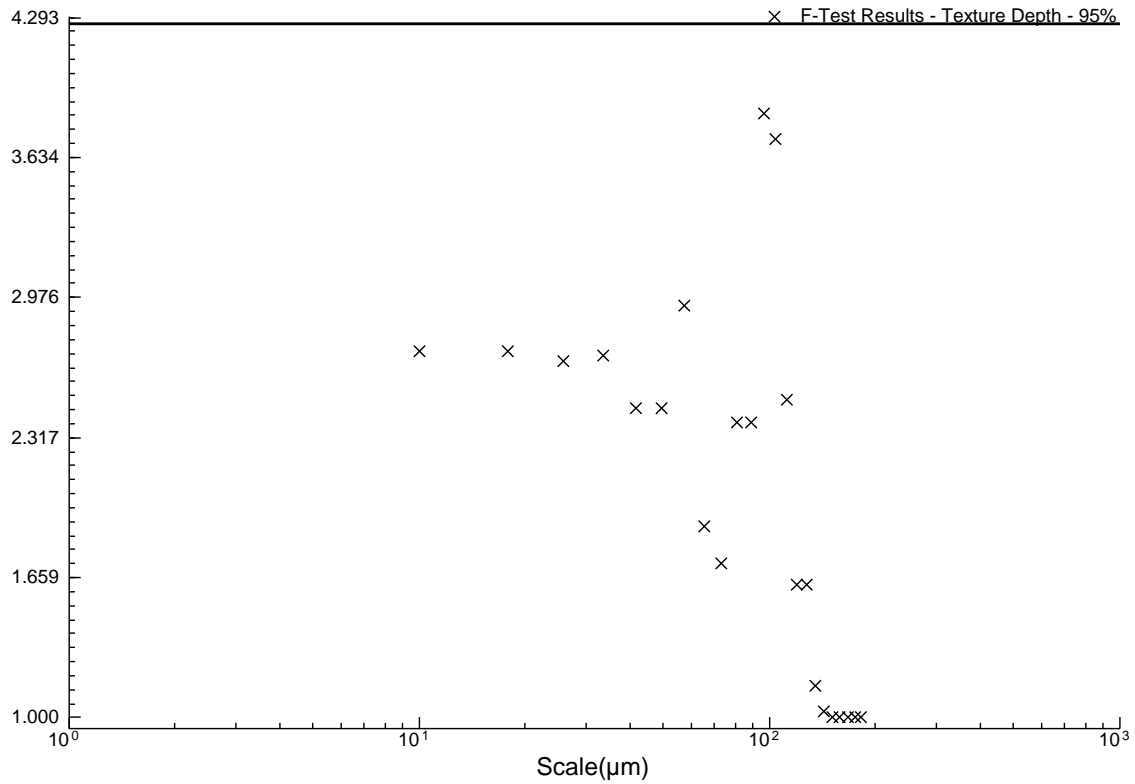


B3DVSW2U

### F-Test Results - Relative Area - 95%

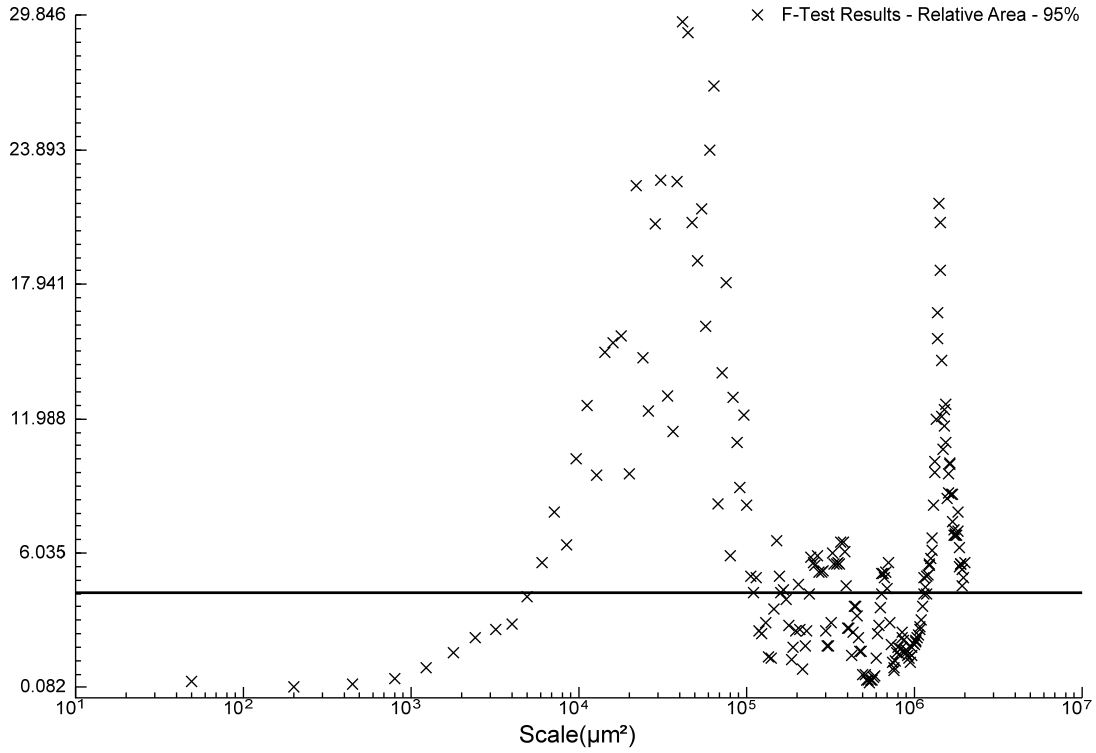


### F-Test Results - Texture Depth - 95%

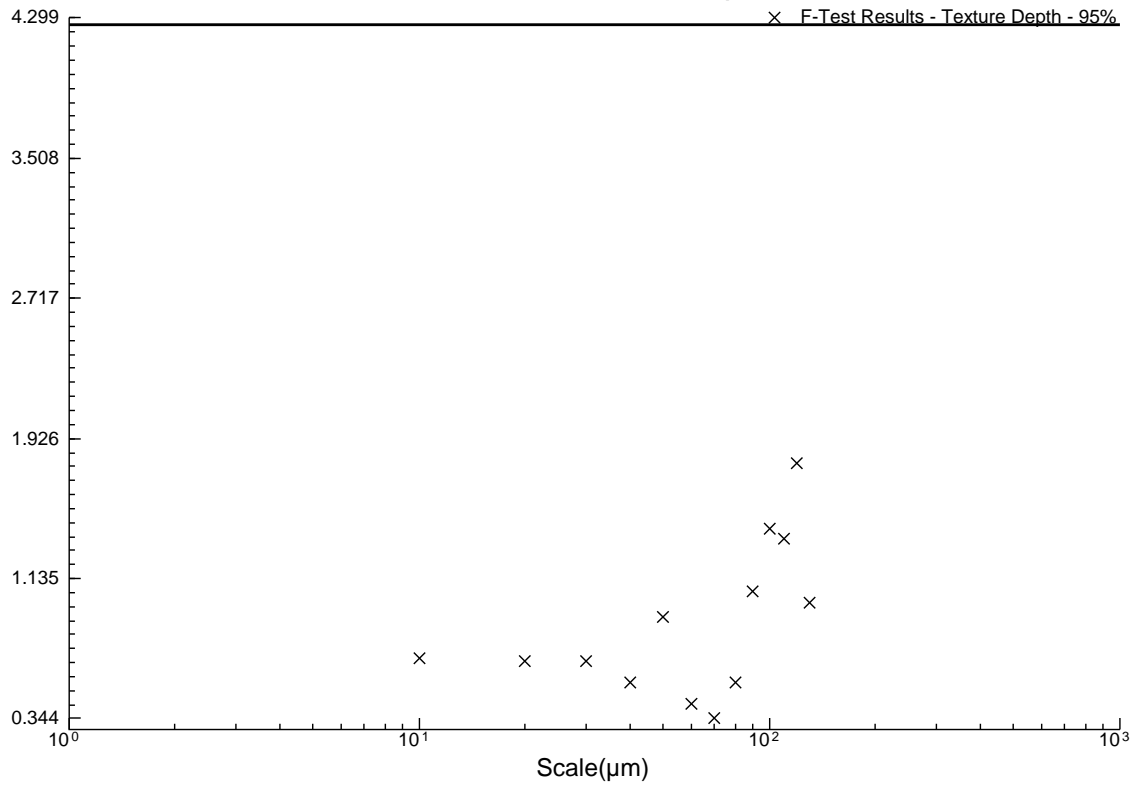


B3DVSW3D

### F-Test Results - Relative Area - 95%

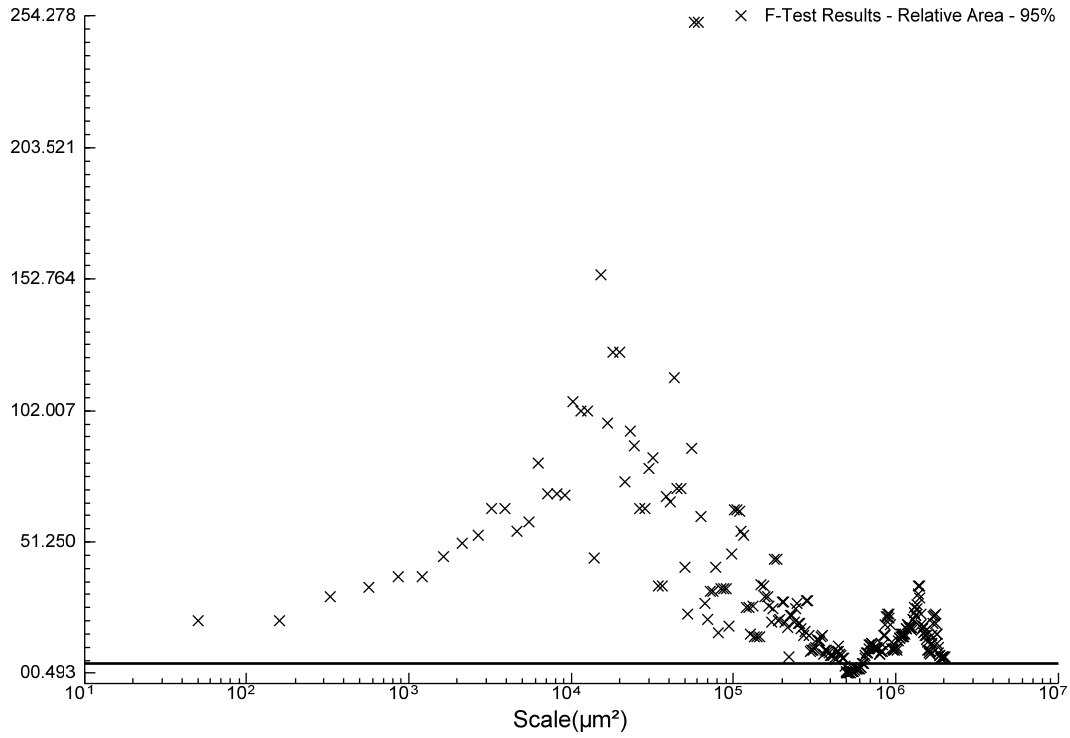


### F-Test Results - Texture Depth - 95%

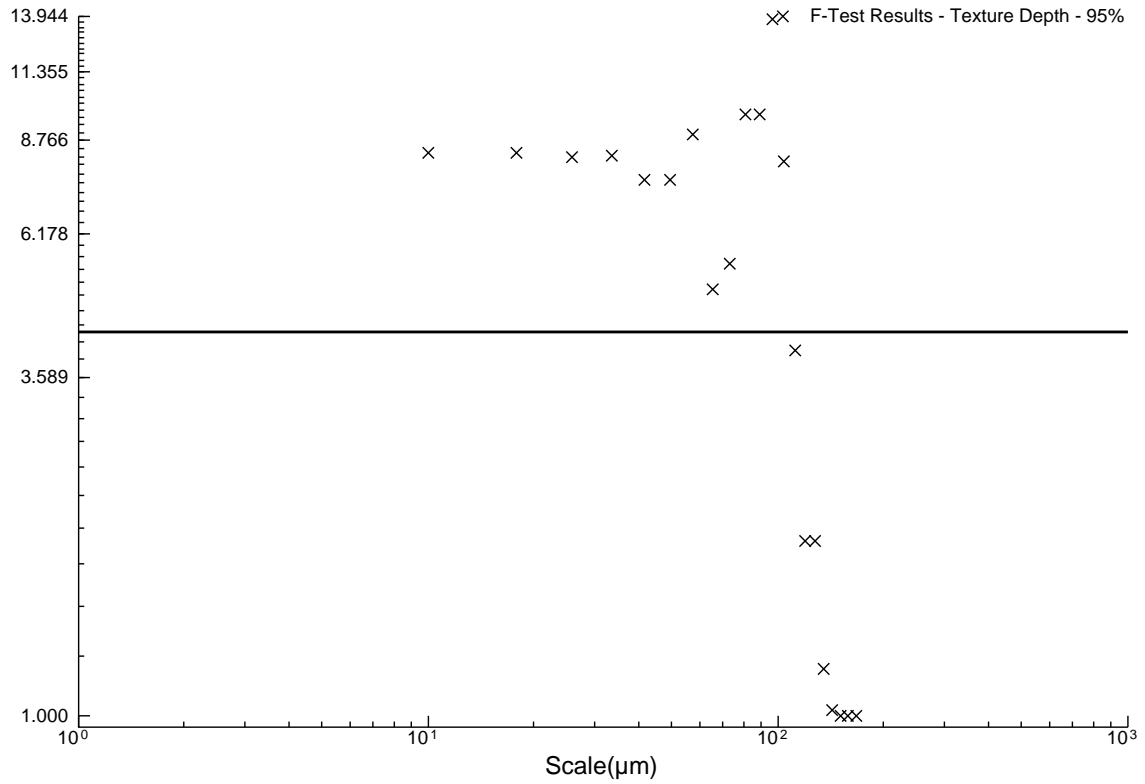


B3DVSW3U

### F-Test Results - Relative Area - 95%

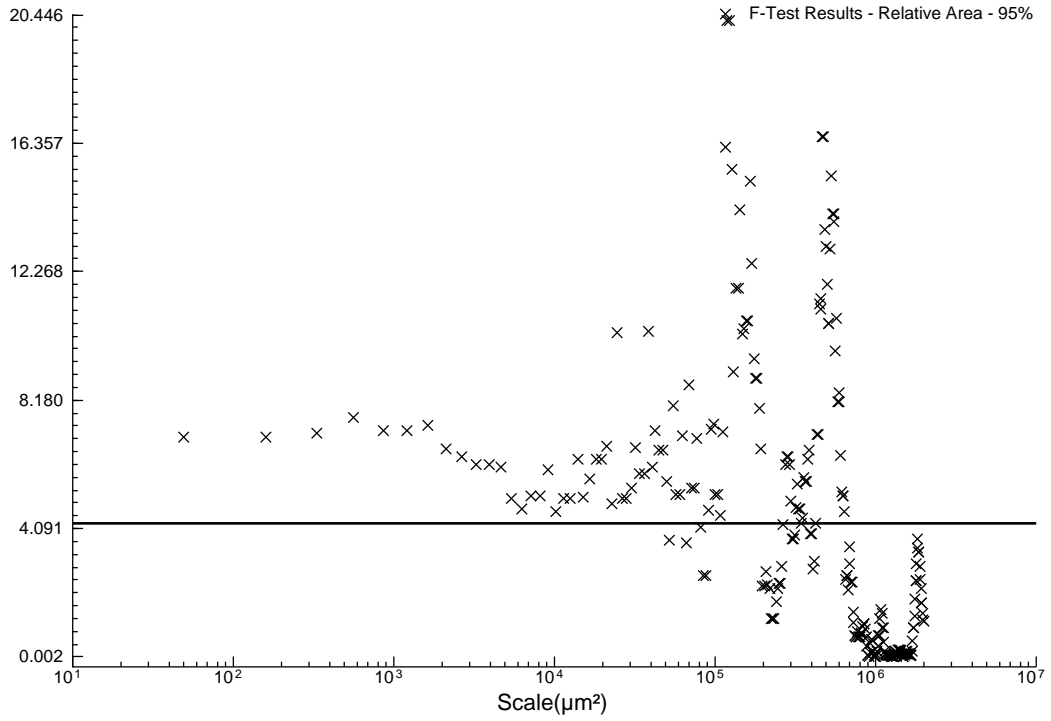


### F-Test Results - Texture Depth - 95%

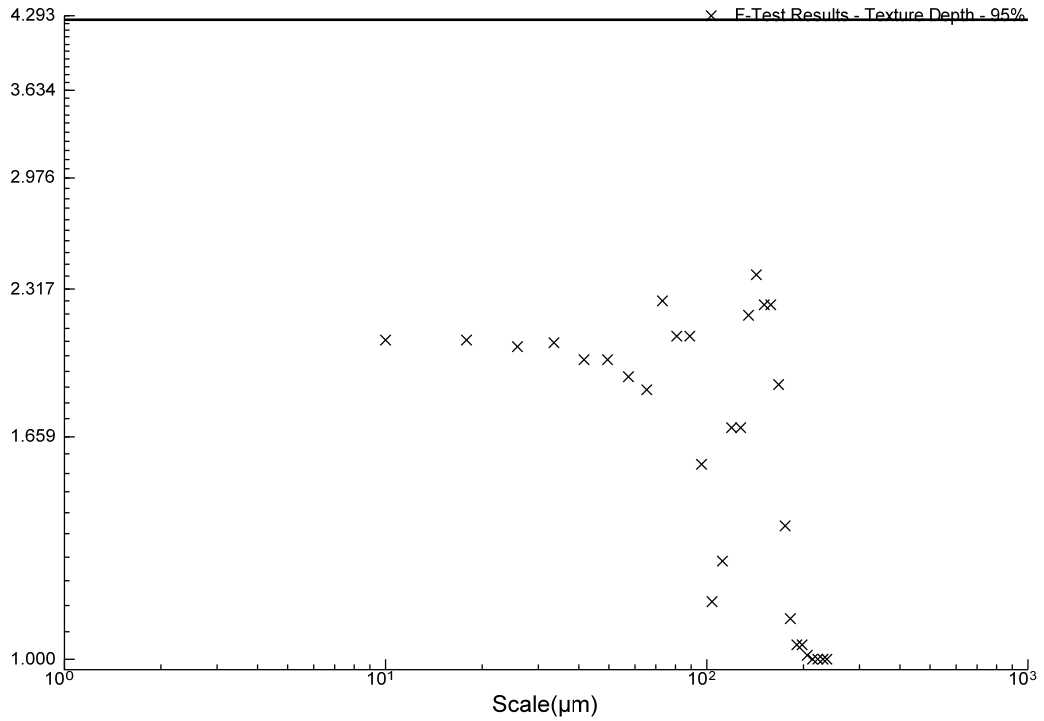


B3UVSW1D

### F-Test Results - Relative Area - 95%

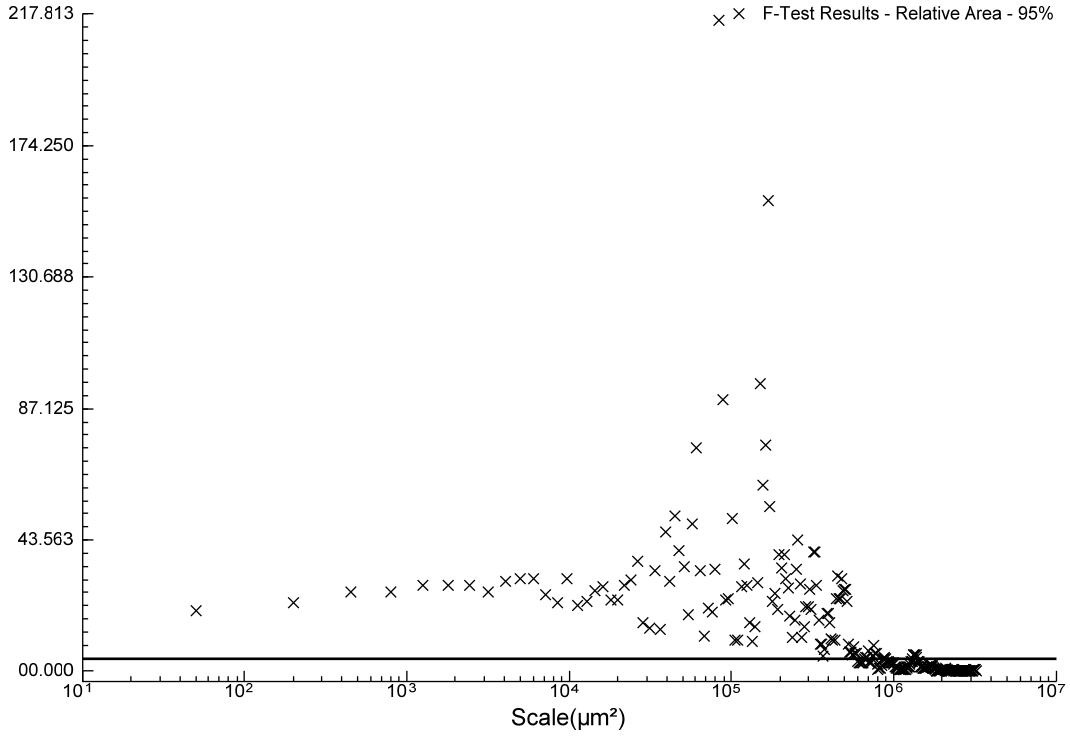


### F-Test Results - Texture Depth - 95%

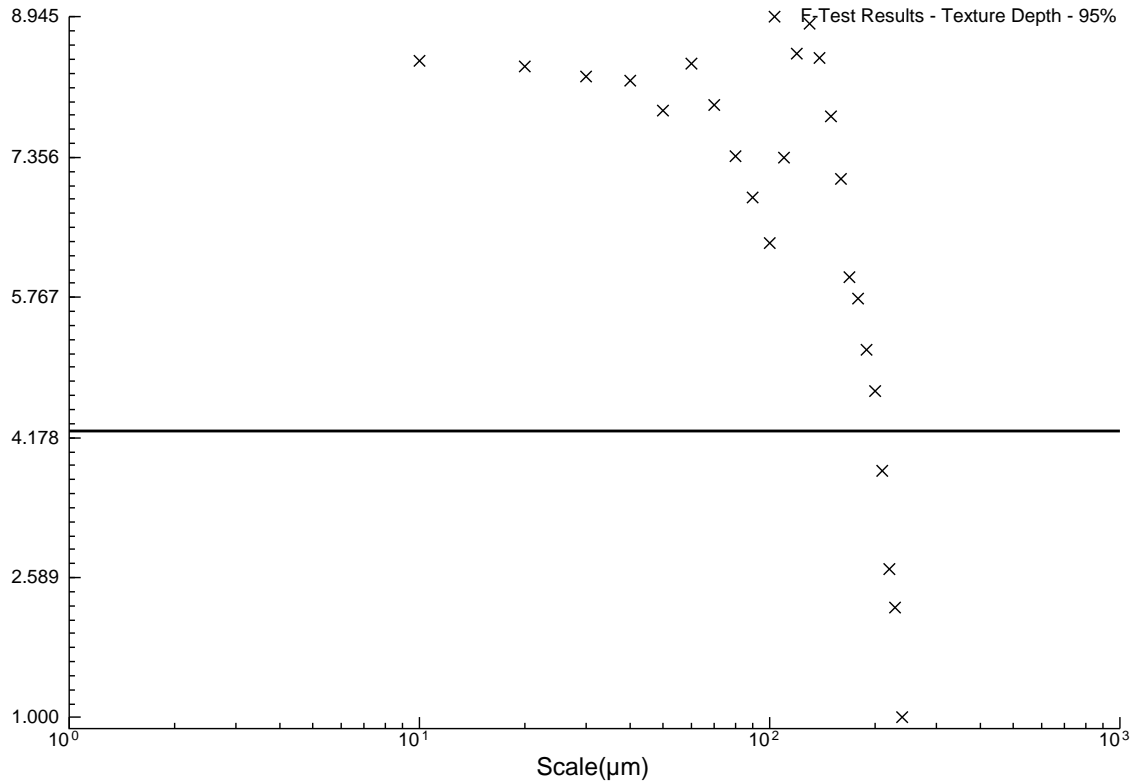


B3UVSW1U

### F-Test Results - Relative Area - 95%

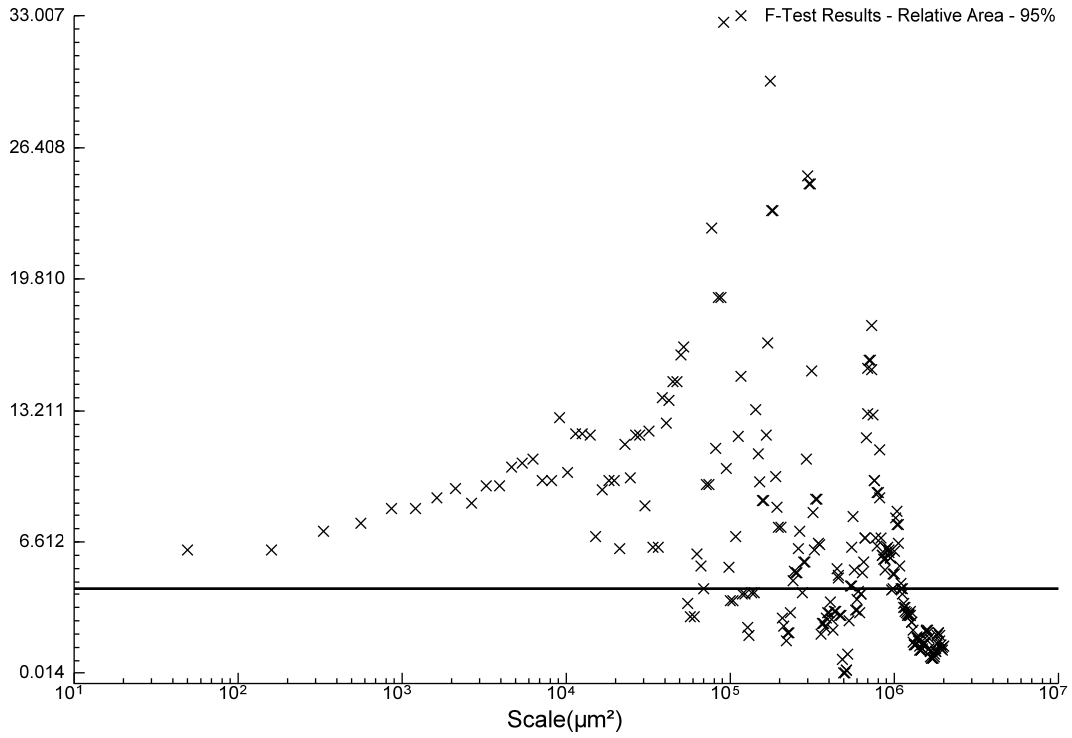


### F-Test Results - Texture Depth - 95%

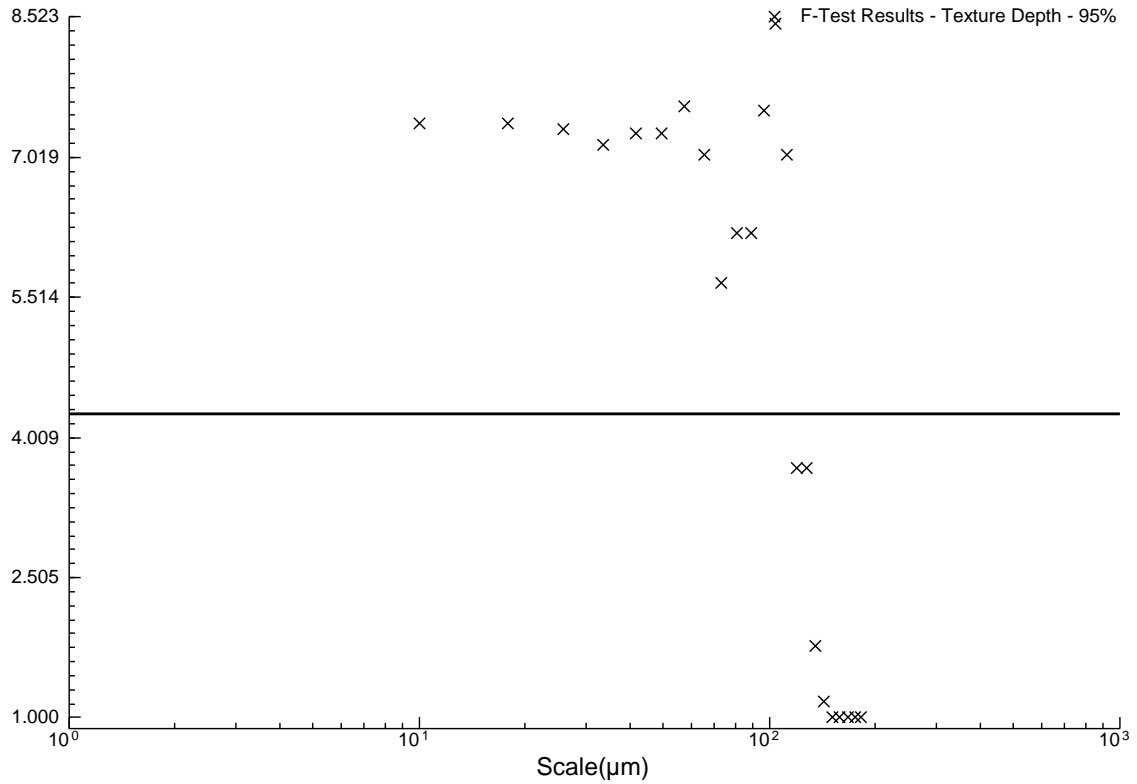


B3UVSW2D

### F-Test Results - Relative Area - 95%

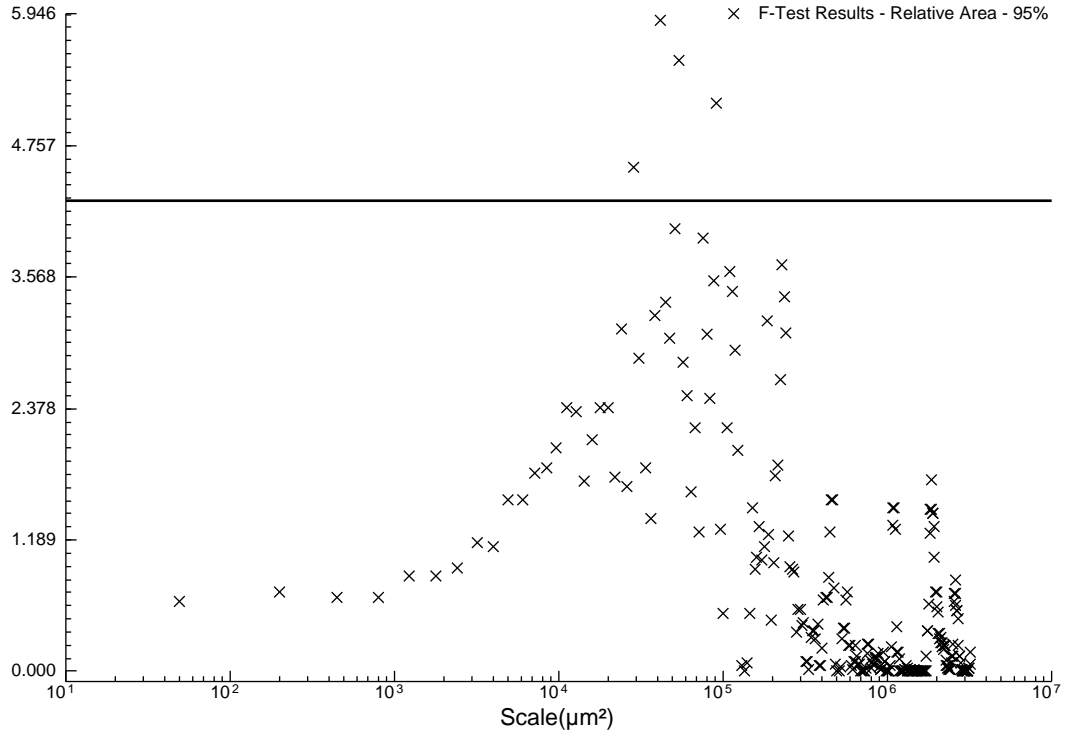


### F-Test Results - Texture Depth - 95%

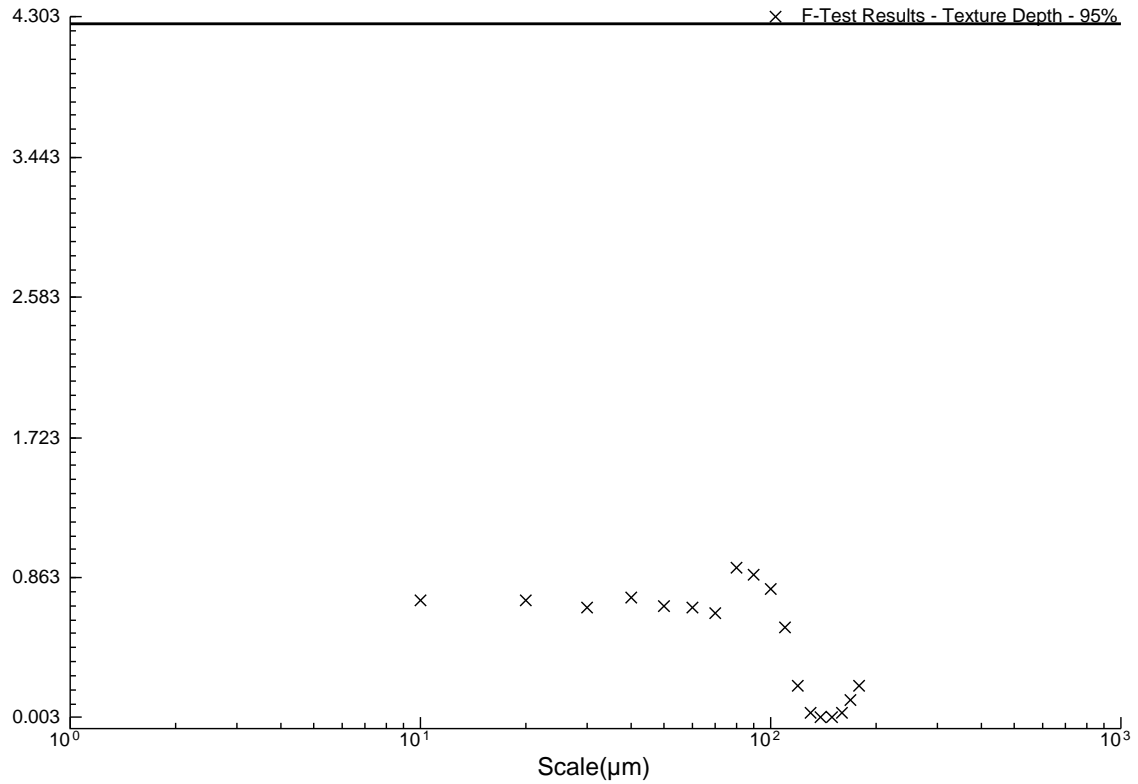


B3UVSW2U

### F-Test Results - Relative Area - 95%

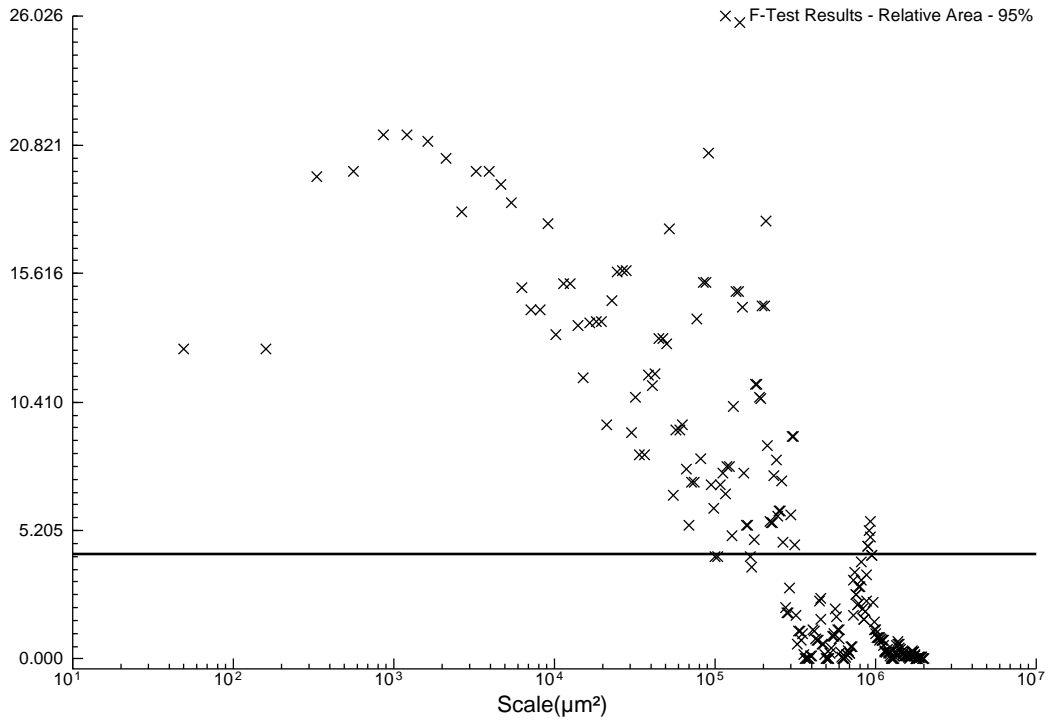


### F-Test Results - Texture Depth - 95%

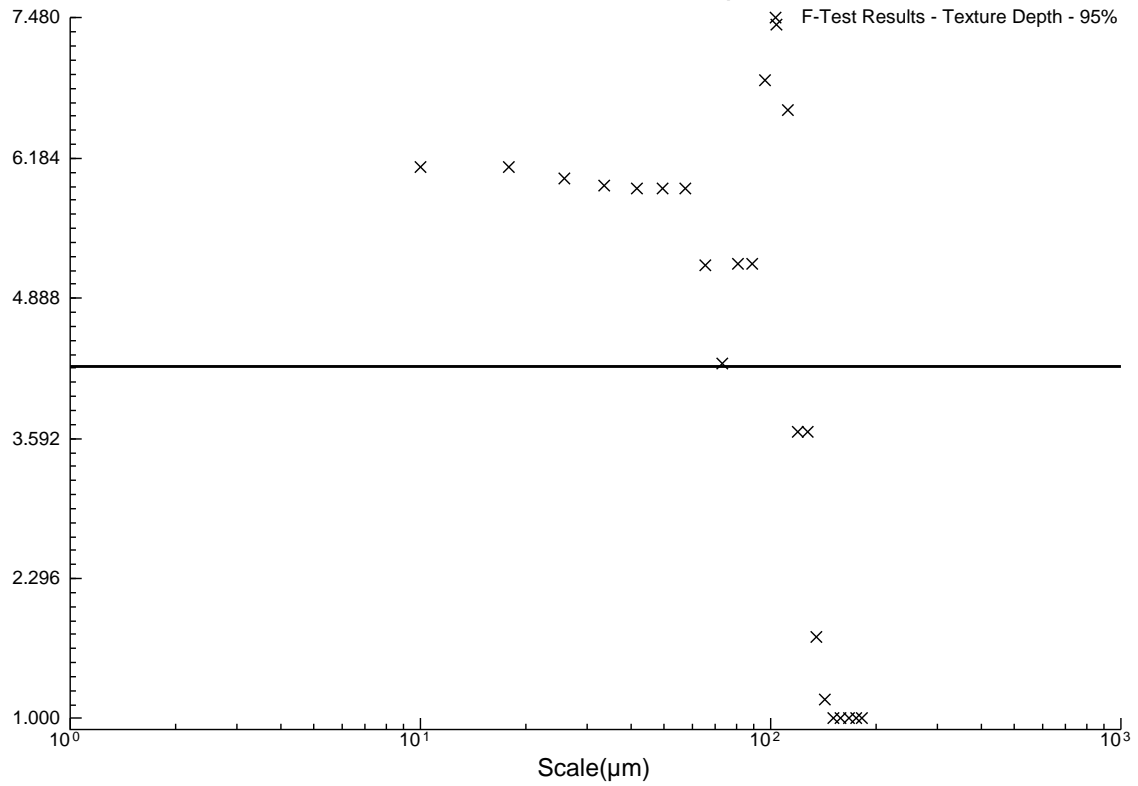


B3UVSW3D

### F-Test Results - Relative Area - 95%

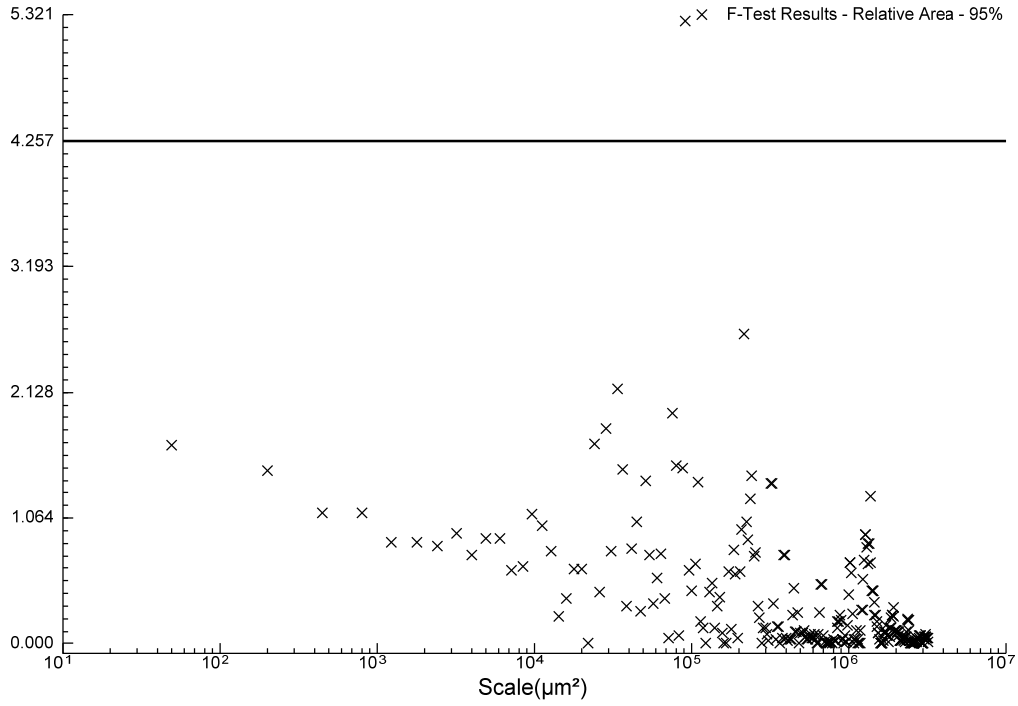


### F-Test Results - Texture Depth - 95%

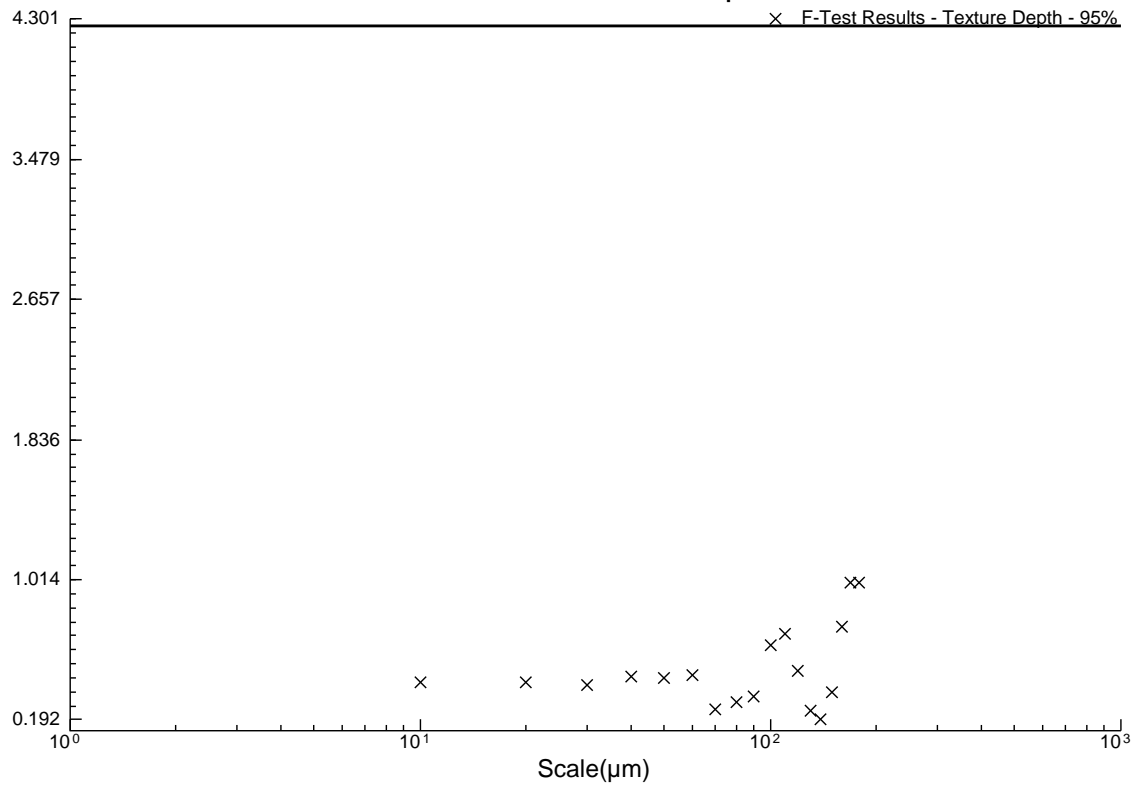


B3UVSW3U

### F-Test Results - Relative Area - 95%

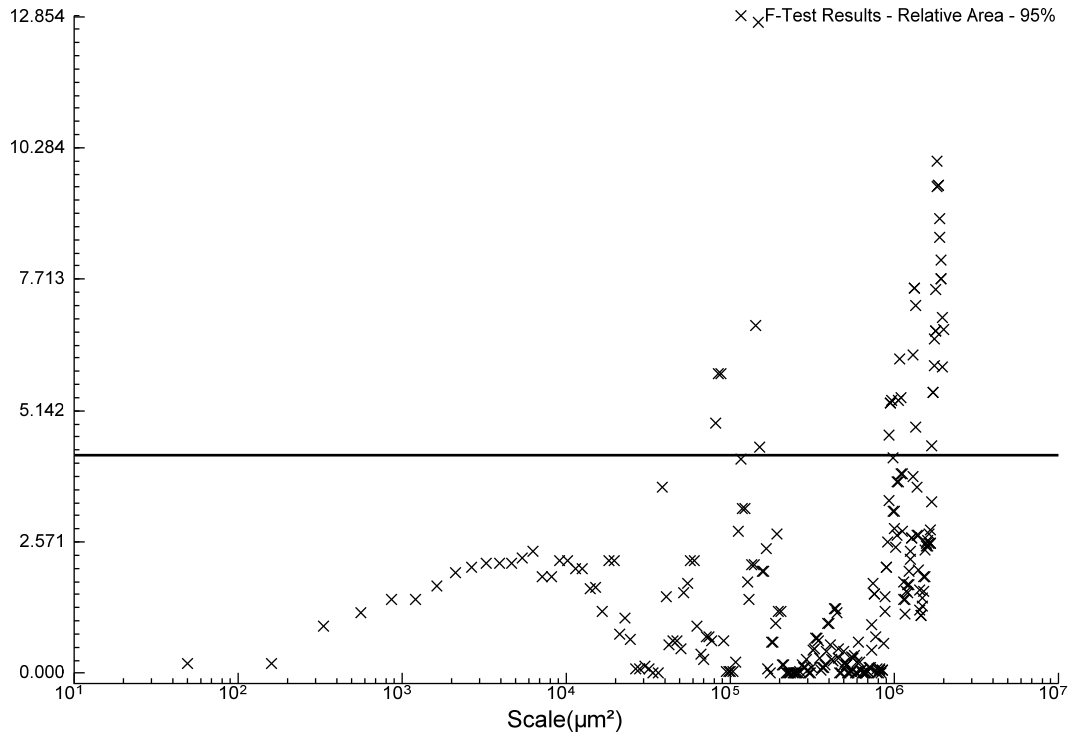


### F-Test Results - Texture Depth - 95%

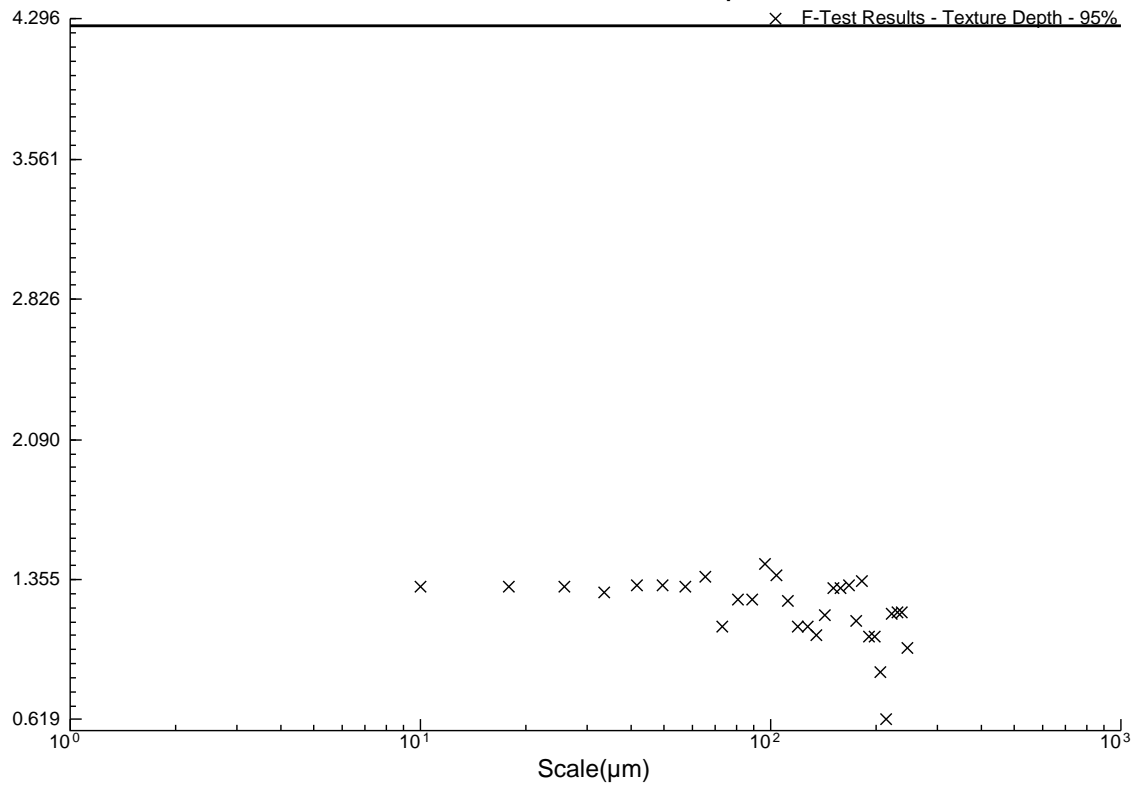


W1DVSW1U

### F-Test Results - Relative Area - 95%

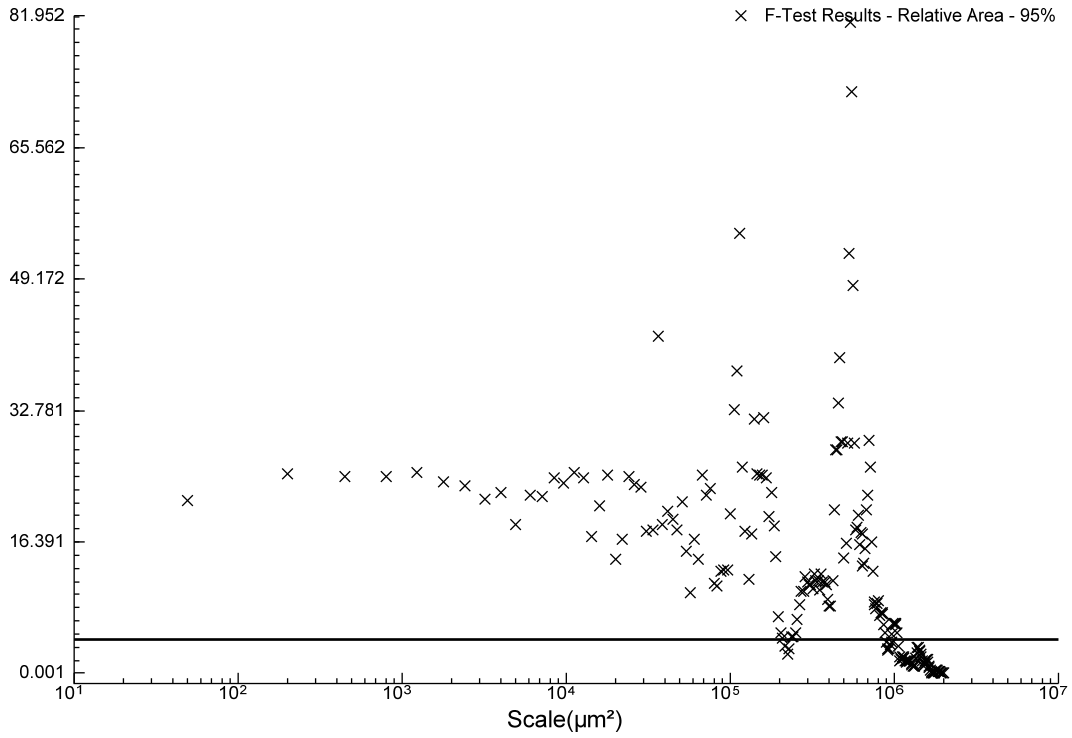


### F-Test Results - Texture Depth - 95%

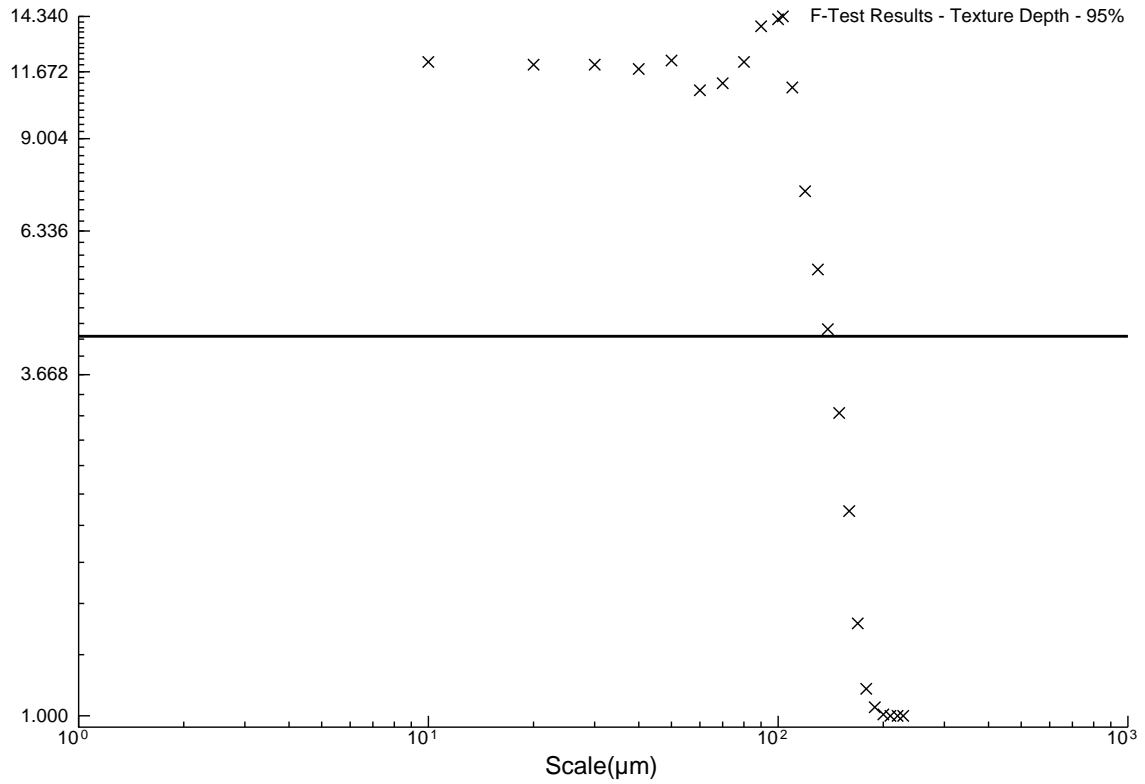


W1DVSW2D

### F-Test Results - Relative Area - 95%

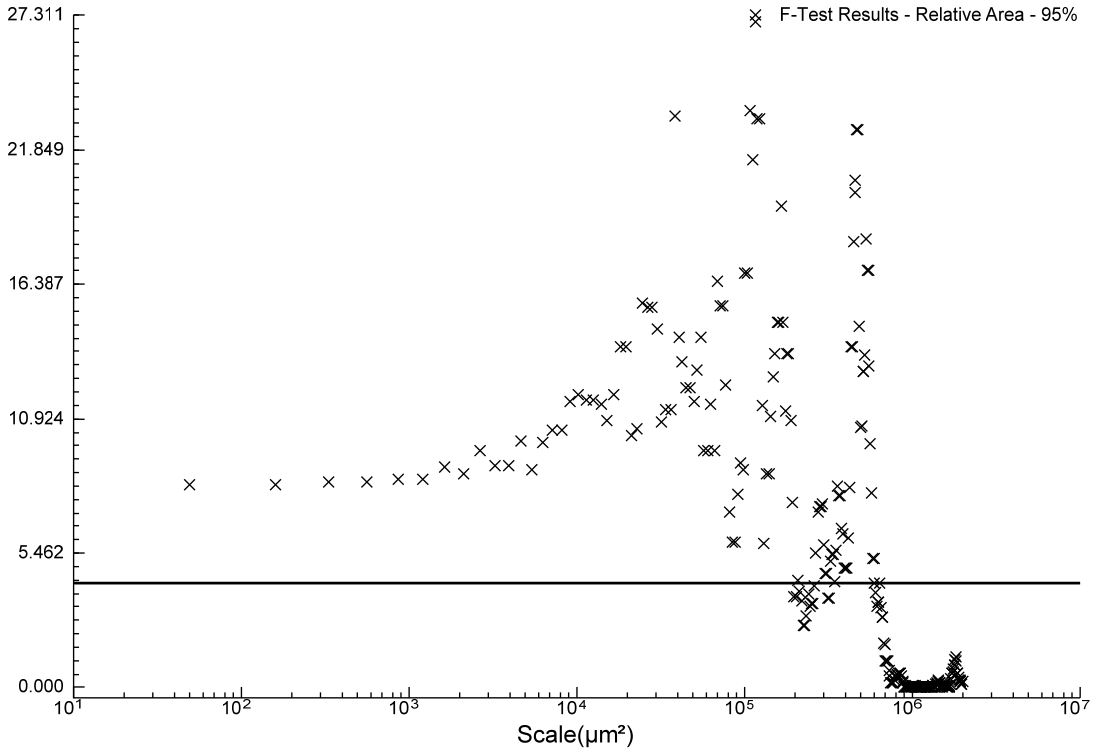


### F-Test Results - Texture Depth - 95%

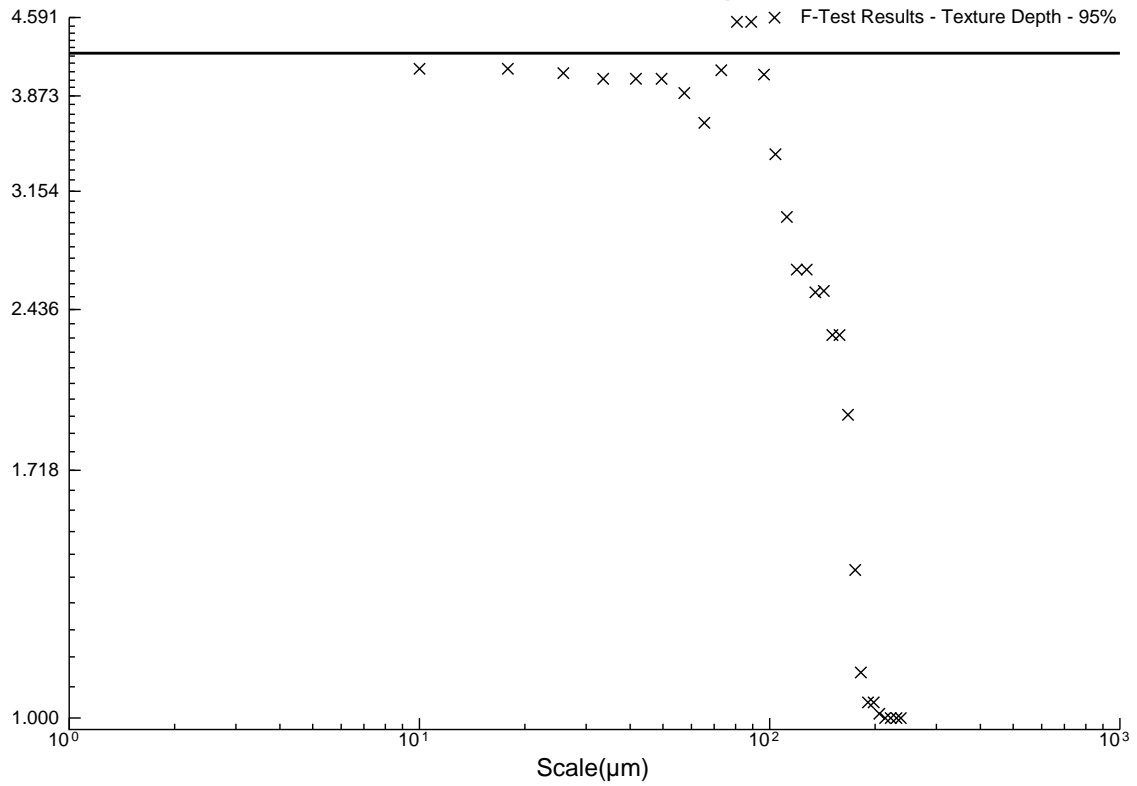


W1DVSW2U

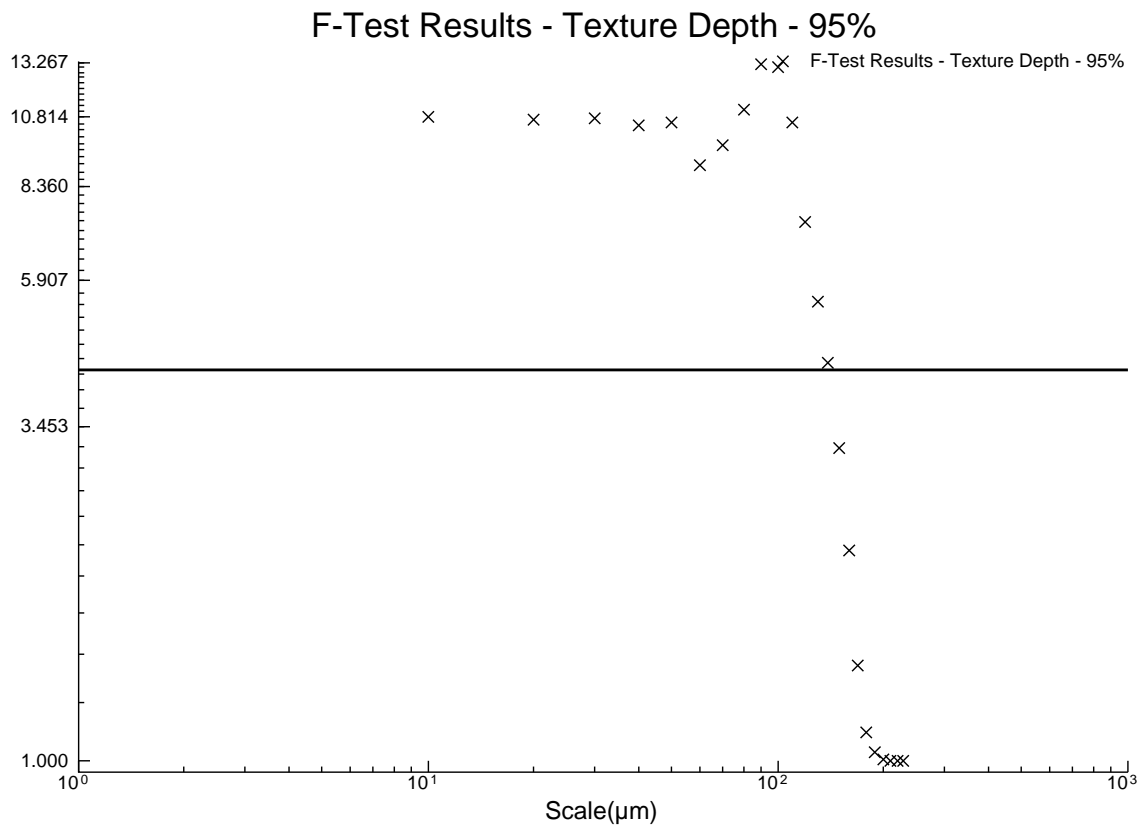
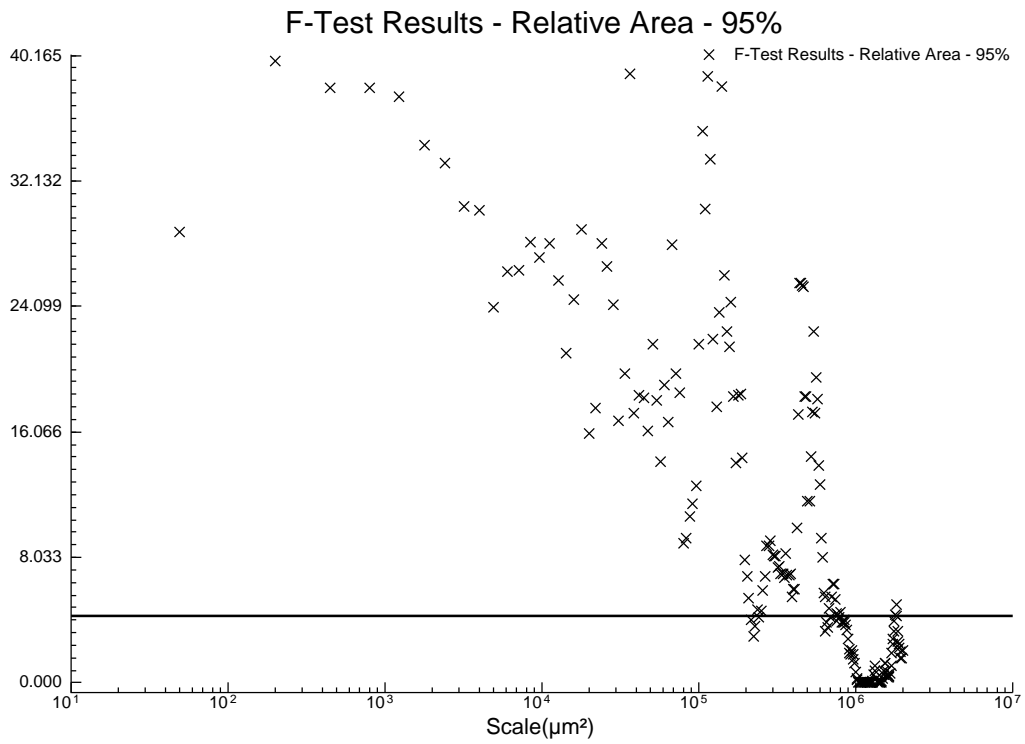
### F-Test Results - Relative Area - 95%



### F-Test Results - Texture Depth - 95%

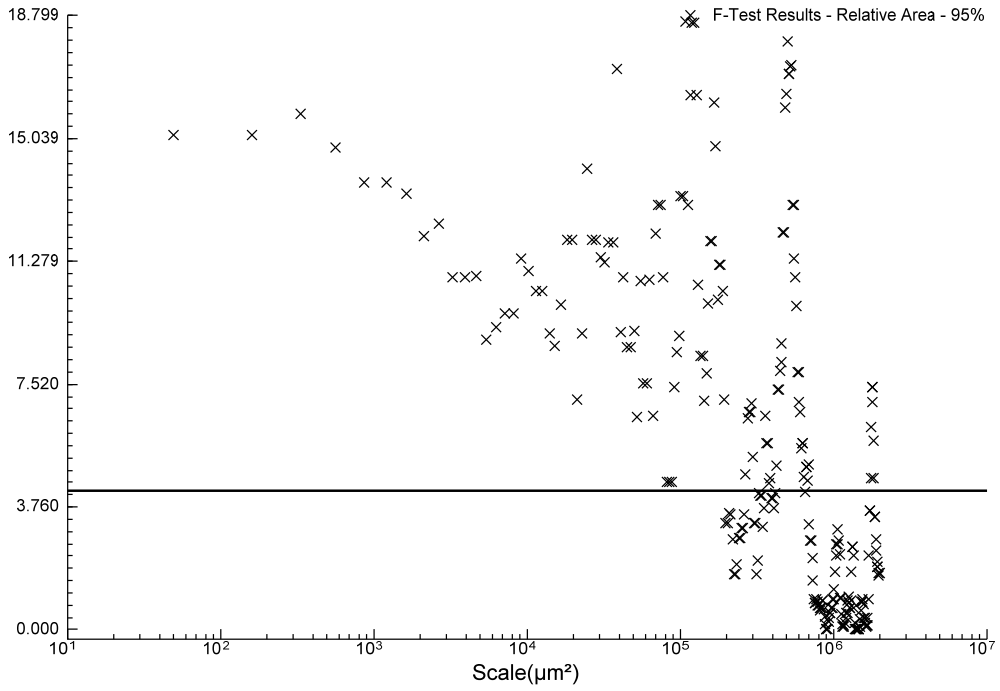


W1DVSW3D

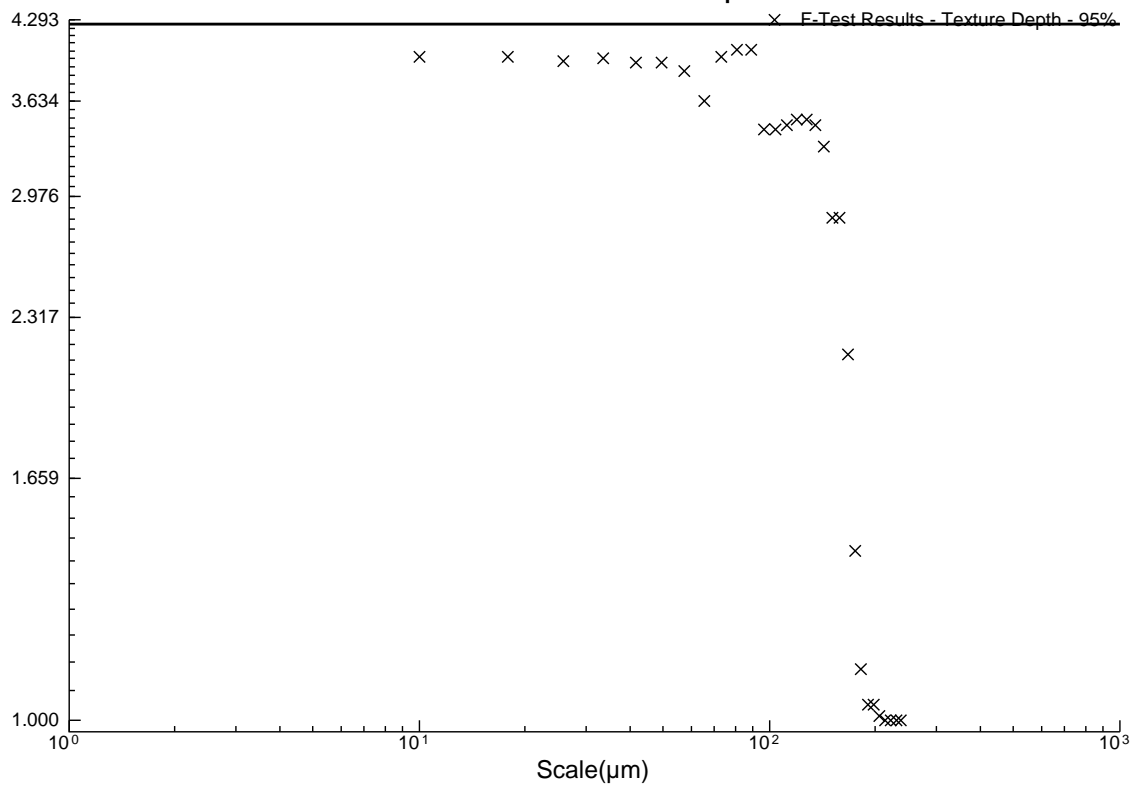


W1DVSW3U

### F-Test Results - Relative Area - 95%

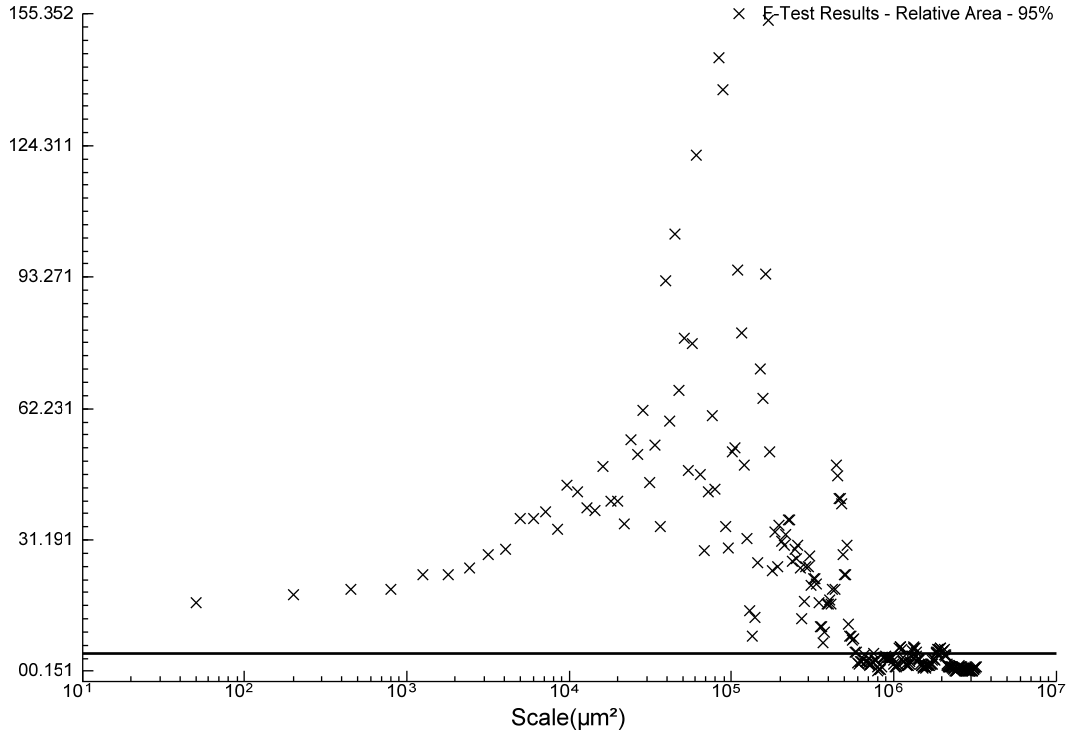


### F-Test Results - Texture Depth - 95%

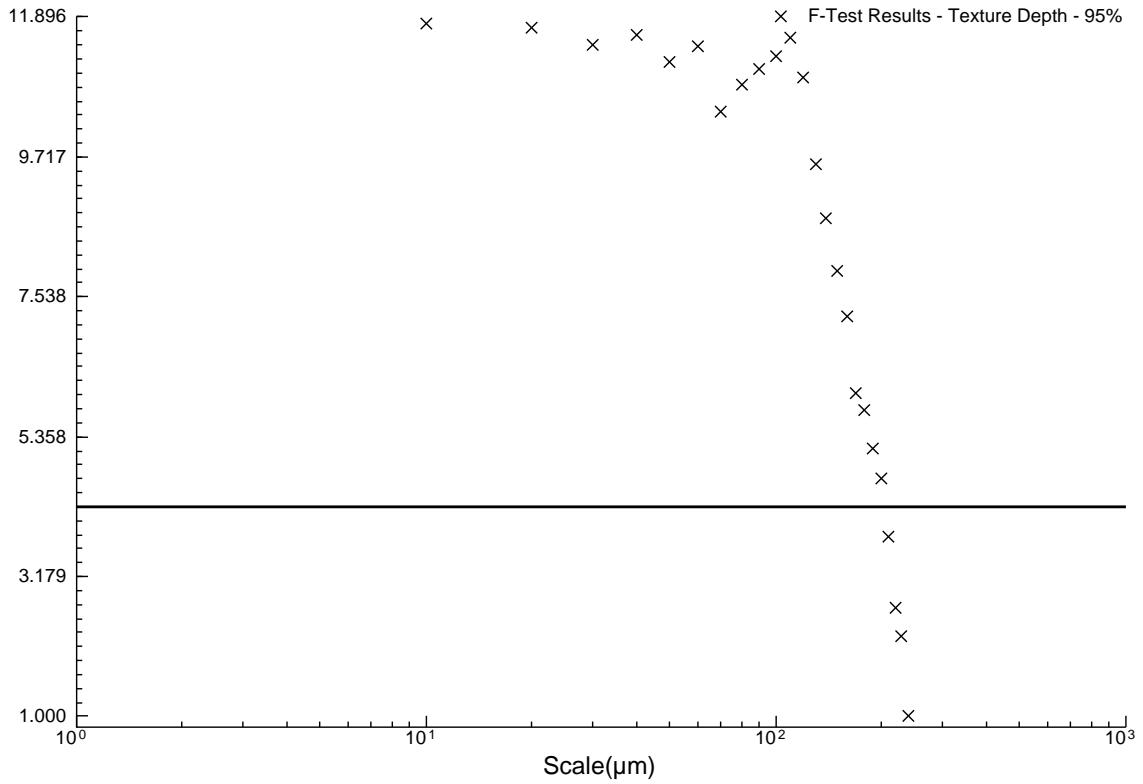


W1UVSW2U

F-Test Results - Relative Area - 95%

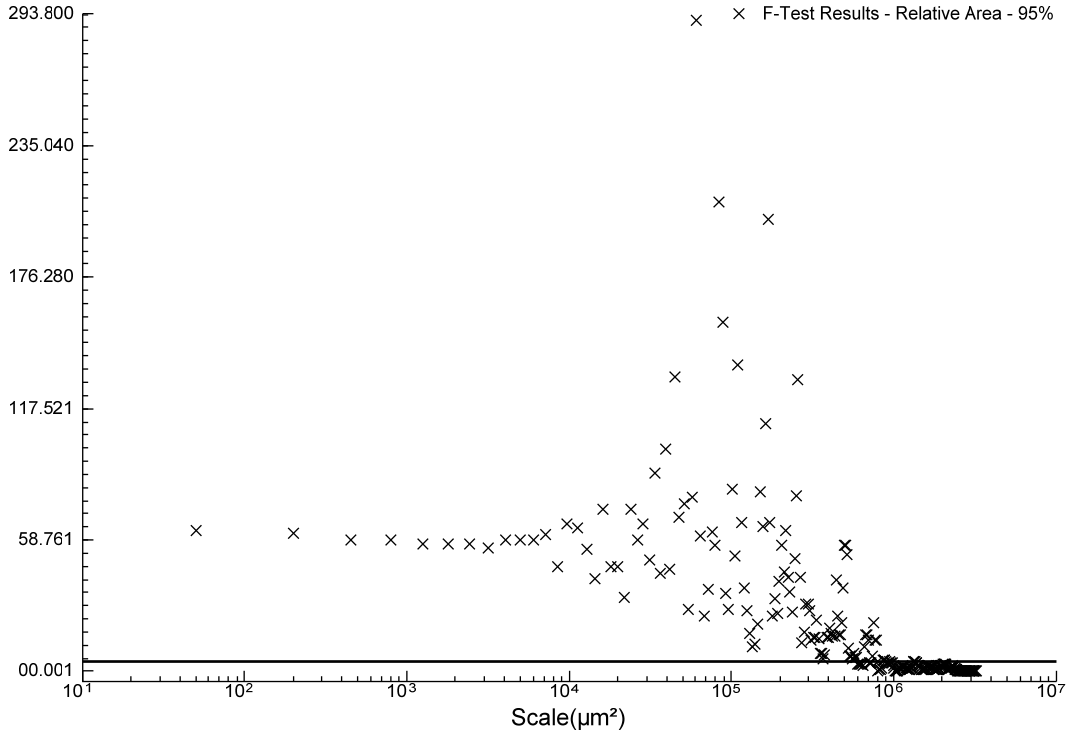


F-Test Results - Texture Depth - 95%

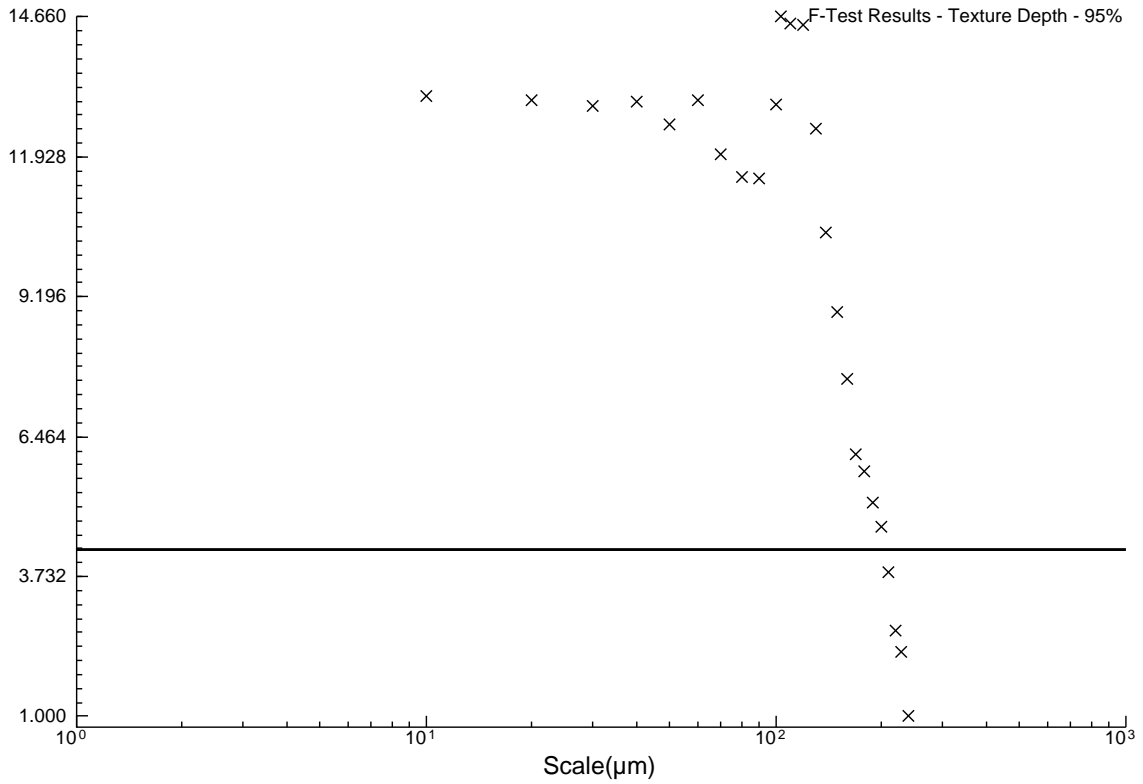


W1UVSW3U

F-Test Results - Relative Area - 95%

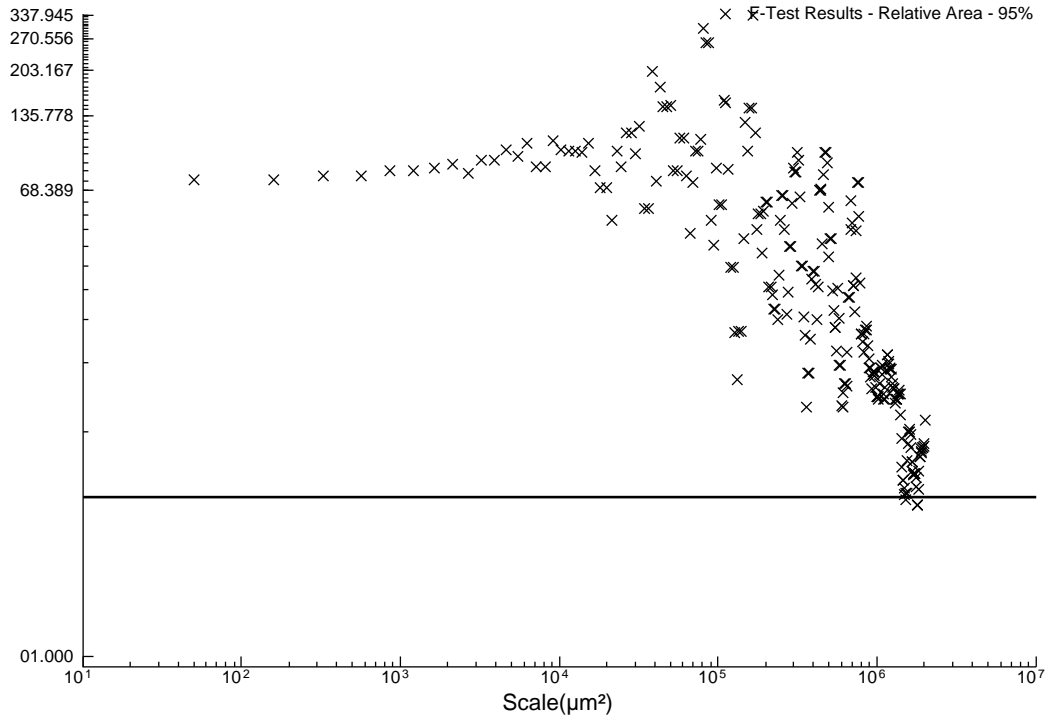


F-Test Results - Texture Depth - 95%

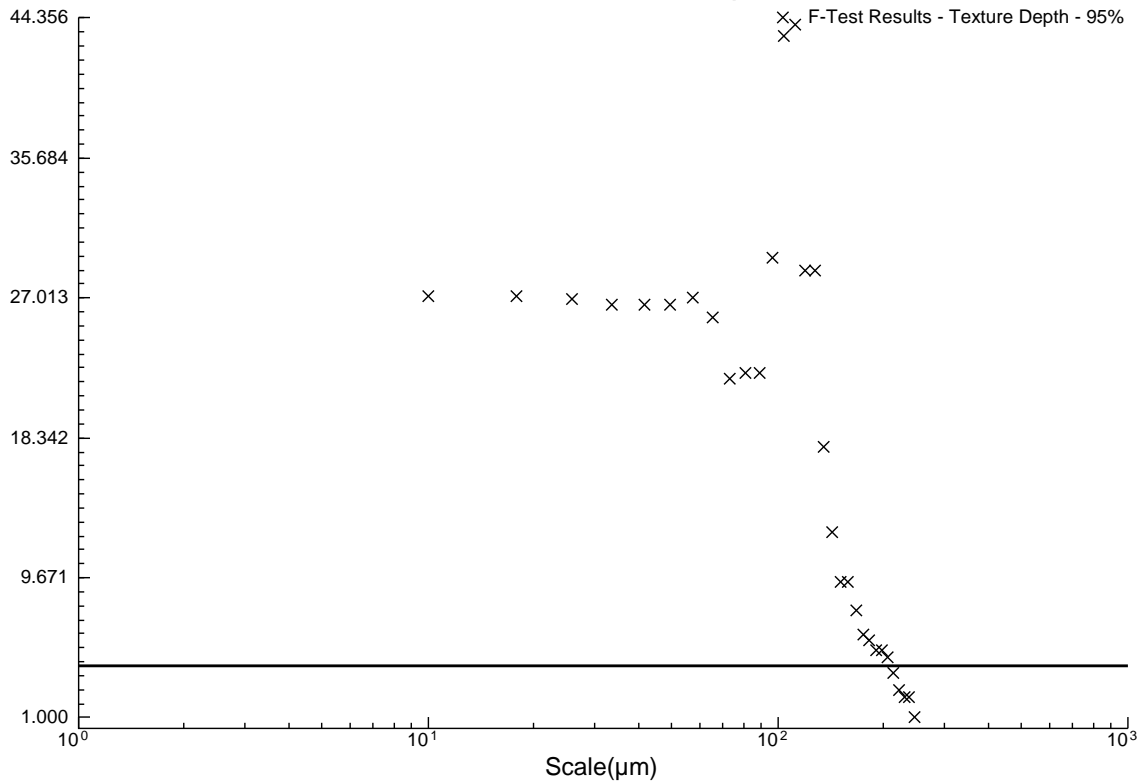


W2DVSW1U

### F-Test Results - Relative Area - 95%

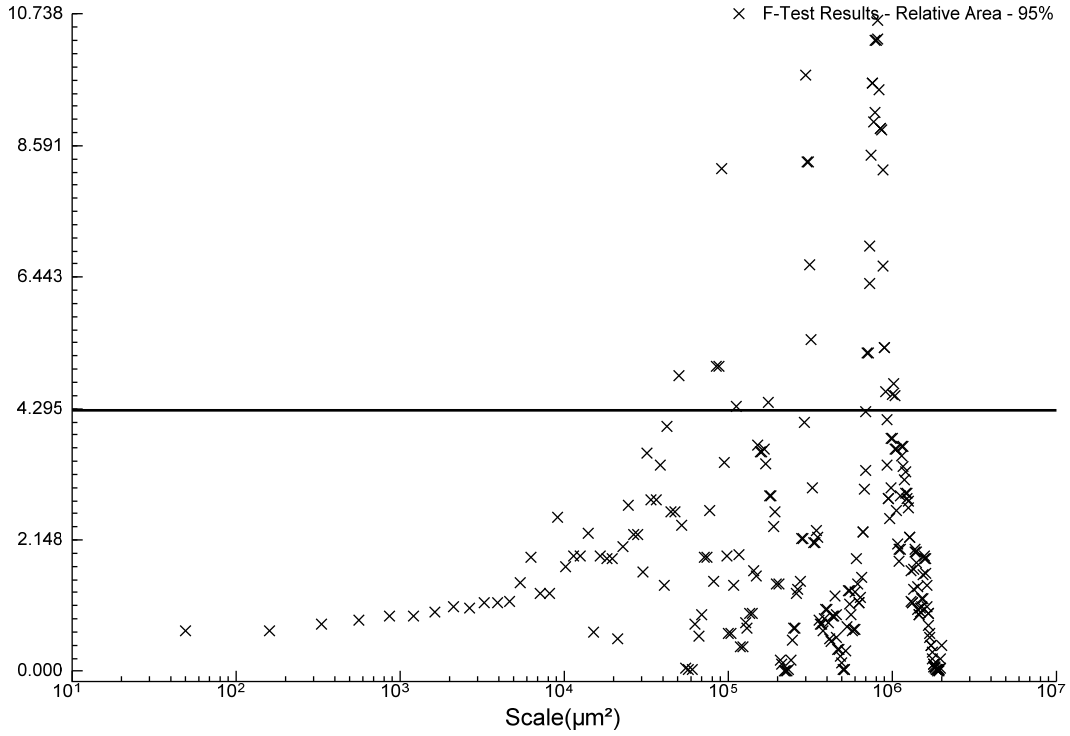


### F-Test Results - Texture Depth - 95%

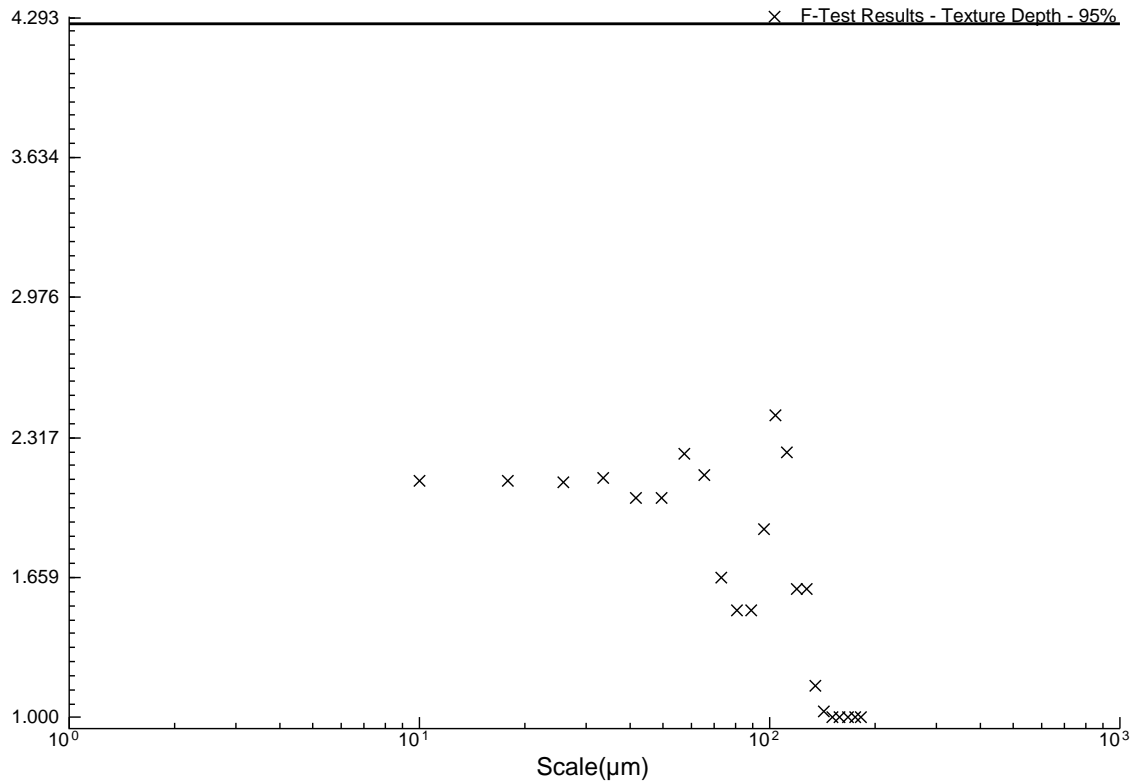


W2DVSW2U

### F-Test Results - Relative Area - 95%

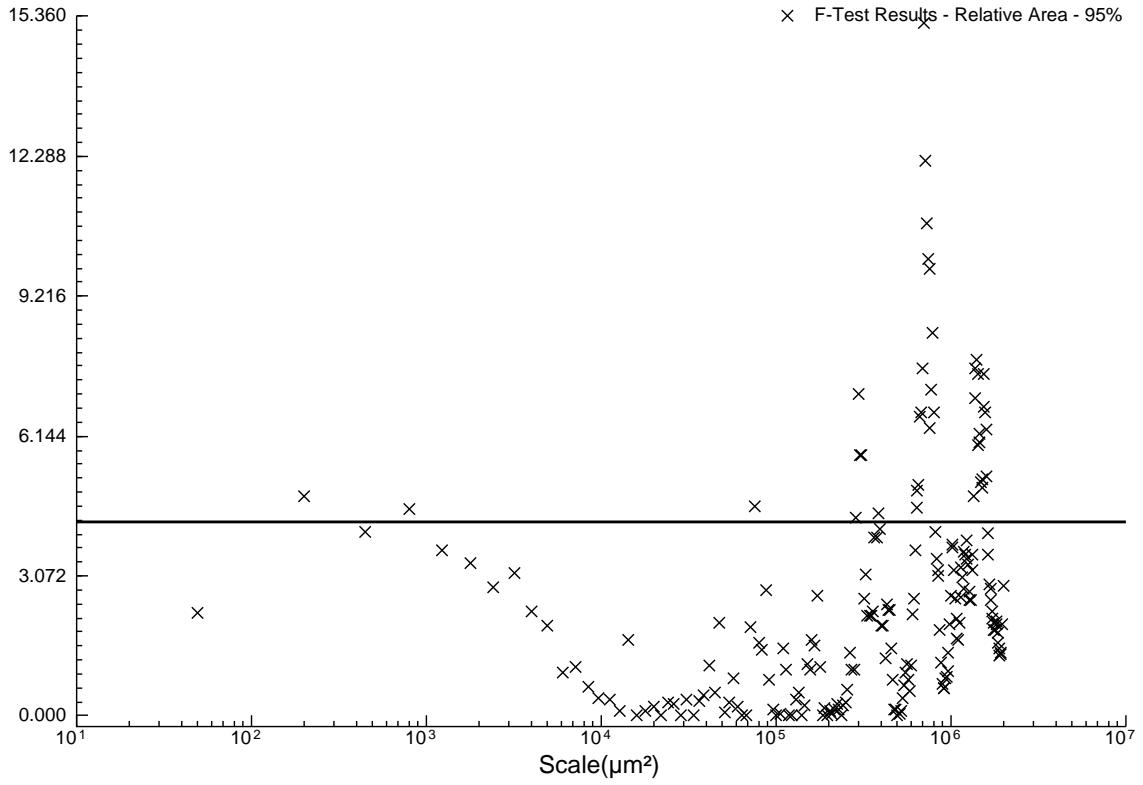


### F-Test Results - Texture Depth - 95%

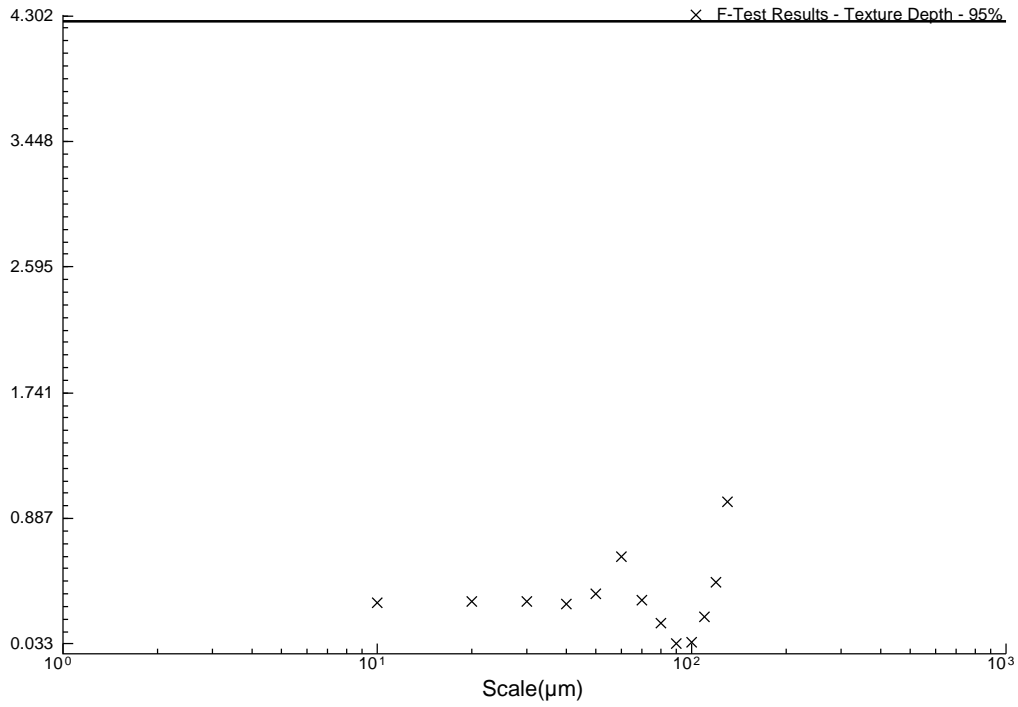


W2DVSW3D

### F-Test Results - Relative Area - 95%

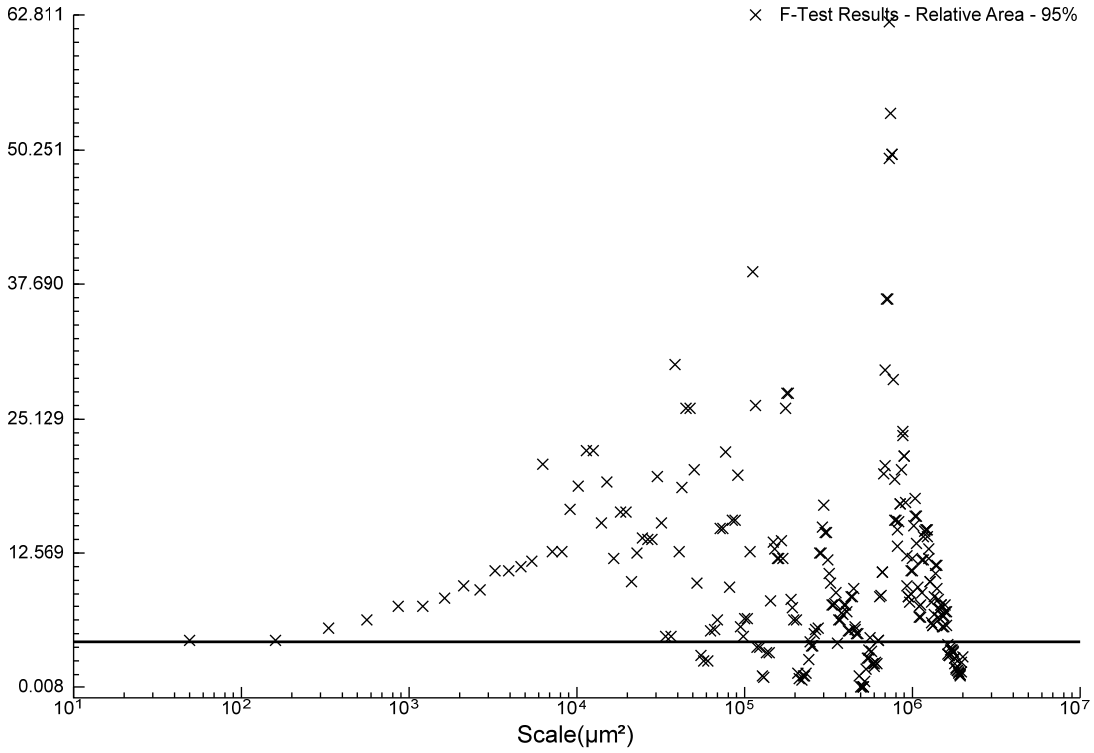


### F-Test Results - Texture Depth - 95%

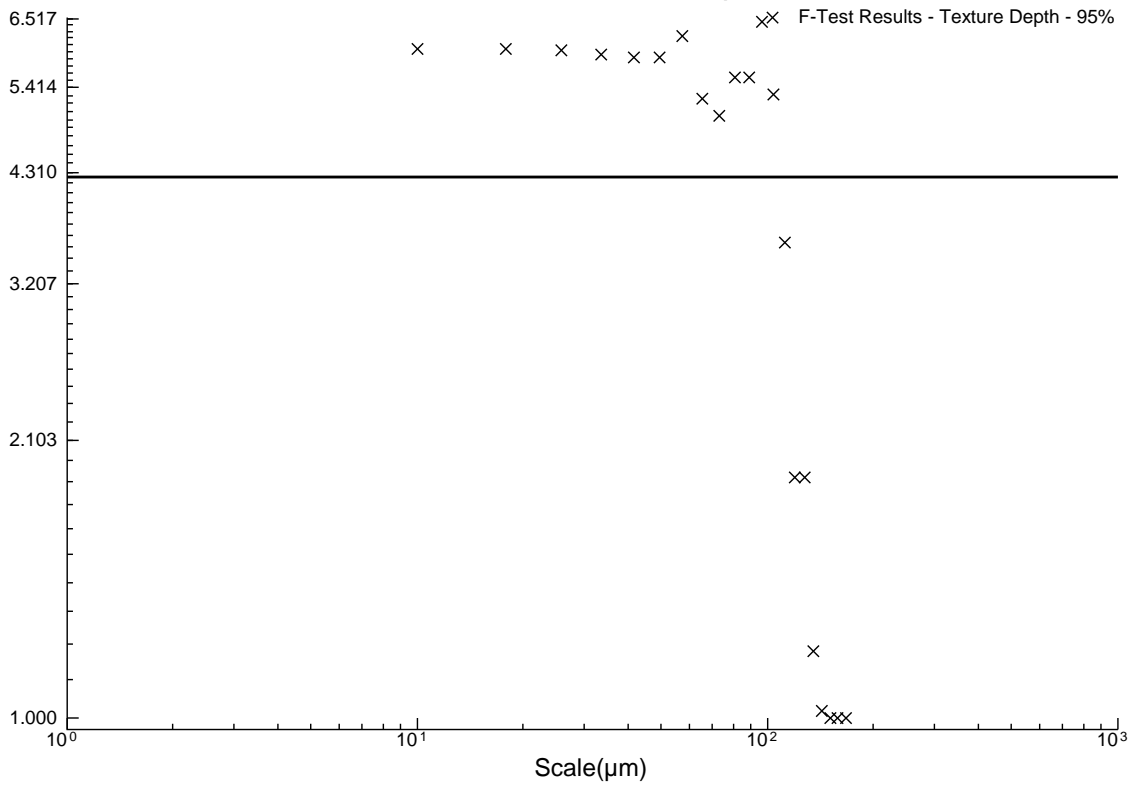


W2DVSW3U

### F-Test Results - Relative Area - 95%

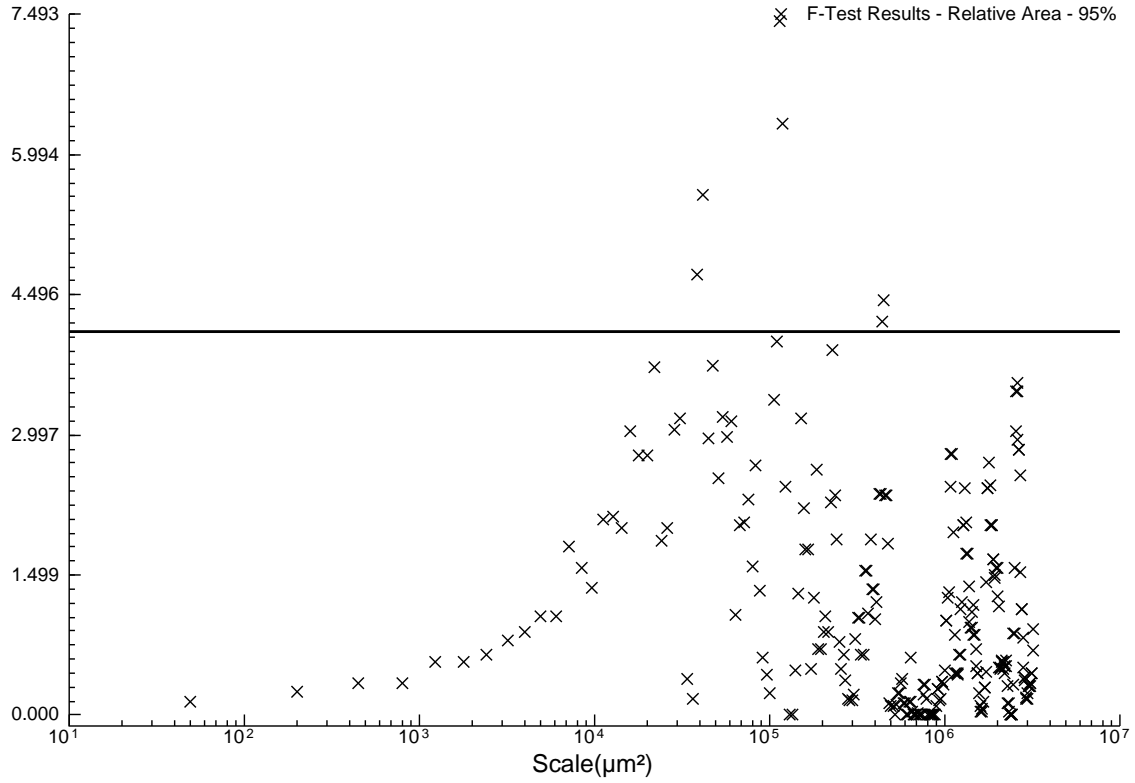


### F-Test Results - Texture Depth - 95%

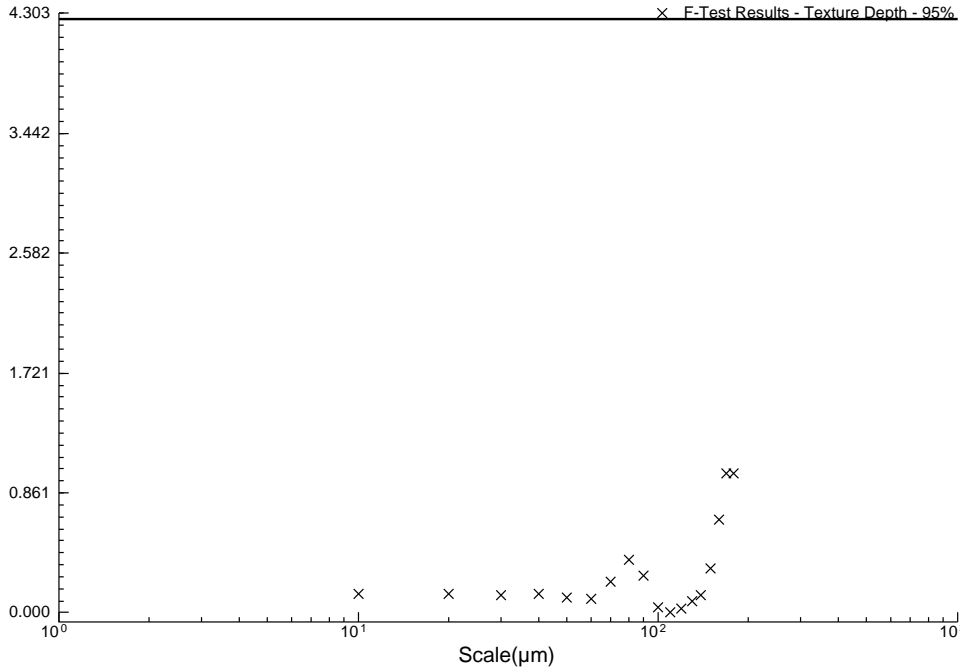


W2UVSW3U

### F-Test Results - Relative Area - 95%

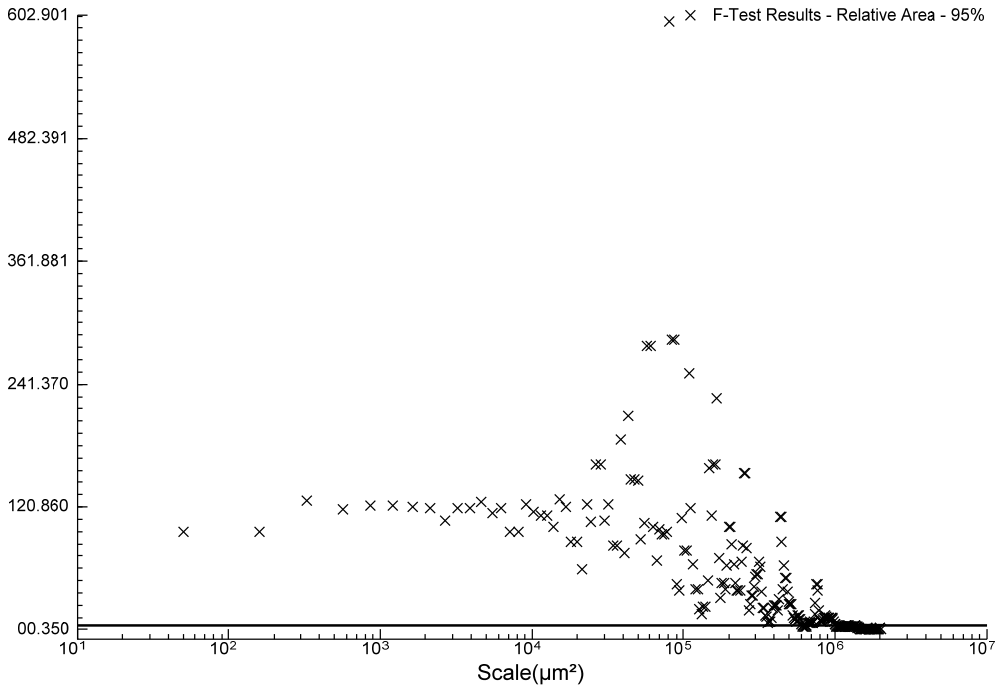


### F-Test Results - Texture Depth - 95%

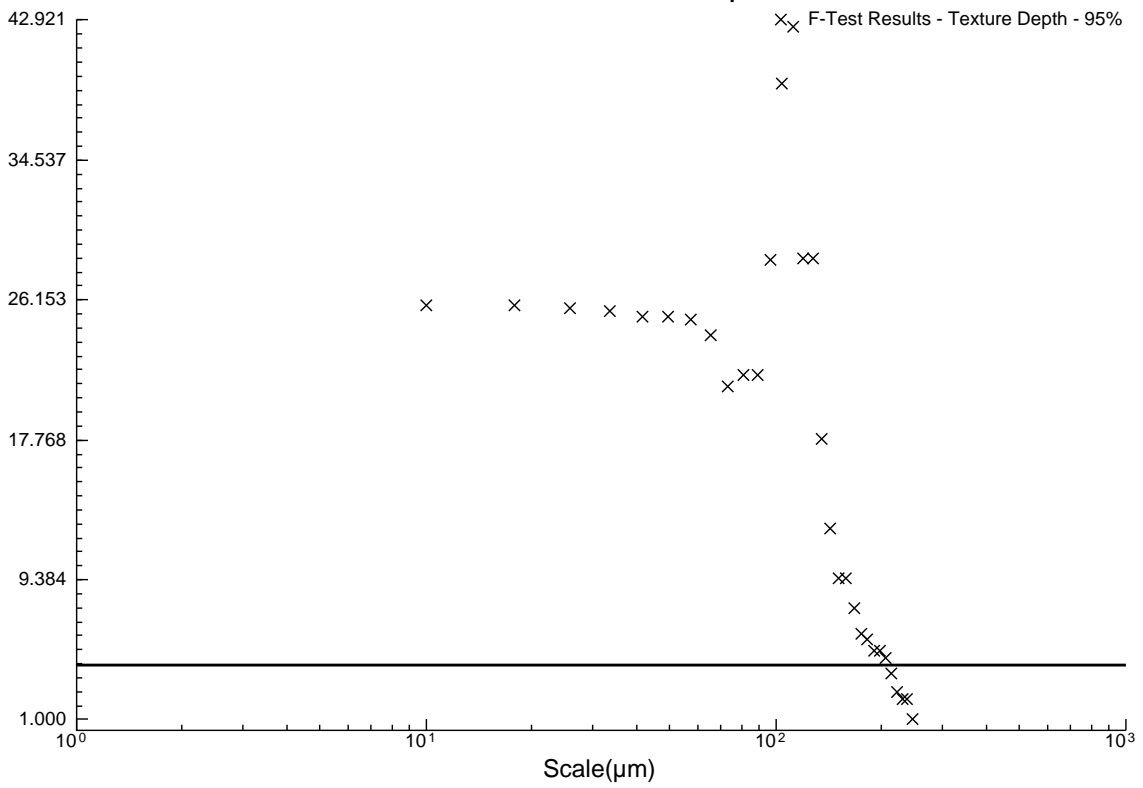


W3DVSWU

F-Test Results - Relative Area - 95%

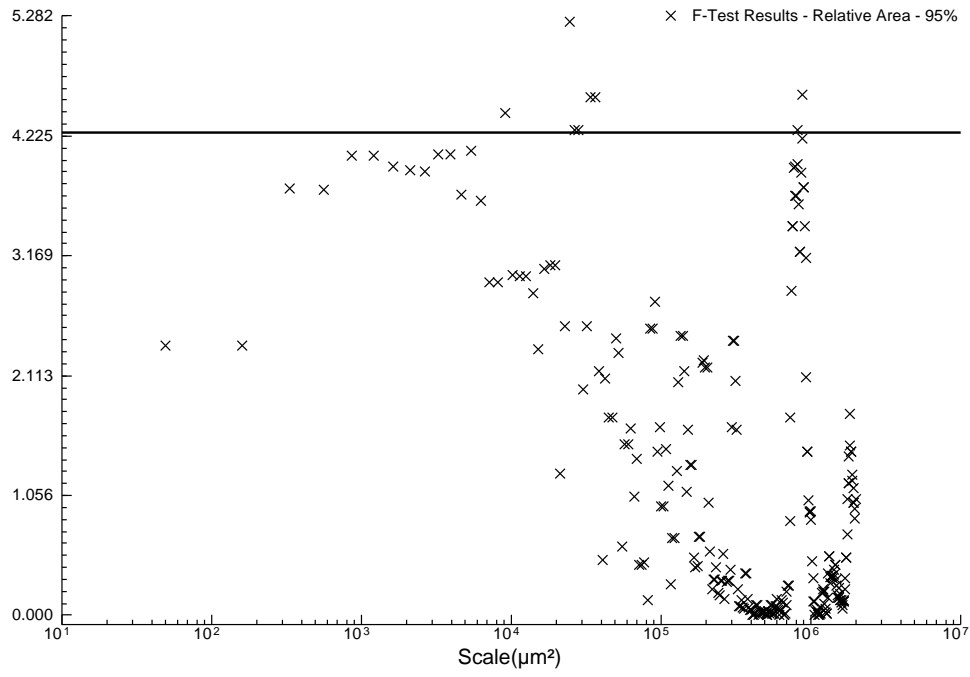


F-Test Results - Texture Depth - 95%

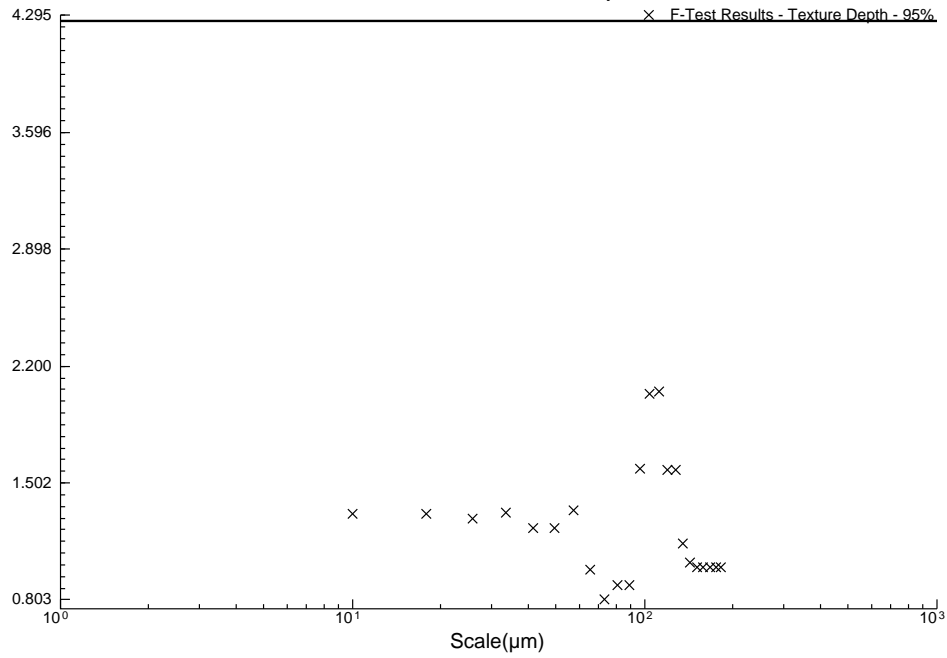


W3DVSW2U

F-Test Results - Relative Area - 95%

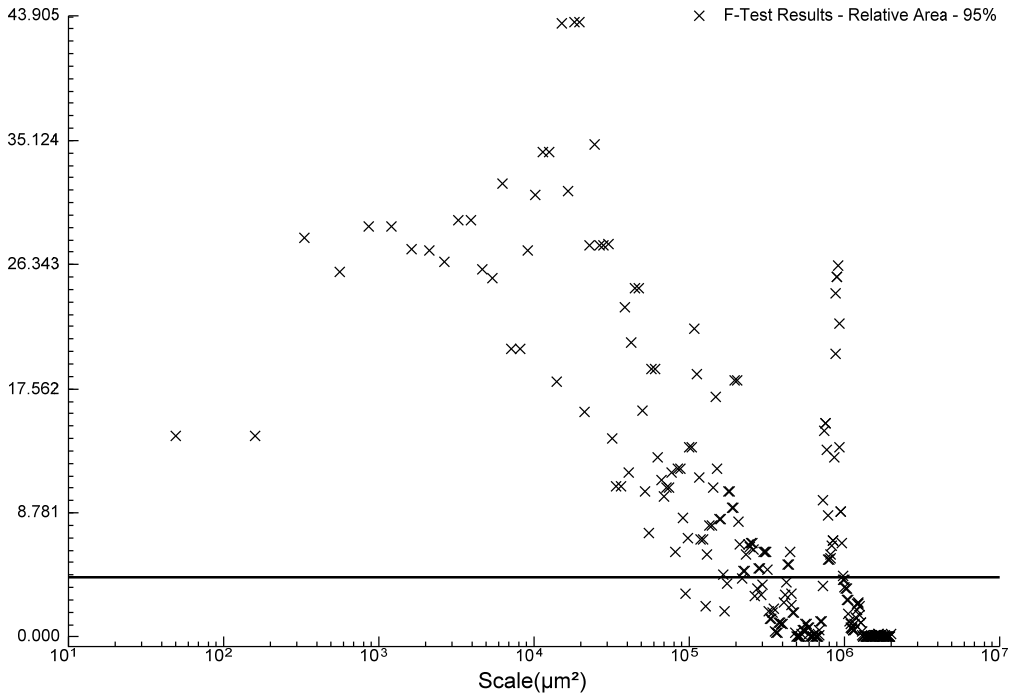


F-Test Results - Texture Depth - 95%



W3DVSW3U

### F-Test Results - Relative Area - 95%



### F-Test Results - Texture Depth - 95%

